UNIVERSITY OF OKLAHOMA

GRADUATE COLLEGE

OUTCROP- SUBSURFACE GEOLOGICAL CHARACTERIZATION OF LA LUNA FORMATION AS AN UNCONVENTIONAL RESOURCE IN THE NORTHWEST LAGO DE MARACAIBO BASIN AND NORTH ANDEAN FLANK, VENEZUELA

A THESIS

SUBMITTED TO THE GRADUATE FACULTY

in partial fulfillment of the requirements for the

Degree of

MASTER OF SCIENCE

By

ANDREINA LIBORIUS PARADA
Norman, Oklahoma
2015

Downloaded from SHAREOK. Persistent Handle URL: https://hdl.handle.net/11244/323460

OU
THESIS
LIB
cop.2

OUTCROP- SUBSURFACE GEOLOGICAL CHARACTERIZATION OF LA LUNA FORMATION AS AN UNCONVENTIONAL RESOURCE IN THE NORTHWEST LAGO DE MARACAIBO BASIN AND NORTH ANDEAN FLANK, VENEZUELA

A THESIS APPROVED FOR THE
CONOCOPHILLIPS SCHOOL OF GEOLOGY AND GEOPHYSICS

BY

[redacted]

© Copyright by ANDREINA LIBORIUS PARADA 2015
All Rights Reserved.

© Copyright by ANDREINA LIBORIUS PARADA 2015
All Rights Reserved.

Pilar, Julio y Nena, esto es para ustedes, los amo!

Acknowledgements

God, for presenting me this amazing opportunity and taught me how to become a better person while facing various difficulties in life.

Dr. Roger Slatt, he gave me the opportunity to learn at the best petroleum geology school in the United States. He taught me that being humble is one of the best traits that anyone can have. Thanks for your unconditional support. I will always be grateful.

Dr. Omar Guerrero, for his guidance during my professional career and his support with my fieldwork while in Venezuela for my thesis.

Dr. Paul Philp, for his amazing lectures that made me realize that I wanted to specialize in geochemistry and his sincere help during my thesis.

My beautiful family, without their support and faith in me I could not have completed this goal of mine. I love you!

I will forever be grateful to **PDVSA** Exploration-Maracaibo for providing me the data for the development of my thesis. I would like to especially thank Dr. Marvin Baquero and Jose Baamonde for their support and Nicanor Mendez and Elber Molina for their help coordinating fieldwork in Zulia.

All of my fellow graduate friends (Lennon Infante, Gabriel Machado, Javier Tellez, Henry Galvis, Emilio Torres among others) who kindly helped me with their experience during my classes and thesis. I learned a lot from you guys, thank you!

To my friends from Venezuela and my friends from OU for always being there as my second family, love you guys!

I want to thank my Alma Mater: Universidad de los Andes, to Dr. Miguel Alvarado and ULA students, especially Carlos Vielma for their help in the fieldwork stage.

Table of Contents

Acknowledgements iv

Table of Contents v

List of Tables ix

List of Figures xi

Abstract xxiii

1. Introduction 1

2. Geological Setting 4

2.1 Geology of study area 4

2.2 Regional Geology 6

2.3 Local Geology 11

3. Methodology 16

3.1 Gathering and analyzing previous information: 16

3.2 Fieldwork: 16

3.3 Description of the outcrops 18

3.4 Laboratory analysis 20

4. Core description and facies analysis of La Luna IX core 21

4.1 La Luna Core 21

4.1.1 Maraca Formation 22

4.1.2 La Luna Formation: 22

4.1.3 Colon Formation 23

4.2 Facies classification present in the 1X WELL: 24

I. Dark gray laminated mudstone: 24

II. Fossiliferous wackstone facies 24

III. Volcanic Ash 25

IV. Laminated mudstone with limestone concretions and packstone 27

V. Siliceous- calcareous laminated mudstone interbedded with black chert filled with calcite veins 27

VI. Siliceous- Calcareous mudstone interbedded with wackstone facies 28

VII. Slightly siliceous- calcareous laminated black mudstone interbedded with calcareous fossiliferous wackstone. 33

VIII. Siliceous green mudstone with authigenic glauconite and Pyrite 33

4.3 Mineral composition 35

4.4 Inorganic Geochemical Parameters 47

4.5 Organic Geochemical Parameters and analyses 53

3.4.1 Source Potential logs 60

3.4.2 Hydrocarbon indicators and maturity logs: 67

4.6 Petrography of core samples: 75

a. Thin section 15568' 75

b. Thin section 15554'. 77

c. Thin section 15496' 78

e. Thin section 15444' 80

f. Thin section 15395' 81

g. Thin section 15382' 82

h. Thin section 15372 83

i. Thin section 15365' 84

j. Thin section 15317' 84

k. Thin section 15303' 85

l. Thin section 15294 86

5.1.1 Las Hernandez Outcrop: 88

5.1.2 Zea Outcrop 92

5.1.3 San Pedro del Rio outcrop: 95

5.1.4 La Azulita-Bachaquero outcrop: 99

5.1.5 Chiguará outcrop 102

5.1.6 Flanco Perijanero outcrop 110

5.2. Geochemical parameters of the outcrops of the North Andean Flank and Lago de Maracaibo basin: 115

5.2.1. Source Potential Logs of the North Andean and Lago de Maracaibo Basin 118

5.3 Productivity/ Preservation 153

5.4 Petrography of outcrop samples 154

1. Las Hernández outcrop 154

Thin section 003: 155

Thin section 004 156

2. Zea outcrop 157

3. San Pedro del Rio outcrop 159

4. Azulita- Bachaquero outcrop 160

5. Chiguará outcrop 161

Thin section 001 161

Thin section 002 162

6. Flanco Perijanero outcrop 163

Thin section 001 164

Thin section 002 164

Thin section 003 165

Thin section 004 166

6. Sequence stratigraphic framework 169

6.1 Sequence stratigraphy of the La Luna formation: 169

6.2 Subregional sequence stratigraphic framework 170

6.3 Total Organic Content Calculation of La Luna 1X 182

6.4 Correlation of La Luna 1X well with outcrops in the North Andean Flank and Lago de Maracaibo Basin 192

7. Definition of the most prospective intervals 200

7.1 Brittleness index 200

7.2 Target intervals 201

Conclusions 206

References 208

List of Tables

Table 1 Stratigraphic Chart of the North Andean Flank in Venezuela 13

Table 2 Name of the towns where the samples were taken in the north Andean Flank and the western Lago de Maracaibo Basin, Venezuela 16

Table 3 Number of samples used for geochemical and petrographical analysis..... 19

Table 4 Mineral percentage of the samples performed for XRD and Facies associated in the 1X La Luna core. 36

Table 5 Summary of elemental paleoenvironmental interpretation. Modified from (Treanton et al., 2014). 47

Table 6 Elemental composition in parts per million in the samples performed for XRF and facies associated in the 1X La Luna core 51

Table 7 Results of the Rock Eval Parameters from La Luna 1X core..... 55

Table 8 Geochemical parameters used for the evaluation of a source rock potential in carbonates and conventional shales. From Philp, R. 2014. 56

Table 9 Source rock parameters, facies associated and results using the carbonate classification in the samples of la Luna 1X core 57

Table 10 Source rock parameters, associated facies and results using the shale classification in the samples of la Luna 1X core 59

Table 11 Maturation parameters of a source rock classification; Production index; Tmax and Vitrinite reflectance. From Philp, R. 2014. 67

Table 12 Summary Chart of facies and major features of thin sections of La Luna IX core. 87

Table 13 Source rock parameters, associated facies and results using the carbonate classification for the samples of the North Andean Flank and Lago de Maracaibo basin outcrops. 115
Table 14 Source rock parameters, associated facies and results using the shale classification in the the North Andean Flank and Lago de Maracaibo basin outcrops. 116
Table 15 Chart summary of facies and major features of thin sections of La Luna outcrops. 168
Table 16 Constituent minerals in the rock used for the Brittleness Index equation (modified from Wang & Gale, 2009) 201

List of Figures

Figure 1 Locations and coordinates of the North Andean Flank- Northwestern Venezuela. 5

Figure 2 Structural geology of the northwest of Venezuela 6

Figure 3 Distribution of Jurassic rocks. 7

Figure 4 Distribution of environments during the Cenomanian-Campanian at the northern edge of the Guayana Shield North. 9

Figure 5 Correlation chart of the most important Late Cretaceous units of Venezuela. 10

Figure 6 Correlation chart for the Paleocene-Eocene of Venezuela.. 11

Figure 7 Map of locations of La Luna Formation outcrops in the North Andean Flank of Venezuela 17

Figure 8 Flow chart for integrated Characterization of unconventional gas shales 20

Figure 9 Facies I. Dark gray laminated mudstone 25

Figure 10 A) Light gray laminated shale displaying a high content of organic matter, B) calcite lenses in a rhythmic deposition towards the top with some erosional surfaces, C) Location of dead oil filled fractures. 26

Figure 11 Laminar and fissile yellowish color with coarse particles of volcanic ash. ... 28

Figure 12 A) Intergrowth of calcareous foraminifera B) calcareous lenses C) micro fractures, stylolite and small bioclast fragments (less than 1cm) D) Fractures, filled with calcite are perpendicular to the bedding plane (15489' interval). 29

Figure 13 Massive calcite nodules (yellow circles); small filled fractures in chert layers (yellow squares). 30

Figure 14 Fractures filled with organic matter perpendicular to the bedding plane. 31

Figure 15 Dark brown mudstone with very small calcite intraclasts 32

Figure 16 A) Change in the sedimentation pattern to a more organic-rich sediment B) marked bioturbation that shows the presence of *Glossifungites* that are Ichnofacies characterized by *Domichnia*. 34

Figure 17 La Luna core in the Upper La Luna interval showing boundary of La Luna Formation with the Socuy Member of the Colon Formation. 35

Figure 18 Summary of the XRD and petrography of the Facies IV. 37

Figure 19 Summary of the XRD and petrography of the Facies V 38

Figure 20 Summary of the XRD and petrography of the Facies V 39

Figure 21 Summary of the XRD and petrography of the Facies V 40

Figure 22 Summary of the XRD and petrography of the Facies V 41

Figure 23 Summary of the XRD and petrography of the Facies V 42

Figure 24 Summary of the XRD and petrography of the Facies V 43

Figure 25 Summary of the XRD and Petrography of the Facies VIII. 44

Figure 26 Representation of the dominant mineralogy of La Luna core 1X based on the samples performed with XRD 46

Figure 27 XRF and GR Profile of La Luna 1X (Lower; Middle and Upper La Luna Formation) 50

Figure 28 Representation of the dominant elemental composition of The La Luna core 1X based on the samples performed with XRF. 52

Figure 29 Pyrogram that represents the distribution of Organic Matter in Rock.. 54

Figure 30 Total Organic Carbon (TOC) is generally lower in carbonates because of better expulsion.. 56

Figure 31 Plot that shows the amount of TOC and Carbonates in la Luna 1X core.. 60

Figure 32 Pyrogram plots from La Luna 1X core showing the best intervals of Potential Hydrocarbon in Facies VII 61

Figure 33 Pyrogram plots from La Luna 1x core showing the best intervals of Potential Hydrocarbon context in Facies VII (La Luna upper interval) 62

Figure 34 Pyrogram plots from La Luna 1x core showing the less prone intervals of Potential Hydrocarbon in Facies V(La Luna upper interval) 63

Figure 35 Pyrogram plots from La Luna 1x core showing the less prone intervals of Potential Hydrocarbon context in the alternancy of Facies V and VI (La Luna upper interval)..... 64

Figure 36 Source Potential logs showing the relationship of the S2 peak between the TOC and the oil potential quality with depth. 65

Figure 37 Source Potential logs showing the relationship between the S2 peak between the TOC with depth. 66

Figure 38 Source Potential logs showing the relationship between the S1 peak/ TOC and the percent of carbonates with depth. 68

Figure 39 Source Potential logs showing the production index changes of La Luna 1X core with depth. 69

Figure 40 Source Potential logs showing Vitrinite reflectance changes of La Luna 1X core with depth. 70

Figure 41 Approximate boundaries for kerogen types I, II, and III. 71

Figure 42 Kerogen type and maturity plot that displays the relationship between the Tmax and the Hydrogen index. 72

Figure 43 Pseudo Van Krevelen diagram showing four different types of kerogen at different maturity levels. 73

Figure 44 Kerogen Quality Plot that correlates TOC and S2. 74

Figure 45 Photographs of thin section 15568' in plane polarized light 76

Figure 46 Photographs of thin section 15554' in plane polarized light 77

Figure 47 Photographs of thin section 15464'. 79

Figure 48 Photographs of thin section 15444' in plane polarized light 80

Figure 49 Photographs of thin section 15395'. 81

Figure 50 Photographs of thin section 15382'. 82

Figure 51 Photographs of thin section 15372'. 83

Figure 52 Photographs of thin section 15365' in cross polarized light. 84

Figure 53 Photographs of thin section 15317'. 85

Figure 54 Photographs of thin section 15317'. 86

Figure 55 Photographs of thin section 15294'. 86

Figure 56 Las Hernandez Outcrop showing the Upper La Luna Interval (Tres Esquinas Member) in the North Andean Flank. 88

Figure 57 Picture that shows how calcite filled chert layers and glauconite are representative of this Upper La Luna interval. 89

Figure 58 Big concretions with concoidal fractures in Las Hernandez outcrop. 90

Figure 59 Geological profile using Ozzies logbook representing the geologic units in Las Hernandez outcrop. 91

Figure 60 Alternation of massive grey to black hard shale represented by Upper La Luna- Colon Formation in Zea Outcrop, Mérida state. 92

Figure 61 Alternation of fissile grey to black hard shale represented by Upper La Luna-Colon Formation in Zea Outcrop, Mérida state..... 93

Figure 62 Geological profile using Ozzies logbook representing the geologic units in Zea outcrop..... 94

Figure 63 San Pedro del Rio outcrop. Yellow dashed lines show the alternation of calcareous mudstone, limestone and black chert..... 95

Figure 64 Limestone concretion in yellow and white lines showing the alternation of limestone, chert and mudstone in "Ftanita del Táchira member" in Táchira state..... 97

Figure 65 Geological profile using Ozzies logbook representing the geologic units in the San Pedro del Rio outcrop..... 98

Figure 66 La Azulita- Bachaquero outcrop, located in La Azulita town, Mérida state.. 99

Figure 67 Image that displays highly weathered and fissile mudstone..... 100

Figure 68 Image that shows mudstone weathering color with small organic matter fragments within..... 100

Figure 69 Geological profile using Ozzies logbook representing the geologic units in La Azulita- Bachaquero outcrop..... 101

Figure 70 Lower La Luna outcrop located in Chiguará town, Mérida state..... 102

Figure 71 Image that shows how weathered and fissile the rock is in this locality. . 103

Figure 72 Calcite concretion (dashed black line) present in the Lower La Luna outcrop. 103

Figure 73 Image that shows the use of the Gamma ray scintilometer in the Lower La Luna outcrop..... 104

Figure 74 Yellow dashed lines display the transition between the Chejende Member (Lower la Luna) and Timbetes member (Upper La Luna) in Chiguará town, Mérida state. 105

Figure 75 NE- SW image showing where the yellow dash lines mark the transition between the Chejende and Timbetes Members. 106

Figure 76 Big chert concretion (yellow dashed lines) and volcanic ash layer (black dashed lines) in the Upper La Luna Formation, Chiguará town- Merida state. 107

Figure 77 Picture that best represents the volcanic ash layer (black dash lines) in the Upper La Luna Formation, Chiguará town- Merida state. 108

Figure 78 Geological profile using Ozzies logbook representing the geologic units in Chiguará outcrop. 109

Figure 79 First section of La Luna stratotype. 110

Figure 80 Second section of La Luna stratotype. 111

Figure 81 Picture that best represents the unconformity of the Albian rocks (Maraca formation) under Cenomanian rocks (Lower La Luna Formation) in the Perijanero Flank, Zulia state. 112

Figure 82 Picture that best represents the Middle La Luna Formation in the Perijanero Flank, Zulia state. 112

Figure 83 Upper La Luna (Tres Esquinas member) in the Perijanero Flank, Zulia state. 113

Figure 84 Geological profile using Ozzies logbook representing the geologic units in Flanco Perijanero outcrop..... 114

Figure 85 Pyrogram plots from Las Hernandez outcrop showing the Potential Hydrocarbon context in Facies V and VII (La Luna Upper interval). 118

Figure 86 Source Potential logs in Las Hernandez outcrop.. 119

Figure 87 Maturity logs in Las Hernandez outcrop..... 120

Figure 88 A. Pseudo Van Krevelen diagram showing four different types of kerogen at different maturity levels. B) Kerogen type and maturity plot that displays the relationship between the Tmax and the Hydrogen index. 122

Figure 89 Kerogen Quality Plot that correlates TOC and S2. 123

Figure 90 Pyrogram plots from Zea outcrop showing the Potential Hydrocarbon context in Facies V, VI and VII (La Luna Upper interval). 124

Figure 91 Source Potential logs in Zea outcrop. 125

Figure 92 Maturity logs in Zea outcrop..... 126

Figure 93 A. Pseudo Van Krevelen diagram showing four different types of kerogen at different maturity levels. B) Kerogen type and maturity plot that displays the relationship between the Tmax and the Hydrogen index. 127

Figure 94 Kerogen Quality Plot that correlates TOC and S2. 128

Figure 95 Pyrogram plots from Azulita-Bachaquero outcrop showing the Potential Hydrocarbon context in Facies I V and V (La Luna Upper interval). 130

Figure 96 Source Potential logs in La Azulita – Bachaquero outcrop. 131

Figure 97 Maturity logs in Las Hernandez outcrop..... 132

Figure 98 A. Pseudo Van Krevelen diagram showing four different types of kerogen at different maturity levels in Azulita- Bachaquero outcrop. 133

Figure 99 Kerogen Quality Plot that correlates TOC and S2. Red diamonds represent Azulita – Bachaquero samples samples. 134

Figure 100 Pyrogram plots from San Pedro del Rio outcrop showing the Potential Hydrocarbon content in Facies I V and V (La Luna Upper interval)..... 136

Figure 101 Source Potential logs in San Pedro del Rio outcrop. 137

Figure 102 Maturity logs in Zea outcrop..... 138

Figure 103 Pseudo Van Krevelen diagram showing four different types of kerogen at different maturity levels. 139

Figure 104 Kerogen Quality Plot that correlates TOC and S2. 140

Figure 105 Pyrogram plots from Chiguará outcrop showing the Potential Hydrocarbon content in Facies V and VII (La Luna Middle and Upper interval). 142

Figure 106 Source Potential logs in Chiguará outcrop..... 143

Figure 107 Maturity logs in Chiguará outcrop. 144

Figure 108 A) Pseudo Van Krevelen diagram showing four different types of kerogen at different maturity levels. B. Kerogen type and maturity plot that displays the relationship between the Tmax and the Hydrogen index. 145

Figure 109 Kerogen Quality Plot that correlates TOC and S2. 146

Figure 110 Pyrogram plots from Flanco Perijanero outcrop showing the Potential Hydrocarbon context in Lower, Middle and Upper La Luna interval..... 148

Figure 111 Source Potential logs in Flanco Perijanero outcrop. 149

Figure 112 Maturity logs in Flanco Perijanero outcrop. 150

Figure 113 A) Pseudo Van Krevelen diagram showing four different types of kerogen at different maturity levels. B. Kerogen type and maturity plot that displays the

relationship between the Tmax and the Hydrogen index. Red diamonds represent Flanco Perijanero samples. 151
Figure 114 Kerogen Quality Plot that correlates TOC and S2. 152
Figure 115 Photographs of thin section 001-Las Hernandez in plane polarized light. 154
Figure 116 Photographs of thin section 002-Las Hernandez in cross polarized light.. 155
Figure 117 Photographs of thin section 003-Las Hernandez in cross polarized light.. 156
Figure 118 Photographs of thin section 004-Las Hernandez in cross polarized light.. 157
Figure 119 Photographs of thin section 001-Zea in cross polarized light. (a and B) Big picture of the thin section represented by micrite cement around the recrystallized foraminifera C) Recrystallized micrite, intraparticle porosity and pyrite fragments D) Micrite cement around the recrystallized foraminifera and pyrite replacement in echinoderm spicule. 158
Figure 120 Photographs of thin section 002-Zea in cross polarized light. 159
Figure 121 Photographs of thin section 001-Chiguara in cross polarized light. 160
Figure 122 Photographs of thin section Azulita- Bachaquero in cross polarized light. 161
Figure 123 Photographs of thin section 001-Chiguara in cross polarized light. 162
Figure 124 Photographs of thin section 002-Chiguara in cross polarized light.. 163
Figure 125 Photographs of thin section 001-Perija in cross polarized light 164
Figure 126 Photographs of thin section 002-Perija. 165
Figure 127 Photographs of thin section 003-Perija. 166
Figure 128 Photographs of thin section 004-Perija. 167
Figure 129 Generalized sequence – stratigraphic model of unconventional resource shales. 171

Figure 130 Subaerial exposure accounted for unconformity (Maraca Fm) and early accumulation of TOC (La Luna Fm).. 172

Figure 131 Left figure shows the second (red arrows) and third order (blue arrows) sequence stratigraphy of Eagle Ford; the right well show the second (red arrows) and third order (green and red arrows) sequence stratigraphy of La Luna Formation..... 173

Figure 132 Generalized sequence stratigraphic model and the corresponding gamma ray log responses, with examples from La Luna Fm. 177

Figure 133 A) Generalized lithology, planktonic foraminiferal biozones, and stage boundaries for the La Luna Formation and surrounding units in La Luna IX. Biostratigraphy is determined after Sliter (1989). B) Age dates for stage boundaries taken from Gradstein et al. (1994), and middle-late Turonian boundary date from Kauffman et al. (1993). 178

Figure 134 First track shows the third order sequences (TST and HST) in La Luna 1X well using lower volcanic ash as a stratigraphic datum. 179

Figure 135 Stratigraphic cross section of third order sequences (TST and HST) in La Luna 1X well using lower volcanic ash (purple line) as a stratigraphic datum. 180

Figure 136 Structural cross section of third order sequences (TST and HST) in La Luna 1X well using volcanic ash are shown as purple lines.. 181

Figure 137 Sonic/ resistivity logs showing the Δlog R separation. After Passey et al. (1990). 183

Figure 138 Relationship between LOM (level of organic metamorphism) and R_o. 185

Figure 139 Relation between LOM and R_o for Woodford Shale basins in Oklahoma. 185

Figure 140 Track 1 corresponds to the GR profile related with the organic rich interval that shows in the Track 2. ΔlogR separations use the Sonic (VE_DT) and Resistivity (RT) overlay. Track 3 corresponds to the ΔlogR profile already generated by the two previous curves. Track 4 corresponds to the TOC data from core and TOC data predicted with the ΔlogR method and TOC Lithology predicted using (RT and VE_DT). Baseline was taken in Aguardiente Fm. 186

Figure 141 Track 1 corresponds to the GR profile related with the organic rich interval that shows in the track 2 ΔlogR separations using the Sonic (VE_DT) and Resistivity (RT) overlay. Track 3 corresponds to the ΔlogR profile already generated by the two previous curves. Track 4 corresponds to the TOC data from core and TOC data predicted with the ΔlogR method and TOC lithology predicted using (RT and VE_DT).Yellow circles show the low TOC content due to the presence of chert content. 187

Figure 142 Track 1 corresponds to the GR profile related with the organic rich interval that shows in Track 2 ΔlogR separations using the Sonic (VE_DT) and Resistivity (RT) overlay. Track 3 corresponds to the ΔlogR profile already generated by the two previous curves. Track 4 corresponds to the TOC data predicted with the ΔlogR method. 189

Figure 143 Track 1 corresponds to the GR profile related with the organic rich interval that shows in Track 2 ΔlogR separations using the Sonic (VE_DT) and Resistivity (RT) overlay. Track 3 corresponds to the ΔlogR profile already generated by the two previous curves. Track 4 corresponds to the TOC data predicted with the ΔlogR method. 190

Figure 144 Track 1 corresponds to the GR profile related with the organic rich interval that shows in the Track 2 ΔlogR separations using the Sonic (VE_DT) and Resistivity

(RT) overlay. Track 3 corresponds to the ΔlogR profile already generated by the two previous curves. Tract 4 corresponds to the TOC data predicted with the ΔlogR method. (Passey et al., 1990). 191

Figure 145 Estimated correlation between La Luna IX well and Las Hernandez outcrop.. 194

Figure 146 Estimated correlation between La Luna IX well and Zea outcrop. 195

Figure 147 Estimated correlation between La Luna IX well and Chiguara outcrop... 196

Figure 148 Estimated Correlation between La Luna IX well and Perijá outcrop.. 197

Figure 149 Identified foraminifera and benthic-planktonic faunal distribution chart showing the standard zonation 198

Figure 150 Identified foraminifera and benthic-planktonic faunal distribution chart showing the standard zonation 199

Figure 151 Relationship of the brittle and ductile couplets based on their stratigraphic correlation with the gamma ray, TOC % wt, BI and RHP. Blue squares show the best target intervals. 203

Figure 152 Definition of the three most prospective target intervals in La Luna1X well 204

Figure 153 Stratigraphic cross section of third order sequences (TST and HST) in La Luna 1X well using lower volcanic ash (purple line) as a stratigraphic datum. 205

Abstract

In recent years, unconventional shale reservoirs have become very important around the world for their high source of energy and for their high economic value. La Luna Formation is of crucial importance in the petroleum geology of northern South America, especially in Venezuela and Colombia. La Luna Formation has been considered for a long time the main focus of study for conventional oil production, since it is the most important source rock in the Maracaibo Basin and in Venezuela. However, recent works on this Upper Cretaceous shale as a prospective exploration target are very few; La Luna is now being considered an unconventional shale prospect (PDVSA-2012).

This study encompasses stratigraphic and geochemical characterization of La Luna Formation from five outcrops and a 345 foot long core along the North Andean flank and the northwest of Lago de Maracaibo Basin, Venezuela. TOC content from the core varies from 3.85 to 9.13 wt % (average 5.10 wt. %). Rock-Eval pyrolysis results indicate Type I and Type II kerogen, a "Good-to-Excellent" oil potential generation and a maturity indicator suggesting a greater likelihood of oil than gas in La Luna 1X core; similar values are represented in La Luna stratotype (Lago de Maracaibo Basin) where TOC content varies from 0.14 to 12.80 wt. % (average 3.60 wt. %). In the North Andean Flank, TOC content is lower,varying from 0.46 to 5.64 wt% (average 2.37 wt. %); kerogen is Type III, indicating a potential generation of dry gas instead of oil in the subsurface near the outcrops.

The Delta Log R method (Passey, 1990) of TOC estimation showed a good agreement with geochemical Rock-Eval results in the core.

Eight lithofacies were defined in the La Luna core. From bottom to top they are: A) Dark gray, laminated mudstone. B) Fossiliferous wackstone. C) Volcanic ash; laminated mudstone with limestone concretions and packstone. D) Calcareous – siliceous laminated mudstone interbedded with black chert filled with calcite veins. E) Calcareous-siliceous mudstone interbedded with wackestone. F) Calcareous slightly siliceous laminated black mudstone interbedded with calcareous fossiliferous wackestone. G) Siliceous slightly calcareous green mudstone with authigenic glauconite and pyrite. Planktonic foraminifera are present in the upper part of the interval.

Based upon petrography, geochemical analysis and facies characterization, the facies comprise a third order sequence. Highstand and Transgressive Systems Tracts. A Maximum Flooding Surface was correlated with the worldwide Cretaceous oceanic anoxic event 2 and also with the volcanic ash found in La Luna Colombia,

Three target intervals were identified in La Luna 1X well. The first interval from bottom to top has a thickness of 14.32 m. and a BI of 0.85. The second interval has a thickness of 7.60m and has a BI of 0.99. The third interval has a thickness of 18 m and has an average BI of 0.93. These results serve as a baseline for current and future study of the La Luna Formation in Venezuela.

1. Introduction

Every day the world demands more energy, requires more power for industries, transport, and homes. Natural gas currently occupies third place as the most important source of energy in the world (after oil and coal). Additionally, natural gas generates about 45% less carbon dioxide (CO_2) than production from coal and 20% less than from fossil fuels. Also during combustion, non-toxic gases, ash and debris are generated.

Unconventional deposits are those that do not naturally produce economic flow rates and that can't be produced profitably without the application of techniques such as hydraulic fracturing or enhanced recovery. They usually occur in regional accumulations and are independent of stratigraphic and structural traps; they are characterized by having low permeability and porosity, therefore in their development they require advanced technology.

According to Gomez (2010), unconventional reservoirs can be classified into four types:

- Gas Shale, whose sediments are clays or silts.
- Tight Gas Sand, whose permeability is so low that the gas would not flow normally.
- Coalbed Methane (CBM) which is the gas coming from the micropores of coal seams.
- Methane Hydrates; although representing another source that is not yet being exploited, should be considered because of its importance for the future.

Gas Shale is considered as one of those unconventional reservoirs of dry gas in shales characterized by a high content of organic matter and a certain degree of thermal

maturity with high retention of gas (both free and absorbed gas) in pores, fractures, and in areas without traps or seals.

Resource shale exploration is currently a worldwide boom. Many countries are increasing their gas reserves by the discovery of this new energy resource. United States is the founder of this new line of technology and it has increased gas production significantly. Many other countries around the world are investing capital in this unconventional resource. The economic success of gas shale in the United States since 2000 (Hughes, J. 2013) has led to rapid development of gas shale in Canada (Newswire, 2012) and, more recently, has spurred interest in Europe (Schulz et al., 2010), Asia (Xu et al., 2011) and Australia (Peter, C. 2013)

The School of Geology and Geophysics of the University of Oklahoma has been working with unconventional deposits globally, including La Luna Formation. Torres, (2013) conducted outcrop studies in the southern and middle parts of the Middle Magdalena Basin (MMB) to assess the gas/oil – shale potential of La Luna formation in Colombia. The Salada and Galembo members have reached the dry gas window for hydrocarbon generation in this area of the MMB. Gomez (2014) conducted an integrated geological characterization and distribution of the Salada Member in the central area of the MMB; which suggested that the facies studied are good to very good source rocks. TOC content varies from 0.5 to 8.15 wt% with an average of 3.62 wt%.

The La Luna Formation is a widespread rock unit that has different names locally (Villamil, T. 2002), which creates confusion in regional understanding in northern South America. La Luna extends from the central part of Ecuador where it is known as the Chonta Formation, is widely distributed in Colombia where it is also

known as Villeta, Chipaque, Gachetá, La Luna, San Rafael and many more. It extends to the west of Venezuela, where it is known as La Luna and Navay in Guanare and the Barinas -Apure basin. It is widely distributed in eastern Venezuela and is known as Querecual. La Luna, known as Naparima Hill, is present in Trinidad, Guyana, Suriname and northern Brazil, but it does not produce much oil because it was not buried deeply enough.

La Luna Formation is widely known for being the most important source rock in Venezuela and has been considered for a long time the focus of study for conventional oil production in the Maracaibo Basin. It plays a crucial role in petroleum geology of northern South America, representing one of the largest generators of hydrocarbons on earth. However, based on this new oil boom of unconventional energy, it seems that La Luna is probably one of the best deposits suitable for gas shale reservoirs.

Venezuela has been dabbling in this new energy phenomenon. Petróleos de Venezuela Sociedad Anónima (PDVSA, 2012) has begun to develop several projects in conjunction with Universidad de los Andes (ULA) focusing on unconventional gas shale in outcrops. *R*esults of these preliminary studies have shown that the shales of La Luna Formation in outcrop have good properties and good conditions for this unconventional exploration study. However, La Luna Formation is a really heterogenic and complex deposit that requires further study in a number of outcrop areas.

2. Geological Setting

2.1 Geology of study area

The study area is located in western Venezuela, (Figure 1). The Zulia State is located to the south of the Gulf of Venezuela and the Caribbean Sea; it is northwest of Mérida, Táchira and Trujillo states; to the west of Falcón and Lara states and to the east of the Republic of Colombia on an oblique convergent margin of the three plates: the oceanic crust (Nazca and Caribbean plates) and the continental crust (South America Plate) (Gonzales de Juana et al., 1980)

This gives a triangular-shaped basin (Figure 2) bordering three larger faults: Oca's Fault located towards the north; Santa Marta-Bucaramanga's fault towards the west; and Bocono Fault towards the east and southeast of Zulia state (Audemard et al., 2004) Inside the basin, the major faults are: Icotea; Urdaneta; La Paz –Mara; Pueblo Viejo and Begote - Burro Negro (Gonzalez de Juana et al., 1980); these faults resulted from the rotation of the blocks in a similar way to a bookcase, through a mechanism called "bookshelf" produced by the relative movement of the limiting faults of the triangular block (Audemard et al., 2004).

The Maracaibo Basin is located in the Zulia state, where the log of the well from the northwest Maracaibo basin was made available for study. This log was correlated with the outcrop natural gamma ray logs obtained in the North Andean Flank.

The North Andean Flank and center of the Venezuelan Andes are in the Táchira Depression (Lobaterita-San Pedro Rivers) to the northwestern edge extending from the border with Colombia and the vicinity of the Chama River, where the most

representative La Luna cross-section for this study is located in Chiguara area in Mérida state.

The most important Cretaceous and Tertiary sequences in the central Andean region are represented by sections located in Jají- Mérida; Los Guaimaros-Mérida; Los Guaimaros-El Vigia; La Azulita- Mérida; Zea- Mérida; La Tendida- Táchira and San Pedro del Rio- Táchira.

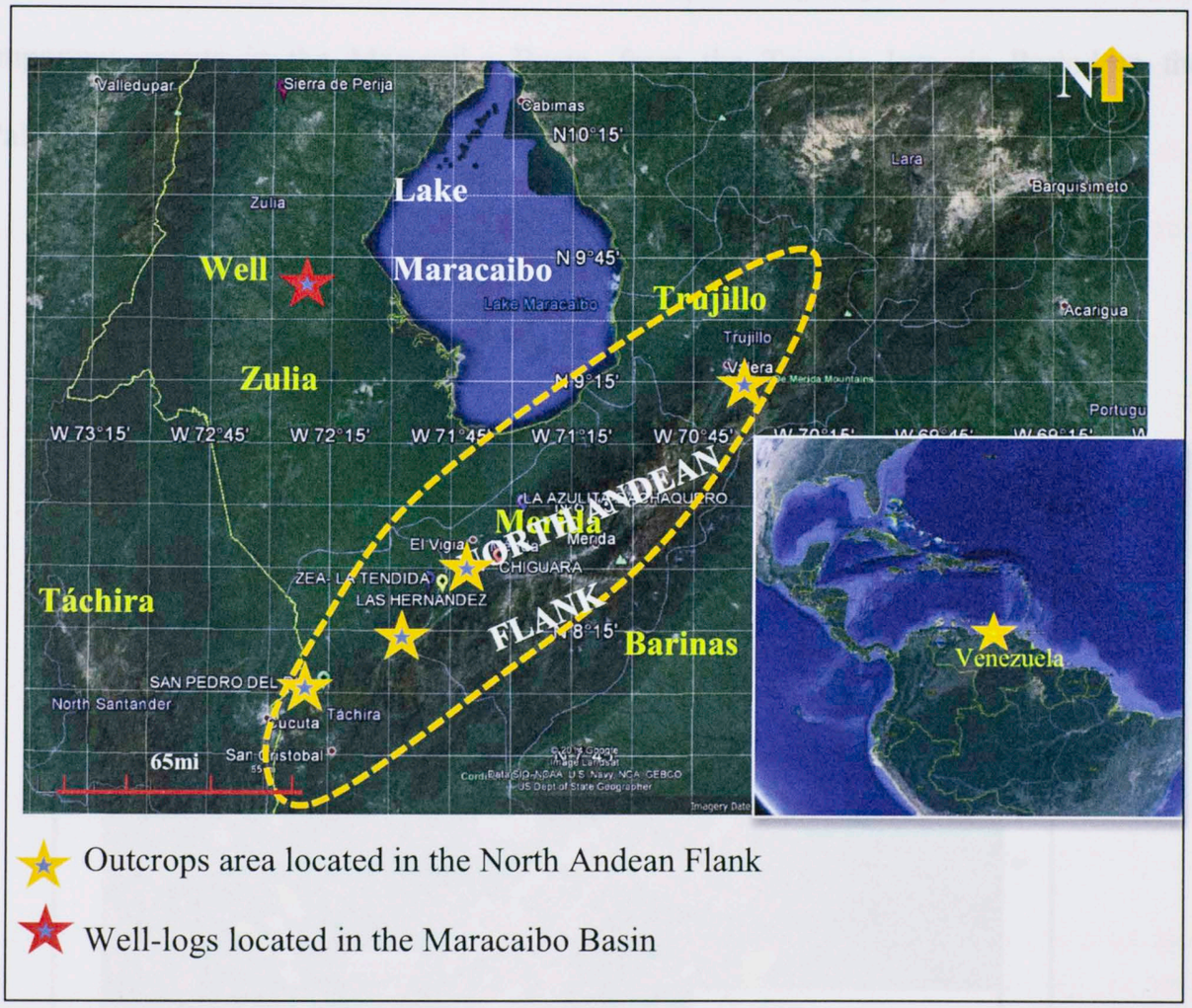

Figure 1 Locations and coordinates of the North Andean Flank- Northwestern Venezuela (Taken from Google Earth, 2014).

2.2 Regional Geology

The Maracaibo Basin is the most important petroliferous basin in Venezuela and is one of the most prolific hydrocarbon basins in the world. Maracaibo Basin covers an area of 50,000 km^2; the main source rock is the La Luna Formation of Late Cretaceous age; its facies extend along all of western Venezuela and Colombia. The Andean orogeny occurred in several phases, resulting in the generation, migration, and accumulation of oil. For the purpose of this study I am going to synthesize the most important events in the Maracaibo Basin, from the Triassic-Jurassic Period to the Paleogene.

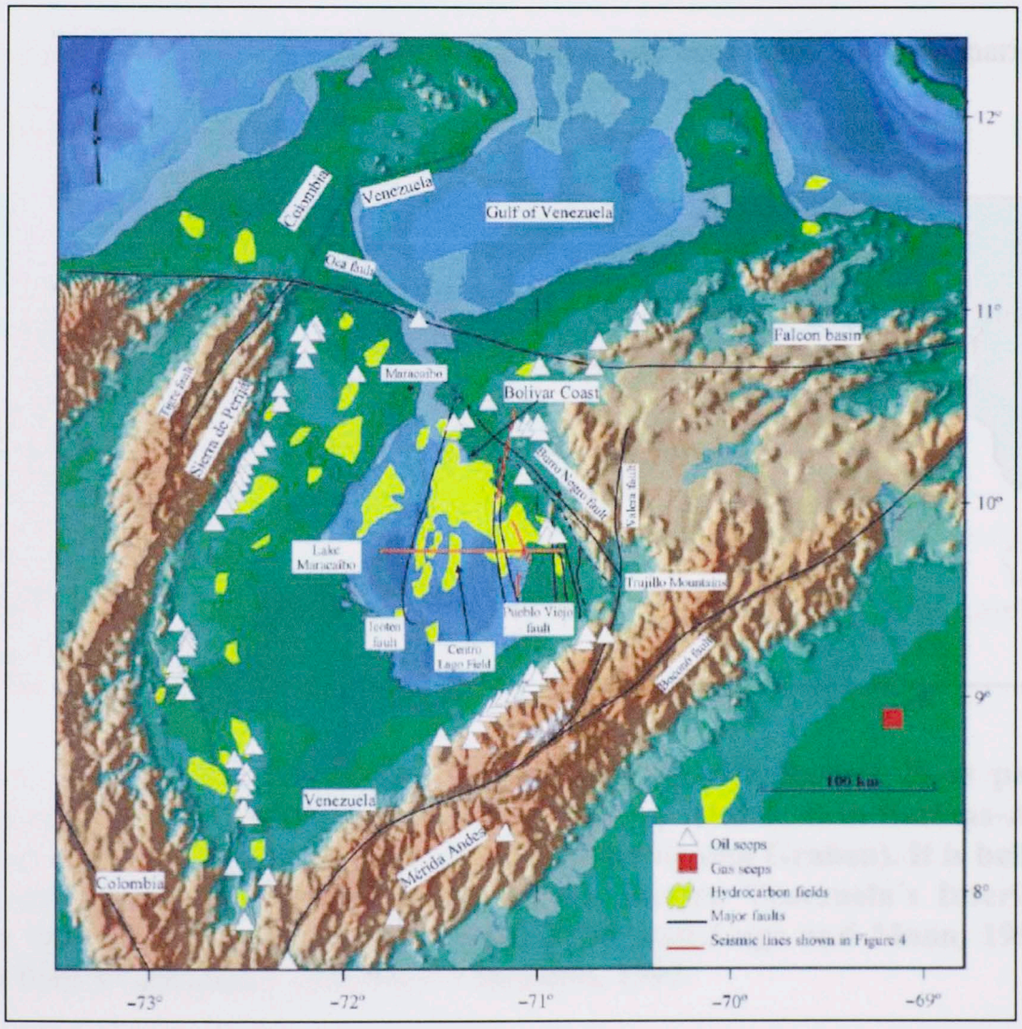

Figure 2 Structural geology of the northwest of Venezuela: Main faults on the triangular Block of the Maracaibo Basin (Modified by Mann and Escalona, 2006).

No Triassic rocks have been found in Venezuela so far. The Lower Jurassic is represented by Volcánicas de la Ge (Sierra de Perijá) and Volcánicas de Guacamayas (Macizo El Baúl), which predated red bed sedimentation of La Quinta Formation and the expansion process related to the Gulf of Mexico or Proto-Caribe opening.

The rifting of Pangea produced several structural features that later influenced the evolution of the Venezuelan sedimentary basins (Acuna, et al., 1997). The Proto-Caribe opening induced the development of northeast-oriented extension valleys or grabens (Figure 2). Among these valleys are the Apure-Mantecal, Espino, Andes-Perijá and Maracaibo grabens. All these grabens were filled during the Jurassic Period by red bed (continental) sediments, diverse volcanics, and occasional shallow-marine clastics and limestone (Acuna *et al.,* 1997).

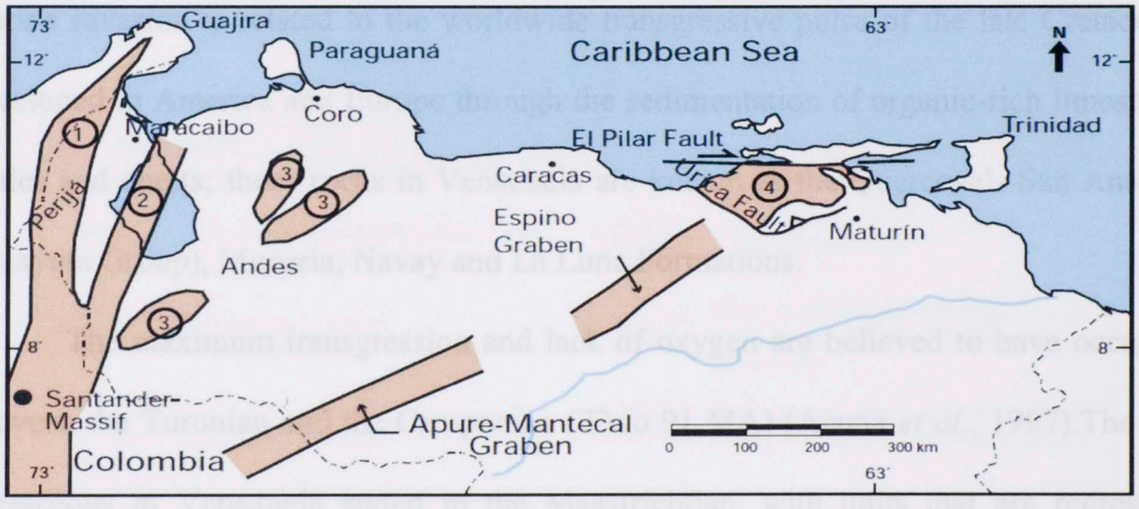

Figure 3 Distribution of Jurassic rocks: 1) in Perijá Range; 2) as part of the economic basement of Maracaibo Basin; 3) in the Andes; 4) in Barinas-Apure and eastern Venezuela Basins (Apure-Mantecal and Espino Graben). It is believed that they are involved in deep thrusting within eastern Venezuela's Interior Range (after Bartok, 1993; Passalacqua et al., 1995; and Lugo and Mann, 1995). Cited from Well Evaluation Conference Venezuela, 1997.

In western Venezuela, the Early Cretaceous was controlled initially by the Jurassic graben faults systems. This is evidenced by the variable thicknesses of Rio

Negro Formation clastics, which range from more than 2 km near the south of Machiques Trough, to only a few meters thick in some parts of the North-Andean Flank. Later, subsidence stabilized and there was an extensive transgression of an open sea over the western Venezuelan shelf causing carbonate sedimentation of the Cogollo Group. The lateral clastic equivalent of these carbonates in the Cratón or Guayana Province Margins is the equivalent to the Aguardiente Formation, (Acuna *et al.,* 1997).

The paleo-environmental distribution and stratigraphic units during the Late Cretaceous are shown in Figure 3 and 4 which encompasses the correlation for these units in Venezuela. A marine invasion began at the end of the Lower Cretaceous, moving from east to west and invading the south of Venezuela, which had been emerged and undergoing erosion since late Jurassic and possibly Paleozoic times. This marine invasion is related to the worldwide transgressive pulse of the late Cretaceous developed in America and Europe through the sedimentation of organic-rich limestone, shales and cherts; these rocks in Venezuela are known as the Querecual- San Antonio (Guayuta Group), Mucaria, Navay and La Luna Formations.

The maximum transgression and lack of oxygen are believed to have occurred between the Turonian and the Campanian (72 to 91 MA) (Acuna *et al.*, 1997).The late Cretaceous in Venezuela ended in the Maastrichtian, with units that are regressive related to the deeper environments of the source rock. In Perijá and the Maracaibo Basin, La Luna Formation grades vertically to glauconitic limestone (Socuy Member). Shales with thin sandstones are defined as the Colon and Mito Juan Formations.

In the North Andean Flank, the glauconitic phosphatic Tres Esquinas Member is present, which is the possible equivalent of the Socuy Member, underlying the dark shales of the Colón Formation. In the South-Andean Flank, the upper contact with the source rock is gradationally erosive with the basal sandstones of the Burgüita Formation (Acuna *et al.*, 1997).

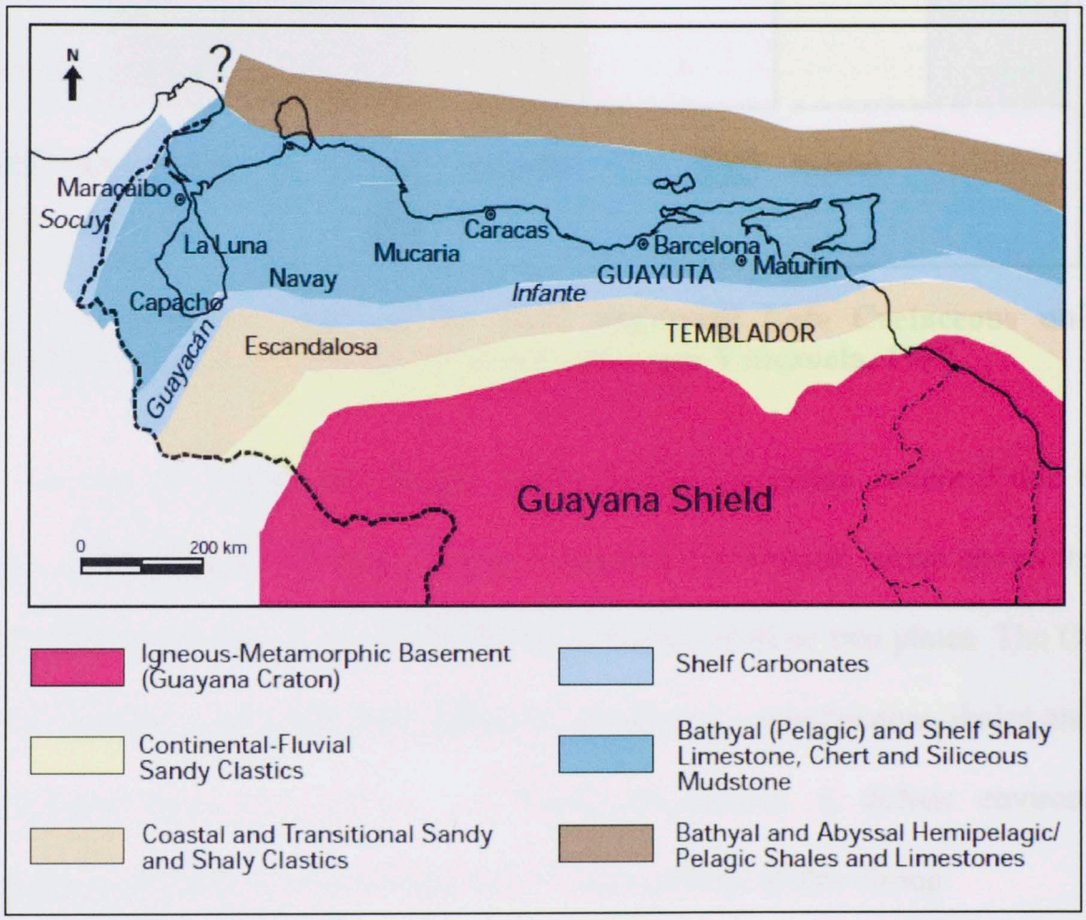

Figure 4 Distribution of environments during the Cenomanian-Campanian at the northern edge of the Guayana Shield North. Typical units of these sets of facies are indicated. Taken from Well Evaluation Conference Venezuela, 1997.

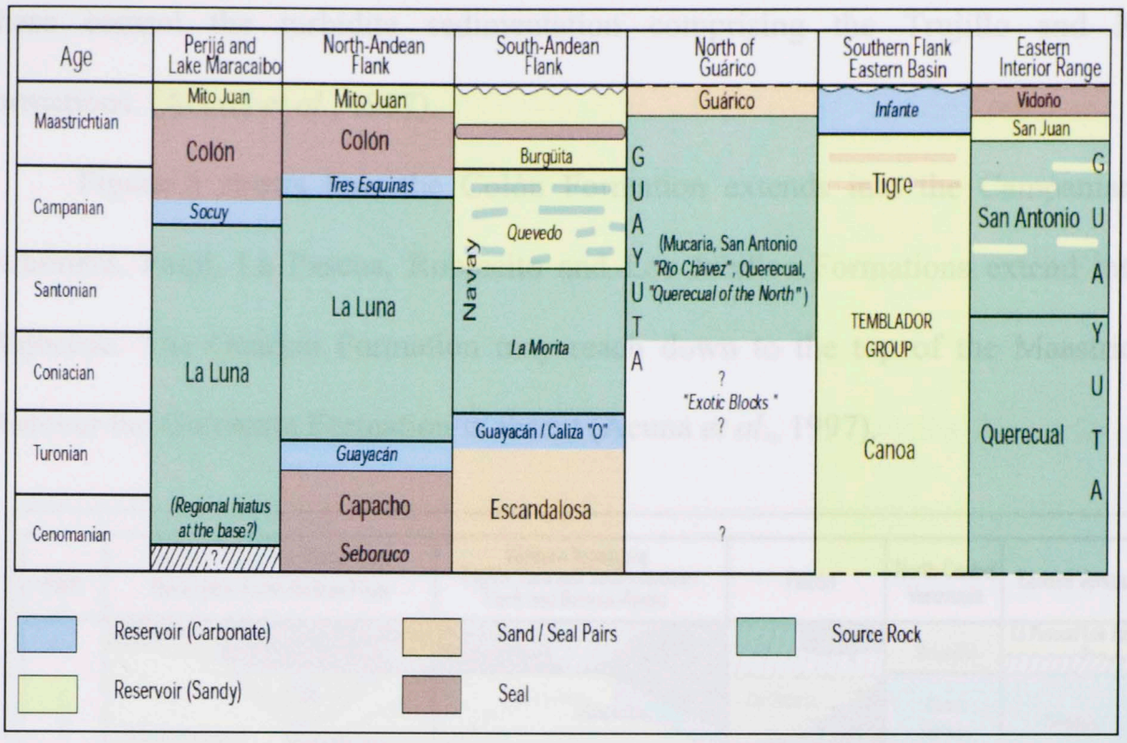

Figure 5 Correlation chart of the most important Late Cretaceous units of Venezuela. Taken from Well Evaluation Conference Venezuela, 1997.

During the Paleocene- Eocene Epoch marine regression occurred due to the collision of the Nazca Plate with western Colombia. The Orocué Group shows that the sedimentation load was controlled by the deformation of these two plates. The Orocué Group is composed of sandstones, siltstones, mudstones, carbonaceous shales and coal seams which form Los Cuervos and Barco Formations. A deltaic environment, interdigitated with fluvial-deltaic deposits, is characteristic of this Group.

Meandriform rivers and fluvial deposits are characteristic of the Eocene Epoch. White fine-grained sandstones with medium thin layers of granules or pebbles of quartz and abundant carbonaceous material form the Mirador Formation.

To the northeast of the South American plate, the oblique collision of the Lesser Antilles Arc generated a series of sheets trending towards the south and southeast.

These control the turbidite sedimentation comprising the Trujillo and Morán Formations. (Acuna *et al.*, 1997).

Figure 5 shows how the Colón Formation extends into the Campanian; the Carbonera, Paují, La Pascua, Roblecito and Los Jabillos Formations extend into the Oligocene. The Guárico Formation may reach down to the top of the Maastrichtian wherever the Garrapata Formation is absent (Acuna *et al.*, 1997).

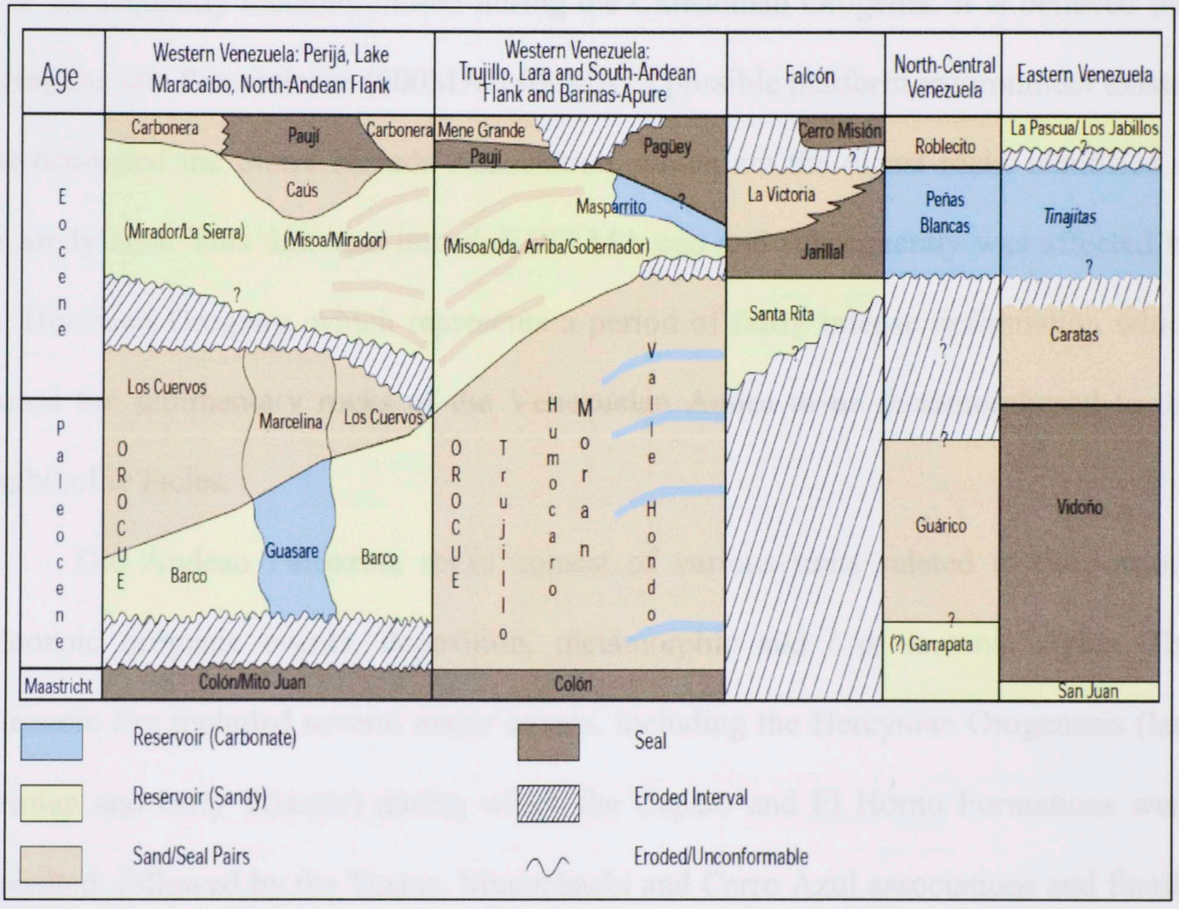

Figure 6 Correlation chart for the Paleocene-Eocene of Venezuela. Taken from Well Evaluation Conference Venezuela, 1997.

2.3 Local Geology

The Andean basement is composed of Precambrian and Paleozoic rocks. The oldest rocks of the Venezuelan Andes are represented by the Precambrian Iglesias

Complex (Gonzales de Juana et al., 1980), also known as Sierra Nevada Association (Bellizia & Pimentel, 1994) which consists of igneous, metamorphic and / or metasedimentary rocks.

According to Burkley (1975) the Venezuelan Andes must have existed during the Precambrian Period (1400-600MA) providing a sedimentary environment that allowed the deposition of the protolithic rocks of the Sierra Nevada Association that were subsequently metamorphosed during the Caledonian Orogenia. It is believed that during the late Precambrian (600MA-1400MA) a possible platform environment existed that deposited the Sierra Nevada Association, which are the oldest rocks identified in the study area. This unit was intruded 600 MA ago and subsequently was affected by the Huronian Orogeny, which represents a period of fairly intense deformation which caused the sedimentary rocks of the Venezuelan Andes to be metamorphosed to the amphibolite facies.

The Andean Paleozoic rocks consist of various units related to the various Paleozoic orogenic events, deposition, metamorphic and / or tectonic styles. The Paleozoic Era included several major events, including the Hercynian Orogenesis (late Permian and early Triassic) during which the Caparo and El Horno Formations were deposited, followed by the Tostos, Mucuchachi and Cerro Azul associations and finally the Sabaneta, Carache and Palmarito Formations.

Table 1 Stratigraphic Chart of the North Andean Flank in Venezuela

Era	Period	Epoch	Geological Events	Sedimentological Deposits	Lithology	North Andean Flank units	
CENOZOIC	TERTIARY	Eocene	-Cretaceous sea withdrew (Marine regression) -Shelf seas	-Fluvial braided rivers and meandering rivers	-Fine to medium white sands with thin layers of granules and pebbles of quartz with an abundant carbonaceous material	Mirador Fm	
		Paleoce		-Deltaic Province: deltaic settings interdigitated with fluvio-deltaic and beach deposits	-Sandstones, siltstones, mudstones,carbonaceous shales and coal seams.	Orocue Fm	Los Cuervos Fm Barco Fm
MESOZOIC	CRETACEOUS	UPPER Maastr	-Regressive conditions. -Start of the Alpine Orogeny. - Maximum marine Transgresion	-Neritic settings, near to the shore with sea periods.	-Marine shale with some sandy intervals, representing the basin fill	Colon Fm	Mitojuan Member Tres esquinas Member
		UPPER Campania					
		UPPER Santonian		-Open marine platform to restricted platform	-Black Chert interbedded with siliceous limestone and black shale layers with fish remains. -Pelagic sediments: dark gray to black fetid limestone and calcareous shales, with abundant finely laminated and dispersed organic matter.	Táchira Chert Member **La Luna Fm**	
		UPPER Coniacian	-Maximum flooding Surface -Deep seas				
		UPPER Turonian		Sedimentological settings that shows the progress of the transgression and deepening.	-Hard dark gray to black shales, hard clear and often fossiliferous limestone		Guayacan Member Seboruco Member La Grita Member
		UPPER Cenomanian					
		LOWER Albian	-Cretaceous transgression over the continental margin of Venezuela. -The geometry of the ocean scatterings centers is changed. - The tectonic styles in the plate boundaries are changed -Pangea separation starts to developed	-Shelf Environment -Fluvio-deltaic environments -Shallow marine environments	-Fossiliferous limestone -Gray and hard quartz sandstones, shales and limestone -Dolomitic shales	-Maraca Fm -Aguardiente Fm -Apón Fm	
		LOWER Aptia		Predominantly fluvial environment, furrow filling.	-Basal clastics: Arkoses and arkosic sandstones.	Rio Negro Fm	
		LOWER Barre					
		LOWER Hauterivi					

These events were influenced by granitic intrusions and regional tectonic metamorphism. Table 1 shows a summary of the main depositional events in the study area from the Mesozoic to the Cenozoic eras in the North Andean Flank of Venezuela:

Mesozoic sedimentation in the Central Venezuelan Andes was affected by different tectonic events, the oldest of which was the intervention of the Permo-Triassic Orogeny of compressional character with intrusive and extrusive igneous activity. The latter was formed by a domain of extensional tectonics (± 200 MA) during the Triassic-Jurassic, whose product was the accumulation of thick layers of red beds and lacustrine strata interbedded with volcanic rocks. During the Cretaceous Period, Pangea continued its expansion, and in the Early Cretaceous Period (± 135 MA) the plate boundaries changed the tectonic styles and produced a marine transgression over the continental margin of Venezuela.

The Andean region was invaded by the waters of an epicontinental sea of the Eastern Cordillera of Colombia, which resulted in shallow marine sedimentation in the Barremian which ended with deep marine sedimentation in the Santonian. In the Upper Cretaceous Period the sedimentary regime became regressive with epiclastic sedimentation dominating.

During the Cenozoic era different orogenic events occurred that affected the sedimentation in this area. The first was a tectonic pulse at the end of the Eocene Epoch, which produced a break in sedimentation and subsequent erosion, resulting in a well-known discordance between the Misoa and La Rosa Formations which are of great importance in the Maracaibo basin. In the middle of the Miocene Epoch, seas again invaded the Lake Maracaibo area, depositing shallow marine and continental sediments

which practically filled the whole basin. The Miocene Epoch began with uplift of the Venezuelan Andean chain, generating two deep trenches towards the southwest and the southeast, where thick intervals of coarse and considerable large conglomerates were deposited. Finally the late Cenozoic Era is characterized by sedimentation of fluvial-deltaic, fluvial, lacustrine, and glacial continental deposits.

3. Methodology

In order to achieve the objective of this thesis, three main geological techniques were used:

3.1 Gathering and analyzing previous information:

This first stage included reading all previous works related to unconventional shales in Venezuela and geological settings of the Maracaibo Basin and North Andean Flank as well as the geological maps of the area.

3.2 Fieldwork:

This stage was accomplished by three weeks in the North Andean Flank and the western area of the Maracaibo Basin in northwest Venezuela in July of 2014. It includes the collection of samples taken in different outcrops where the La Luna Fm. is present, including Mérida, Táchira and Zulia (Figure 7). It also includes the definition of facies present in the La Luna Formation and the measurements of the GR Scintilometer in order to develop an outcrop gamma ray log for the outcrops. The locations, including the most representative outcrops are listed in Table 2.

Table 2 Name of the towns where the samples were taken in the north Andean Flank and the western Lago de Maracaibo Basin, Venezuela

State	Location	Coordinates X,Y (UTM)
Mérida	La Azulita-Bachaquero	(231537; 965696)
	Zea	(188909;930139)
	Chiguará	(222572;943942)
Táchira	Las Hernandez	(186413; 927137)
	San Pedro del Rio	(199990;883675)
Zulia	Flanco Perijanero	(778064;1148259)

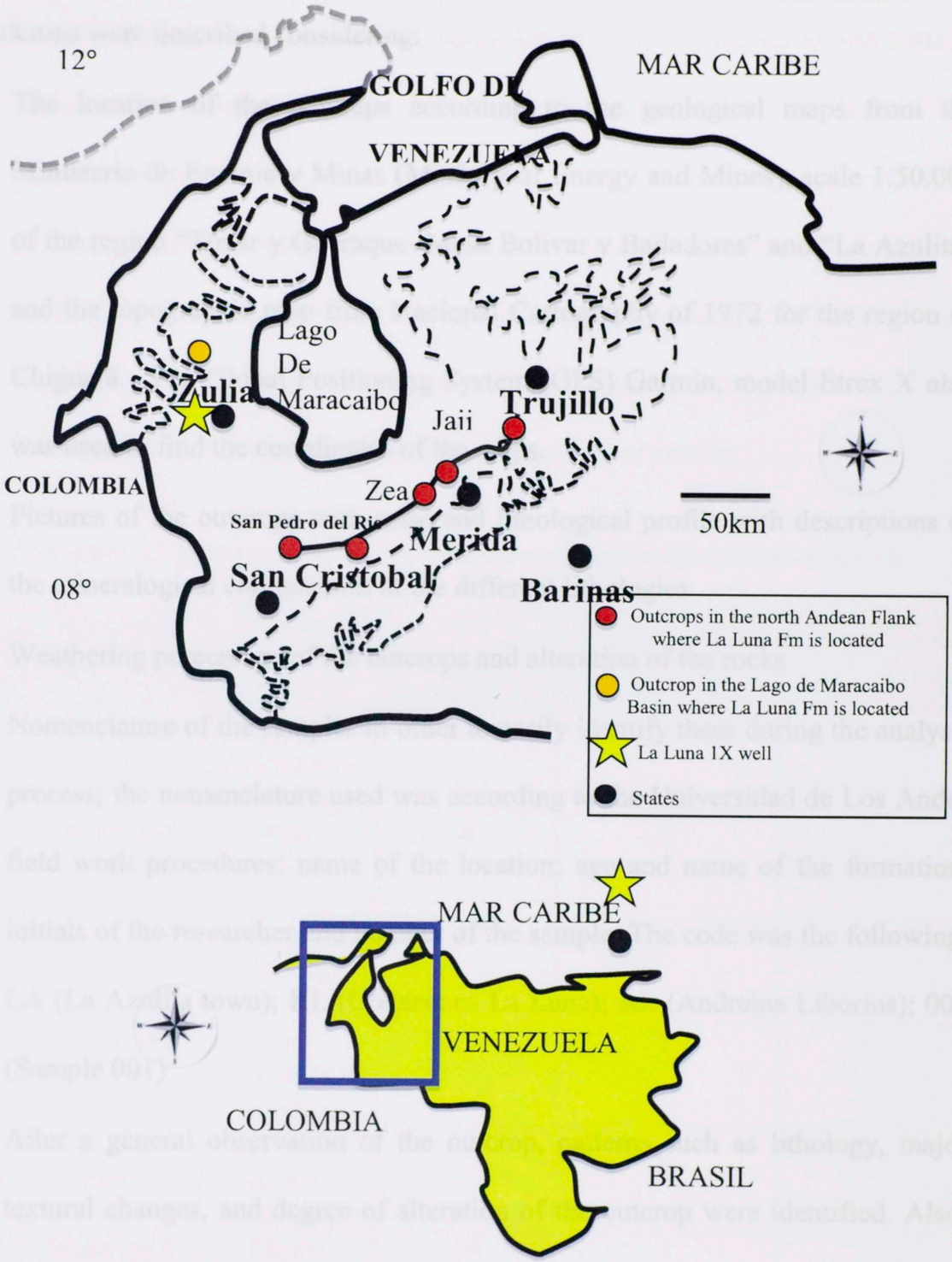

Figure 7 Map of locations of La Luna Formation outcrops in the North Andean Flank of Venezuela

3.3 Description of the outcrops

The outcrops were described considering:

- The location of the outcrops according to the geological maps from the Ministerio de Energia y Minas (Ministry of Energy and Mines), scale 1:50.000 of the region "Tovar y Guaraque- Mesa Bolivar y Bailadores" and "La Azulita" and the topographic map from Nacional Cartography of 1972 for the region of Chiguará. The Global Positioning System (GPS) Garmin, model Etrex X also was used to find the coordinates of the maps.
- Pictures of the outcrops with scale and lithological profile with descriptions of the mineralogical composition of the different lithologies
- Weathering percentage of the outcrops and alteration of the rocks
- Nomenclature of the samples in order to easily identify them during the analysis process; the nomenclature used was according to the Universidad de Los Andes field work procedures: name of the location; age and name of the formation, initials of the researcher and number of the sample. The code was the following: LA (La Azulita town); KL (Cretaceous La Luna); AL (Andreina Liborius); 001 (Sample 001)
- After a general observation of the outcrop, patterns such as lithology, major textural changes, and degree of alteration of the outcrop were identified. Also, samples collected were representative of the most important geological outcrops.
- Collected samples were oriented along the magnetic north, indicating the same position from the top and bottom of the sample at the time of the removal from the outcrop.

- Sampling was conducted in a fresh outcrop and different criteria were used for sample collection, but, in general, included: rock type, lithological and textural changes and type of analysis that were subsequently made on each of the samples.
- In total, 40 samples were collected; in Table 3 samples are shown according to: members, lithological changes and type of analysis for each sample. It is worth mentioning that only some samples were subjected to petrographic and Rock Eval analysis because macroscopic descriptions were similar.

Table 3 Number of samples used for geochemical and petrographical analysis

Unit	Lithology types	Location	Number of samples taken	Geochemistry (Rock Eval)	Petrography
La Luna Fm	Shales and chert	La Azulita Bachaquero, Mérida	4	2	2
La Luna Fm	Shales and chert	Zea, Mérida	4	5	2
La Luna Fm	Shales and chert	Chiguara, Mérida	8	6	3
La Luna Fm	Shales and chert	Las Hernandez, Táchira	10	5	4
La Luna Fm	Shales and chert	San Pedro del Rio, Tachira	5	3	1
La Luna Fm	Shales and chert	Flanco Perijanero, Zulia	10	7	6
La Luna Fm	Shales and chert	La Luna 1X core	40	20	12

3.4 Laboratory analysis

A successful reservoir characterization is based on a variety of datasets which provide information at different scales. The methodology proposed by Slatt et al. (2012) (Figure 8) was applied to the geologic characterization of La Luna Formation samples

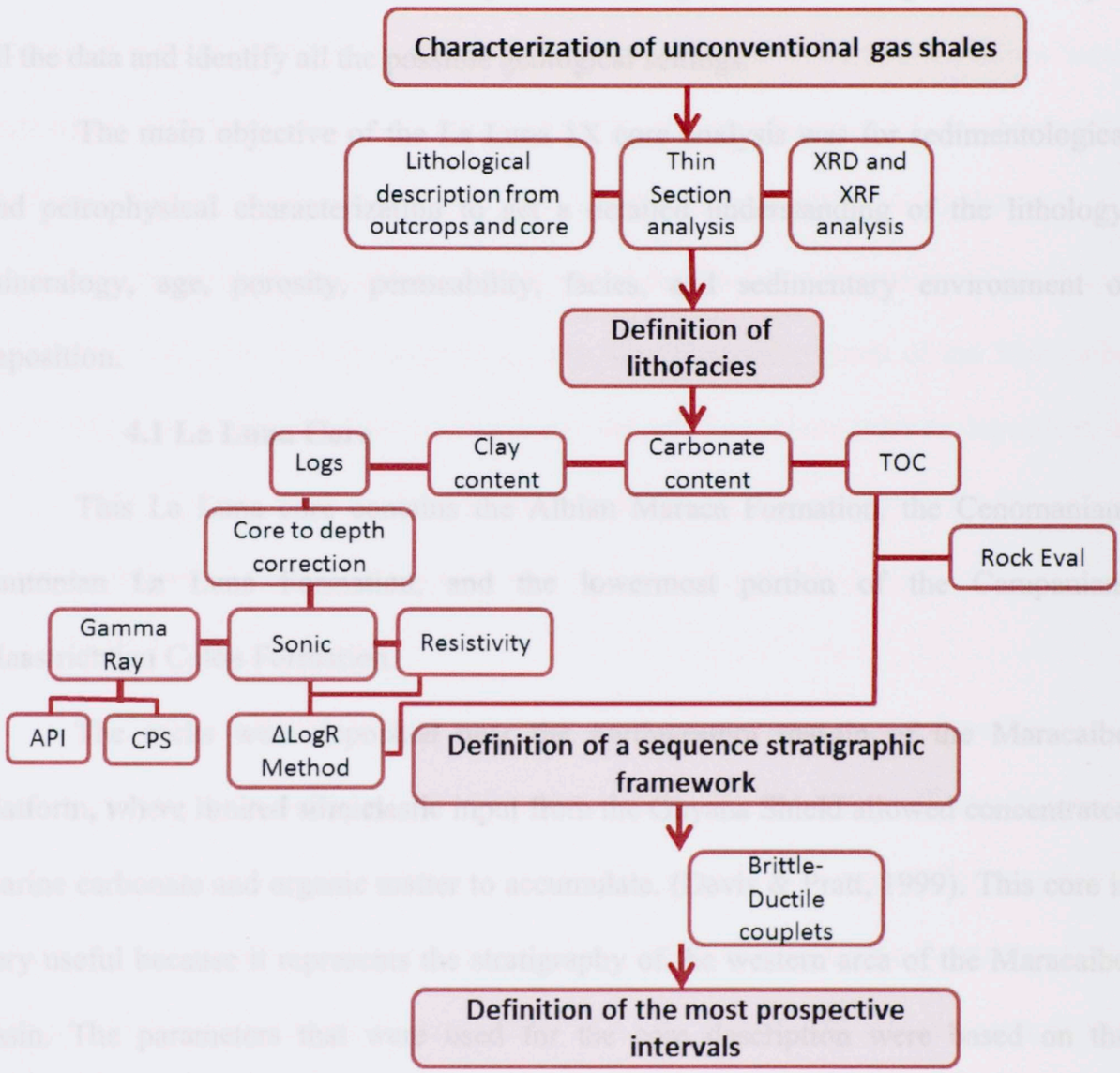

Figure 8 Flow chart for integrated Characterization of unconventional gas shales (Modified from Slatt et al., 2012, AAPG Memoir 97, p. 1-24.).

4. Core description and facies analysis of La Luna IX core

In order to characterize the La Luna Fm in the Lago de Maracaibo basin, a 345 foot long core was provided by the Venezuelan national oil company, Petroleos de Venezuela S.A (PDVSA) in Zulia state, Venezuela. This core was analyzed in the summer of 2014 and was studied every 0.5 feet using Ozzie's core logbook to compile all the data and identify all the possible geological settings.

The main objective of the La Luna 1X core analysis was for sedimentological and petrophysical characterization to get a detailed understanding of the lithology, mineralogy, age, porosity, permeability, facies, and sedimentary environment of deposition.

4.1 La Luna Core

This La Luna core contains the Albian Maraca Formation, the Cenomanian-Santonian La Luna Formation, and the lowermost portion of the Campanian-Maastrichtian Colón Formation.

The rocks were deposited near the northwestern margin of the Maracaibo platform, where limited siliciclastic input from the Guyana Shield allowed concentrated marine carbonate and organic matter to accumulate. (Davis & Pratt, 1999). This core is very useful because it represents the stratigraphy of the western area of the Maracaibo basin. The parameters that were used for the core description were based on the lithology, sedimentological analysis, and core to well calibration. The type of lithology was determined based on the color, grain size, mineral composition, organic content, and type of cement. Sedimentological analyses were identified based on trace fossils, macrofossils, stratification, accessory minerals, and contacts in order to define geologic

facies and trends. Organic geochemical, XRF, and XRD analysis were conducted for the La Luna core in order to characterize the core into different facies, which was based on the change in TOC, trace and major elements.

4.1.1 Maraca Formation

The Maraca Formation is a laminated packstone that is becoming more calcareous moving stratigraphically up section. It is made up of bioclastic shallow water carbonates, which represent the latest stage in the development of the Maracaibo Platform. Resting unconformably on top of the Maraca platform, carbonates are laminated, fine-grained bituminous limestone of the La Luna Formation. Dissolution and infilling at the top of the Maraca are reported from other parts of the Maracaibo Basin, suggesting paleokarst development and subaerial exposure prior to deposition of the La Luna (Trukowski et al., 1996). These features are also present in the Woodford and Barnett shales (Slatt et al., 2015).

4.1.2 La Luna Formation:

La Luna sediments in the western Maracaibo region were deposited in a hemipelagic to pelagic environment, with water depths of ~200–300 m (Perez-Infante et al., 1996). The La Luna is overlain in the ALP- 6 core by a regionally recognized phosphatic and glauconitic hardground marking the base of the Colón Formation (Tres Esquinas Member). Martinez & Hernandez (1992) suggest that maximum water depths of 600 m were reached during deposition of this hardground.

There is global evidence suggesting that the mid-Cretaceous (Aptian-Santonian) was a major time interval of organic matter accumulation in marine sediments (e.g., Arthur et al., 1986). The Cenomanian-Santonian La Luna Formation and equivalent

organic-rich shales accumulated in a wide area across the northern margin of South America. These strata appear to constitute a significant fraction of worldwide organic carbon accumulation during this time interval (David & Pratt, 1999).

The core has clay-sized grains and represents certain features which allow it to be classified as Upper, Middle, and Lower members of La Luna Formation. When moving stratigraphically from the base up, the La Luna Formation (which is in unconformable contact with the Maraca Formation) changes from a laminated mudstone to a mudstone with recrystallized calcite and micrite lenses (15610'-15574').

There is also reworking of the La Luna Formation in certain areas because there is a large presence of bioclasts probably coming from the Maraca Fm.

4.1.3 Colon Formation

The upper interval of the Colon formation is called the Socuy Member and consists of approximate 35 meters of olive-gray, hemipelagic limestone. Alternation of well-laminated layers with layers where bioturbation partially destroys lamination is a common feature. Some cyclicity is present toward the top of the unit. There is a presence of terrigenous clays, fine sand-sized quartz, feldspar, red siltstones, and volcanic and plutonic fragments. Planktonic and benthicforaminifera are dominant. Phosphates are present as well. Pyrite occurs in framboids and nodules, but glauconite occurs as sand-size grains.

4.2 Facies classification present in the 1X WELL:

Eight facies were defined in the La Luna core from bottom to top.

I. Dark gray laminated mudstone:

(Interval 15581' – 15560'): The lower section of the La Luna in the 1X core starts at the upper contact of the Maraca Formation with a series of conchiferous bivalves (Figure 9A). A dark gray, laminated mudstone filled with calcite veins is present in this interval. High levels of organic matter are also shown by the presence of micro slumps. Micrite lenses (Figure 9B) and recrystallization of benthic foraminifera, are visible with the presence of minor reworking from the Maraca formation. This interval changes gradually from calcareous-organic in character. There is a presence of erosion surfaces, lag deposits and calcite-filled fractures almost perpendicular to bedding with slight bioturbation towards the top (Figure 9C). This lithology reflects the depositional sequence proposed by David & Pratt (1999) who named this interval the LL1. It is thought that during the earliest La Luna deposition in the western Maracaibo basin a marine transgression decreased the supply of terrigenous alumino-silicate sediments to the shelf with moderate marine productivity and deep waters that were depleted in oxygen, creating reducing conditions in the benthic environment.

II. Fossiliferous wackstone facies

(Interval 15560' - 15552'): This is a light gray laminated shale displaying a high content of organic matter and rhythmic calcite lenses towards the top with some erosional surfaces (Figure 10A and B). There is a presence of foraminifera in a micrite matrix and the upper part of this interval contains organic matter-filled fractures containing dead oil (Figure 10C). This is probably related to the tectonic settings of the

basin during the Cretaceous period. Cone-in –cone structures are also present representing an area of overpressure during sedimentation (Cobbold et al., 2013).

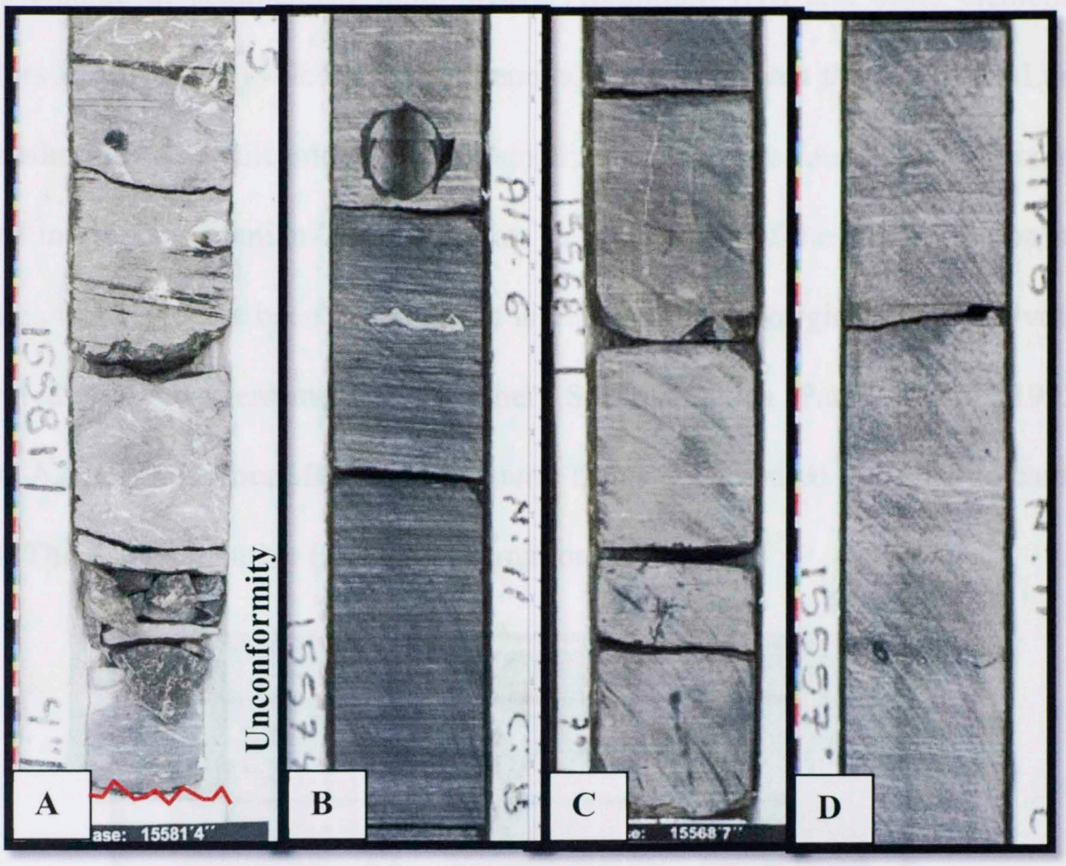

Figure 9 Facies I. Dark gray laminated mudstone: A) conchiferous bivalves, B) micrite lenses C) Presence of calcite veins and fractures are almost perpendicular to bedding D) Slight bioturbation occurs towards the top of the interval.

III. Volcanic Ash

(Interval 15552'- 15548'): Two volcanic ash pulses were found in La Luna 1X core. The base of this interval is represented by a laminar and fissile, yellowish colored bed with coarse particles of volcanic ash (Figure 11). They look like grains of sand, but are euhedral crystals that are locally called "coffee grains". After this layer there is a gap in the core (15548'- 15537') maybe due to its friable character. This interval was probably thicker than the remaining strata described in the core. Towards the top of this interval

the volcanic ash is intercalated with laminated black shale. This interval is correlated with the LL2 interval (David & Pratt, 1999) where it is described as representing a marked change in sedimentary input where Aluminum (Al) and other elements are indicators of increased (volcanic + terrigenous) input. Towards the top of La Luna IX core another pulse of volcanic ash but in small amount is also found. Ash horizons are reported in the Cenomanian-Turonian strata in other areas of the Maracaibo basin. In Colombia this layer has been found and it is believed that it originated from a volcanic arc located on the western margin of northern South America (Parnaud et al., 1995 and Gomez, A., 2014). Gomez also in her Master's thesis documented a similar volcanic ash layer in The Salada member (La Luna Formation, Colombia).

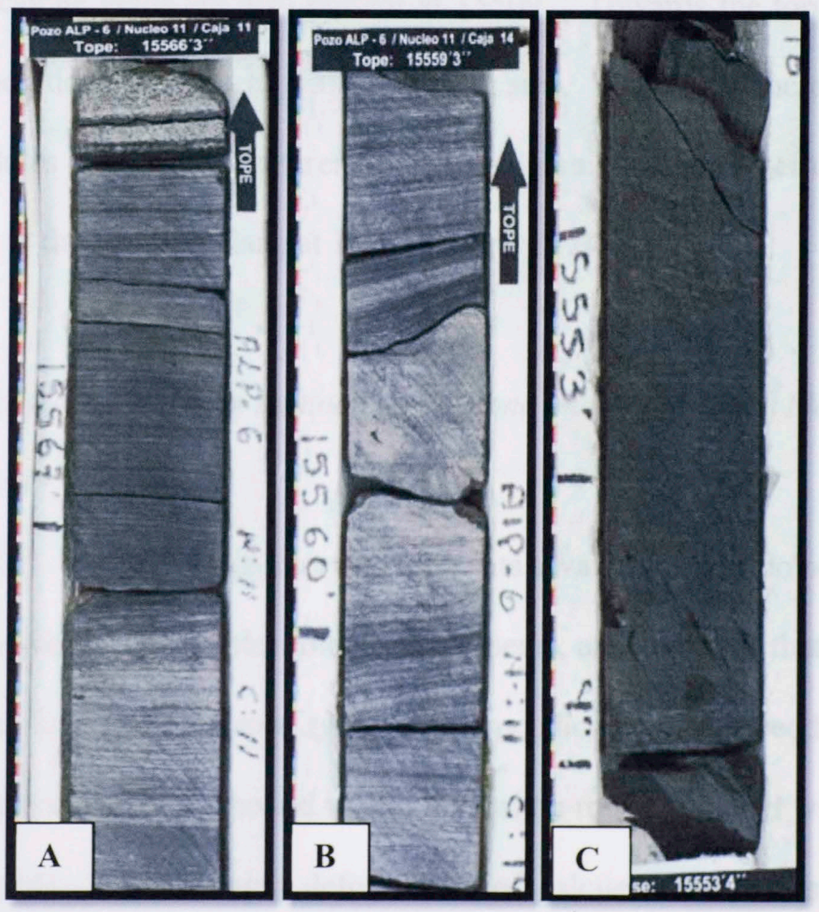

Figure 10 A) Light gray laminated shale displaying a high content of organic matter, B) calcite lenses in a rhythmic deposition towards the top with some erosional surfaces, C) Location of dead oil filled fractures.

IV. Laminated mudstone with limestone concretions and packstone

(Interval 15537'- 15471'): The bottom of the interval consists of light gray mudstone containing calcareous foraminifera that are spread out in some segments of this facies (Figure 12A). There are calcareous lenses around the whole interval, as well (Figure 12B). The interval from 15523'-15522' represents a weathered reddish color that may be confused with red beds, but is just a weathering effect due to the time of exposure of the core. Micro fractures and small bioclast fragments (less than 1 cm) are also present at 15519' (Figure 12C).

Towards the top there is a darker coloration corresponding to an increase in organic matter and, in return, less carbonate. Foraminifera are dispersed along the segment and calcite veins are also present at 15509'. Towards the top of this interval limestone concretions are present with increasing size. There is an increase in plankton and small nodules at 15485'. Fractures filled with organic matter or perhaps dead oil are perpendicular to the bedding plane at 15489' (Figure 12D).

V. Siliceous- calcareous laminated mudstone interbedded with black chert filled with calcite veins

(Interval 15471'- 15458'): This interval represents a variation in lithology (Figure 13). There are massive calcite nodules, bioclast fragments, and fractures that are filled with dead oil or calcite. Both fracture types are perpendicular to the bedding plane. The fractures in the concretion are bound within this brittle rock compared with surrounding shale (Figure 14). Soft sediment deformation of calcite nodules has deformed the

lamination. Beds occur rhythmically with alternations of black chert, laminated mudstone, and big calcite concretions.



Figure 11 Laminar and fissile yellowish color with coarse particles of volcanic ash.

VI. Siliceous- Calcareous mudstone interbedded with wackstone facies

(Interval 15458'- 15456'): This facies is a dark brown mudstone with very small calcite intraclasts. The amount of organic matter is higher than in the lower intervals (Figure 15). From 15456'-15382 the layers are related to facies V with a distinct variation in black chert, laminated mudstone, (more organic matter than before) and calcite concretions. The black chert layers and chert concretions increase towards

the top of the interval. The increase in chert concretions is probably related to a lowstand systems tract that caused the reduction in the productivity of calcareous organisms and an increase in the productivity of siliceous organisms. These features could be related to the LL4 facies of David & Pratt (1999). At 15382' facies VI appears again, which transitions into a rhythmic alternating sequence from facies V to facies VI up to 15311'.

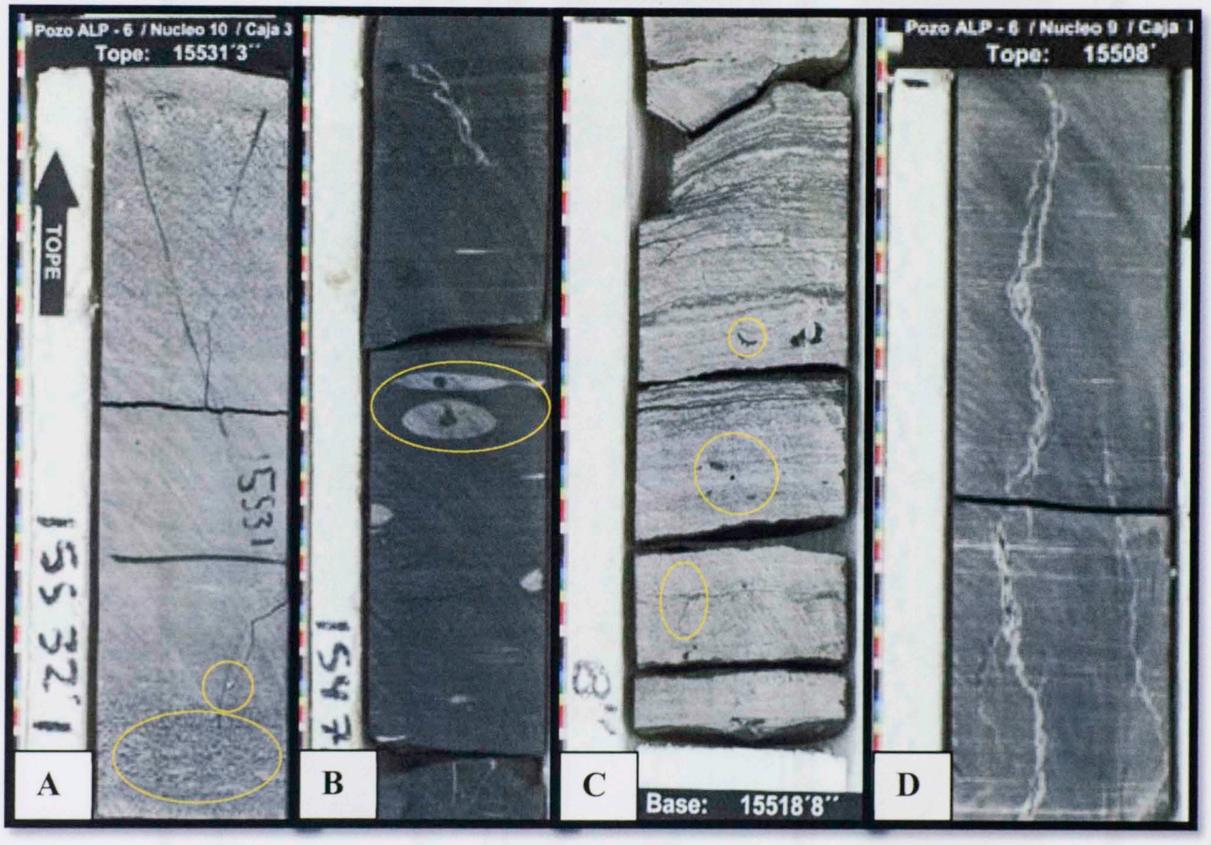

Figure 12 A) Intergrowth of calcareous foraminifera B) calcareous lenses C) micro fractures, stylolite and small bioclast fragments (less than 1cm) D) Fractures, filled with calcite are perpendicular to the bedding plane (15489' interval).

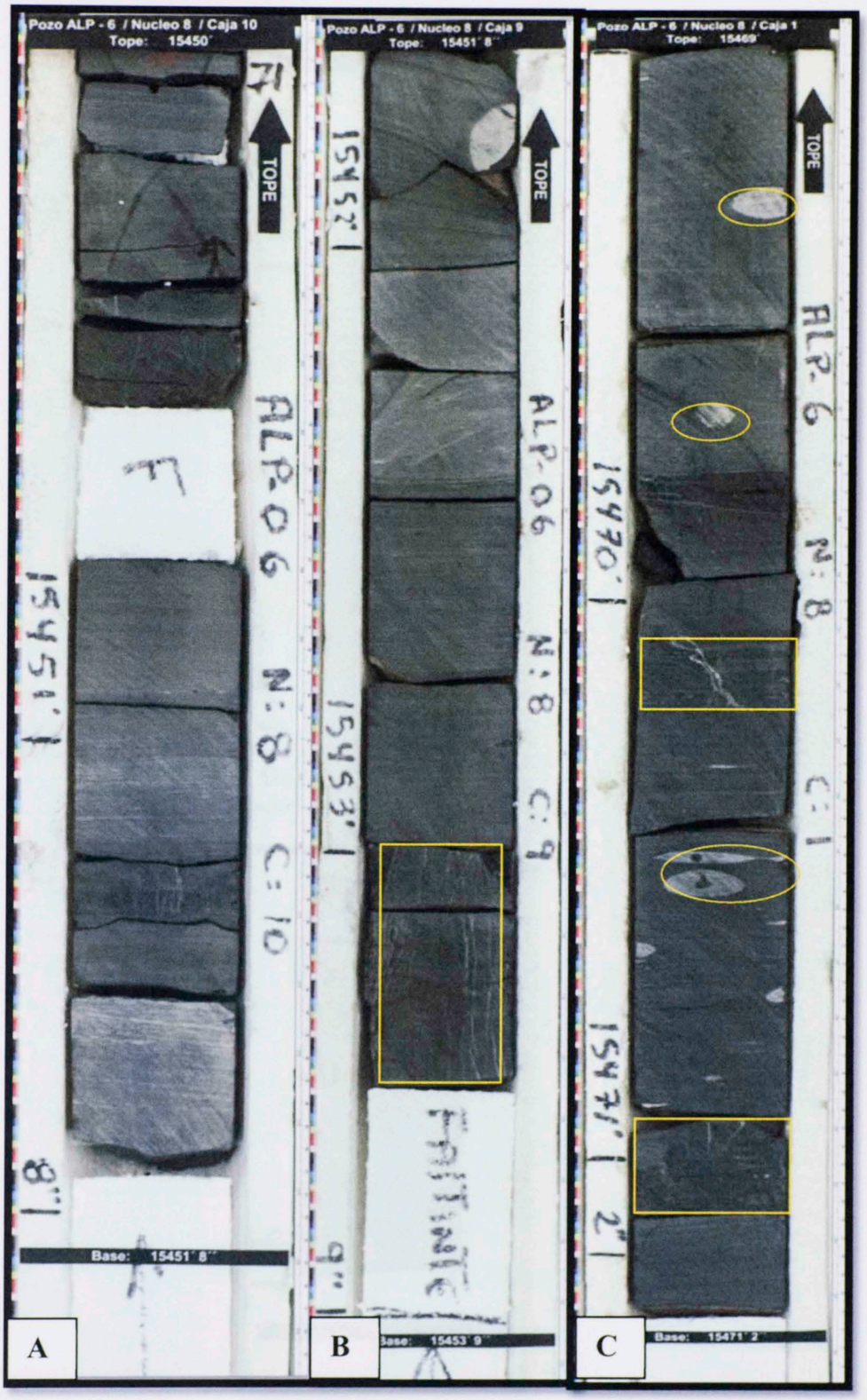

Figure 13 Massive calcite nodules (yellow circles); small filled fractures in chert layers (yellow squares).

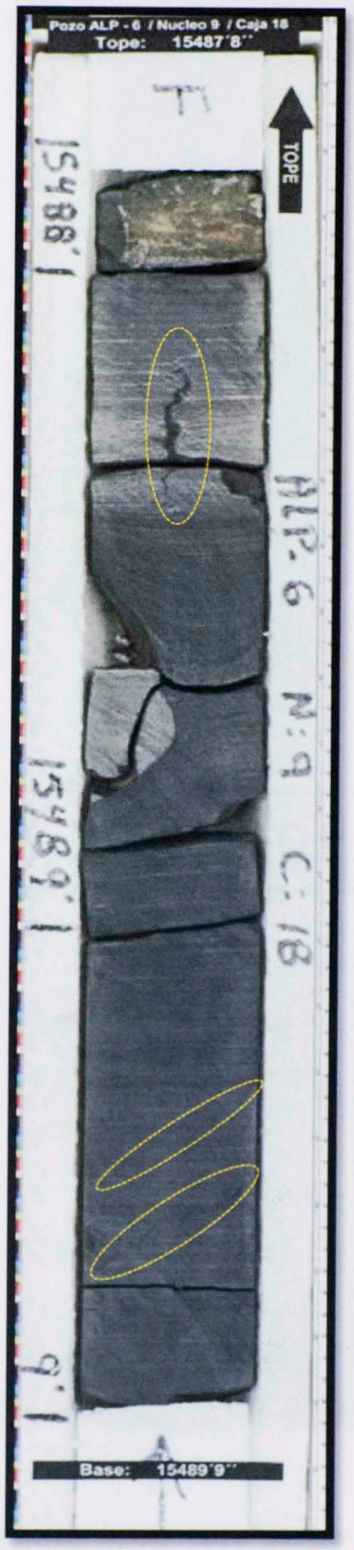

Figure 14 Fractures filled with organic matter perpendicular to the bedding plane.

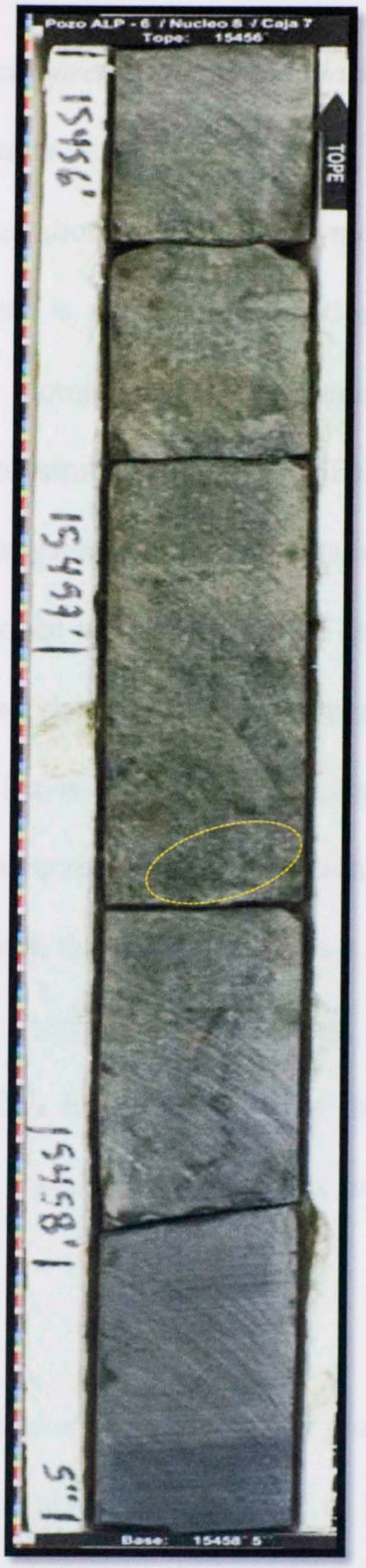

Figure 15 Dark brown mudstone with very small calcite intraclasts This core contains a large increment of organic matter and strong petroleum odor in facies VI.

VII. Slightly siliceous- calcareous laminated black mudstone interbedded with calcareous fossiliferous wackstone.

(15311'- 15281'): The sedimentation trend becomes more organic rich in this interval (Figure 16A). At 15311' there is marked bioturbation by *Glossifungites* that is an ichnofacies characterized by domichnia (*Glossifungites* and *Thalassinoides*) and sometimes plant root penetration structures (Figure 16B). These characteristics occur in firm, but not lithified sediments, such as muds and silts in marine intertidal and shallow subtidal zones. They are developed in shallow marine environments where erosion has stripped off superficial, unconsolidated layers of sediment. This interval can be related to one of the facies defined by Davis & Pratt (1999) where the levels of benthic oxygen are inferred to be low, but an increase of oxygenation likely occurred in the upper portion of the LL5 interval. Above this interval there is a large increase in the content of organic matter. There is a presence of dark gray, finely laminated, planktonic foraminifera with occasional fish fragments towards the base. Interbedded nodules disturb the bedding of shales. Occasional packstones with abundant foraminifera are also present.

VIII. Siliceous green mudstone with authigenic glauconite and Pyrite

Interval (15281'- 15267'): In the interval from 15280' to 15275' there is a succession of fining upward sequences with brown/grey wackstone and fish remains at the base (5-15cm). There are laminated shales with planktonic foraminifera and laminations at the top (30-120 cm) exhibit erosive bases. At 15270' there is a presence of micrite wackstone, phosphatic glauconite, and dolomite at the base. In some parts of this

interval, vertical burrows are present that extend from 7-10 cm in height. There is also some calcite fill with a sinuous shape caused by compaction. Towards the top there is gray to green wackstone – packstone that is altered to glauconite, phosphate, and pyrite. Along this interval there are bioturbated *Zoophycos,* which occur between the abyssal zone and the shallow continental shelf with normal background conditions of sedimentation. There are also benthic and planktonic foraminifera along with amounts of organic matter. Davis and Pratt (1999) associated this lithology with the lowermost portion of the overlying Colon Formation, (Tres Esquinas Member) which is characterized by high concentrations of Fe and S. This is expected for low marine productivity and starved basin sedimentation, which is associated with the formation of authigenic glauconite and pyrite under suboxic conditions (Davis and Pratt, 1999).

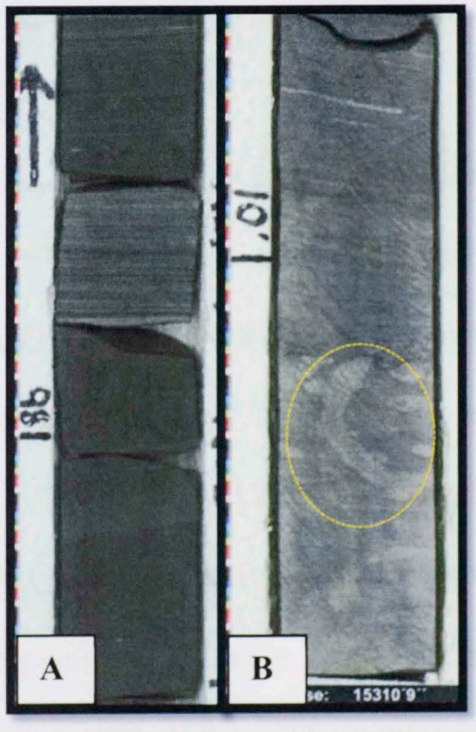

Figure 16 A) Change in the sedimentation pattern to a more organic-rich sediment B) marked bioturbation that shows the presence of *Glossifungites* that are Ichnofacies characterized by *Domichnia*.

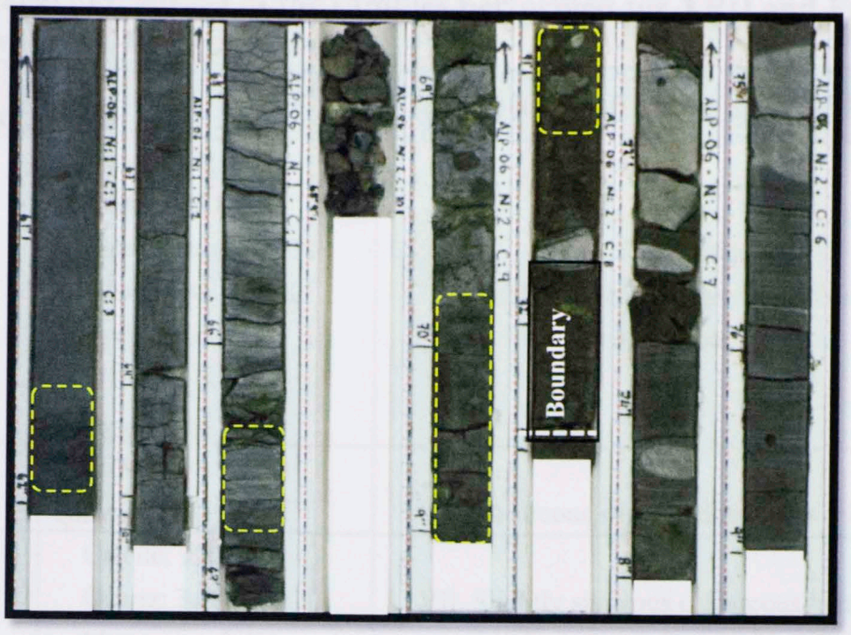

Figure 17 La Luna core in the Upper La Luna interval showing boundary of La Luna Formation with the Socuy Member of the Colon Formation. The characteristic green olive coloration of the glauconitic segments is present in the Socuy Member; bioturbation is notorious in the segment of the core (highlighted by yellow dashed lines).

4.3 Mineral composition

"An important aspect to understanding shale reservoirs is determining their mineralogy and TOC (total organic carbon) content, since these will essentially control reservoir quality" (Radcliffe et al., 2013). Typically, this is achieved using X-Ray diffraction (XRD), X-ray fluorescence (XRF), and LECO TOC analysis, respectively. Eight samples were taken for XRD analysis, 12 for XRF, and 20 were performed for the LECO TOC analysis. The purpose of this was to tie all this information to the facies developed in the core description in order to match the results obtained in these samples. Table 3 shows the results of the XRF samples and their relationship with the facies performed for the La Luna 1X core. Figures 18- 24 display the summary of the XRD, core description and petrography that represents each interval.

Table 4 Mineral percentage of the samples performed for XRD and Facies associated in the 1X La Luna core.

Sample/Depth	Mineral percentage (%)	Facies association in La Luna IX core
15267'	Illite: 42.7% Quartz: 25.8% Fluorapatite: 10.9% Glauconite: 10.1% Pyrite: 6.5% Gypsum: 3.2% Calcite: 0.8%	VIII. Siliceous green mudstone with authigenic glauconite and Pyrite
15300'	Calcite: 95.9% Quartz: 4.1%	VI. Calcareous slightly siliceous wackstone
15334'	Calcite: 92.3% Quartz: 3.5% Muscovite: 3.4% Montmorillonite: 0.9%	VII. Slightly siliceous calcareous laminated black mudstone interbedded with calcareous fossiliferous wackstone
15357'	Calcite: 58.8% Quartz: 35.8% Dolomite: 4.7% Hematite: 0.7%	VII. Siliceous calcareous laminated black mudstone interbedded with calcareous fossiliferous wackstone
15376'	Calcite: 95.9 % Gypsum: 2.5% Quartz: 1.6%	VII. Slightly siliceous calcareous laminated black mudstone interbedded with calcareous fossiliferous wackstone
15401'	Calcite: 96.2% Quartz: 3.8%	VII. Slightly siliceous calcareous laminated black mudstone interbedded with calcareous fossiliferous wackstone
15465'	Calcite: 70.9% Quartz: 16.1% Muscovite: 9.7% Gypsum: 1.4%	V. Siliceous- calcareous laminated mudstone interbedded with black chert filled with calcite veins
15568'	Illite: 27.5% Calcite: 25.4% Quartz:21.8% Albite:11.8% Pyrite: 8.5% Gypsum: 3.1% Glauconite: 2%	IV. Laminated mudstone with limestone concretions and packstone

Facies IV: Laminated mudstone with limestone concretions and packstone. Interval 15568'

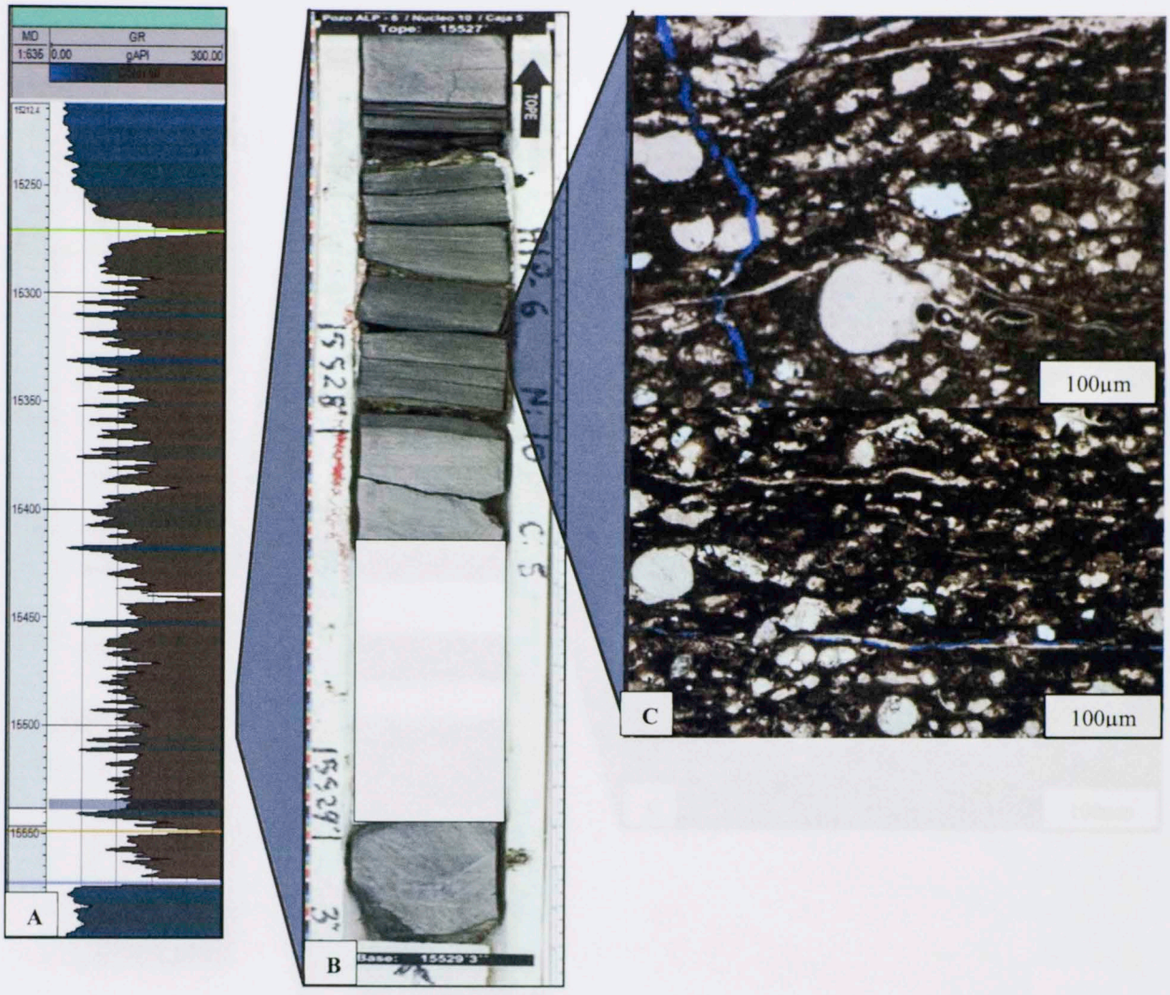

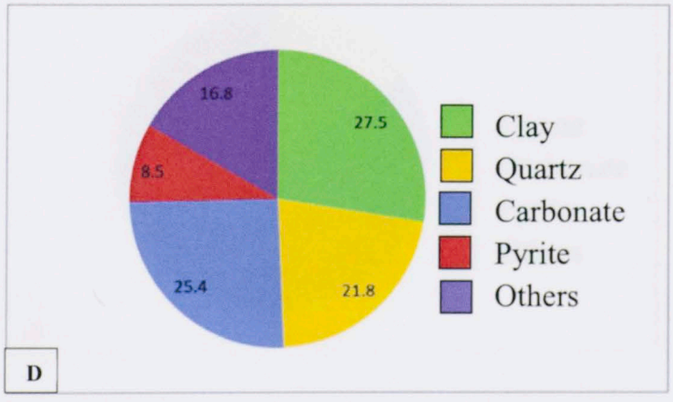

Clay	27.5 wt. %
Quartz	21.8 wt. %
Carbonate	25.4 wt. %
Pyrite	8.5 wt. %
Others	16.8 wt. %

Figure 18 Summary of the XRD and petrography of the Facies IV. A) Log interval where the sample was taken B) Picture of the interval of the core where the sample was taken C) Photograph of thin section showing recrystallized forams and small quartz grains in an organic matrix D) Mineralogical composition based on XRD values.

Facies V: Calcareous – siliceous laminated wackstone interbedded with black chert filled with calcite veins. Interval 15465'

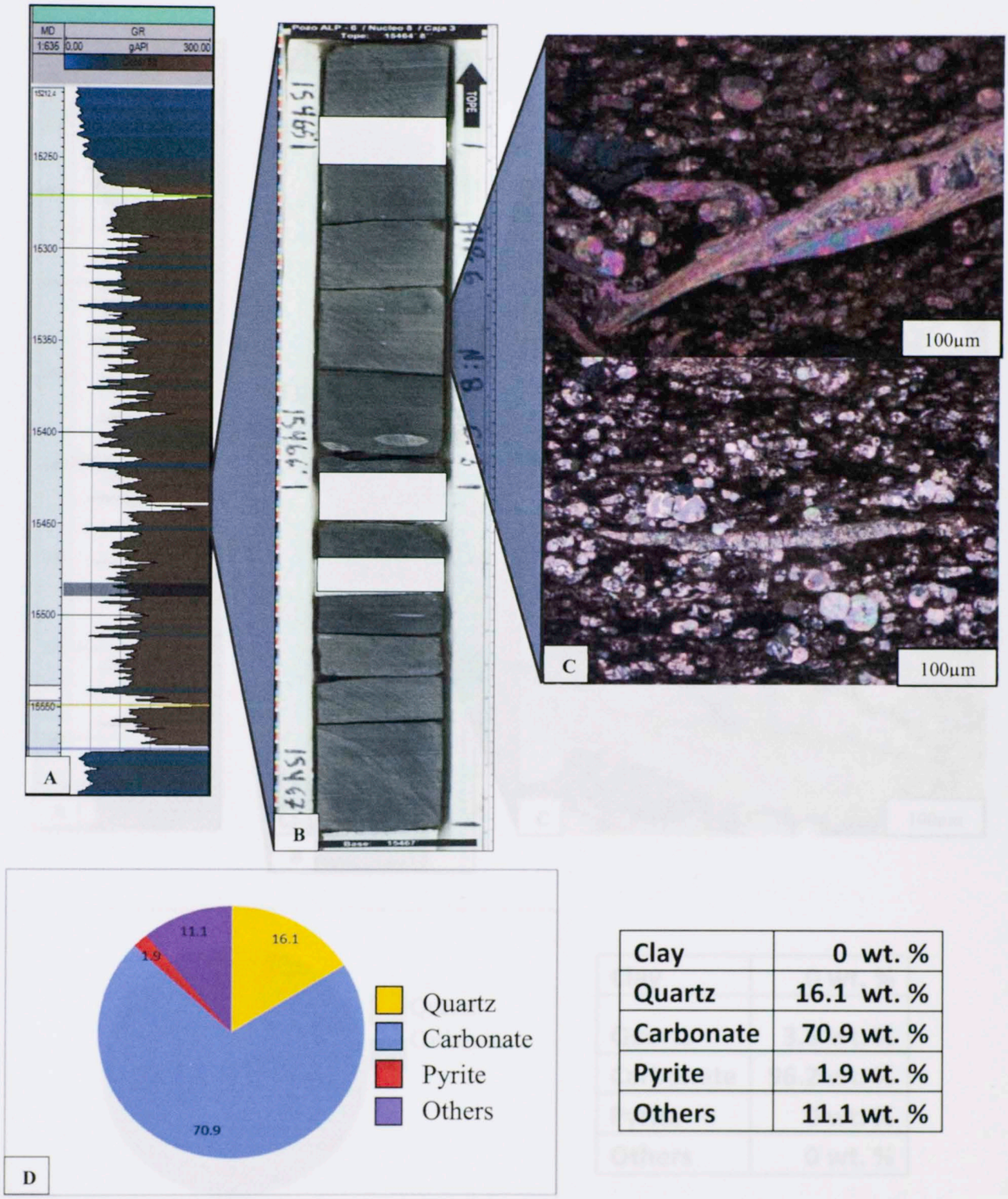

Clay	0 wt. %
Quartz	16.1 wt. %
Carbonate	70.9 wt. %
Pyrite	1.9 wt. %
Others	11.1 wt. %

Figure 19 Summary of the XRD and petrography of the Facies V A) Log interval where the sample was taken B) Picture of the interval of the core where the sample was taken C) Photograph of thin section showing recrystallized forams, spicules of Echinoderms and small quartz grains in an organic matrix D) Mineralogical composition based on XRD values.

Facies VII: .Calcareous slightly siliceous laminated black mudstone interbedded with calcareous fossiliferous wackstone. Interval 15401'

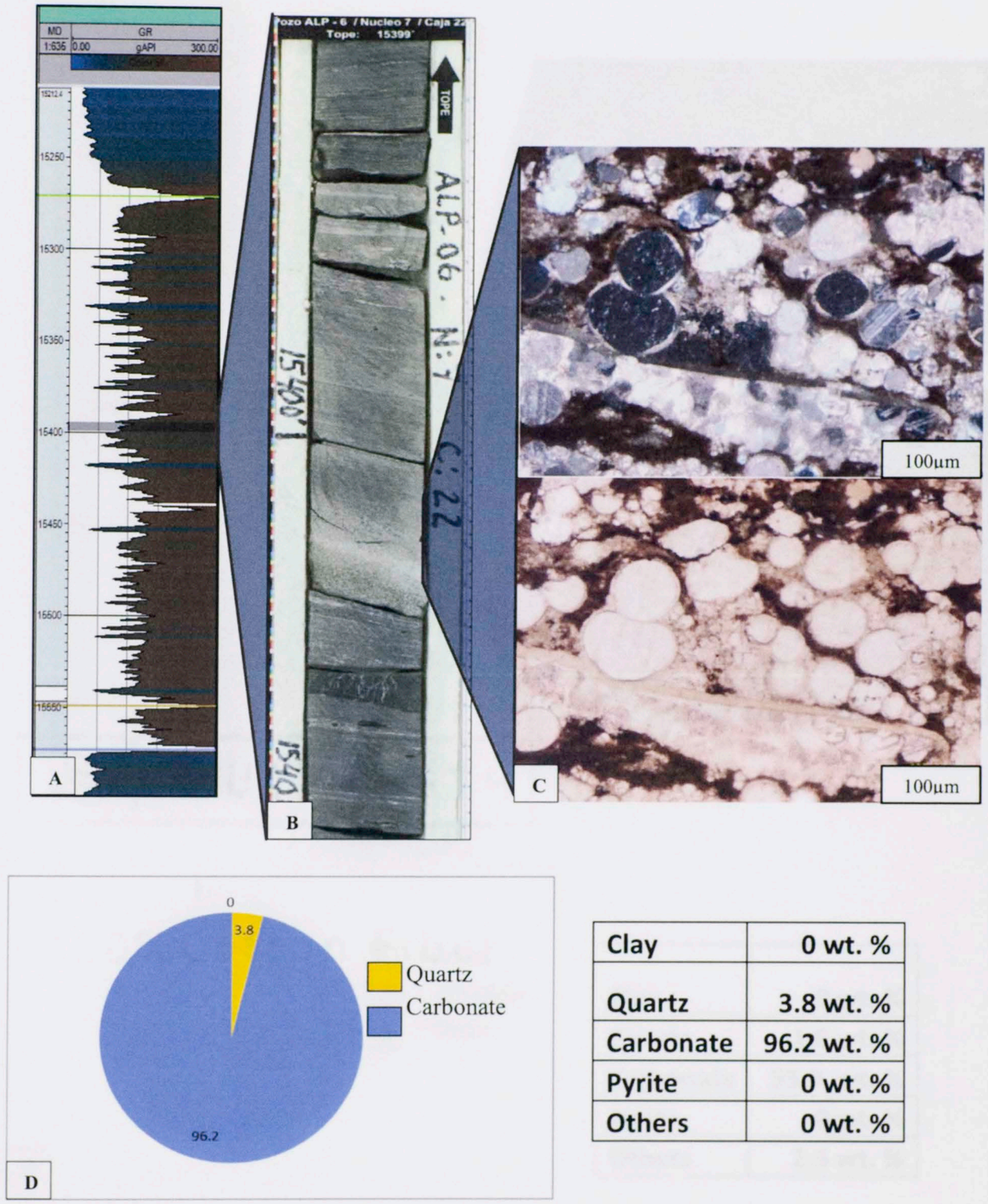

Clay	0 wt. %
Quartz	3.8 wt. %
Carbonate	96.2 wt. %
Pyrite	0 wt. %
Others	0 wt. %

Figure 20 Summary of the XRD and petrography of the Facies V A) Log interval where the sample was taken B) Picture of the interval of the core where the sample was taken C) Photograph of thin section showing recrystallized forams of a larger size, spicules of Echinoderms and small quartz grains in a carbonate matrix D) Mineralogical composition based on XRD values.

Facies VII: Calcareous, slightly siliceous, laminated, black mudstone interbedded with calcareous fossiliferous wackstone. Interval 15376'

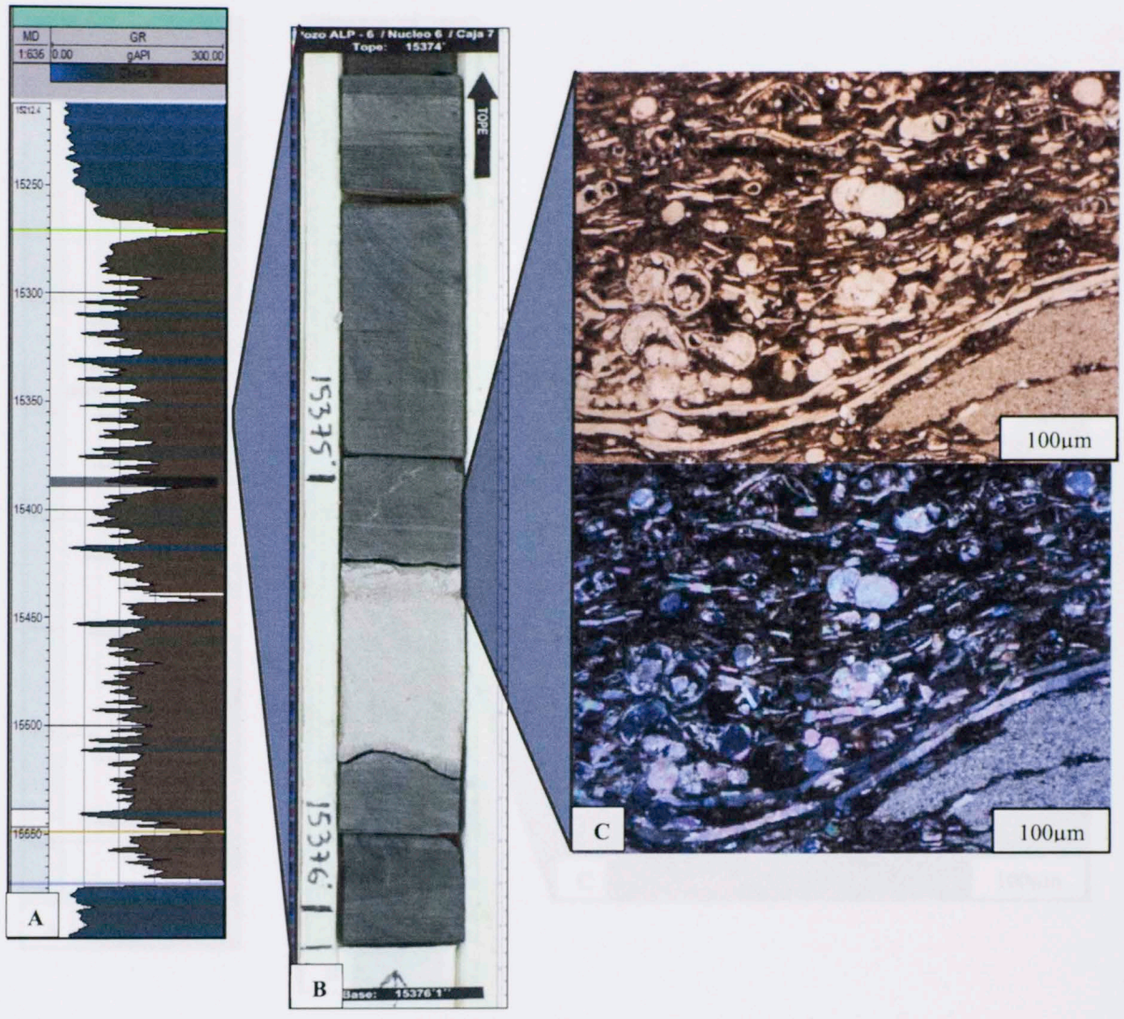

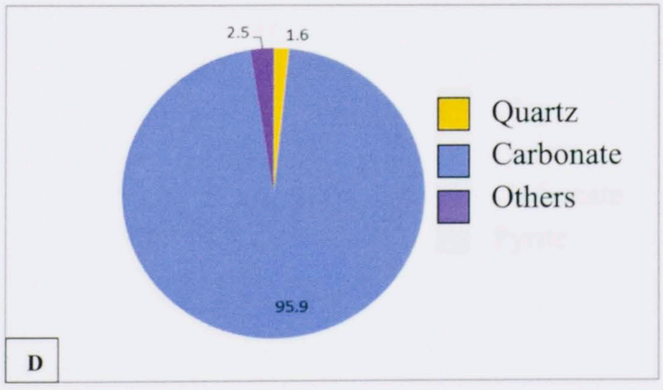

Clay	0 wt. %
Quartz	1.6 wt. %
Carbonate	95.9 wt. %
Pyrite	0 wt. %
Others	2.5 wt. %

Figure 21 Summary of the XRD and petrography of the Facies V A) Log interval where the sample was taken B) Picture of the interval of the core where the sample was taken C) Photograph of thin section showing recrystallized forams, pellets and small quartz grains in a carbonate matrix D) Mineralogical composition based on XRD values.

Facies VII: Calcareous, slightly siliceous, laminated black mudstone interbedded with calcareous fossiliferous wackstone. Interval 15357'

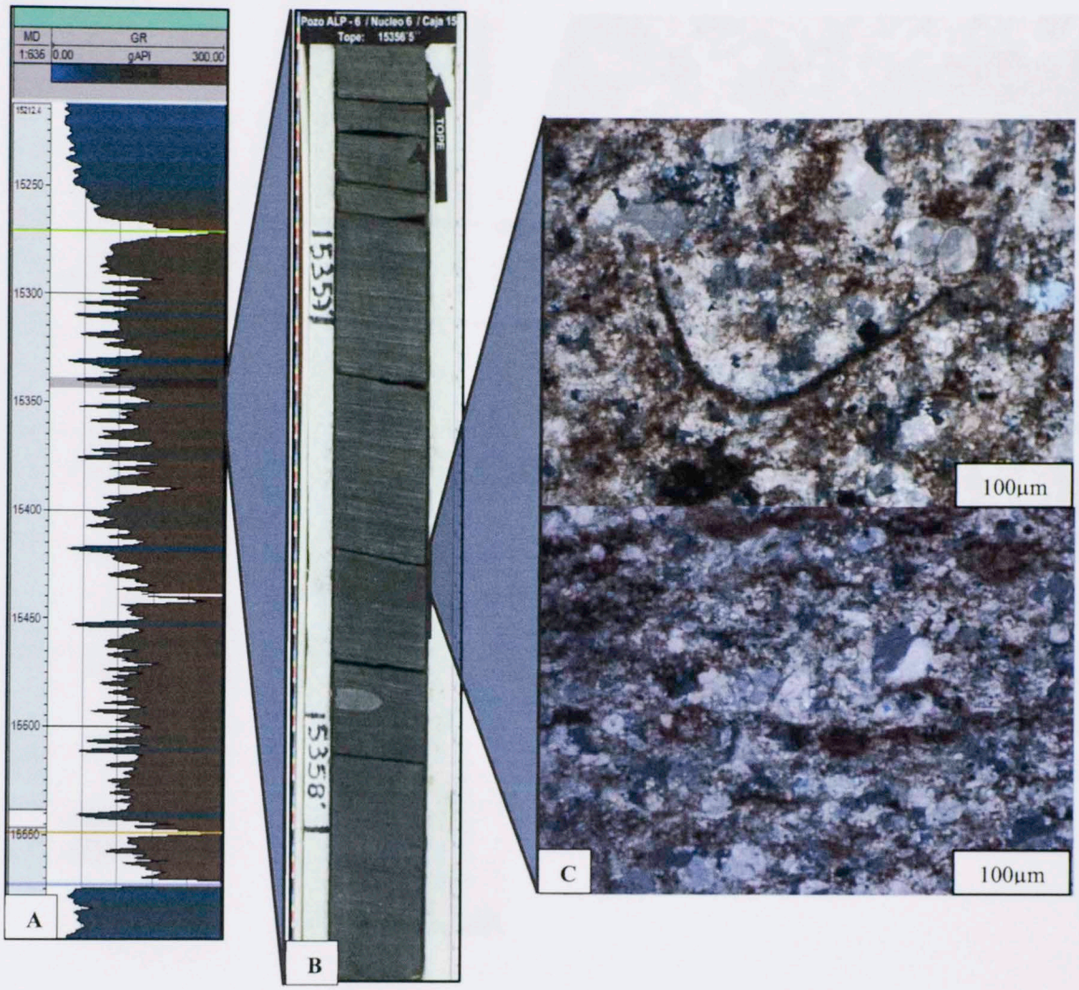

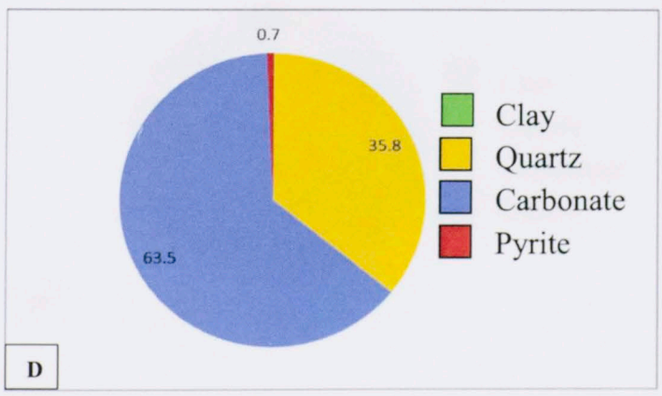

Clay	0 wt. %
Quartz	35.8 wt. %
Carbonate	63.5 wt. %
Pyrite	0 wt. %
Hematite	0.7 wt. %

Figure 22 Summary of the XRD and petrography of the Facies V. A) Log interval where the sample was taken B) Picture of the interval of the core where the sample was taken C) Photograph of thin section showing recrystallized forams and quartz grains in a carbonate matrix D) Mineralogical composition based on XRD values.

Facies VI: Calcareous- siliceous mudstone interbedded with wackstone facies. Interval 15334'

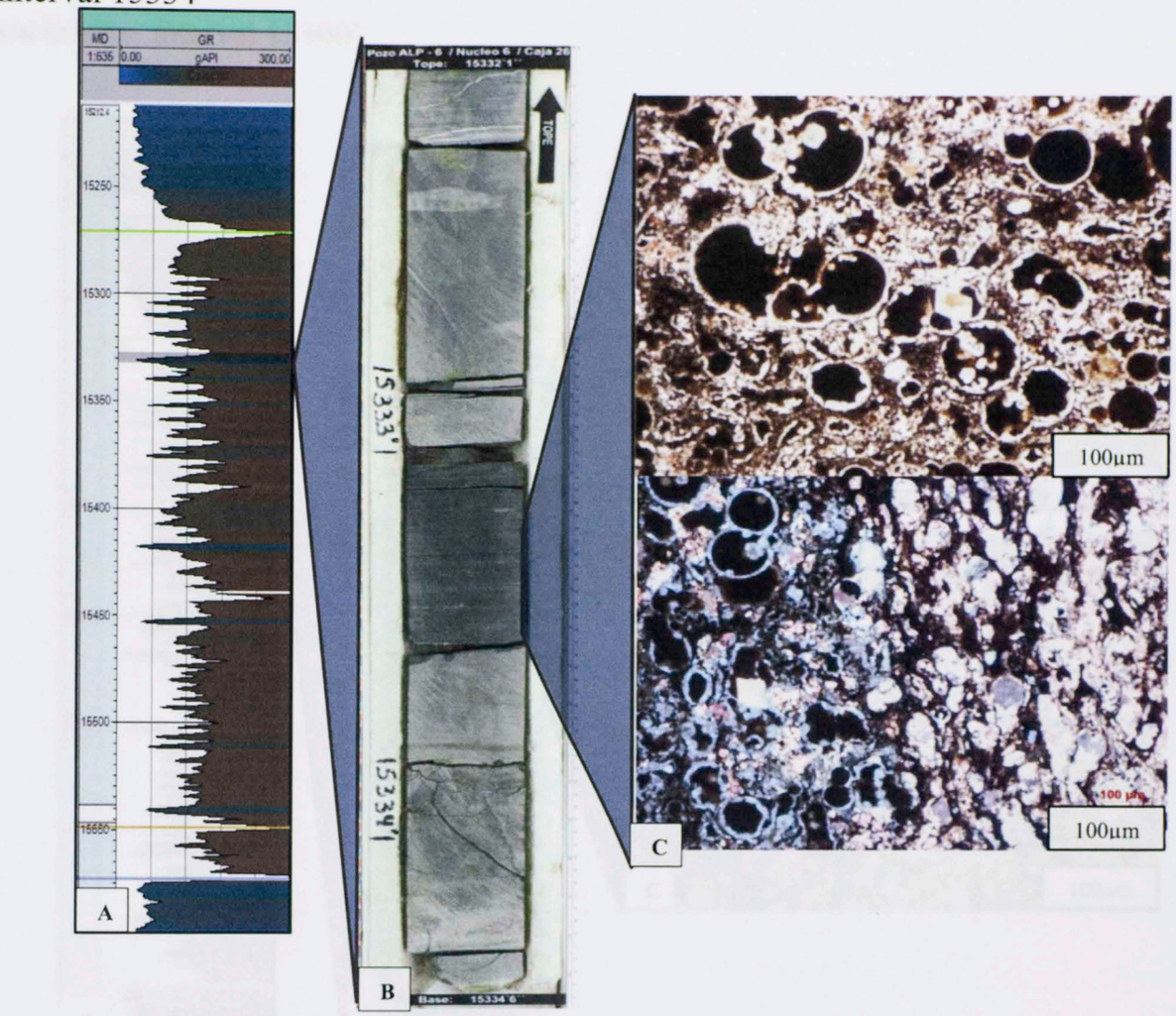

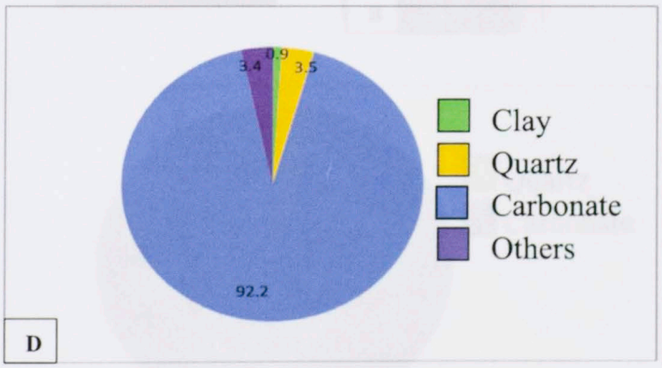

Clay	0.9 wt. %
Quartz	3.5 wt. %
Carbonate	92.2 wt. %
Pyrite	0 wt. %
Others	3.4 wt. %

Figure 23 Summary of the XRD and petrography of the Facies V. A) Log interval where the sample was taken B) Picture of the interval of the core where the sample was taken C) Photograph of thin section showing recrystallized forams in an organic matrix D) Mineralogical composition based on XRD values.

Facies VI: Calcareous -laminated black mudstone interbedded with fossiliferous wackstone. Interval 15300'

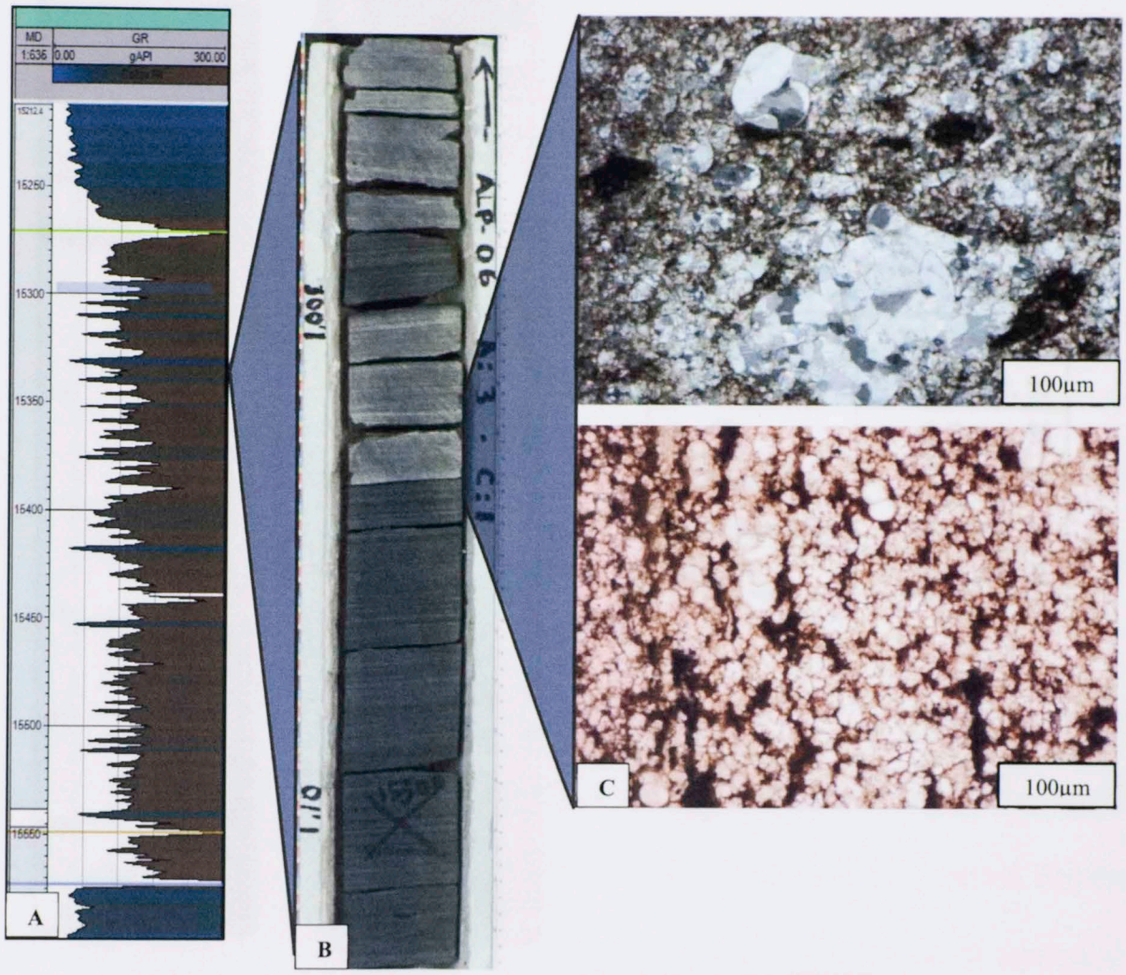

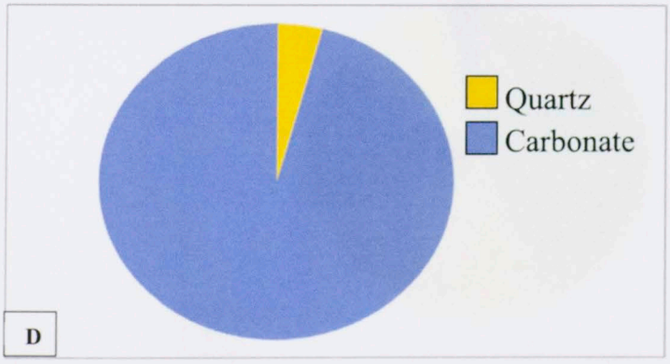

Clay	0 wt. %
Quartz	4.1 wt. %
Carbonate	95.9 wt. %

Figure 24 Summary of the XRD and petrography of the Facies V. A) Log interval where the sample was taken B) Picture of the interval of the core where the sample was taken. C) Photograph of thin section showing abundant parallel layers of *Globoratalia* and small quartz grains in a carbonate matrix D) Mineralogical composition based on XRD values.

Facies VIII: Siliceous, slightly calcareous, green mudstone with authigenic glauconite and Pyrite. Interval 15267'

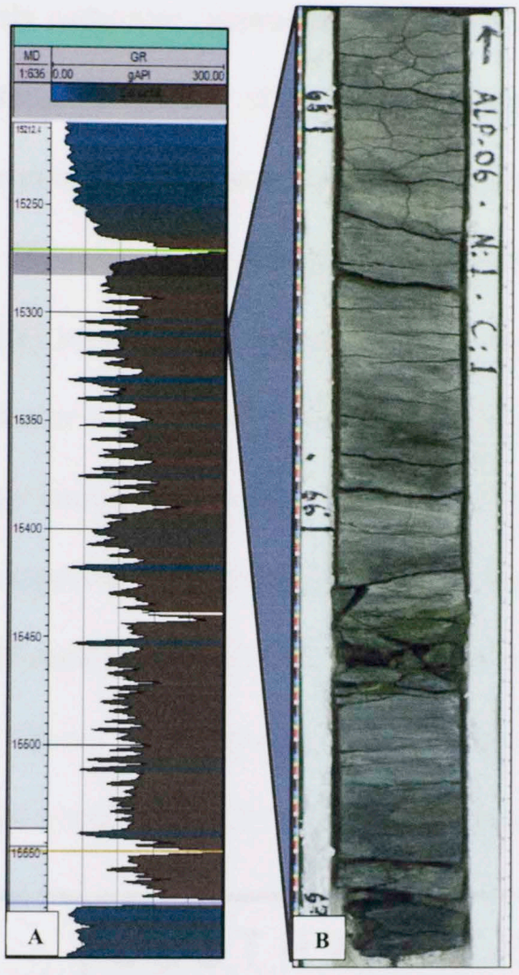

Clay	42.7 wt. %
Quartz	25.8 wt. %
Carbonate	0.8 wt. %
Pyrite	6.5 wt. %
Glauconite	10.1 wt. %
Fluorapatite	10.9 wt. %
Others	3.2 wt. %

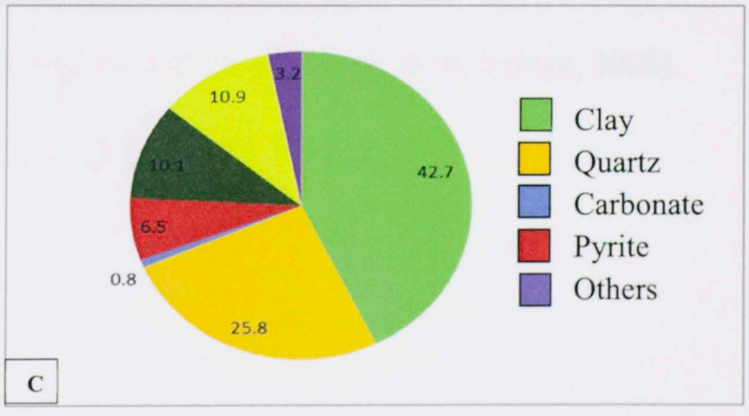

Figure 25 Summary of the XRD and Petrography of the Facies VIII. A) Log interval where the sample was taken B) Picture of the interval of the core where the sample was taken C) Mineralogical composition based on XRD average values.

Figure 26 shows the total distribution of main minerals of the lithofacies containing quartz, calcite, dolomite and clay. The mineral composition of La Luna 1X is primarily carbonate (approximately 90%). This is due to the sedimentation of the thick and lateral succession of mixed carbonates in Lago de Maracaibo basin during the passive margin of northern South America (Davis & Pratt, 1999).

However, as is shown in figure 26, the lower and upper parts of the core display some clay minerals in comparison to the rest of the samples that are mostly carbonates. In the lower zone (15528'- 15469) there is 2 to 5 average % illite and in the upper zone the clay content increases noticeably up to 42.7 %, representing facies VIII which clearly represents the top of the La Luna Fm (Tres Esquinas Member). Table 6 displays the XRF results and the facies association related to each interval.

"X-ray Fluorescence Spectroscopy (XRF) was used to determine the bulk chemical composition of a sample. Elements from fluorine to uranium in the periodic table can be analyzed with detection limits varying from 0.5 ppm for heavier elements like Mo to 100 ppm for the lightest element F. Everything in the sample is analyzed to enable accurate matrix corrections" (Loubser & Verryn, 2008).

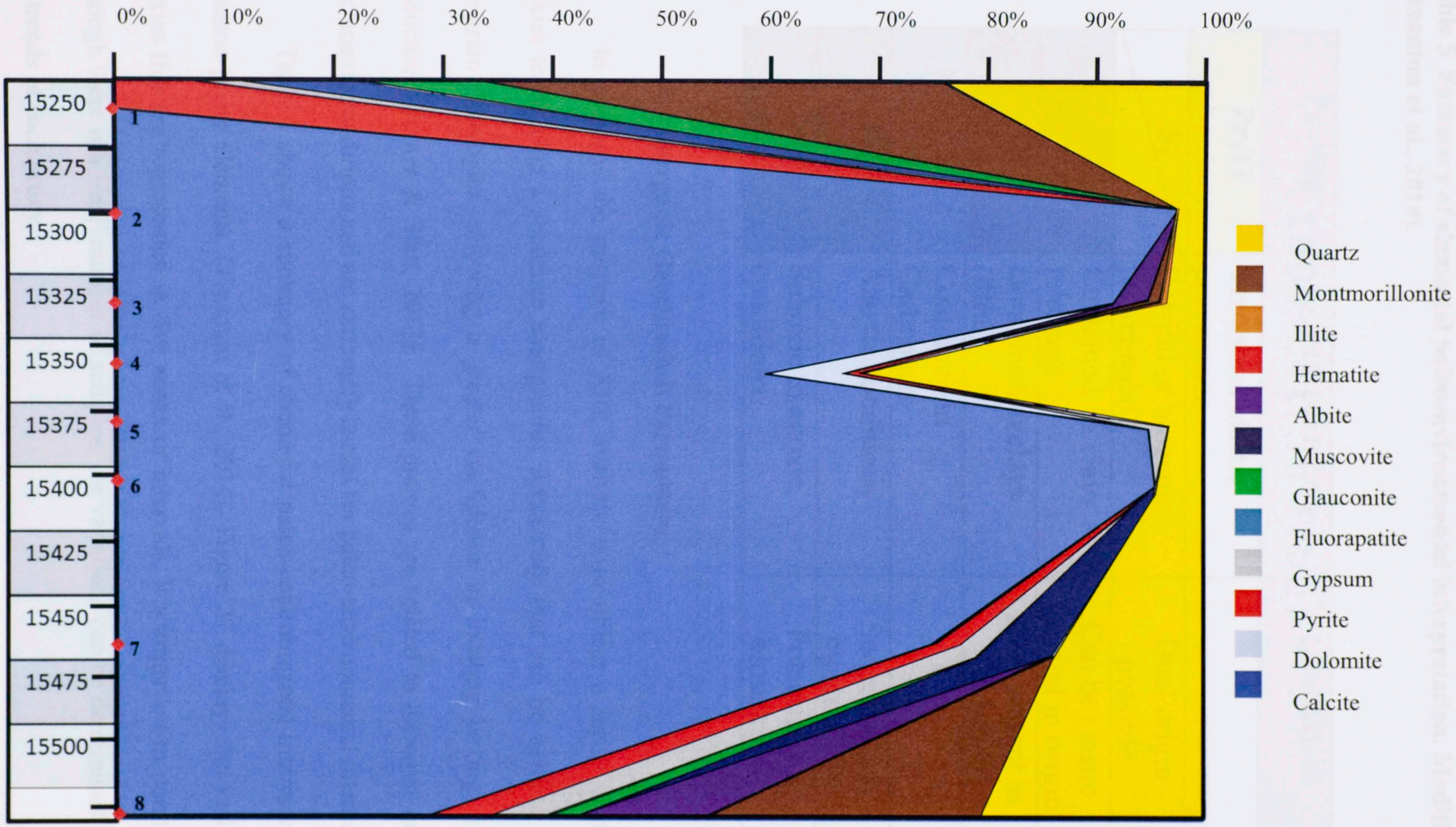

Figure 26 Representation of the dominant mineralogy of La Luna core 1X based on the samples performed with XRD

Table 5 Summary of elemental paleoenvironmental interpretation. Modified from (Treanton et al., 2014).

Proxies	Interpretation	Limitations
Zr,Ti	Terrestrial clastic provenance	
Si	Detrital or biogenic provenance	Dual origin possible
Al	Contained in clays and feldspars	Can be clastic detrital in origin
K	Contained in clays (illite)	Also present in feldspar
Mg, Ca, Sr	Contained in Carbonates	
Mo	Anoxic conditions	Sequestration mechanism
V	Suboxic to anoxic conditions	Potentially a bionutrient

4.4 Inorganic Geochemical Parameters

In geology, the purpose of XRF analysis is to utilize a series of elemental proxies to develop a sequence stratigraphic framework that can be used to correlate fine-grain lithologies, allowing a greater confidence in locating landing zones for production (Turner & Slatt, 2013). These proxies are related to different influx and oxic/anoxic conditions and are extremely useful for paleo-environmental interpretation.

Table 5 shows a summary of elemental paleo-environmental interpretation for common proxy elements. (Treanton et al., 2014). Figure 27 displays the variations in proxies that are represented in five zones or intervals. It's important to point out that although there is a small number of samples, the variations can be determined based on the trends of each proxy.

Interval I is characterized by a slight increment of clastic detrital content towards the top (Zr), the clastic input (Si/Al) is very low but when Si is compared with Ti for the estimation of biogenic input, clastic content increases in the first stages and then decreases to the top of interval I, Ti and Si increases when GR is Low. This suggests relatively important changes with respect to sediment input and hence either sea level and/or distance from sediment source. The clay influx represented by Al, and K highly suggest that K and Al are dominantly associated with detrital feldspars and/or illite. Carbonate content is high in the entire interval but Sr decreases in the uppermost area. Mo and V are present in the middle zone; a high peak is related with anoxic conditions because of a correlation with a high peak in the gamma ray response.

Interval II is characterized by a slight increase in Ti and Si; suggesting some biogenic input and biogenic calcite since these rocks are mainly carbonate. When Si/Al are compared, there is a small increase in the clastic input compared to interval I, but it's still low compared to the other intervals. The clay influx represented by Al, and K is lower and correlates in trend with the Mo and V which has a large peak in the middle that can be related with anoxic conditions correlating with the gamma ray response.

In interval III, elements like Ti and Zr that represent continental influx decrease dramatically. Al, K and Si are very low as well. An increase in biogenic silica is reflected in the Si/Al which undergoes a significant shift in base values. In contrast, the carbonate content remains very high and the Mo, V present low peaks that can be related with oxic conditions, showing a correlation with low peak responses in the gamma ray log.

Interval IV marks another change with all elemental base values shifting significantly. The continental input given by the Zr and Ti increase dramatically. K and Al also increase, which suggests a relative increase in the presence of detrital feldspars or clay. The carbonate content remains high, but there is cyclicity in the Sr that starts to decrease towards the top of Interval IV. The Mo and V increase again, indicating relatively anoxic conditions.

Interval V represents the Upper La Luna Formation (Tres Esquinas Member); the levels of Zr, Ti, P and specially K increase in a high rate. This suggests another increment of continental input. Phosphates are common. In contrast, the Mo and V decrease, suggesting oxic conditions. Figure 28 represents the mineralogy of La Luna core 1X based on the samples performed with XRF; when compared with the XRD (figure 26) the same trend is evident.

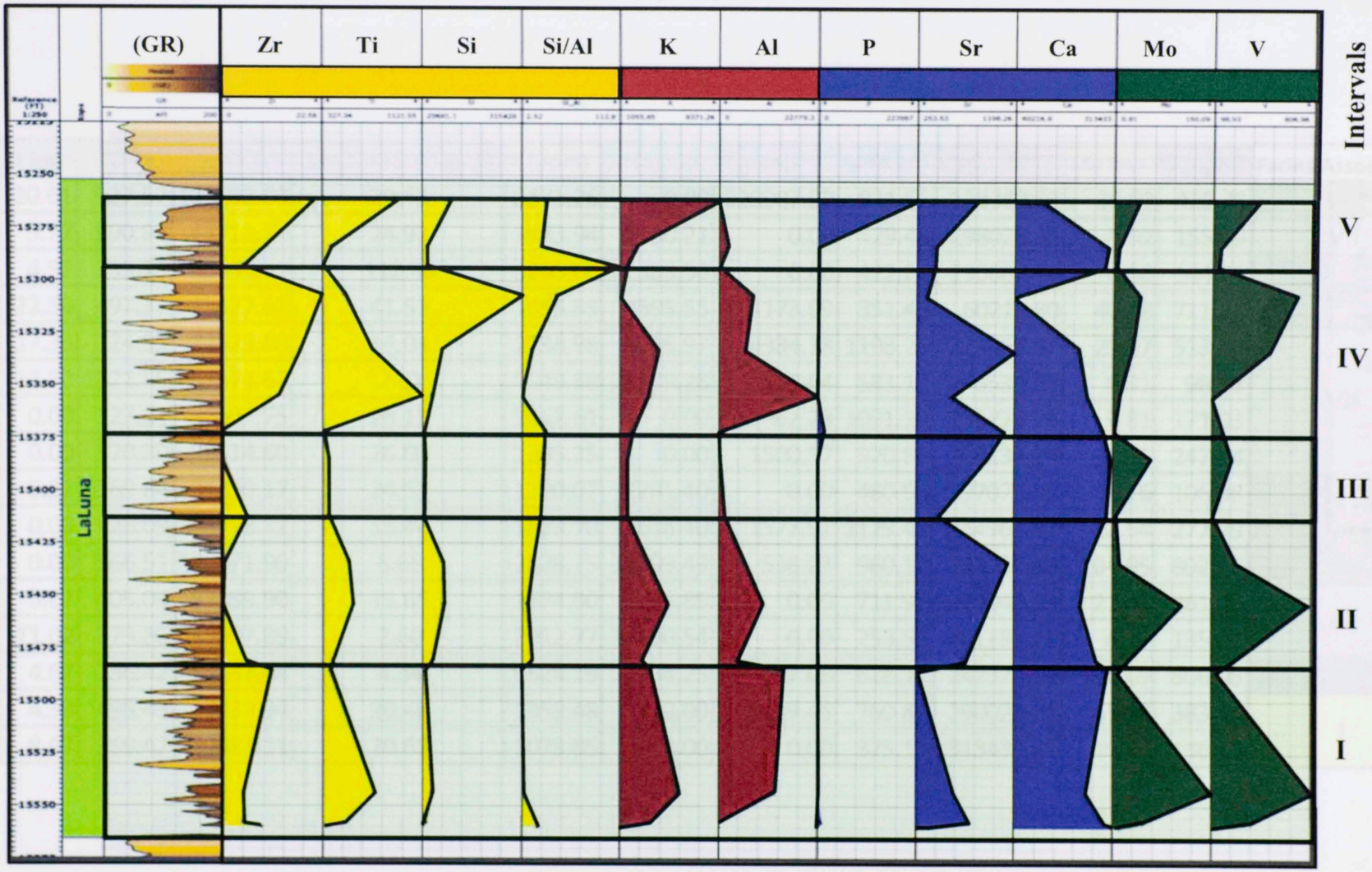

Figure 27 XRF and GR Profile of La Luna 1X (Lower; Middle and Upper La Luna Formation)

Table 6 Elemental composition in parts per million in the samples performed for XRF and facies associated in the 1X La Luna core

Depth	Zr (ppm	Ti (ppm)	Si (ppm)	Interpretted Si/Al	K (ppm)	Al (ppm0	P (ppm)	Sr (ppm)	Ca (ppm)	Mo (ppm	V (ppm)	Facies Association
15272	20.61	927.57	109192.80	29.43	8371.26	0.00	223987.23	831.66	128340.53	36.60	420.78	VIII
15294	9.77	390.81	43711.22	24.97	1473.94	1750.21	0.00	429.48	298026.66	5.92	155.09	VII
15303	4.52	333.13	43492.41	112.80	1200.00	385.56	0.00	422.26	290867.95	6.50	144.21	VI
15317	22.58	497.37	315427.62	41.53	1055.85	7595.55	1173.09	351.42	60216.80	40.48	711.11	
15343	17.35	724.95	87423.88	14.04	2338.96	6225.97	4334.18	1198.26	223464.67	29.97	513.67	VII
15365	12.50	1121.55	57474.62	2.52	1949.68	22779.28	157.54	583.10	245539.53	8.31	98.93	
15382	0.00	327.34	36907.75	28.19	1342.61	0.00	10962.28	1091.19	286774.76	0.81	171.03	
15395	0.00	370.30	38514.60	26.00	1205.35	0.00	1500.57	920.92	303137.89	57.95	247.84	
15422	5.27	369.84	31410.17	24.51	1220.07	1281.40	0.00	460.98	297075.85	6.16	106.98	V
15444	0.00	528.09	86728.12	15.44	1853.70	5616.40	1577.91	1129.43	244961.87	11.54	277.79	
15464	0.00	566.51	88671.90	8.69	2828.75	10199.49	538.23	960.12	228734.48	104.95	802.86	
15491	5.07	405.09	57839.90	13.65	1674.00	4235.89	0.00	711.97	274040.53	21.47	261.49	IV
15496	11.02	379.86	38697.89	2.60	2012.77	14900.54	0.00	253.53	301131.27	6.17	135.22	
15554	4.67	736.42	55283.84	4.34	3524.19	12734.25	977.08	628.11	242378.10	150.09	806.96	II
15568	4.39	498.43	40837.94	20.48	1959.48	0.00	9119.45	760.84	290020.21	45.78	383.14	I
15570	8.67	359.42	29681.11	20.65	1078.85	0.00	0.00	375.19	313433.21	10.88	136.12	

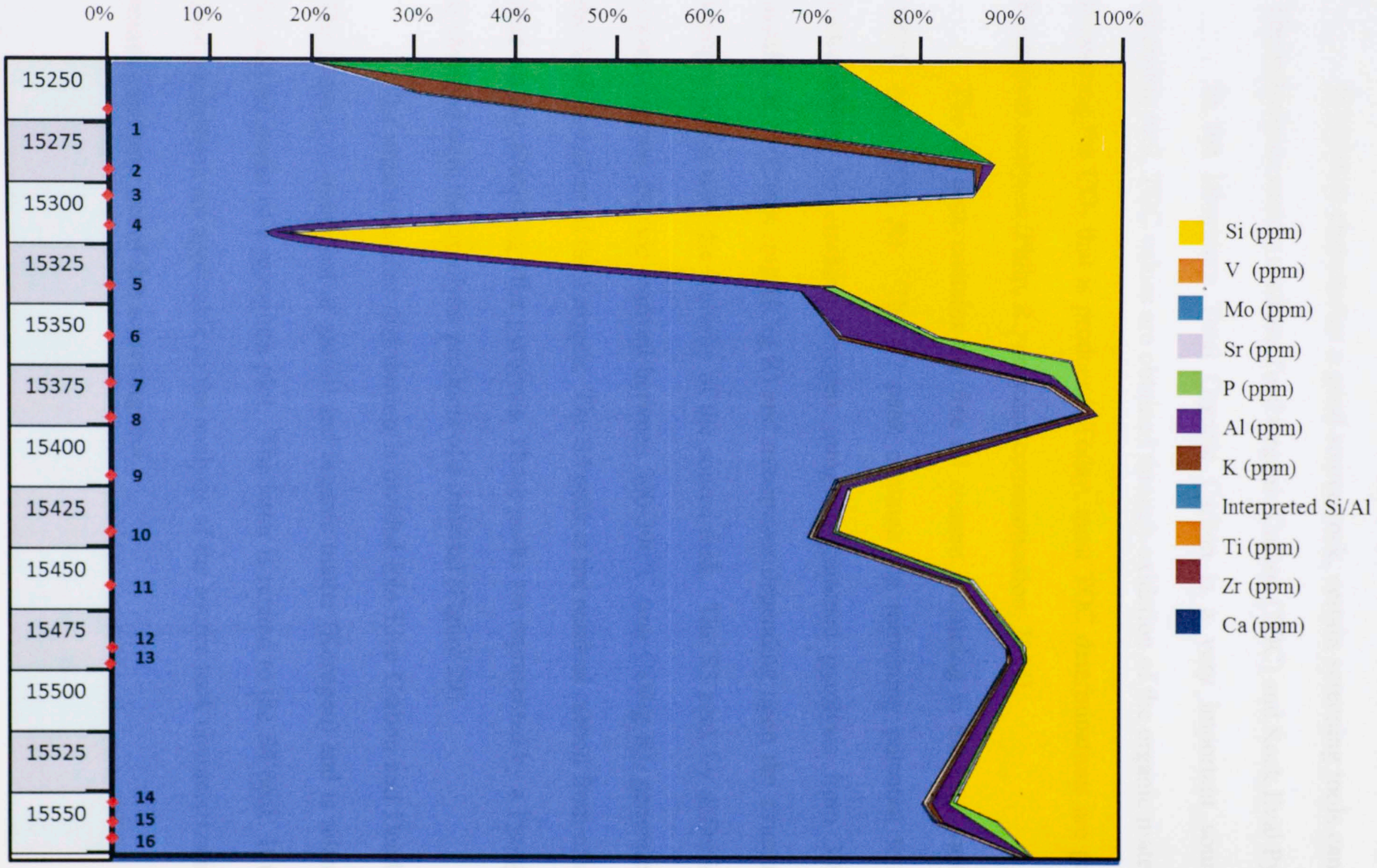

Figure 28 Representation of the dominant elemental composition of The La Luna core 1X based on the samples performed with XRF.

4.5 Organic Geochemical Parameters and analyses

In order to characterize a good source rock, certain screening tools can be used. The techniques mostly used are Total Organic Carbon (TOC) and Rock Eval Pyrolysis.

In the laboratory Total Organic Carbon is a very important source rock-screening tool. TOC values are obtained through oxidation of the organic material, then measuring the CO_2 that is produced. Today, most TOC determinations are part of the Rock Eval analyses (Philp, R.; personal communication. 2014).

The S1 peak contains the free oil content remaining in the rock vaporized at 300°C (mg HC/g R). The S2 peak contains the remaining potential to generate hydrocarbons by cracking kerogen using programmed pyrolysis from 300-600°C, usually at 25°C/min (mg HC/g R) and maximizes depending upon the structure of the kerogen along with the maturity of the source rock. The S3 peak by definition is the organic carbon dioxide evolved between 300-390°C (mg CO2/g R), generated during the decomposition of the kerogen. The S4 peak is the residual carbon from oxidation of dead carbon remaining after pyrolysis. These peaks are represented by a Pyrogram that is obtained from the pyrolysis products of a material (Figure 29).

The organic matter distribution is divided into Live Carbon and Dead Carbon. The former, is composed of gas/oil and organic matter (Kerogen) and is related to the S1 and S2 peaks of a pyrogram plot. The latter is related to the S4 peak. If the Rock Eval parameters are applicable to the analysis of the source rock characterization, good results can come out of this screening tool.

In the same manner, other parameters are linked to the S1, S2, S3, and S4 peaks. The Tmax parameter is the temperature of maximum evolution of the S2 hydrocarbons and an indication of thermal maturity (°C). Also, using these three parameters (S1, S2 and S3) together with the TOC content of the sample, two important parameters are developed (Philp, 2014). The former is the hydrogen index; (HI) which is the S2 peak normalized to the TOC and gives a measure of the amount of kerogen in the rock and indirectly the hydrogen content. The latter is the oxygen index, (OI) which is the S3 peak normalized to the TOC and shows a measure of the organic oxygen content of the kerogen. Lastly, the production index (PI) is the ratio of S1 to S1+S2.

S1 and PI increases with maturation and most reservoirs have very high (anomalous) PI values. The TOC in the La Luna Formation samples were measured using the Leco TOC, Rock-Eval-2, and Maturity Testing generated by Geomark Research Laboratories. Twenty samples were taken at depths that show variance in lithology and organic matter.

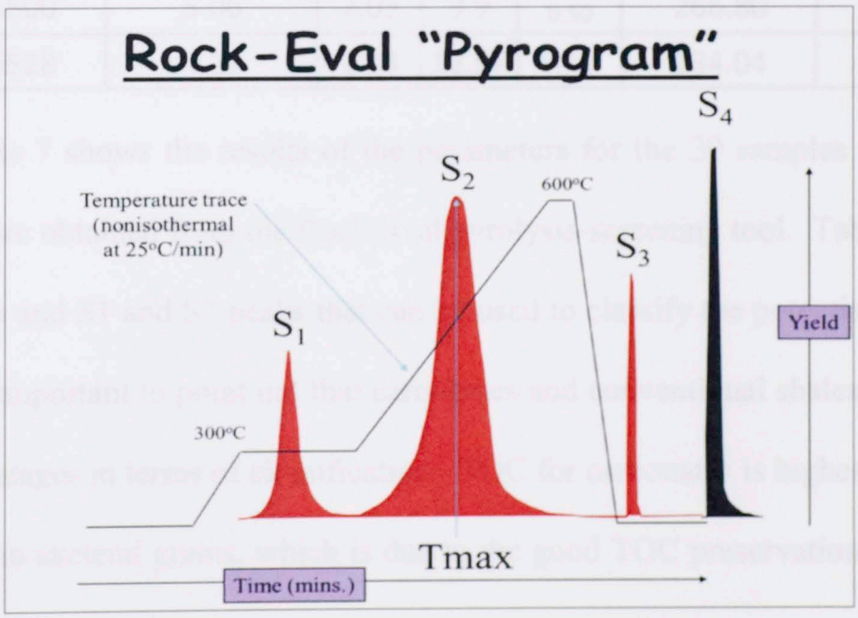

Figure 29 Pyrogram that represents the distribution of Organic Matter in Rock. From Philp, R. 2014.

Table 7 Results of the Rock Eval Parameters from La Luna 1X core

Depth	TOC Leco (%wt)	S1	S2	S3	Hydrogen Index (S2x100/TOC)	Oxygen Index (S3x100/TOC)
15267	0.98	0.42	0.72	0.37	73.62	37.83
15274	4.74	2.82	20.37	0.62	429.75	13.08
15278	3.85	1.61	15.13	0.54	392.99	14.03
15280	4.4	1.9	18.76	0.63	426.36	14.32
15287	4.43	1.92	17.18	0.61	387.81	13.77
15300	0.88	0.22	2.1	0.25	238.91	28.44
15314	4.12	1.75	12.7	0.55	308.25	13.35
15334	0.84	0.41	3.28	0.47	388.63	55.69
15342	0.75	0.67	2.13	0.54	284.00	72.00
15351	6.44	2.93	21.04	0.90	326.71	13.98
15357	9.13	5.4	38.26	1.06	419.06	11.61
15376	0.22	0.07	0.28	0.15	125.56	67.26
15378	3.87	2.09	19.88	0.63	305.94	16.28
15401	6.12	1.99	11.84	0.84	324.84	13.73
15415	4.78	1.92	12.02	0.66	251.49	13.81
15430	6.16	4.64	22.38	0.93	363.31	15.10
15444	4.07	1.96	10.11	0.67	248.40	16.46
15469	5.11	0.99	13.5	0.55	245.99	10.76
15500	5.06	2.03	9.9	0.50	266.80	9.88
15528	4.23	1.14	12.57	0.59	234.04	13.95

Table 7 shows the results of the parameters for the 20 samples taken from La Luna 1X core obtained from the Rock Eval pyrolysis-screening tool. Table 8 shows the TOC values and S1 and S2 peaks that can be used to classify the potential of the source rocks. It is important to point out that carbonates and conventional shales have different TOC percentages in terms of classification. TOC for carbonates is highest in lime muds and lowest in skeletal grains, which is due to the good TOC preservation in low energy areas (coastal areas).

Table 8 Geochemical parameters used for the evaluation of a source rock potential in carbonates and conventional shales. From Philp, R. 2014.

TOC (wt %) (Shales)	TOC (wt %) (Carbonates)	S1	S2	Quantity
0.00 – 0.50	0.00 – 0.12	0 – 0.5	0 -2.5	Poor
0.50 – 1.00	0.12 – 0.25	0.5 - 1	2.5 - 5	Fair
1.00 – 2.00	0.25 – 0.50	1-2	5 - 10	Good
2.00 – 4.00	0.50 – 1.00	2+	10+	Very Good
4.00 – 8.00	1.00 – 2.00			Excellent
8.00 +	2.00+			

Table 8 and Figure 30 show that Total Organic Carbon (TOC) is generally lower in carbonates. Carbonates will have more potential to generate oils at lower TOC values since the oil is more readily expelled from carbonates than shales. (Philp, 2014). Also figure 31 shows that the amount of TOC is lower when compared with the percent of carbonates in the samples. The trend shows that the La Luna 1X core is composed of almost 95 % carbonates in the Middle La Luna Fm.

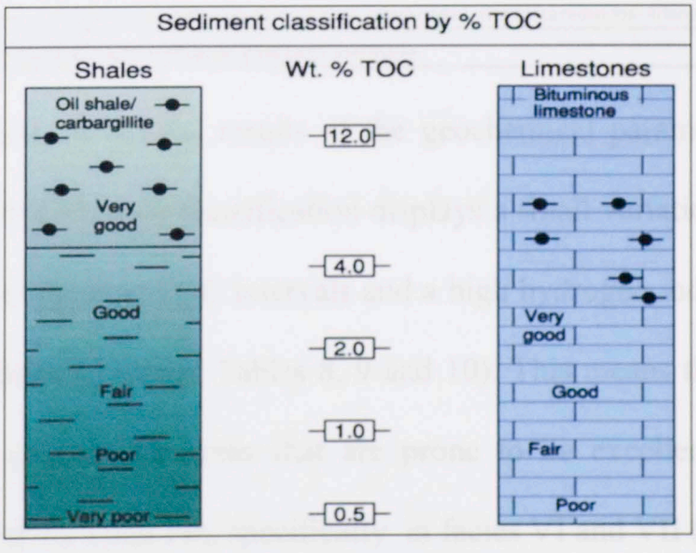

Figure 30 Total Organic Carbon (TOC) is generally lower in carbonates because of better expulsion. From Philp, R. 2014.

Table 9 Source rock parameters, facies associated and results using the carbonate classification in the samples of la Luna 1X core

Depth	TOC(%wt)	s1	s2	S3	Hydrogen Index (S2x100/TOC)	Oxygen Index (S3x100/TOC)	Production Index (S1/(S1+S2)	Facies
15267	0.98	0.42	0.72	0.37	73.6196319	37.8323108	0.3684211	VIII
15274	4.74	2.82	20.37	0.62	429.746835	13.0801688	0.1216041	
15278	3.85	1.61	15.13	0.54	392.987013	14.025974	0.0961768	
15280	4.40	1.90	18.76	0.63	426.363636	14.3181818	0.0919652	VII
15287	4.43	1.92	17.18	0.61	387.810384	13.7697517	0.1005236	
15300	0.88	0.22	2.10	0.25	238.90785	28.4414107	0.0948276	
15314	4.12	1.75	12.70	0.55	308.252427	13.3495146	0.1211073	VI
15334	0.84	0.41	3.28	0.47	388.625592	55.6872038	0.1111111	
15342	0.75	0.67	2.13	0.54	284	72	0.2392857	
15351	6.44	2.93	21.04	0.90	326.708075	13.9751553	0.1222361	
15357	9.13	5.40	38.26	1.06	419.05805	11.6100767	0.123683	
15376	0.22	0.07	0.28	0.15	125.560538	67.264574	0.2	VII
15378	3.87	2.09	19.88	0.63	305.943152	16.2790698	0.1438901	
15401	6.12	1.99	11.84	0.84	324.836601	13.7254902	0.0951297	
15415	4.78	1.92	12.02	0.66	251.485356	13.8075314	0.1377233	
15430	6.16	4.64	22.38	0.93	363.311688	15.0974026	0.1717246	
15444	4.07	1.96	10.11	0.67	248.402948	16.4619165	0.1623861	V
15469	5.11	0.99	13.50	0.55	245.988258	10.7632094	0.083151	
15500	5.06	2.03	9.90	0.50	266.798419	9.88142292	0.068323	IV
15528	4.23	1.14	12.57	0.59	234.042553	13.9479905	0.1701593	

	Fair
	Very Good
	Excellent
IV	Laminated mudstone with limestone concretions and micropackstone
V	Siliceous- calcareous laminated mudstone interbedded with black chert filled with calcite veins
VI	VI. Siliceous- Calcareous mudstone interbedded with wackstone facies
VII	Slightly siliceous- calcareous laminated black mudstone interbedded with calcareous fossiliferous wackstone.
VIII	Siliceous green mudstone with authigenic glauconite and Pyrite

Tables 9 and 10 list the results of the geochemical parameters using the two classifications. This carbonate classification displays a small variation in the richness of the source rock, but the best TOC intervals and a high hydrogen index are consistent in the two classifications (compare Tables 8, 9 and 10). This means that according to the results, the most prospective areas that are prone to be excellent source rocks are located in the Upper La Luna Fm, specifically in facies VI and VII (Figure 32 and 33).

It is important to point out that it wasn't possible to take samples for geochemistry analysis for depths from the interval 15581'- 15548 (facies I, II, and III described in the core), thus it is difficult to geochemically relate the first three facies. According to the TOC richness results, and thin sections (specifically 15444'-15464' interval, see Table 12) facies V (Laminated mudstone interbedded with black chert filled with calcite veins) is the more prospective facies that shows a good source rock potential since it represents the highest TOC.

However, figures 34 and 35 in the Rock Eval pyrograms (which provide information about the maturity of the organic matter present in the rock), shows that even with organic matter richness that is classified as "Excellent" in the TOC, the S1, S2, S3, and S4 peaks show that they aren't the best intervals. Thus, it is important to be very careful when looking at the peaks because Rock Eval analyses are not just a representation of the number of the TOC values by itself but also, maturity is very important.

From the pyrograms, the best intervals of potential oil generation are present in facies VI and VII. The organic matter content is also shown in the thin section intervals (15382'; 15372; 15365; 15317; 15303; 15294) where facies VII is present as well (see Table 12). Lowest values may occur in the middle section of the La Luna core due to the alternation of chert and shales that affect the Rock Eval results.

Table 10 Source rock parameters, associated facies and results using the shale classification in the samples of la Luna 1X core

Depth	TOC Leco (%wt)	s1	s2	S3	Hydrogen Index (S2x100/TOC)	Oxygen Index (S3x100/TOC)	Production Index (S1/(S1+S2)	Facies
15267	0.98	0.42	0.72	0.37	73.6196319	37.8323108	0.3684211	VIII
15274	4.74	2.82	20.37	0.62	429.746835	13.0801688	0.1216041	VII
15278	3.85	1.61	15.13	0.54	392.987013	14.025974	0.0961768	
15280	4.40	1.90	18.76	0.63	426.363636	14.3181818	0.0919652	
15287	4.43	1.92	17.18	0.61	387.810384	13.7697517	0.1005236	
15300	0.88	0.22	2.10	0.25	238.90785	28.4414107	0.0948276	VI
15314	4.12	1.75	12.70	0.55	308.252427	13.3495146	0.1211073	
15334	0.84	0.41	3.28	0.47	388.625592	55.6872038	0.1111111	
15342	0.75	0.67	2.13	0.54	284	72	0.2392857	VII
15351	6.44	2.93	21.04	0.90	326.708075	13.9751553	0.1222361	
15357	9.13	5.40	38.26	1.06	419.05805	11.6100767	0.123683	
15376	0.22	0.07	0.28	0.15	125.560538	67.264574	0.2	
15378	3.87	2.09	19.88	0.63	305.943152	16.2790698	0.1438901	
15401	6.12	1.99	11.84	0.84	324.836601	13.7254902	0.0951297	
15415	4.78	1.92	12.02	0.66	251.485356	13.8075314	0.1377233	V
15430	6.16	4.64	22.38	0.93	363.311688	15.0974026	0.1717246	
15444	4.07	1.96	10.11	0.67	248.402948	16.4619165	0.1623861	
15469	5.11	0.99	13.50	0.55	245.988258	10.7632094	0.083151	
15500	5.06	2.03	9.90	0.50	266.798419	9.88142292	0.068323	IV
15528	4.23	1.14	12.57	0.59	234.042553	13.9479905	0.1701593	

	Poor
	Fair
	Very Good
	Excellent
IV	Laminated mudstone with limestone concretions and micropackstone
V	Siliceous- calcareous laminated mudstone interbedded with black chert filled with calcite veins
VI	VI. Siliceous- Calcareous mudstone interbedded with wackstone facies
VII	Slightly siliceous-calcareous laminated black mudstone interbedded with calcareous fossiliferous wackstone.
VIII	Siliceous green mudstone with authigenic glauconite and Pyrite

3.4.1 Source Potential logs

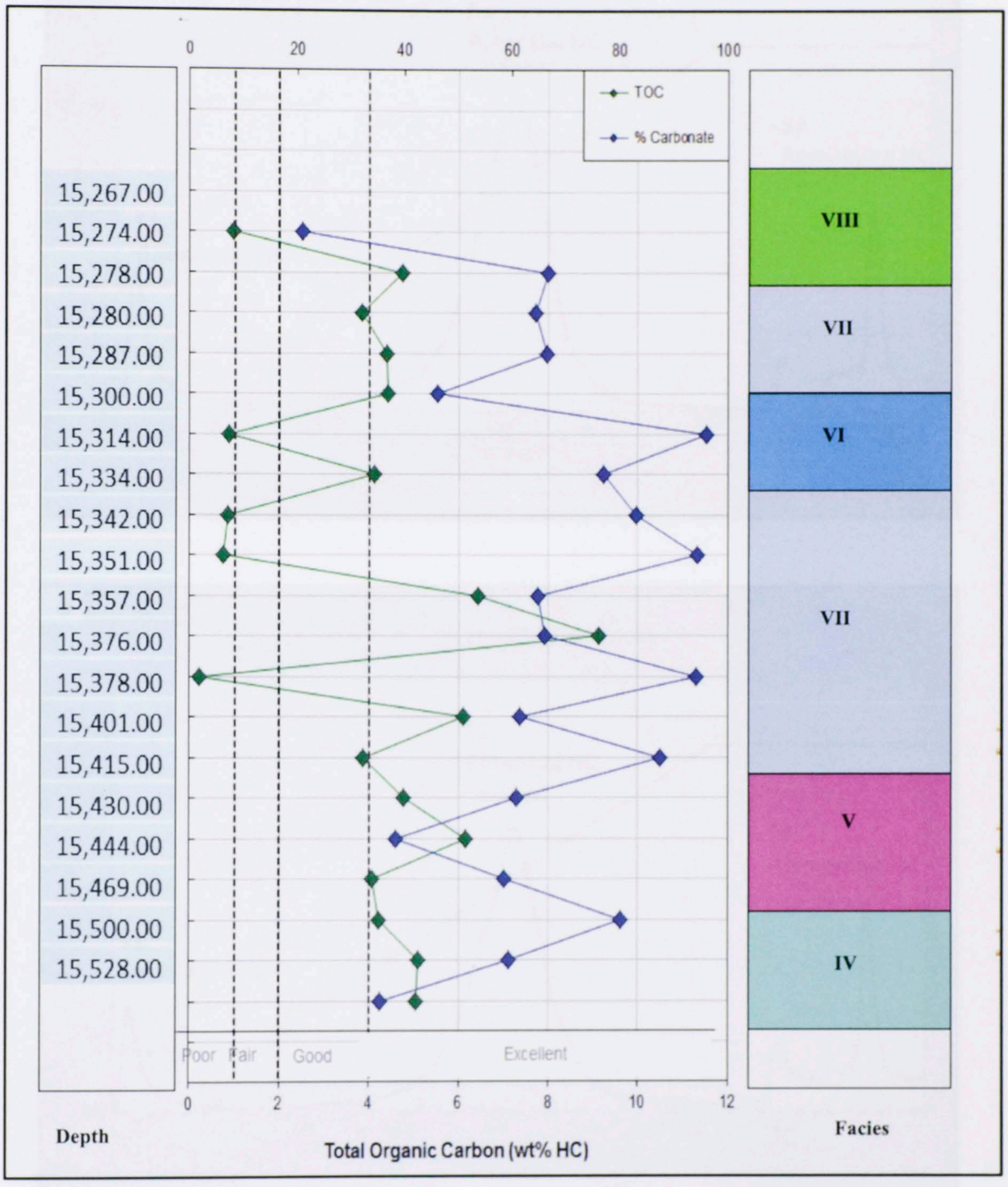

Figure 31 Plot that shows the amount of TOC and Carbonates in la Luna 1X core. Green diamonds represent the TOC content and blue diamonds represent the percent of carbonates.

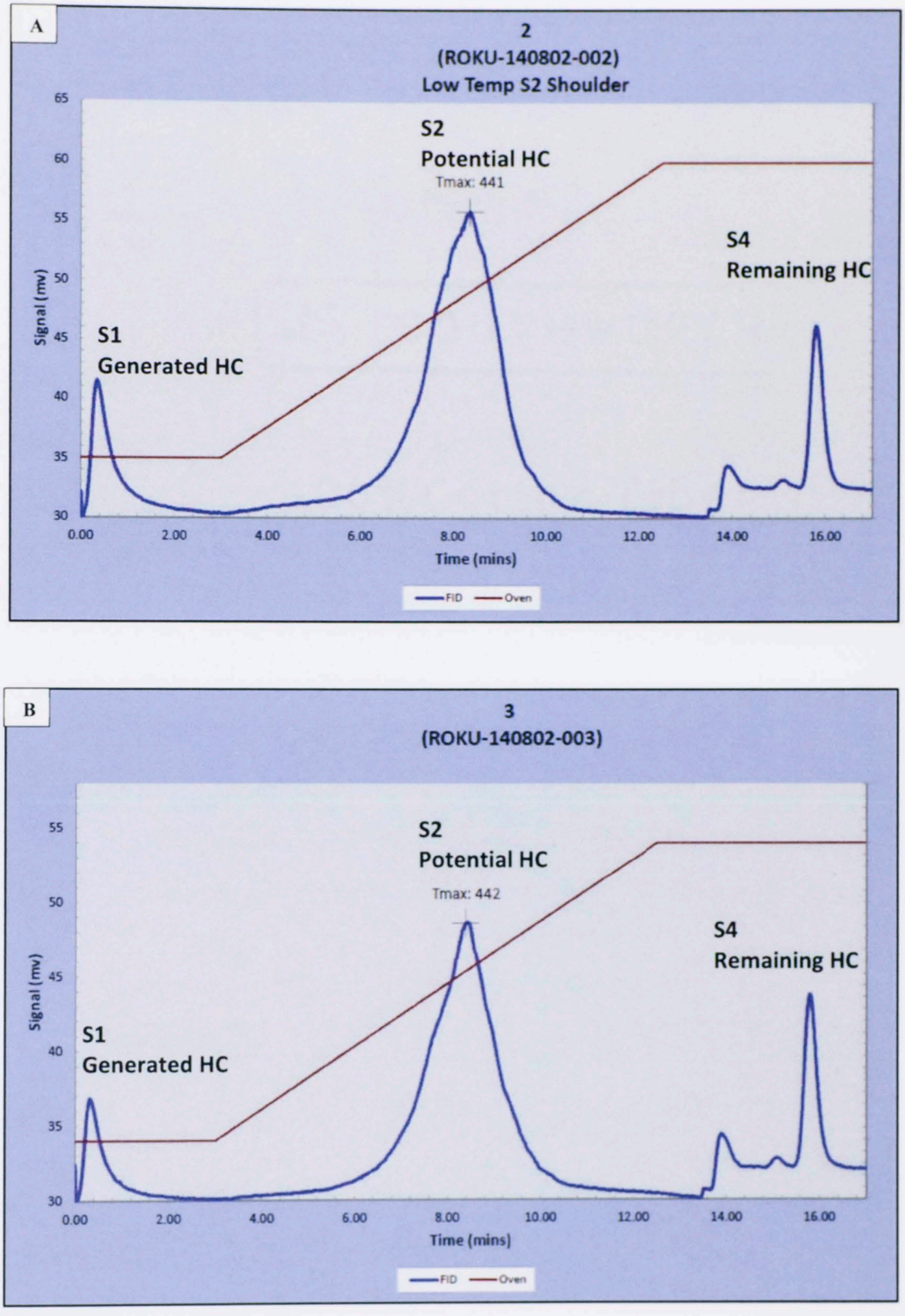

Figure 32 Pyrogram plots from La Luna 1x core showing the best intervals of Potential Hydrocarbon in Facies VII (La Luna Upper interval) A) Plot at 15274' B) Plot at 15278'.

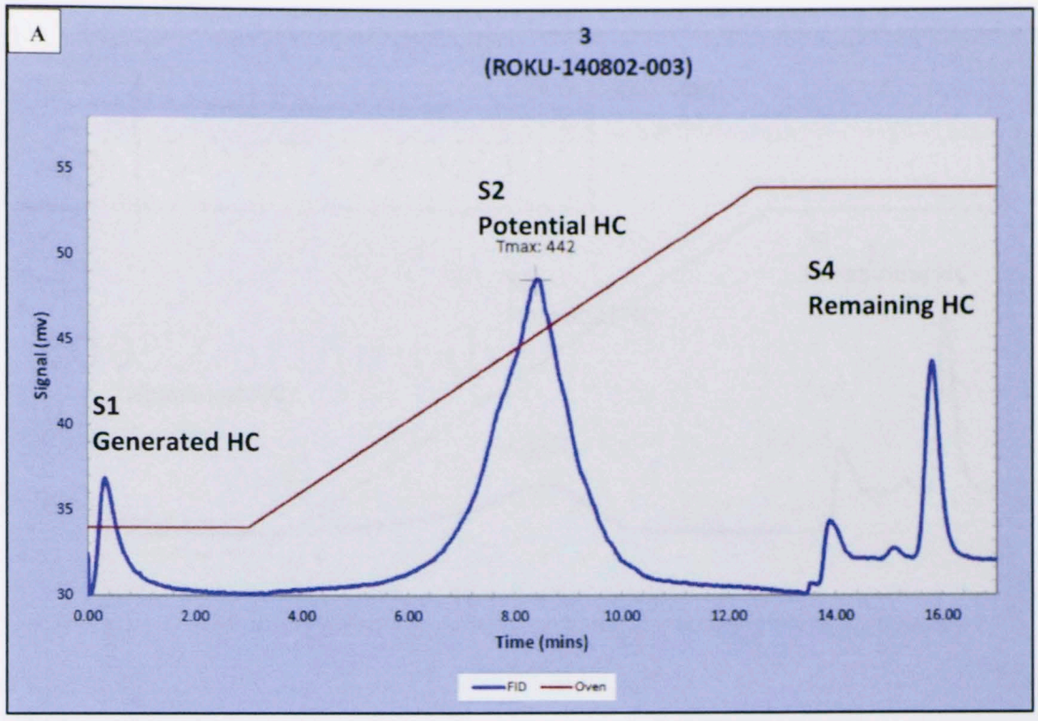

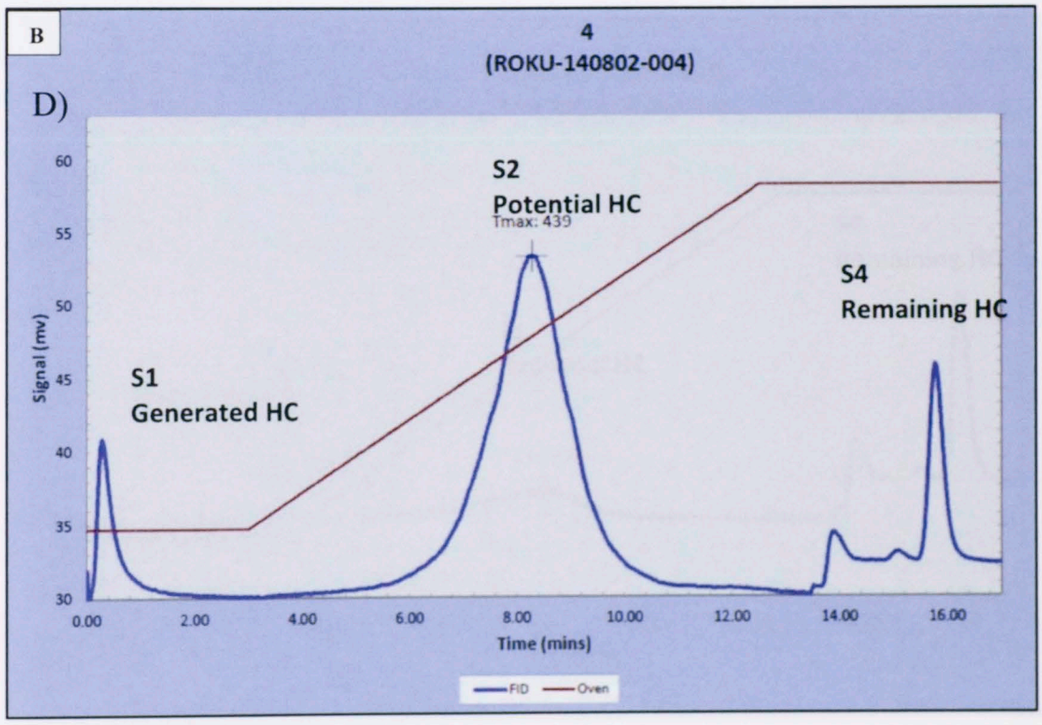

Figure 33 Pyrogram plots from La Luna 1x core showing the best intervals of Potential Hydrocarbon context in Facies VII (La Luna upper interval) A) Plot at 15278' B) Plot at 15280'.

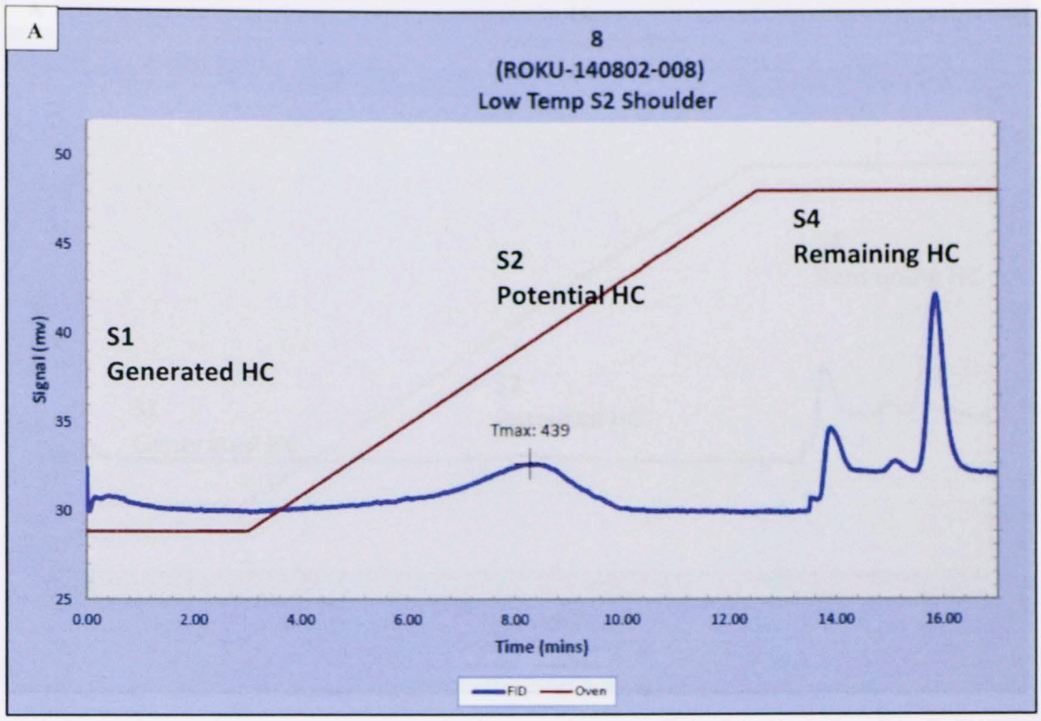

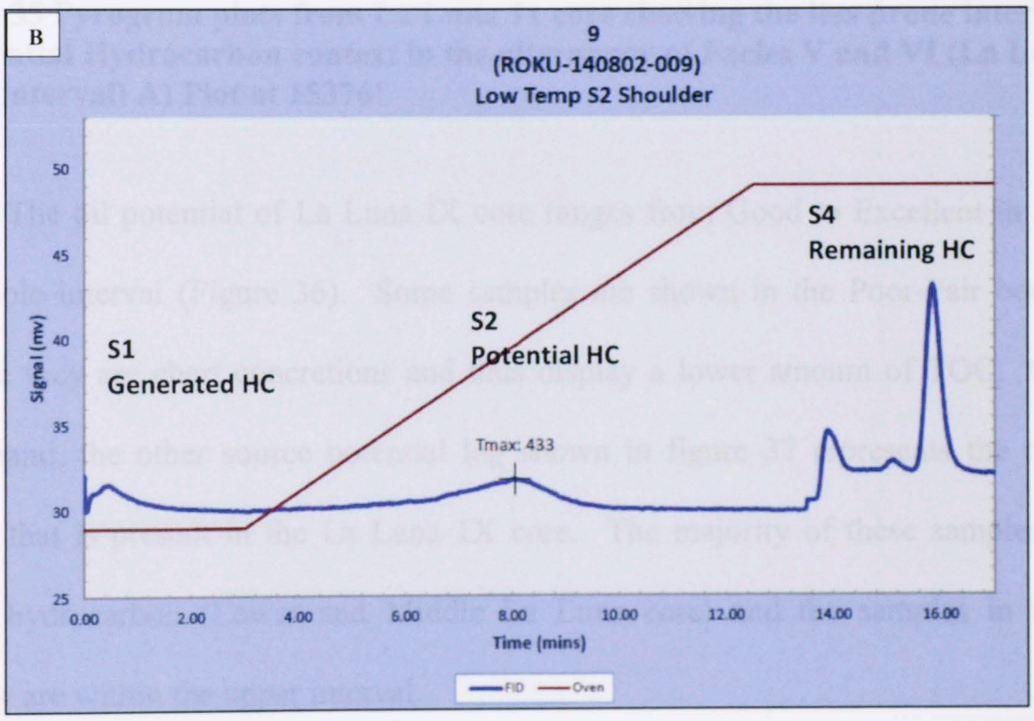

Figure 34 Pyrogram plots from La Luna 1x core showing the less prone intervals of Potential Hydrocarbon in Facies V(La Luna upper interval) A) Plot at 15334' B) Plot at 15342'.

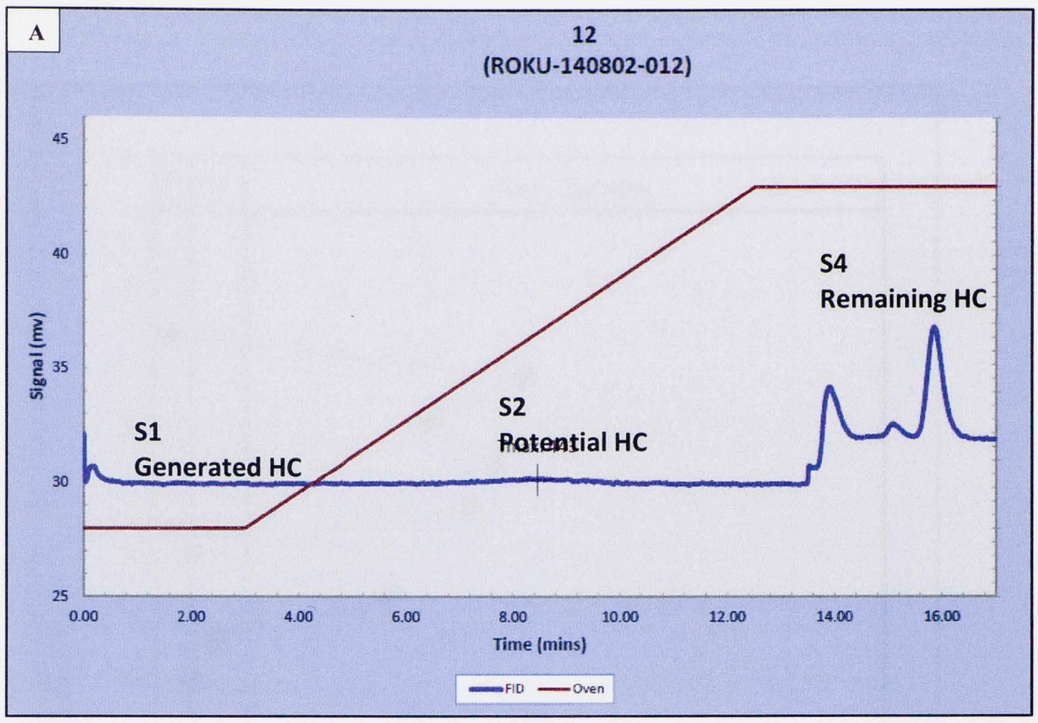

Figure 35 Pyrogram plots from La Luna 1x core showing the less prone intervals of Potential Hydrocarbon context in the alternancy of Facies V and VI (La Luna upper interval) A) Plot at 15376'

The oil potential of La Luna IX core ranges from Good to Excellent in almost the whole interval (Figure 36). Some samples are shown in the Poor-Fair boundary because they are chert concretions and thus display a lower amount of TOC. On the other hand, the other source potential log shown in figure 37 represents the type of oil/gas that is present in the La Luna 1X core. The majority of these samples are a mixed hydrocarbon (Lower and Middle La Luna core) and the samples in the oil window are within the upper interval.

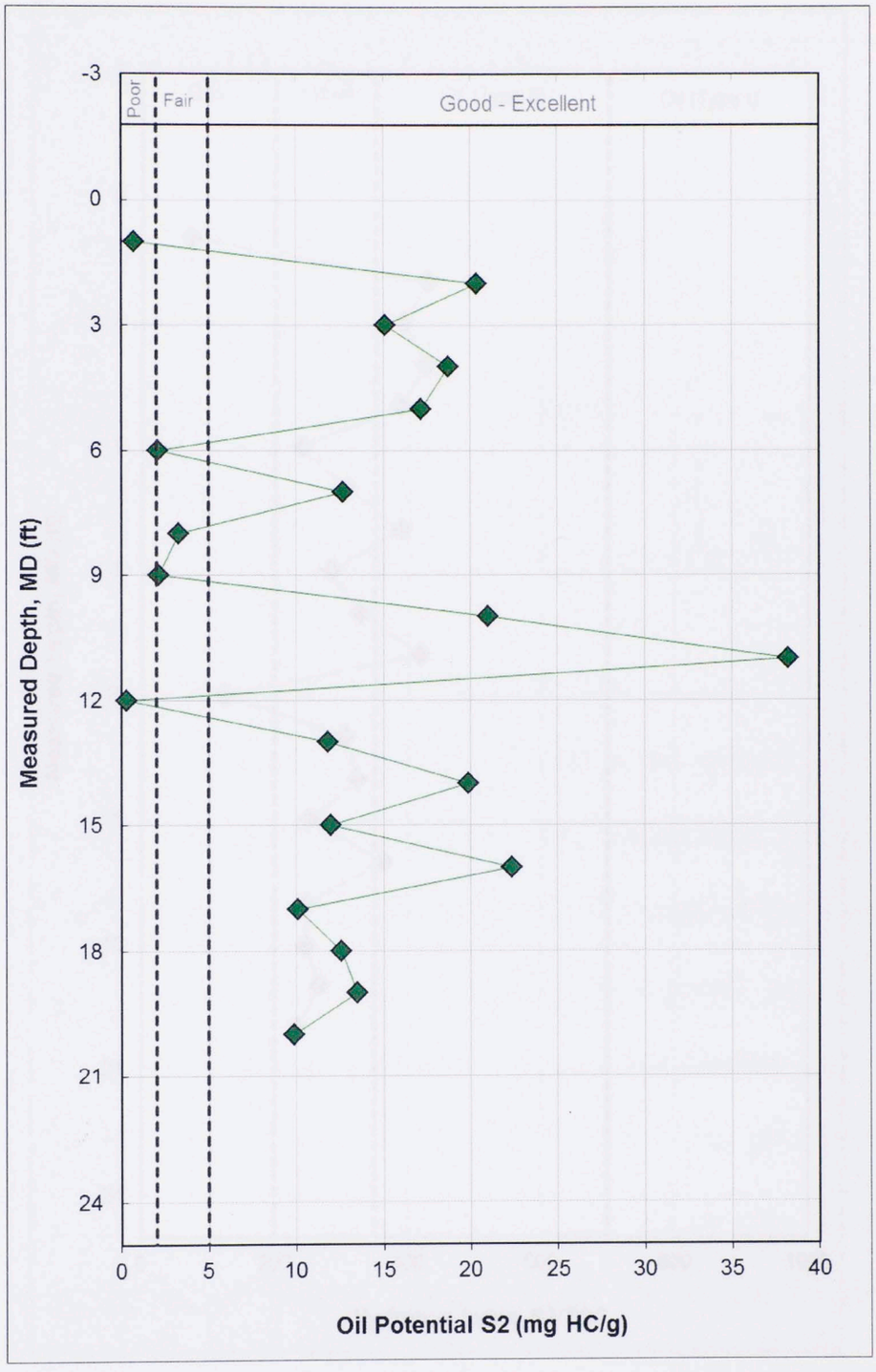

Figure 36 Source Potential logs showing the relationship of the S2 peak between the TOC and the oil potential quality with depth.

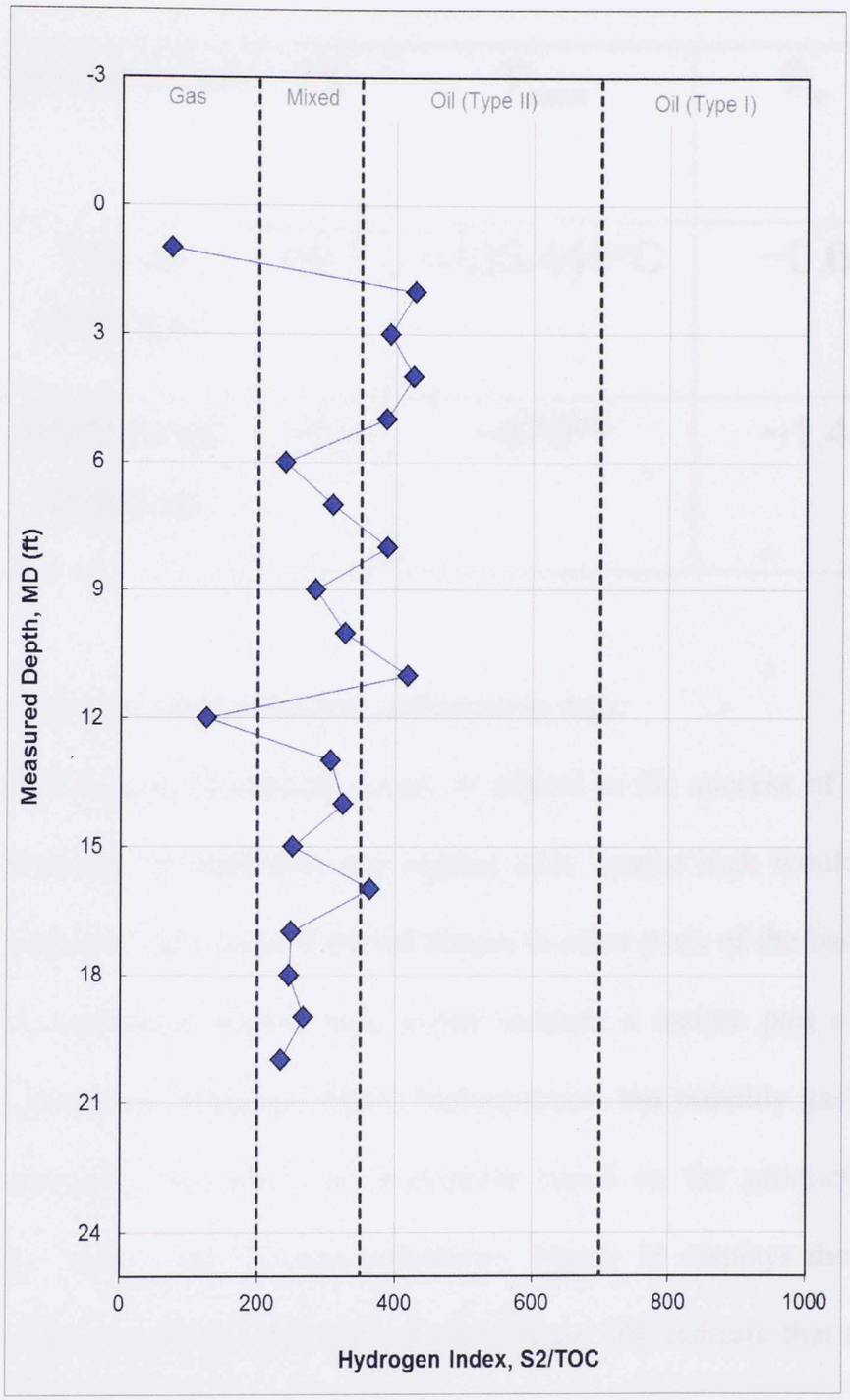

Figure 37 Source Potential logs showing the relationship between the S2 peak between the TOC with depth.

Table 11 Maturation parameters of a source rock classification; Production index; Tmax and Vitrinite reflectance. From Philp, R. 2014.

Maturation	PI	T_{max}	R_o
Top oil Window	~0.1	~435-445°C	~0.6
Bottom oil Window	~0.4	~470°C	~1.4

3.4.2 Hydrocarbon indicators and maturity logs:

"Determination of maturity levels is critical to the success of any exploration program. Recovery of immature, but organic rich, source rock would indicate good source potential for such rocks if buried deeper in other parts of the basin. At the other extreme, an overmature source rock would indicate a mature part of the basin not capable of generating additional liquid hydrocarbons, but possibly gas" (Philp, 2014). Table 11 represents the levels of maturation based on the production index (PI= S1/(S1+S2). , Tmax, and Vitrinite reflectance. Figure 38 displays the normalized oil content for different depths (S1/TOC). Levels below 100 indicate that the La Luna 1X core is mostly early mature with a high carbonate content from 40 to almost 95 percent. The production index (figure 39) ranges from 0.10-0.30 up to 0.40 in the shallowest sample, which means that most of the samples are in the oil window.

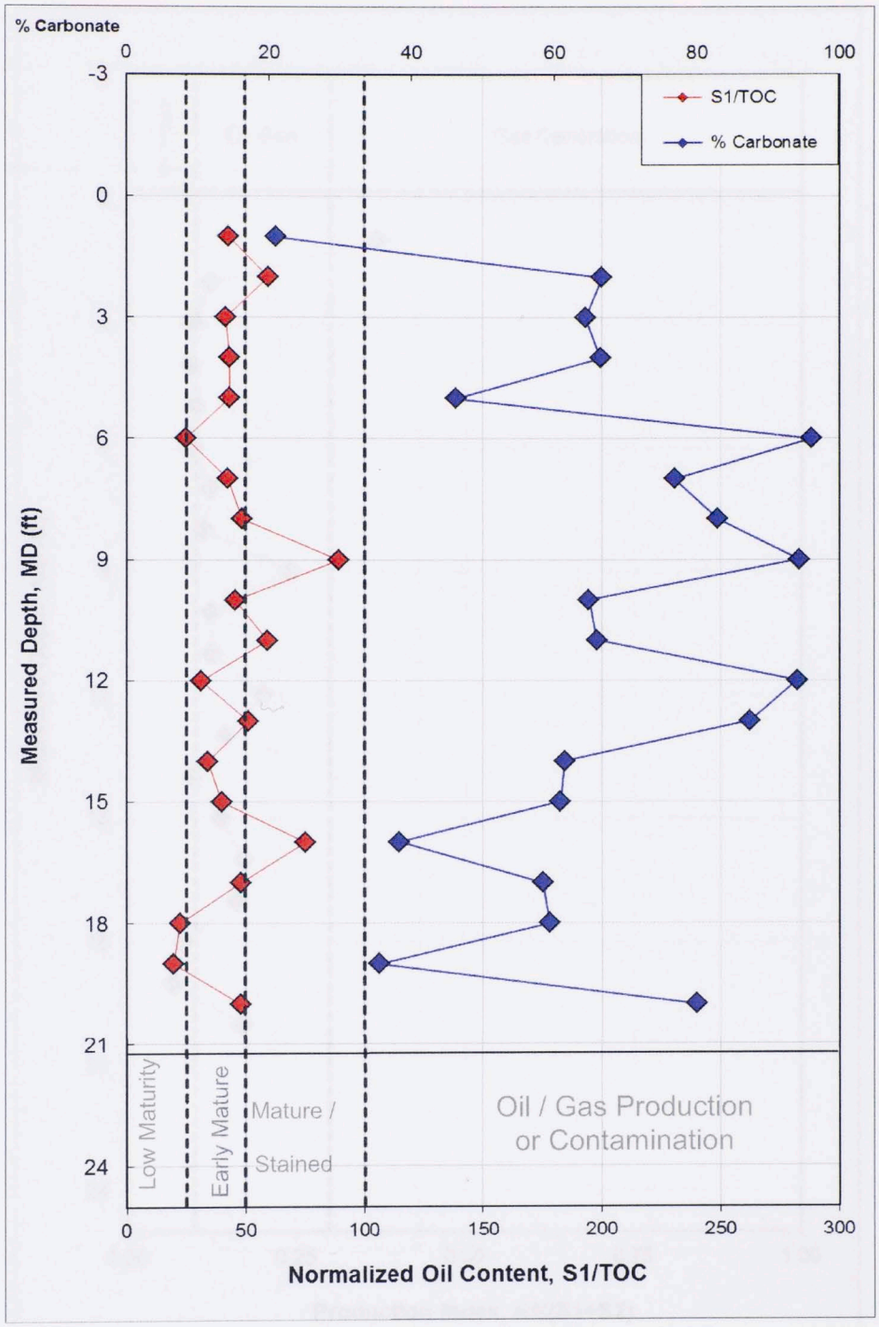

Figure 38 Source Potential logs showing the relationship between the S1 peak/ TOC and the percent of carbonates with depth.

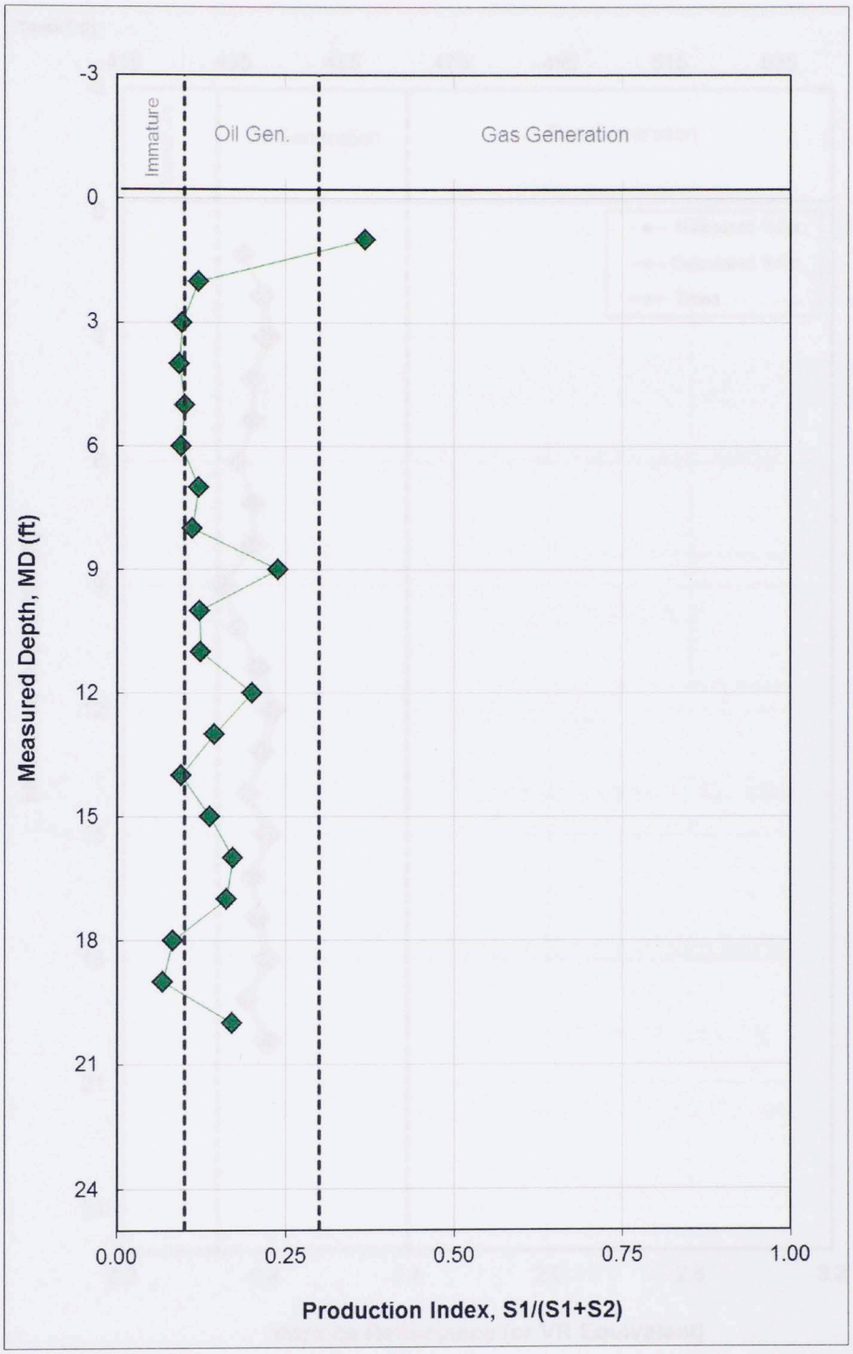

Figure 39 Source Potential logs showing the production index changes of La Luna 1X core with depth.

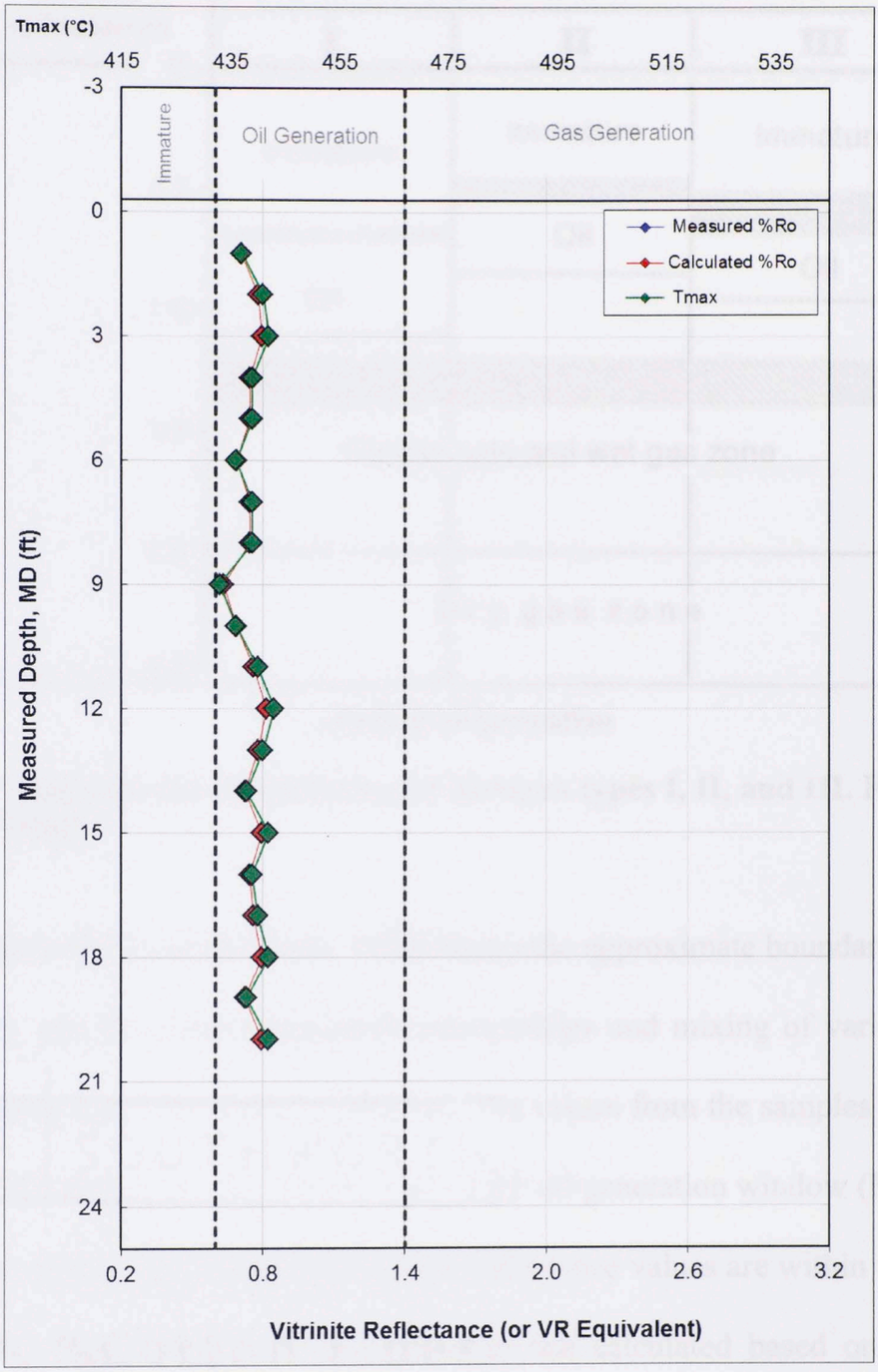

Figure 40 Source Potential logs showing Vitrinite reflectance changes of La Luna 1X core with depth.

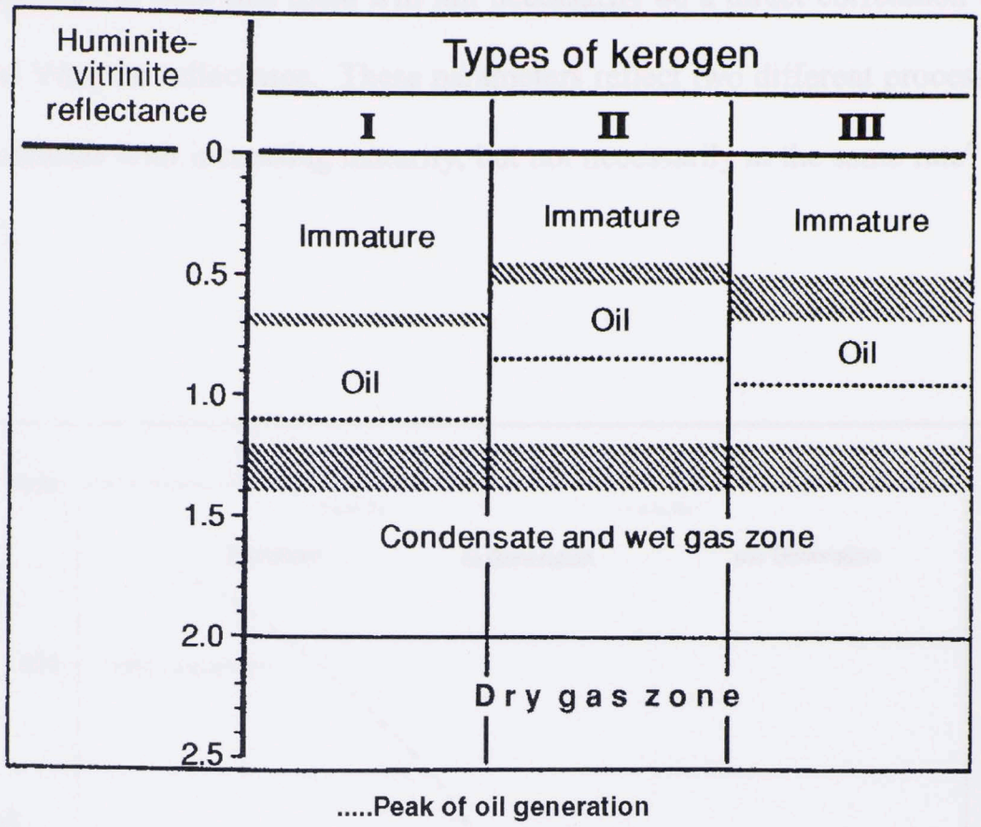

Figure 41 Approximate boundaries for kerogen types I, II, and III. From (Tissot & Welte, 1984)

Figure 41 (Tissot & Welte, 1984) shows the approximate boundaries for kerogen Types I, II, and III. Time-temperature relationships and mixing of various sources of organic matter may alter these boundaries. The values from the samples of La Luna IX vary from 0.6 up to 0.9, which forms part of the oil generation window (Figure 41). The kerogen is mostly Type II and the Vitrinite reflectance values are within the oil window (Figure 41). These values are not measured, but calculated based on T max. "The increase in the temperature at which S2 is maximized reflects an increase in the temperature at which S2 is maximized and reflects an increase in the temperature at which the residual material in the rocks breaks down. As the maturity level increases, the temperature required to degrade the residual material also increases" (Philp, 2014).

It is important to note that there will not necessarily be a direct correlation between T max and Vitrinite reflectance. These parameters reflect two different processes both of which increase with increasing maturity, but not necessarily at the same rate" (Jarvie, et al 2007).

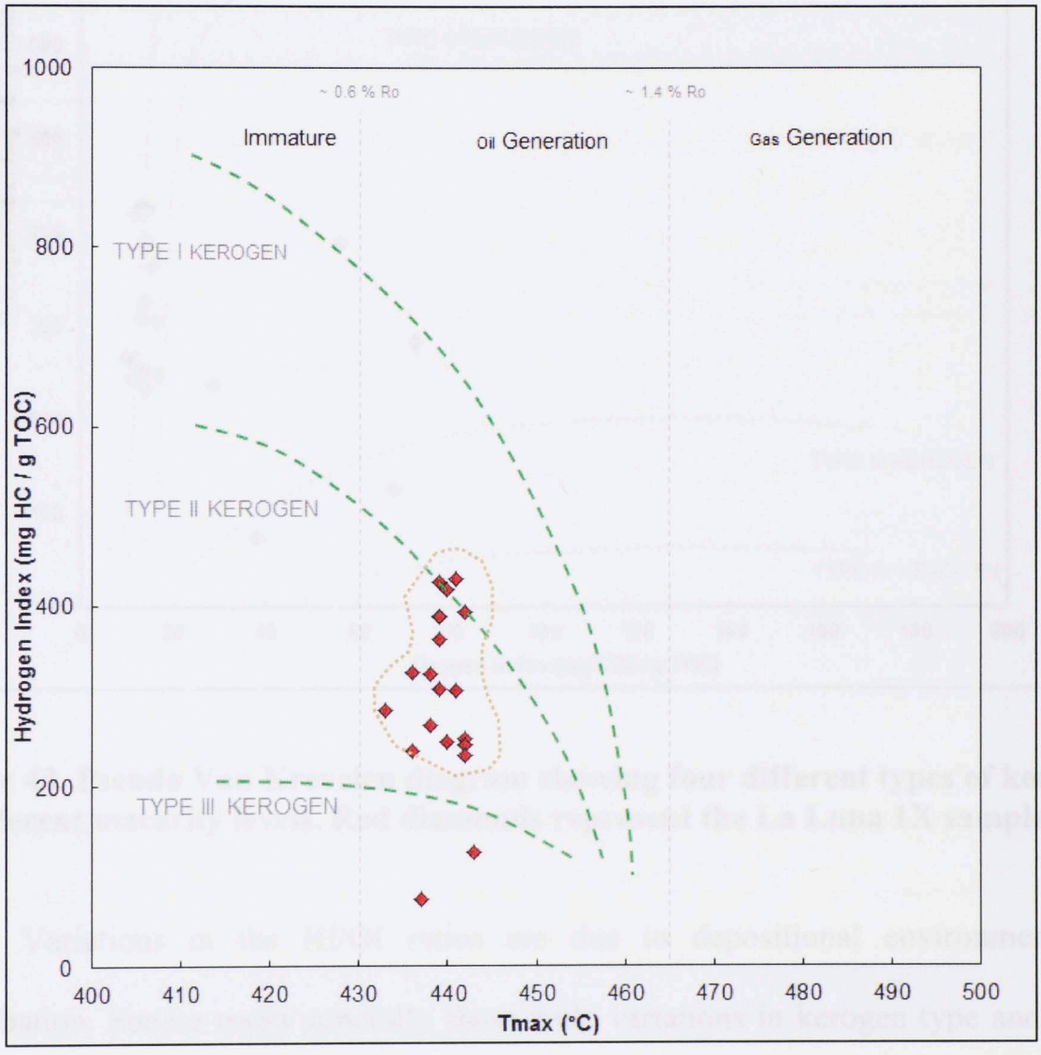

Figure 42 Kerogen type and maturity plot that displays the relationship between the Tmax and the Hydrogen index. Red diamonds represent the La Luna 1X samples

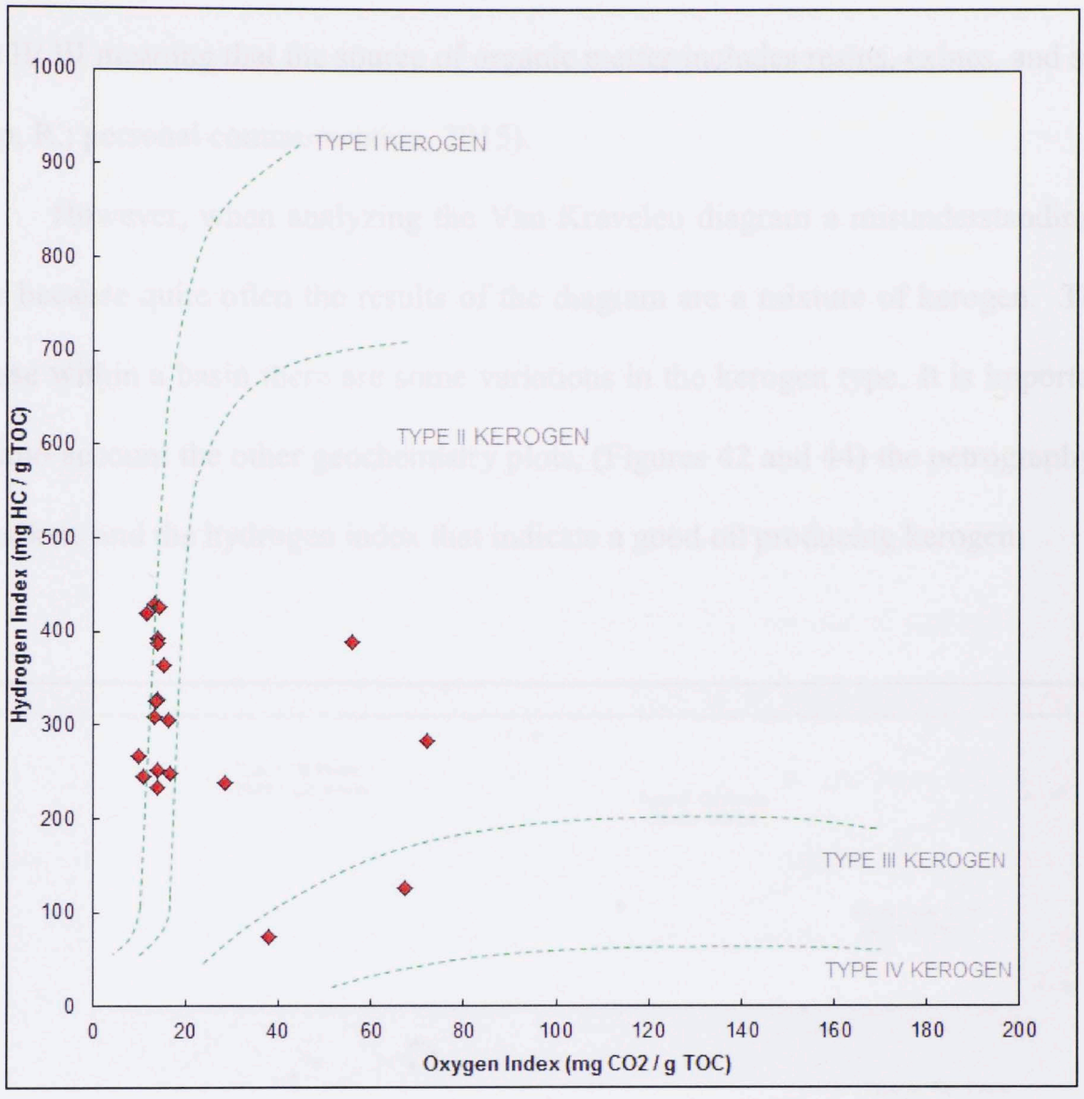

Figure 43 Pseudo Van Krevelen diagram showing four different types of kerogen at different maturity levels. Red diamonds represent the La Luna 1X samples

Variations in the HI/OI ratios are due to depositional environments and bioturbation. Source rocks generally show wide variations in kerogen type and source potential and it is generally not possible to assign a single kerogen type, and values tend to vary as a result of source depositional environments and maturity (Philp, 2014).

"It has been shown that the HI and OI are directly proportional to the H/C and O/C ratios and therefore a plot of HI against OI can be used to replace the H/C and O/C

values" (Philp, 2014). This plot shows that most of the kerogen is mainly Type II and Type II/ III meaning that the source of organic matter includes resins, exines, and spores (Philp, R.; personal communication, 2015).

However, when analyzing the Van Krevelen diagram a misunderstanding can occur because quite often the results of the diagram are a mixture of kerogen. This is because within a basin there are some variations in the kerogen type. It is important to take into account the other geochemistry plots, (Figures 42 and 44) the petrography, the biomarkers and the hydrogen index that indicate a good oil producing kerogen.

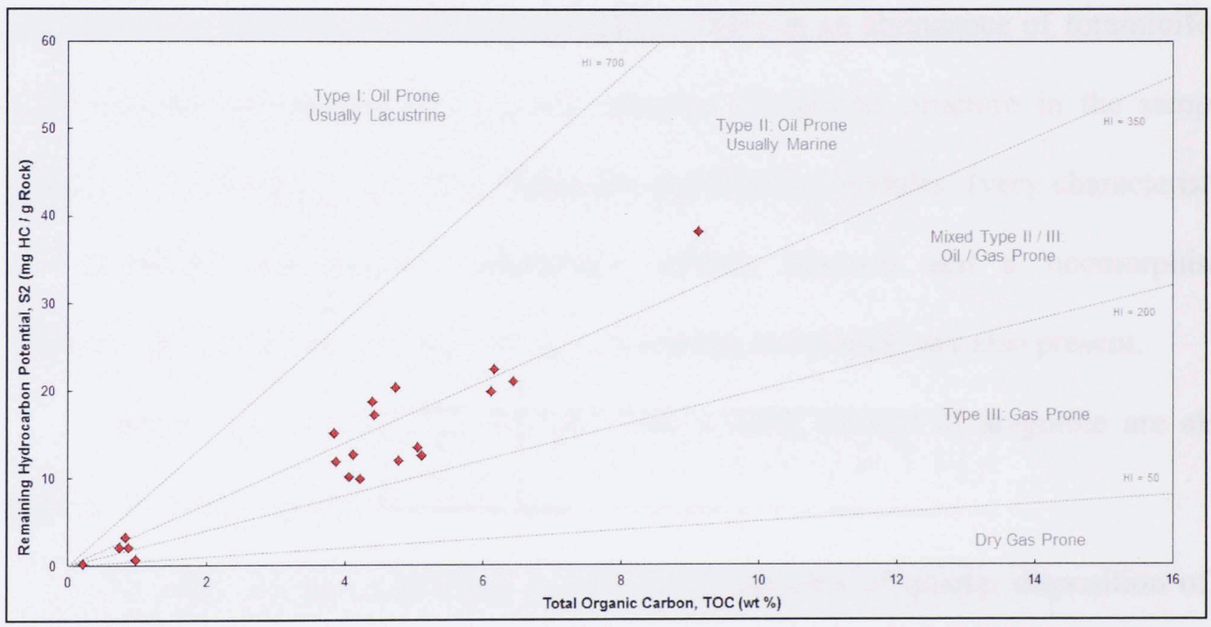

Figure 44 Kerogen Quality Plot that correlates TOC and S2. Red diamonds represent the La Luna 1X samples.

4.6 Petrography of core samples:

Depositional facies and diagenetic patterns determine the physical and chemical properties of carbonates, which control their reservoir potential. In order to correlate the facies characterization from the core with the XRD, XRF and the geochemistry of La Luna formation, thin sections of 12 samples from the core were described.

a. Thin section 15568'

This thin section (Figure 45) shows an abundance of fossils and dark-colored areas represented by various types of fine-grained sediment. In carbonates, the micrite matrix contains microspars. This process also reduces the amount of unstable aragonite and calcite by replacing it with normal calcite. There is an abundance of foraminifera with uniserial morphology and a micro granular compound structure in the sample (Figure 45C). In figure 45d, shell fragments, pyrite micro-nodules, (very characteristic of an anoxic environment) radiolarians, (chert), bitumen and a neomorphism recrystallization process (changes the size of crystals in the rock) are also present.

Moldic and inter-particle porosity with a small amount of aragonite are also present in a small amount (Figure 45B).

In other settings, extraclasts include small amounts of quartz; disposition of a micro-foraminifera nest; less than 1% of glauconite and light pink calcite. The type of contact is grain to grain and the sample also shows mica deformation.

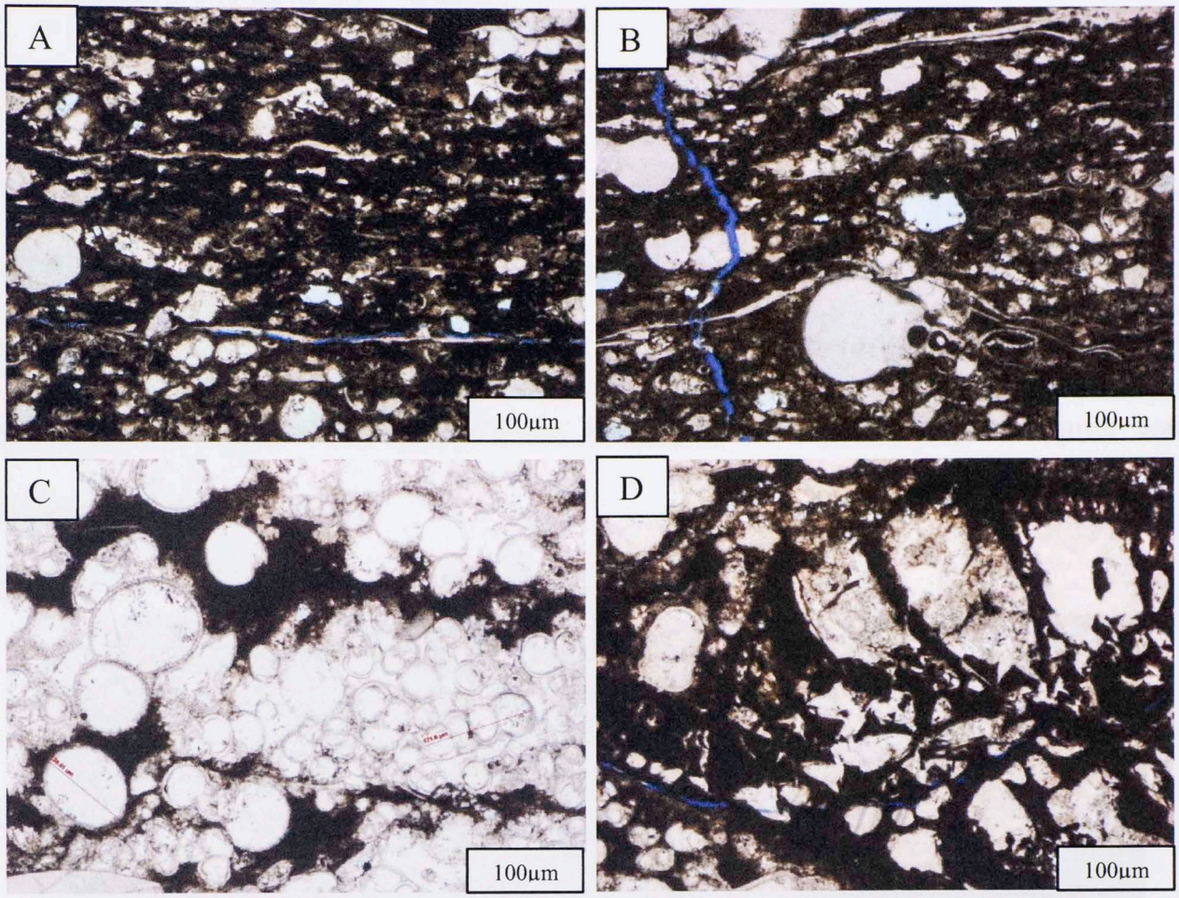

Figure 45 Photographs of thin section 15568' in plane polarized light. A) Abundant fossils and dark- colored areas represented by various types of fine- grained sediment B)Moldic; dissolution and inter-particle porosity with a small amount of aragonite are also present C)Large foraminifera with uniserial morphology and a micro granular compound structure D) Shell fragments; Pyrite micro-nodules; radiolarians (chert) are also present in the sample.

b. Thin section 15554'

This thin section is represented by a Wackstone-Packstone with various types of smaller and finer- grained sediments and micrite cement around the grains (Figure 46a and D). Algal structures and Foraminifera with uniserial morphology and a micro granular compound structure are characteristic in the sample (46B). Also, in figure 46A and c, thin brachiopods and gastropods are highly oriented or aligned (quiet water environment).

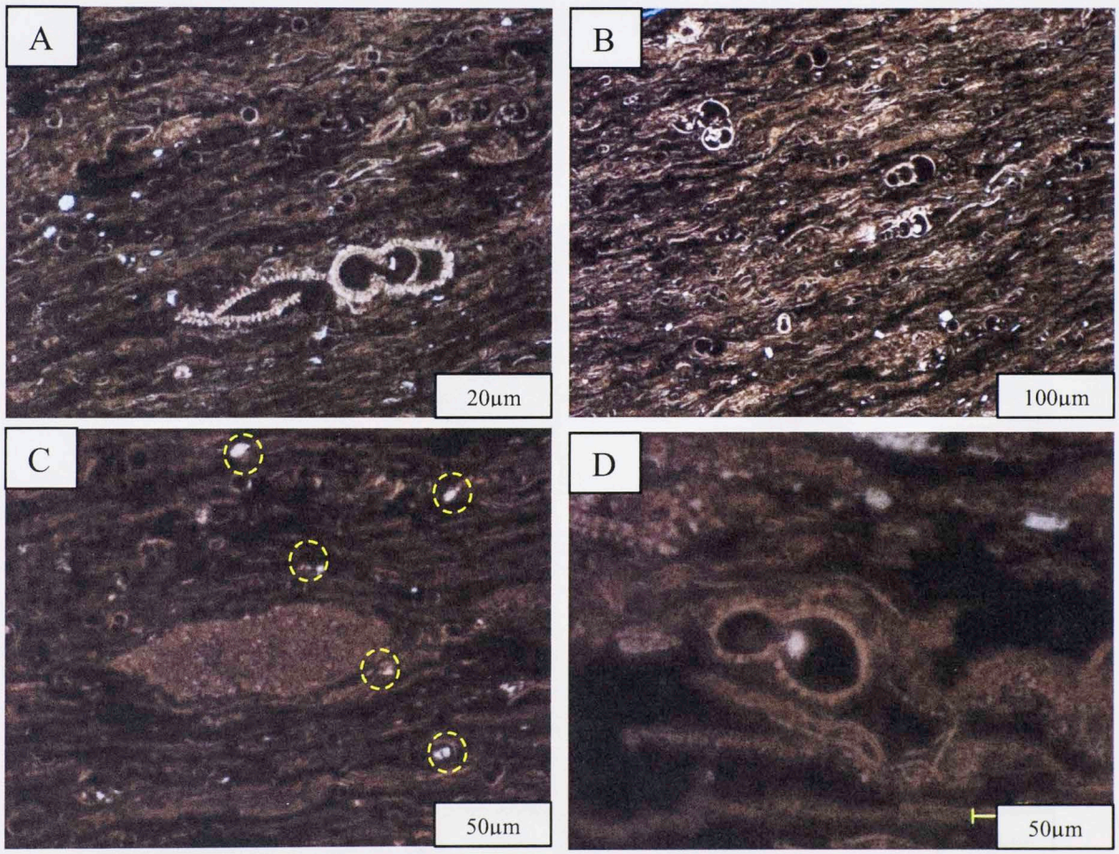

Figure 46 Photographs of thin section 15554' in plane polarized light A) Big picture of the thin section represented by various types of fine- grained sediment and micrite cement around the grains B) Dissolution porosity and Foraminifera with uniserial morphology and a micro granular compound structure C) Qtz overgrowth and the presence of pellets in a fine grained sediment D) Moldic cementation; shell fragments and fine- grained sediments and micrite cement are around the grains.

Elongated and aligned pyrite micro-nodules and pyrite cement are also present (Figure 46A). A very small amount of dissolution porosity by organic matter is also present in a small amount (Figure 46D) as radioaxil, sictacxil and moldic cementation. Shell fragments; Qtz overgrowth and the presence of pellets are also characteristic in certain areas of the sample.

c. Thin section 15496'

This sample shows a different arrangement compared to the previous depths. Micrite recrystallization of big sparite grain sizes is present (Figure 47 A and B) and it shows a high amount of interparticle porosity and dispersed micrite fragments. Some fractures are lined with bitumen.

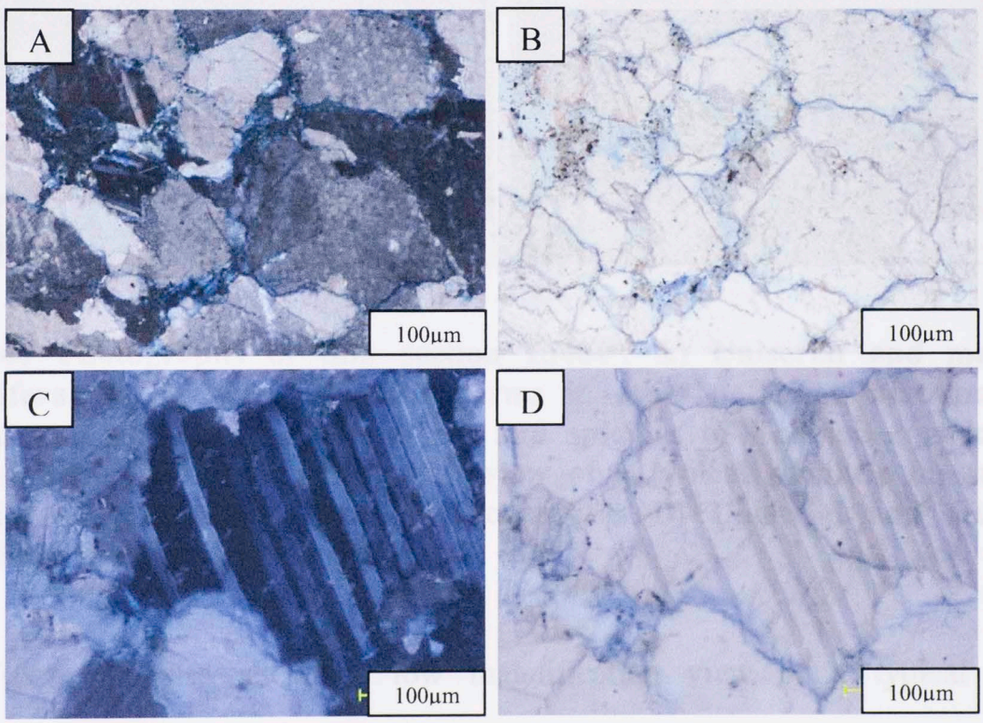

Figure 47 Photographs of thin section 15496'. A) Presence of micrite recrystallization of big sparite grain sizes in cross polarized illumination. B) Presence of micrite recrystallization of big sparite grain sizes in plane- polarized light. C) Qtz Extraclasts; pyrite fragments and possible ankerite in traces in cross polarized illumination D) Qtz Extraclasts, pyrite fragments and possible traces of ankerite in traces in plane- polarized light.

d. Thin section 15464'

This packstone is predominately composed of abundant uniserial and multiserial foraminifera and spicules of Echinoderms. (Figure 47).

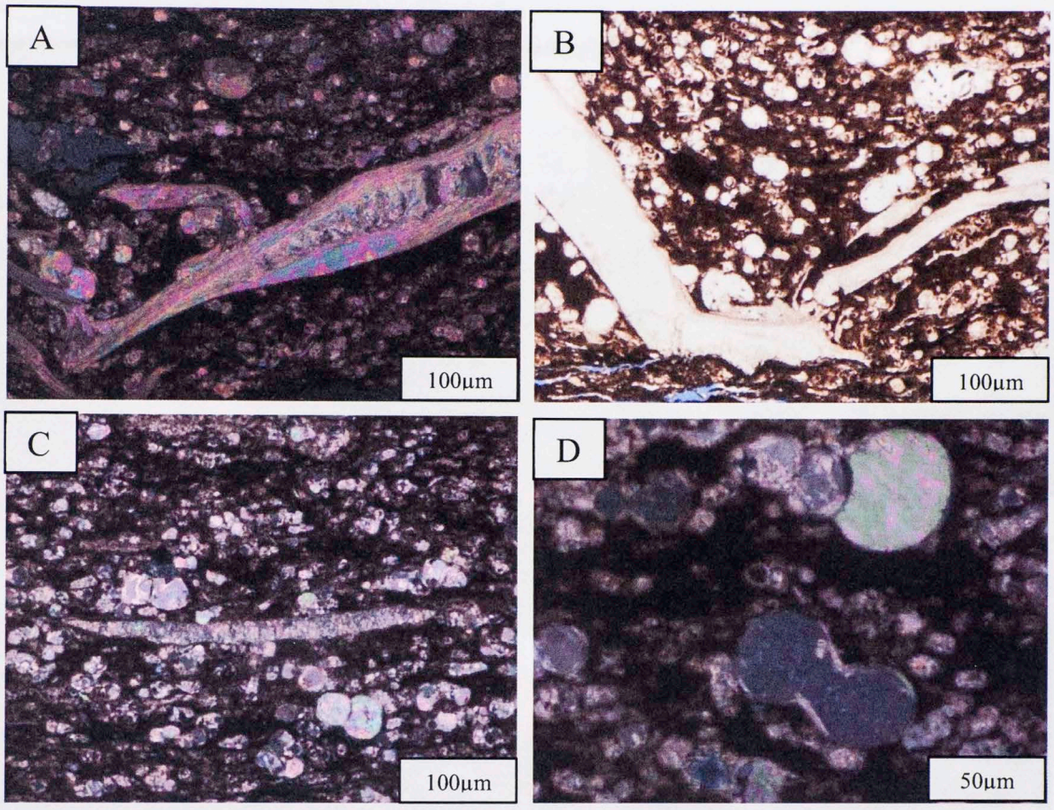

Figure 47 Photographs of thin section 15464'. A) Uniserial and multiserial foraminifera and spicules of Echinoderms in cross polarized illumination B) Uniserial and multiserial foraminifera and spicules of Echinoderms in plane-polarized light C) Low magnification view of a typical planktic foraminiferal biomicrite with multiple spar- filled chambers D) Uniserial and multiserial foraminifera in a fine grained sediment.

Figure 48 also shows a low magnification view of a typical planktic foraminiferal biomicrite showing multiple and spar- filled chambers. Dissolution porosity in the matrix and aragonite cementation by replacement are common.

e. Thin section 15444'

This sample is a packstone with equigranular cementation of calcite, shell fragments and recrystallized quartz (Figure 49). The type of porosity is by dissolution due to the fragmentation of the bioclasts (Figure 49A). The presence of organic matter cementation and smaller foraminifera are noticeable (Figure 49 B).

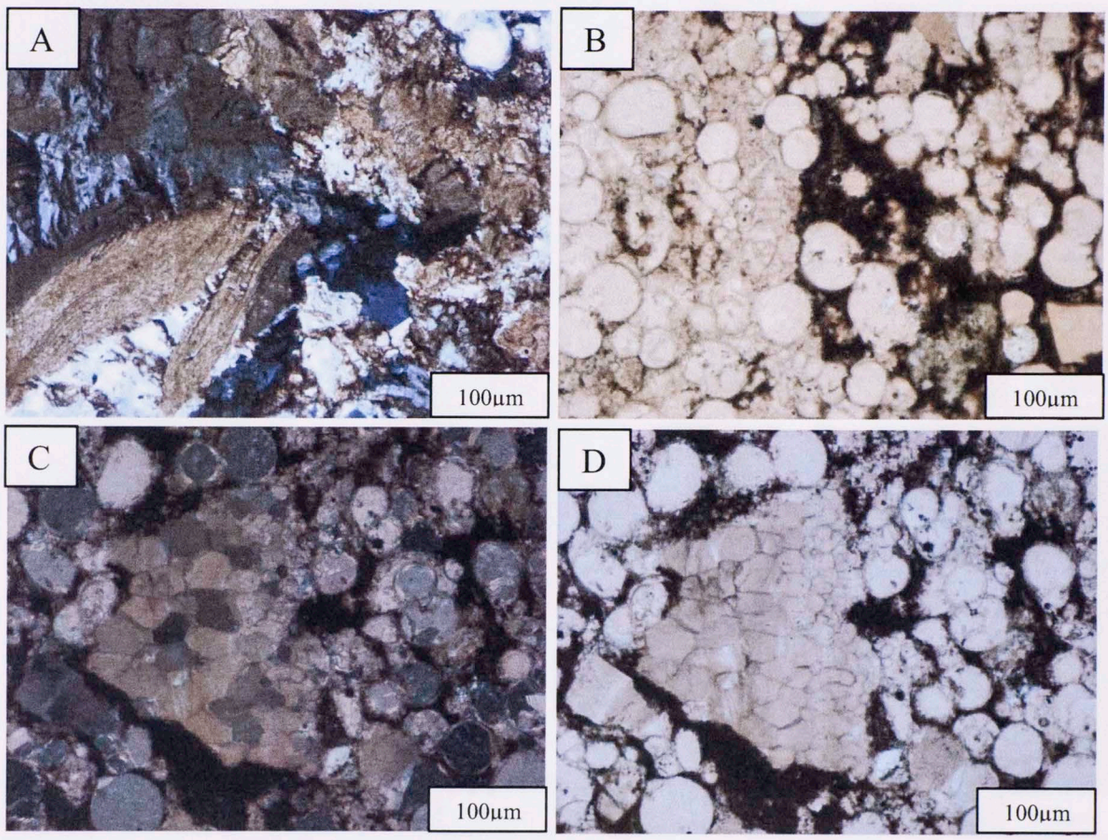

Figure 48 Photographs of thin section 15444' in plane polarized light A) Porosity by dissolution due to the fragmentation of the bioclasts B) Presence of organic matter cementation and smaller foraminifera. C) Contact between packstone and foraminifera traces in cross polarized illumination D) Contact between packstone and foraminifera traces in plane- polarized light.

In certain areas, a contact between packstone and foraminifera was noticeable (Figure 49 C and D). Pyrite fragments of 5% were also described in the sample.

f. Thin section 15395'

This sample is a packstone with an increment of the foraminifera size of around 30% compared with the last sample (15444). Micrite is around 10-15% and broken shell fragments are present (Figure A and B).

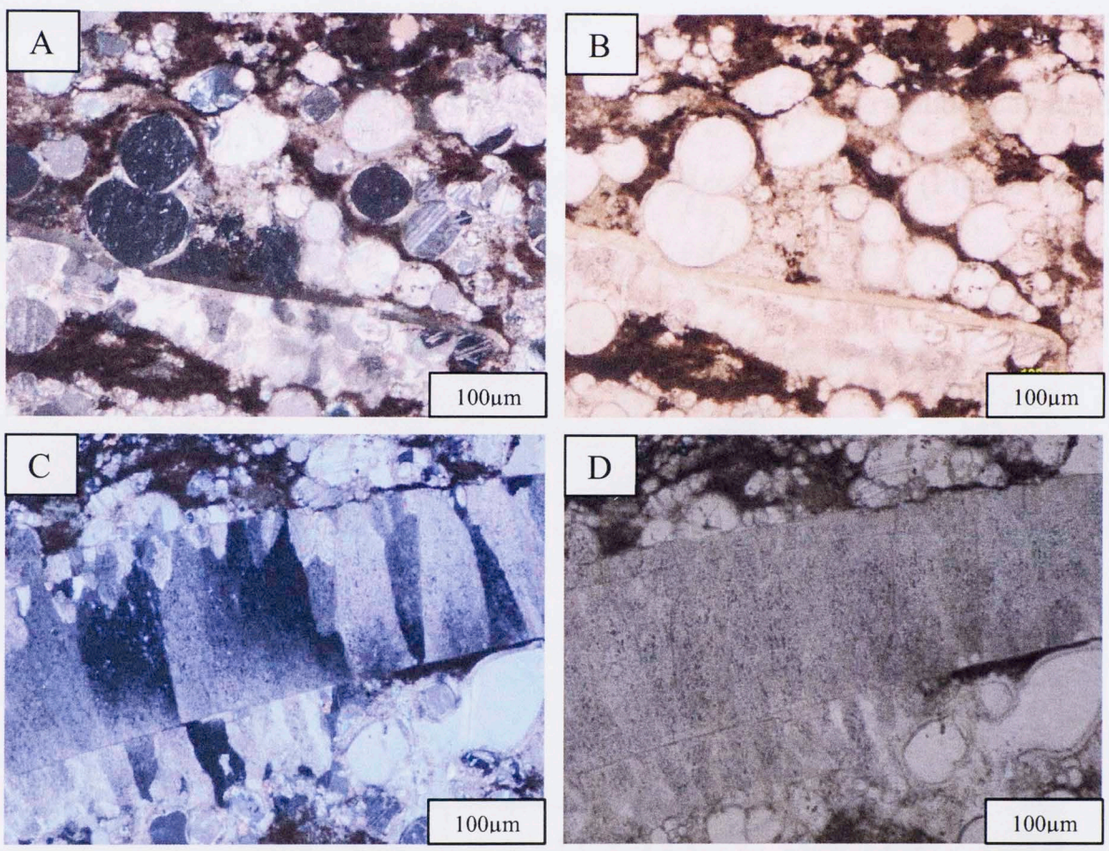

Figure 49 Photographs of thin section 15395' A) Packstone micrite in cross polarized illumination. B) Packstone and micrite in plane- polarized light. C) A cross polarized light view of a bivalve shell with coarsely prismatic structure. D) A plane polarized light view of a bivalve shell with coarsely prismatic structure.

Scholle & Ulmer-Scholle (2003) state that when the coarse prisms that compose the shell wall can be seen as an extension from one shell margin to the other (Figure 50C) a complete diagenetic removal of a secondary, presumably aragonitic, shell layer is indicated. The coarseness and inclusion- rich nature of the prisms may indicate that they too have undergone some diagenetic modification. In plane polarized light (Figure

50D), the margin-parallel lines of inclusions may be original layering within the shell. More subtle margin-normal inclusion traces mark the edges of the individual prisms. (Scholle & Ulmer-Scholle, 2003).

g. Thin section 15382'

This is a packstone composed of calcite cement and recrystallized foraminifera with interparticle porosity (Figure 51 A and B).

Organic matter fragments, recrystallized micrite, equigranular calcite-filled stylolite fractures occur along with some bioclasts altered to micrite (Figure 51 C and D). Hydrocarbons and some pyrite micro nodules are present.

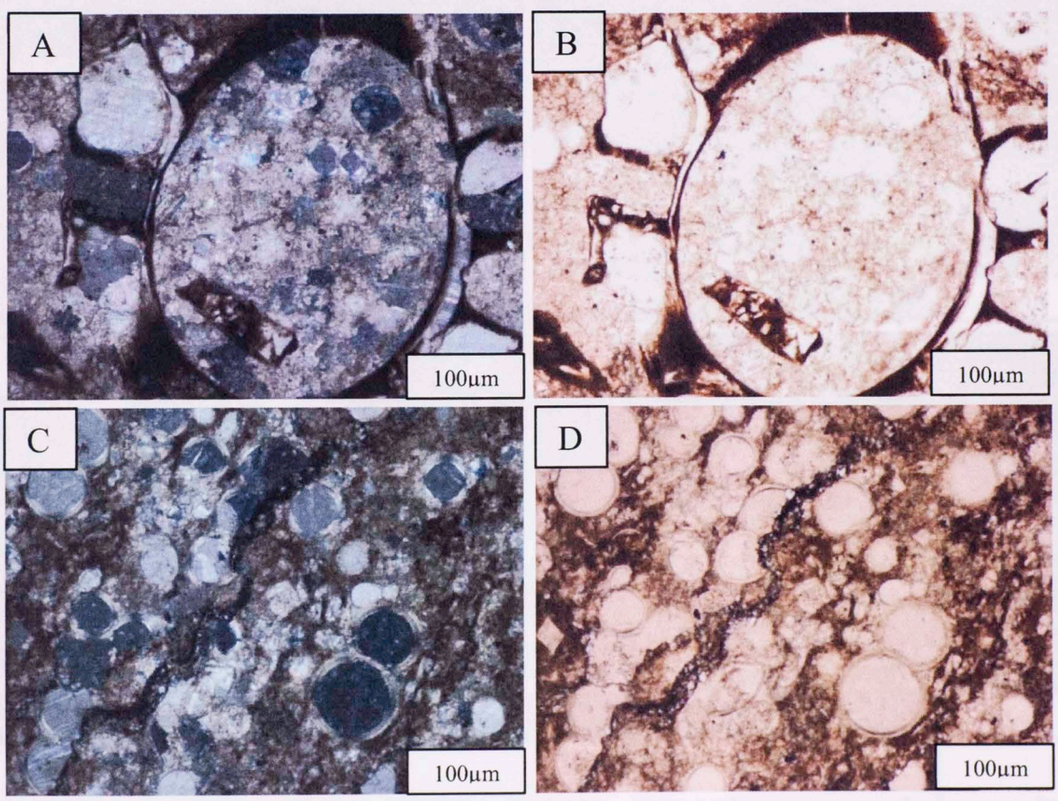

Figure 50 Photographs of thin section 15382'. A) Presence of the organic matter and interparticle porosity in the sample in cross polarized light. B) Presence of the organic matter and interparticle porosity in the sample in plane polarized light. C) Presence of some stylolites filled with organic matter and multiserial foraminifera in cross polarized light. D) Presence of some stylolites filled with organic matter and multiserial foraminifera in plane polarized light.

h. Thin section 15372

This sample shows a wackstone- packstone with a high concentration of organic matter, high content of Echinoderms', spicules and uniserial and multiserial foraminifera (Figure 52A and B). A microfossil of smaller size also occurs (Figure 52C). The porosity is by dissolution. Dispersed pyrite grains and aligned pellets are present (Figure 52D).

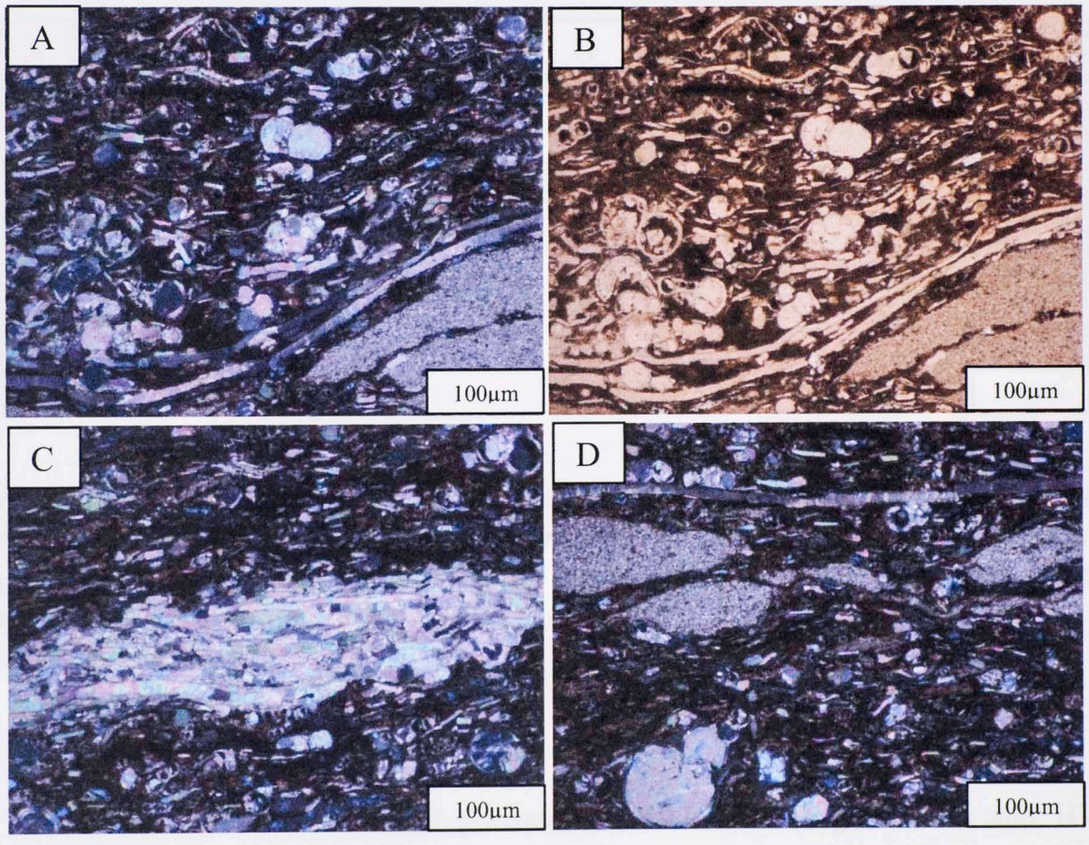

Figure 51 Photographs of thin section 15372'. A) wackstone- packstone with high concentration of organic matter, Echinoderms' spicules and uniserial and multiserial foraminifera (cross polarized light). B) wackstone- packstone with high concentration of organic matter, Echinoderms' spicules and uniserial and multiserial foraminifera in polarized light C) microfossil' nest surrounded by organic matter and foraminifera D) Dispersed pyrite grains and aligned pellets in cross polarized light.

i. Thin section 15365'

This sample is a wackstone- packstone which contains smaller multiserial foraminifera with organic matter and bitumen (Figure 53A).

Cements change along the sample. Calcite cementation is in the inner part with scattered micrite around the sample and micrite intraclasts (Figure 53B).Presence of fractures, fenestral porosity and large number of pelloids, equigranular aragonite and pyrite fragments occur.

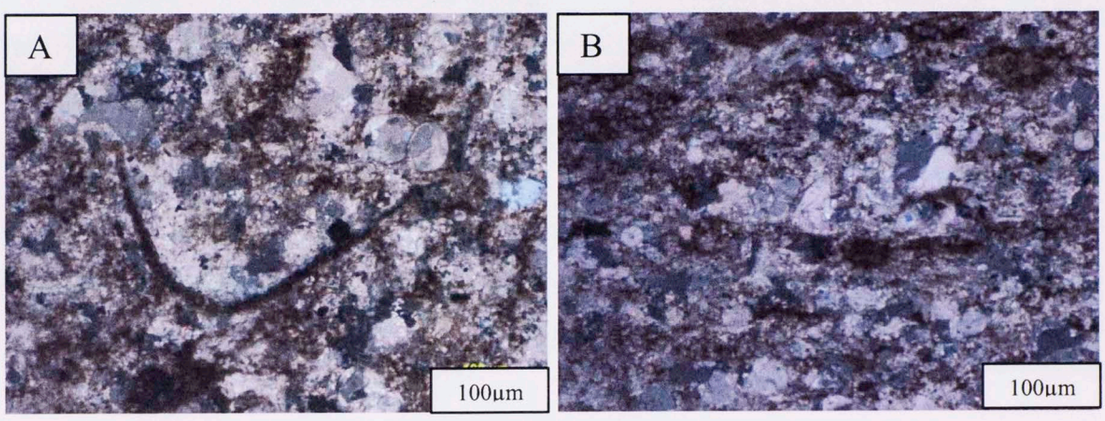

Figure 52 Photographs of thin section 15365' in cross polarized light. A) Wackstone- packstone which contains smaller and multiserial foraminifera with organic matter and bitumen. B) Calcite cement in the inner part with scattered micrite around the sample and micrite intraclasts.

j. Thin section 15317'

This sample is a reworked packstone- wackstone (Figure 54A and B) with abundant foraminifera filled with organic matter (Figure 54C) and a high amount of uniserial foraminifera cemented with calcite within an organic matrix (Figure 54D). Textures in this sample are massive and laminated. Radioaxil- sictacxil aragonite cements with druse porosity is according to Scholle & Ulmer-Scholle (2003) "a crust

or coating of crystals lining a cavity , specifically sparry calcite lining the pores of a limestone with crystal sizes increasing from the edges to the center of the pores" .

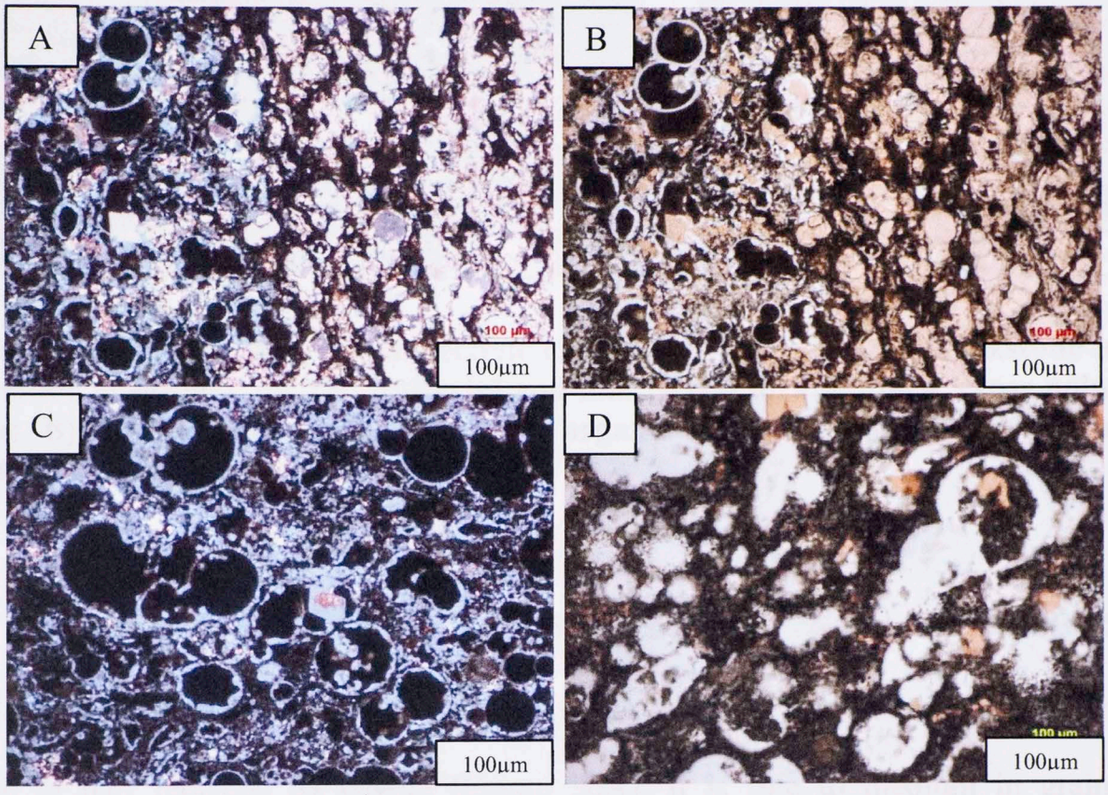

Figure 53 Photographs of thin section 15317'. A) Contact of a reworked packstone-wackstone with abundant foraminifera filled with organic matter; cross polarized light. B) Contact of a reworked packstone- wackstone with abundant foraminifera filled with organic matter; plane polarized light. C) Serial and multiserial foraminifera filled with organic matter and recrystallized calcite. D) Serial and multiserial foraminifera with recrystallized calcite.

k. Thin section 15303'

This sample is a recrystallized wackstone with uniserial and multiserial foraminifera and a small amount of micrite cement and recrystallized foraminifera (Figure 54A and B). The grain size is smaller than the previous samples and there are also traces of micro grains of aragonite and pyrite.

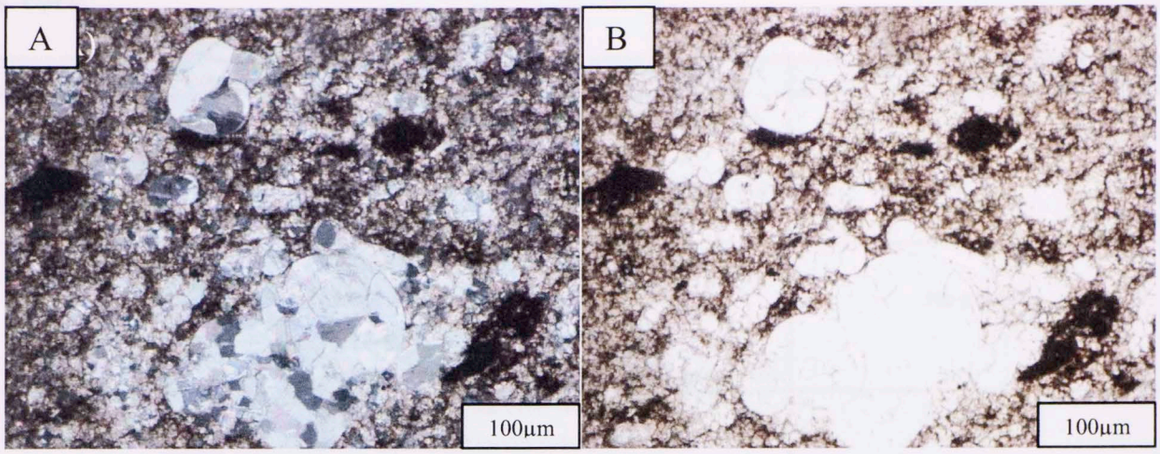

Figure 54 Photographs of thin section 15317'. A) Recrystallized wackstone in the presence of organic matter, uniserial and multiserial foraminifera; cross polarized light. B) Recrystallized wackstone with organic matter, uniserial and multiserial foraminifera; plane polarized light.

l. Thin section 15294

This sample is a wackstone, with 45 percent micrite cement (Figure 56B). Some shell fragments occur (Figure 56B) as uniserial and multiserial foraminifera that have been in part replaced by calcite (Figure 56A). It is fine to medium in grain size (mudstone – wackstone like). Traces of Pyrite occur (Figure 56A and B).

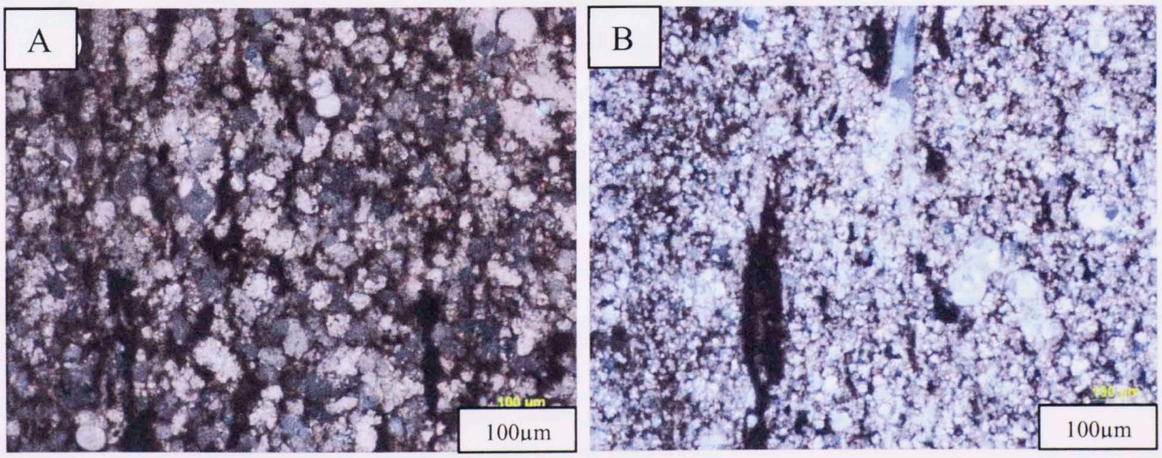

Figure 55 Photographs of thin section 15294'. A) Wackstone and uniserial and multiserial foraminifera that are in part replaced to calcite; cross polarized light. B) Micrite cement of almost 45 percent. Shell fragments and pyrite traces occur. Plane polarized light.

Table 12 Summary Chart of facies and major features of thin sections of La Luna IX core.

Thin sections	Facies related	Mayor Features	Porosity
15294	VII	Wackstone, with 45 percent micrite cement, some shell fragments occur as uniserial and multiserial foraminifera that have been in part replaced by calcite	No porosity
15303	VII	Recrystallized wackstone, uniserial and multiserial foraminifera and amount of micrite cement, small recrystallized foraminifera. Smaller grain size	No porosity
15317	VII	Reworked Packstone- wackstone with abundant foraminifera filled with organic matter and a high amount of uniserial foraminifera cemented with calcite within an organic matrix	Druse porosity
15365	VII	Wackstone- Packstone which contains smaller multiserial foraminifera with organic matter and bitumen	By fractures Fenestral
15372	VII	Packstone with a high concentration of organic matter, high content of Echinoderms', spicules and uniserial	By dissolution
15382	VII	Multiserial foraminifera and organic matter fragments, recrystallized micrite, equigranular calcite-filled stylolite fractures occur along with some	Interparticle
15395	V	Packstone with an increment of the foraminifera size of around 30% Micrite is around 10-15% and broken shell fragments are present	No porosity
15444	V	Packstone with equigranular cementation of calcite, shell fragments and recrystallized quartz	Dissolution
15464	V	Packstone predominately composed of abundant uniserial and multiserial foraminifera and spicules of Echinoderms	By reeplacement
15496	IV	Micrite recrystallization of big sparite grain sizes	Interparticle
15554	IV	Wackstone-Packstone with various types of smaller and finer- grained sediments and micrite cement around the grains	Dissolution
15568	IV	Wackstone with shell fragments, pyrite micro-nodules, (anoxic environment)	Moldic Inter-particle
IV	Laminated mudstone with limestone concretions and Packstone		
V	Siliceous- calcareous laminated mudstone interbedded with black chert filled with calcite veins		
VII	Slightly siliceous- calcareous laminated black mudstone interbedded with calcareous fossiliferous wackstone.		

5. North Andean Flank and Lago de Maracaibo Basin

5.1.1 Las Hernandez Outcrop:

This outcrop is part of the Upper La Luna formation and is represented by the Tres Esquinas member in the North Andean flank of Venezuela. It's located in La Tendida, Táchira state (boundary between Mérida and Táchira states).



Figure 56 Las Hernandez Outcrop showing the Upper La Luna Interval (Tres Esquinas Member) in the North Andean Flank. Dashed yellow lines are characteristic concretions of The Tres Esquinas Member.

The outcrop is 16m wide and 6.6m long (Figure 57). The lithology is laminated mudstone with representative chert layers (Figure 58) and intervals of massive limestone, some of them filled with calcite. In some intervals, glauconite is also present and there is a strong petroleum odor. Concretions in the outcrop show concoidal fractures and are up to 70 cm wide and 50cm long (Figure 59). This outcrop represents the highest percent of organic matter of the North Andean flank according to the geochemical Rock Eval results.



Figure 57 Picture that shows how calcite filled chert layers and glauconite are representative of this Upper La Luna interval.



Figure 58 Big concretions with concoidal fractures in Las Hernandez outcrop.

Figure 60 shows the geological profile using Ozzies logbook; GR Scintilometer profile; trend; and facies are described for each interval.



Figure 59 Geological profile using Ozzies logbook representing the geologic units (Vertical scale; lithological pattern; GR scintilometer and Facies) in Las Hernandez outcrop. Yellow dashed line represents the GR scintilometer measured profile.

5.1.2 Zea Outcrop

The Upper La Luna Zea outcrop and Colon formation (Socuy Member) are located 112Km away from The Las Hernandez Outcrop in the boundary of Mérida state. This is a lateral facies change from the Upper La Luna to the Colon Formation. It's mostly composed of an alternation of massive to fissile, dark grey to black, hard, glauconitic, phosphatic and pyritic, concoidal to irregular-fractured shale. (Figures 60 and 61).

The rock reacts with HCL and represents the transition towards the Colon Formation. TOC content is very low and geochemical Rock Eval analysis shows a low index of oil generation.



Figure 60 Alternation of massive grey to black hard shale represented by Upper La Luna- Colon Formation in Zea Outcrop, Mérida state. Dashed lines show beds.



Figure 61 Alternation of fissile grey to black hard shale represented by Upper La Luna- Colon Formation in Zea Outcrop, Mérida state. Dashed lines show beds.

Figure 62 shows the geological profile using the Ozzies logbook; GR Scintilometer profile; trend; and facies associated with each interval.

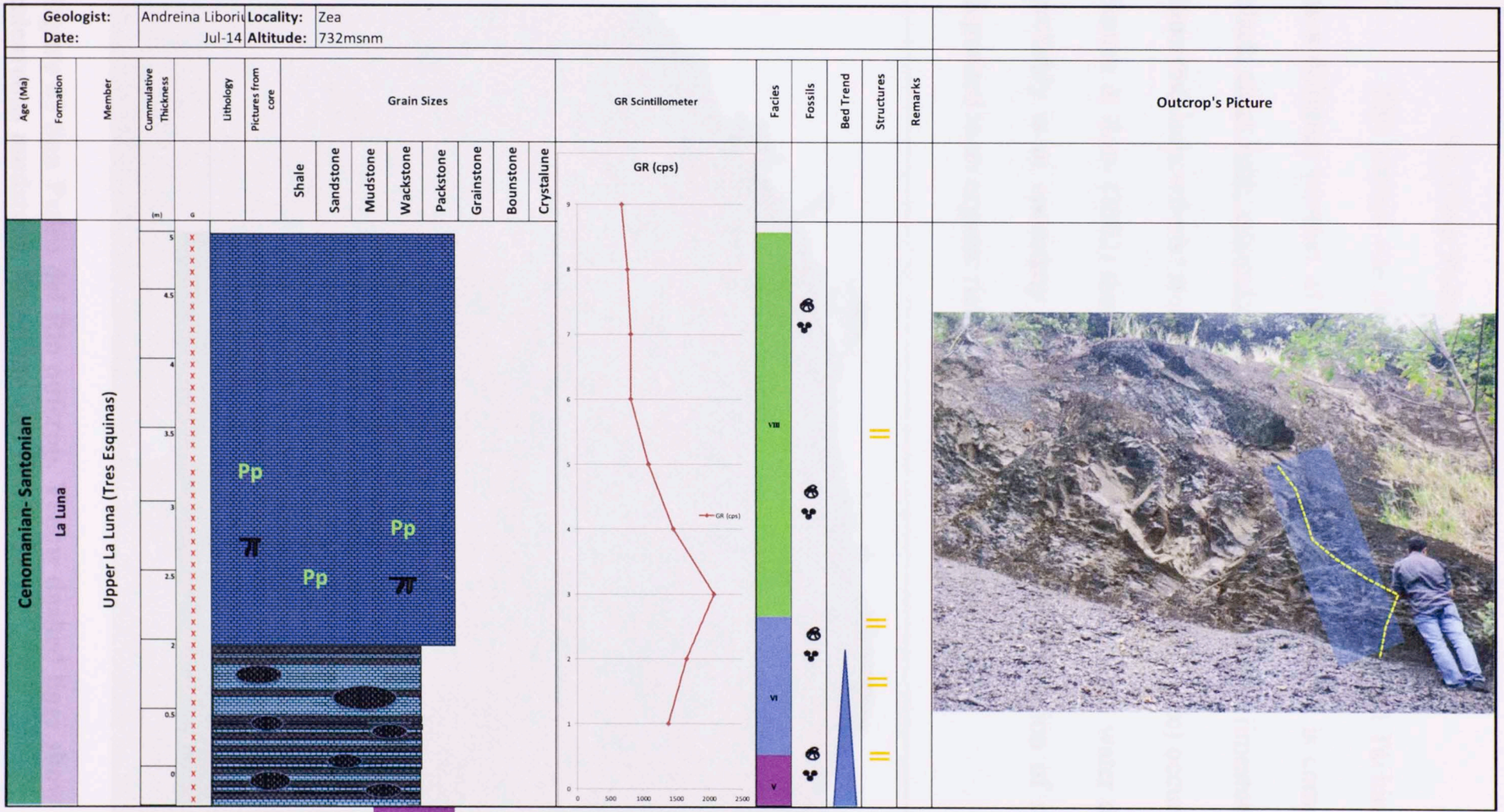

Figure 62 Geological profile using Ozzies logbook representing the geologic units (Vertical scale; lithological pattern; GR scintilometer and Facies) in Zea outcrop.

5.1.3 San Pedro del Rio outcrop:

This section was defined by Renz (1959) "Ftanita del Táchira" (Táchira's chert) as a different member of the Upper La Luna Formation. It is composed of laminated black chert with intercalations of siliceous mudstone and limestone lenticular, small limestone concretions (around 10-20 cm long and 10 cm wide) occur. According to Dos Santos & Soto (2002) this section was deposited in marine water depths of 300 m. It probably is of secondary origin derived from the dissolution of siliceous organisms deposited in an organic rich oxygenated environment.



Figure 63 San Pedro del Rio outcrop. Yellow dashed lines show the alternation of calcareous mudstone, limestone and black chert.

The location where the samples were taken was in La Chiriria Creek located in San Pedro del Rio Town. The whole outcrop is around 65m thick but the thickness where the samples were taken is approximately 13.5m thick. It is composed of calcareous mudstones, limestone and black laminated chert.

According to Dos Santos & Soto (2002) La Luna Formation in this study area might be divided into three informal lithological units: the lower unit is composed of mostly dark calcareous mudstones with an average thickness of 1.50m intercalated with thin limestone beds (0.50m). This unit is approximately 24m thick in this section, the middle unit represents a transition interval with intercalations of limestone, mudstones and chert with predominance of limestone beds. This unit is around 30m thick.

The Upper unit is characterized by the presence of siliceous-mudstone, limestone and characteristic phosphates (around 0.30 m) that marks the top of the sequence, representing a thickness of around 10m. One of the limitations of this outcrop was its difficult access to take samples and to take natural gamma ray measurements (it was very steep and with a lot of vegetation), thus, few samples were taken.

Based on the lithology description made by Dos Santos & Soto (2002) the study interval is located in the middle unit of the outcrop, since the same lithology occurs where the samples were taken. The TOC results for this outcrop are 1.08-2.14 % . Figure 65 shows the geological profile using Ozzies logbook, GR Scintilometer profile, trend,and facies associated with each interval.



Figure 64 Limestone concretion in yellow and white lines showing the alternation of limestone, chert and mudstone in "Ftanita del Táchira member" (Táchira's chert member of La Luna Formation) in Táchira state.



Figure 65 Geological profile using Ozzies logbook representing the geologic units (Vertical scale; lithological pattern; GR scintillometer and facies) in the San Pedro del Rio outcrop.

5.1.4 La Azulita-Bachaquero outcrop:

This outcrop is located in La Azulita town. It's approximately 14m long and 20m wide and is composed of dark gray, laminated mudstones with an alternation of limestone (Figure 66) and chert. Towards the base of the outcrop are chert concretions that are approximately 10cm wide and 7cm long. (Figure 67). Mudstones are very fissile and there is a certain cyclicity to the deposition of chert concretions and laminated mudstone. This outcrop is highly weathered (especially mudstones); the mudstone weathering color is light gray with small organic matter fragments (Figures 67 and 68).



Figure 66 La Azulita- Bachaquero outcrop, located in La Azulita town, Mérida state. Dashed lines show beds.



Figure 67 Image that displays highly weathered and fissile mudstone.

The TOC for this outcrop shows values of 1.08-2.14 %. The rock reacts a lot with HCL. It is the transition towards the Colon Formation. Rock Eval shows a low index of oil generation. Figure 69 shows the geological profile using Ozzies logbook; GR Scintilometer profile, trend, and facies associated with each interval.



Figure 68 Image that shows mudstone weathering color with small organic matter fragments within.

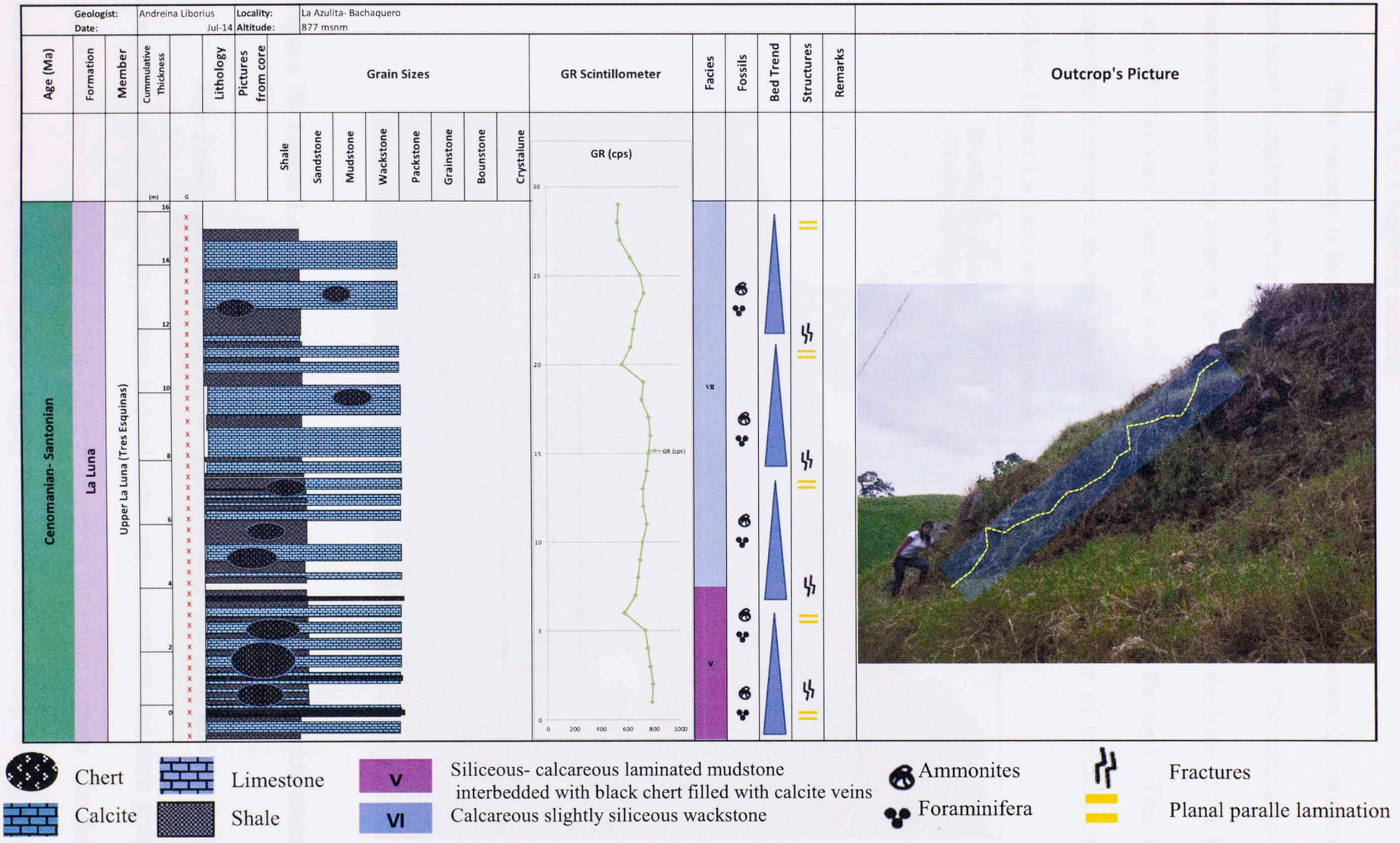

Figure 69 Geological profile using Ozzies logbook representing the geologic units (Vertical scale; lithological pattern; GR scintilometer and Facies) in La Azulita- Bachaquero outcrop.

5.1.5 Chiguará outcrop

This outcrop is located towards the west of Chiguará town. It represents one of the most complete sections of the Middle and Upper La Luna. The natural gamma ray measurements were done in the entire Middle La Luna and at the base of the Upper La Luna (it was very steep and with a lot of vegetation towards the top). This section is important because it shows high iron levels and also a layer of volcanic ash in the Middle- Upper La Luna transition zone.



Figure 70 Lower La Luna outcrop located in Chiguará town, Mérida state.

The Lower La Luna outcrop is approximately 8m long and 7m wide. It is composed of rhythmically, calcite bedded light, gray limestone and dark gray, tabular calcareous mudstones, with calcite-filled fractures in the entire section. The thickness is less towards the top where beds are highly laminated. This outcrop is highly weathered

and shales are highly fissile (Figure 72), however samples were taken in the fresher areas. Some calcite nodules around 15cm wide and 8 long were found (Figure 72). Natural gamma ray measurements were completed though the entire section (Figure 73).



Figure 71 Image that shows how weathered and fissile the rock is in this locality. The rock has an orange- brownish weathered alteration color.



Figure 72 Calcite concretion (dashed black line) present in the Lower La Luna outcrop.

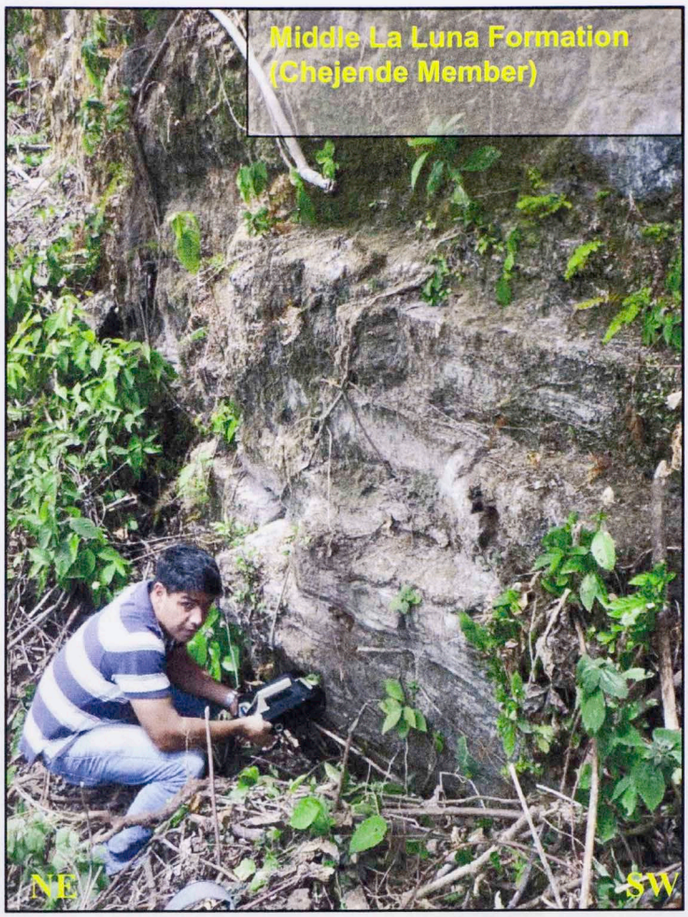

Figure 73 Image that shows the use of the Gamma ray scintilometer in the Lower La Luna outcrop

The second outcrop is located approximately 100 m towards the east of the Lower La Luna outcrop in the same locality. It is approximately 20m long and 22 m wide and represents the transition between the top of the Lower La Luna (Chejende) member and the basal Upper La Luna (Timbetes) member (Figures 75 and 76).

Lithology in the Chejende Member is a cyclical sequence of calcareous mudstone and concretions. The amount of chert increases towards the top of Timbetes member, displaying a contrast in coloration between the two members (Figure 75).

A 10cm bed of reddish sediments (Figures 76 and 77) occurs in the Upper La Luna outcrop; the natural gamma ray response shows high values in that interval. This interval may be a volcanic ash deposit related to the La Luna in Colombia. This layer has been found and it is believed (as stated before in La Luna IX core) that it originated from a volcanic arc located on the western margin of northern South America (Parnaud et al., 1995; Gomez.,2014). Figure 78 shows the geological profile using the Ozzies logbook, GR Scintillometer profile, trend, and facies of each interval.

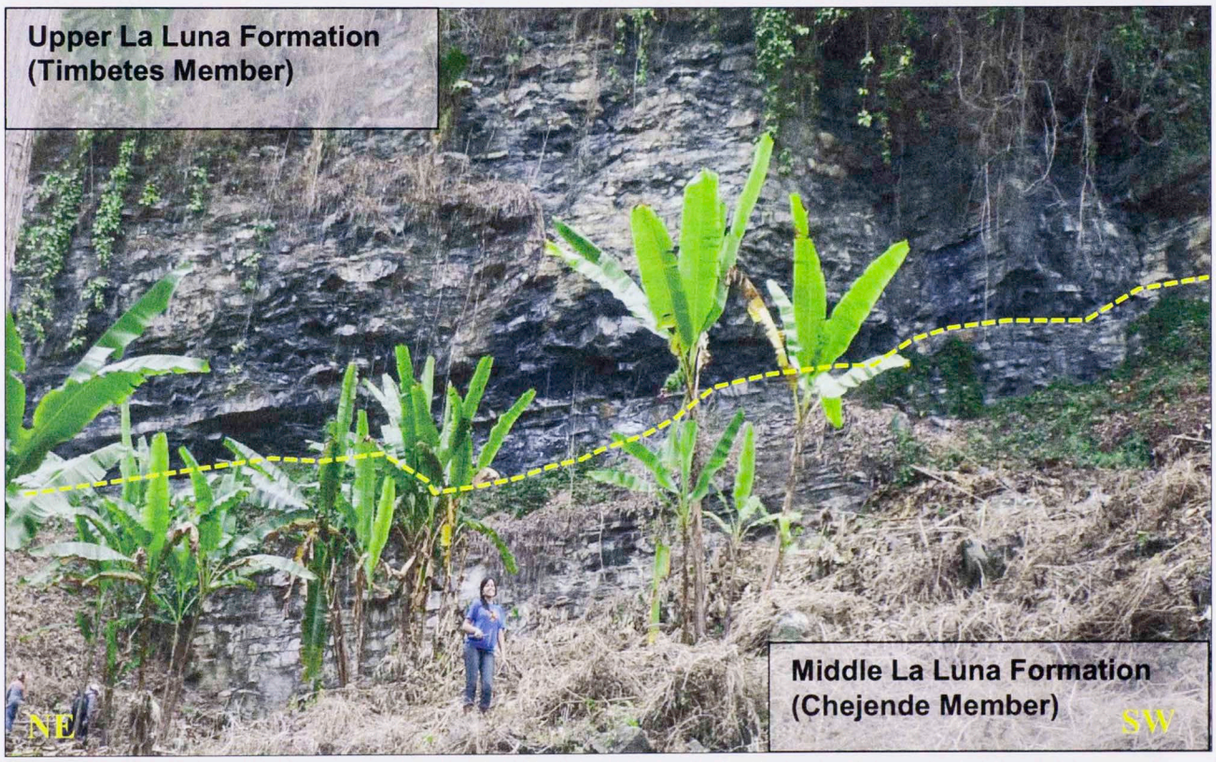

Figure 74 Yellow dashed lines display the transition between the Chejende Member (Lower la Luna) and Timbetes member (Upper La Luna) in Chiguará town, Mérida state.

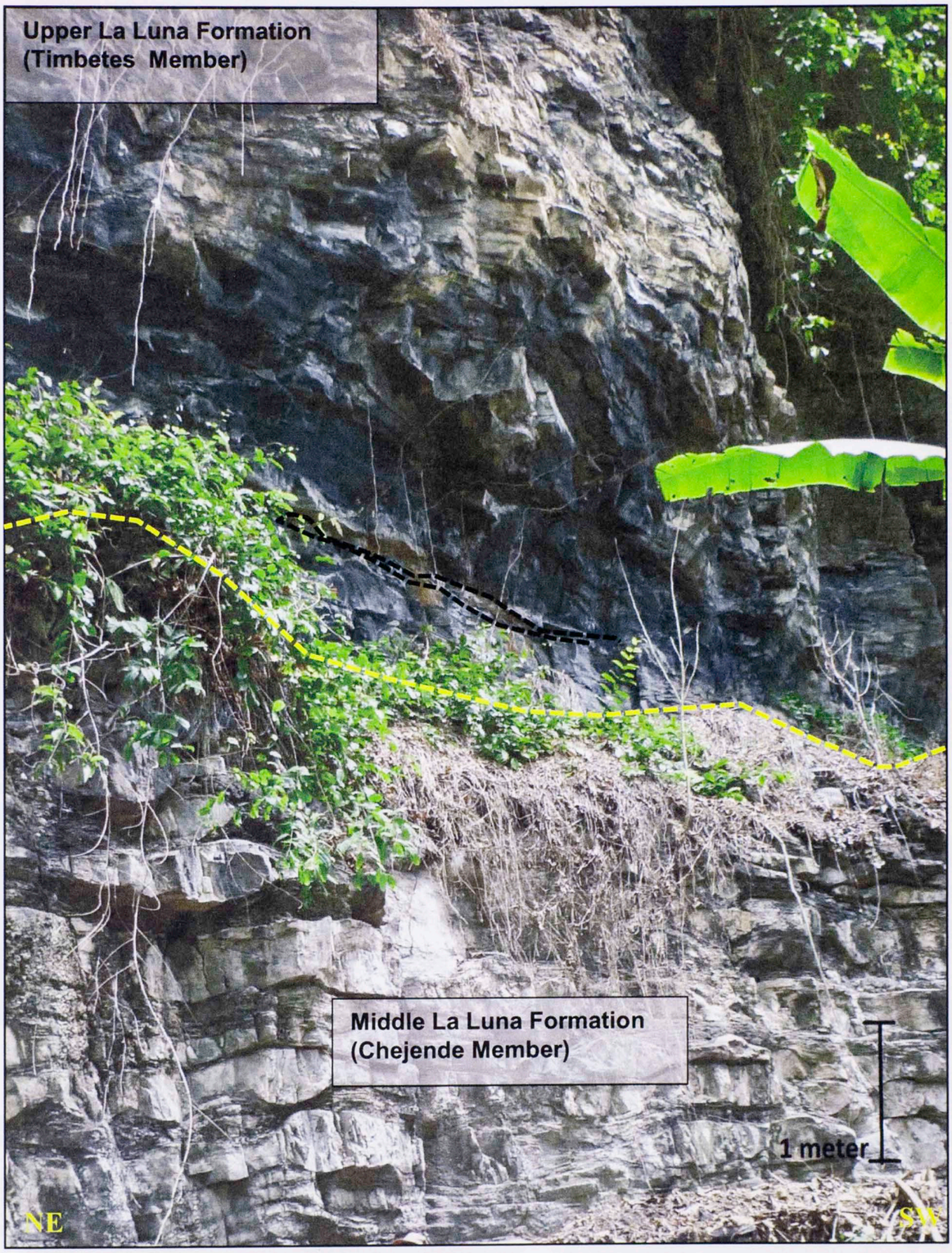

Figure 75 NE- SW image showing where the yellow dash lines mark the transition between the Chejende and Timbetes Members. A small fraction of the volcanic ash beds are noticeable in this picture by a black dashed line.



Figure 76 Big chert concretion (yellow dashed lines) and volcanic ash layer (black dashed lines) in the Upper La Luna Formation, Chiguará town- Merida state.



Figure 77 Picture that best represents the volcanic ash layer (black dash lines) in the Upper La Luna Formation, Chiguará town- Merida state.

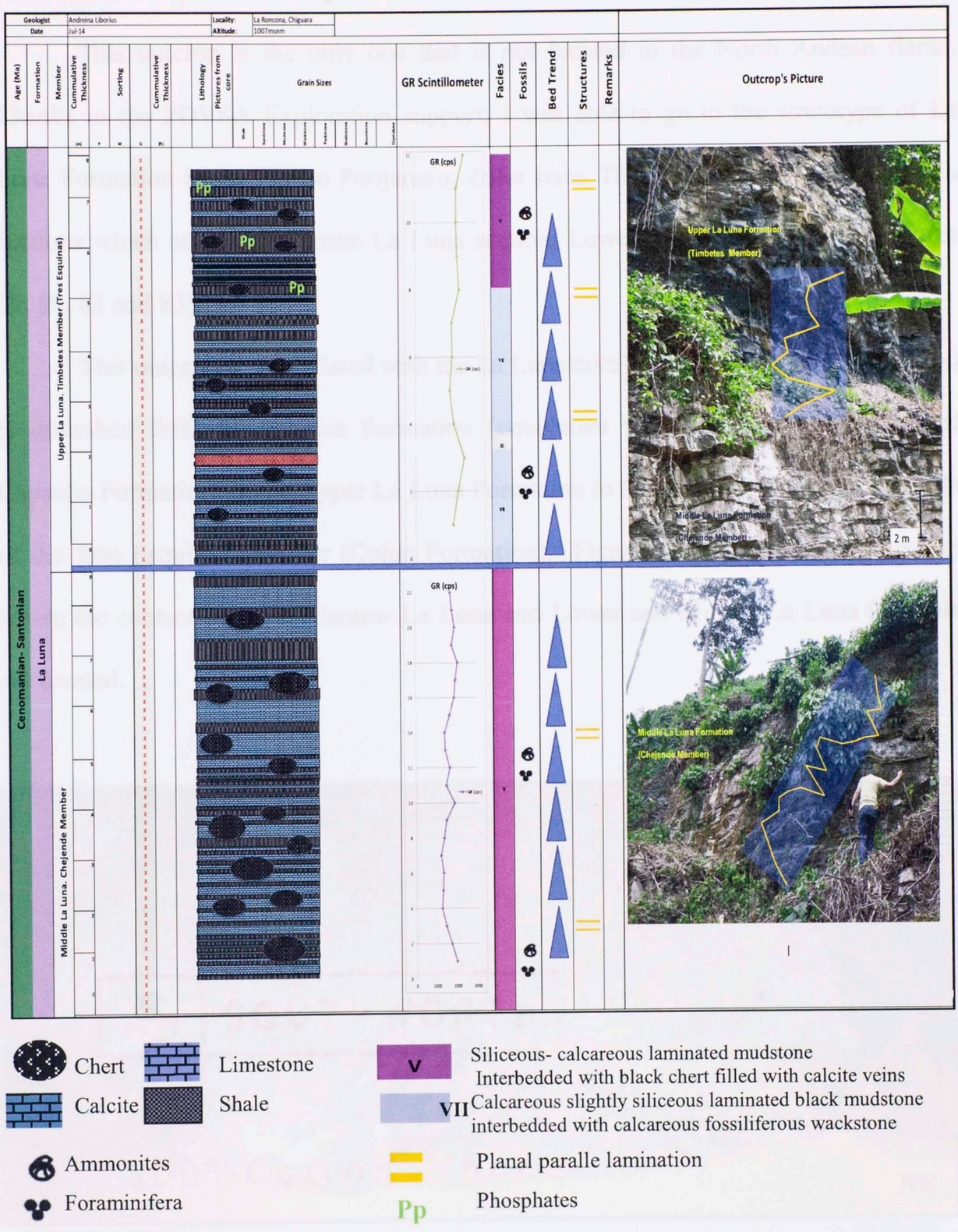

Figure 78 Geological profile using Ozzies logbook representing the geologic units (Vertical scale; lithological pattern; GR scintillometer and Facies) in Chiguará outcrop.

5.1.6 Flanco Perijanero outcrop

This outcrop is the only one that is not located in the North Andean flank.. Thanks to the PDVSA Exploration support, I was able to go to the stratotype of La Luna Formation in the Flanco Perijanero, Zulia state. This outcrop is divided into two sections which contain the entire La Luna section: Lower, Middle and Upper (Figures 79, 80, 82 and 83).

This outcrop is also related with the La Luna core described earlier. This outcrop is described from the Maraca Formation (equivalent to the Guayacán Member of Capacho Formation) to the Upper La Luna Formation to the top of the phosphatic levels of the Tres Esquinas Member (Colon Formation). Figure 80 displays the first section where the contact between Maraca- La Luna and Lower and Middle La Luna intervals are located.

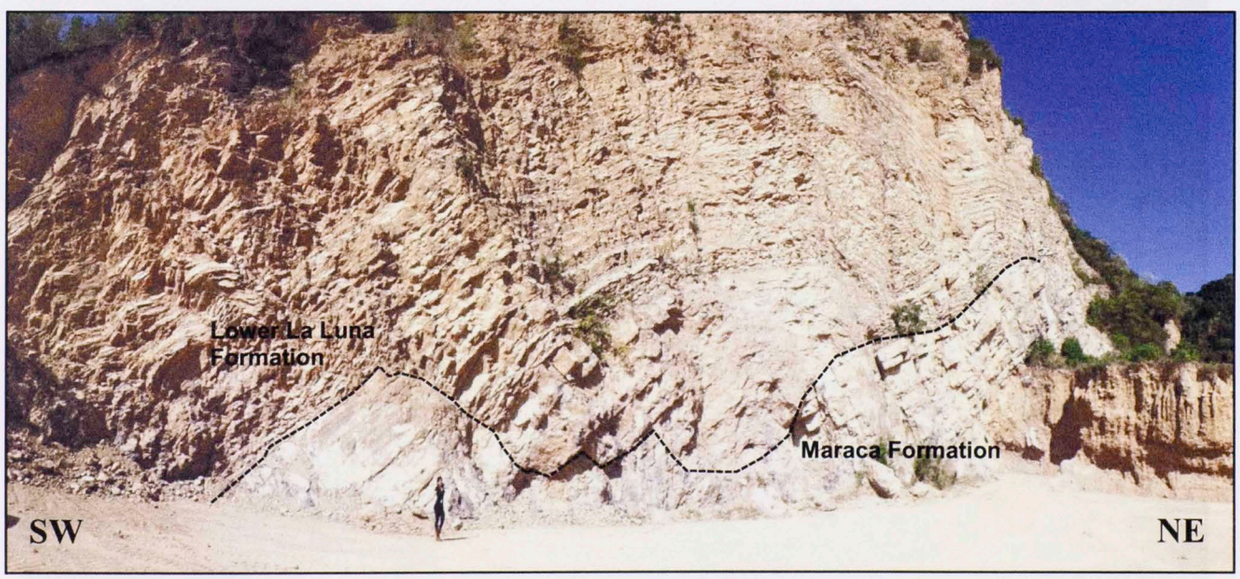

Figure 79 First section of La Luna stratotype. Black dashed lines shows the erosional contact of the Maraca and La Luna Formation. This image represents the Lower-Middle la Luna formation.

"An unconformity between the Maraca and overlying La Luna formations is easily recognized biostratigraphically in the northwestern and central parts of the Maracaibo Basin" (Canache et al., 1994; Truskowski et al., 1995, in Erlich, R., 1999) as shown in this figure. This outcrop is representative of how Upper Cenomanian rocks overlie Upper Albian rocks. "The precise cause of the unconformity is unclear; while drowning appears to be a significant factor of most of Maracaibo, the frequent occurrence of paleokarst at the top of the Upper Maraca formation in western Maracaibo indicates some period of subaerial exposure" (Truskowski et al., 1995, in Erlich, R., 1999). According to Erlich (1999) in northwestern and central Maracaibo, the drowning unconformity is expressed as a submarine hardground, however the abrupt shift from shallow water to "deeper" water deposits over a lithostratigraphic thickness of 1m suggests a hiatus may be present.



Figure 80 Second section of La Luna stratotype. Black dashed lines show the concretions of the Upper La Luna Formation. This image represents the Middle-Upper La Luna formation

Erlich, (1999) also stated that "Lower-Upper Cenomanian rocks in the northwestern Maracaibo Basin still contain an admixture of *in situ* fecal pellets and *Inoceramus* spp. fragments, indicating at least the proximity of oxygenated bottom waters. Nevertheless, this facies quickly grades upwards into microlaminated planktic foraminiferal oozes typical of the La Luna formation thoughout western Venezuela".



Figure 81 Picture that best represents the unconformity of the Albian rocks (Maraca formation) under Cenomanian rocks (Lower La Luna Formation) in the Perijanero Flank, Zulia state (Yellow dashed lines).

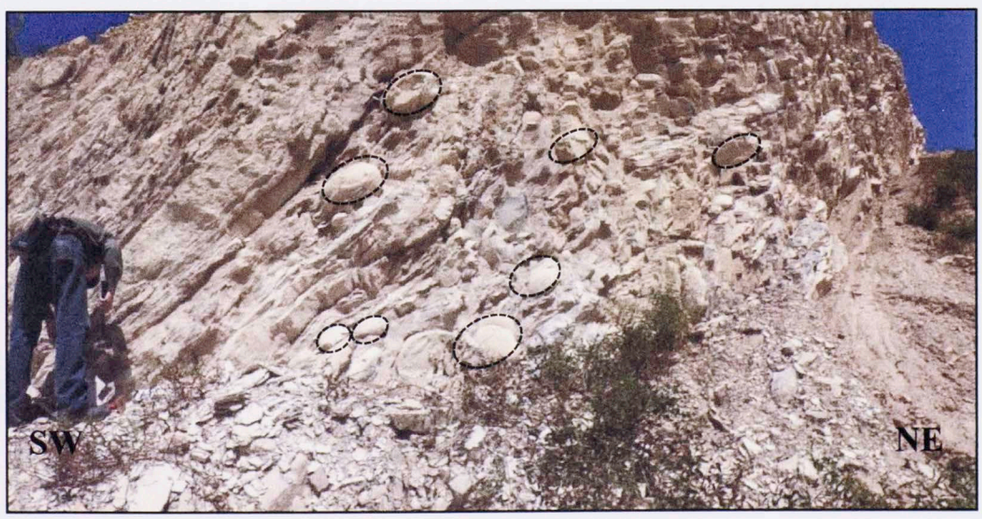

Figure 82 Picture that best represents the Middle La Luna Formation in the Perijanero Flank, Zulia state. The calcite concretions (black dashed lines) that are representative of this interval are noticeable.

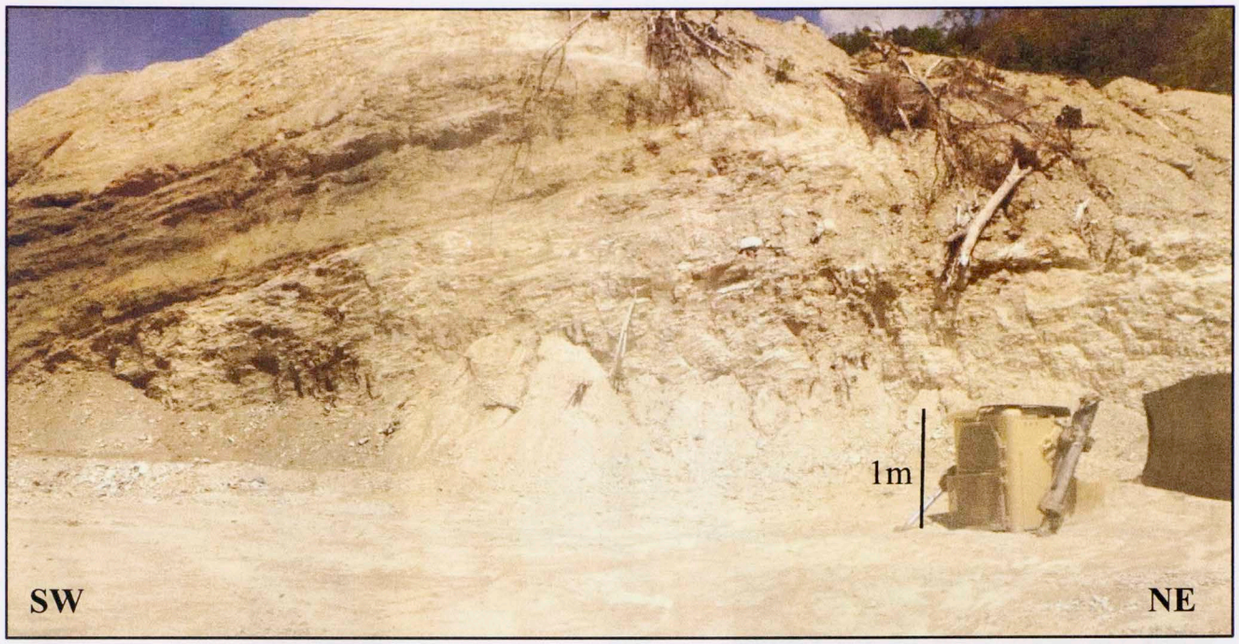

Figure 83 Upper La Luna (Tres Esquinas member) in the Perijanero Flank, Zulia state. The phosphatic and glauconitic composition is representative of this interval.

Figure 84 shows the geological profile using the Ozzies logbook; GR Scintilometer profile; trend; and facies associated with each interval.

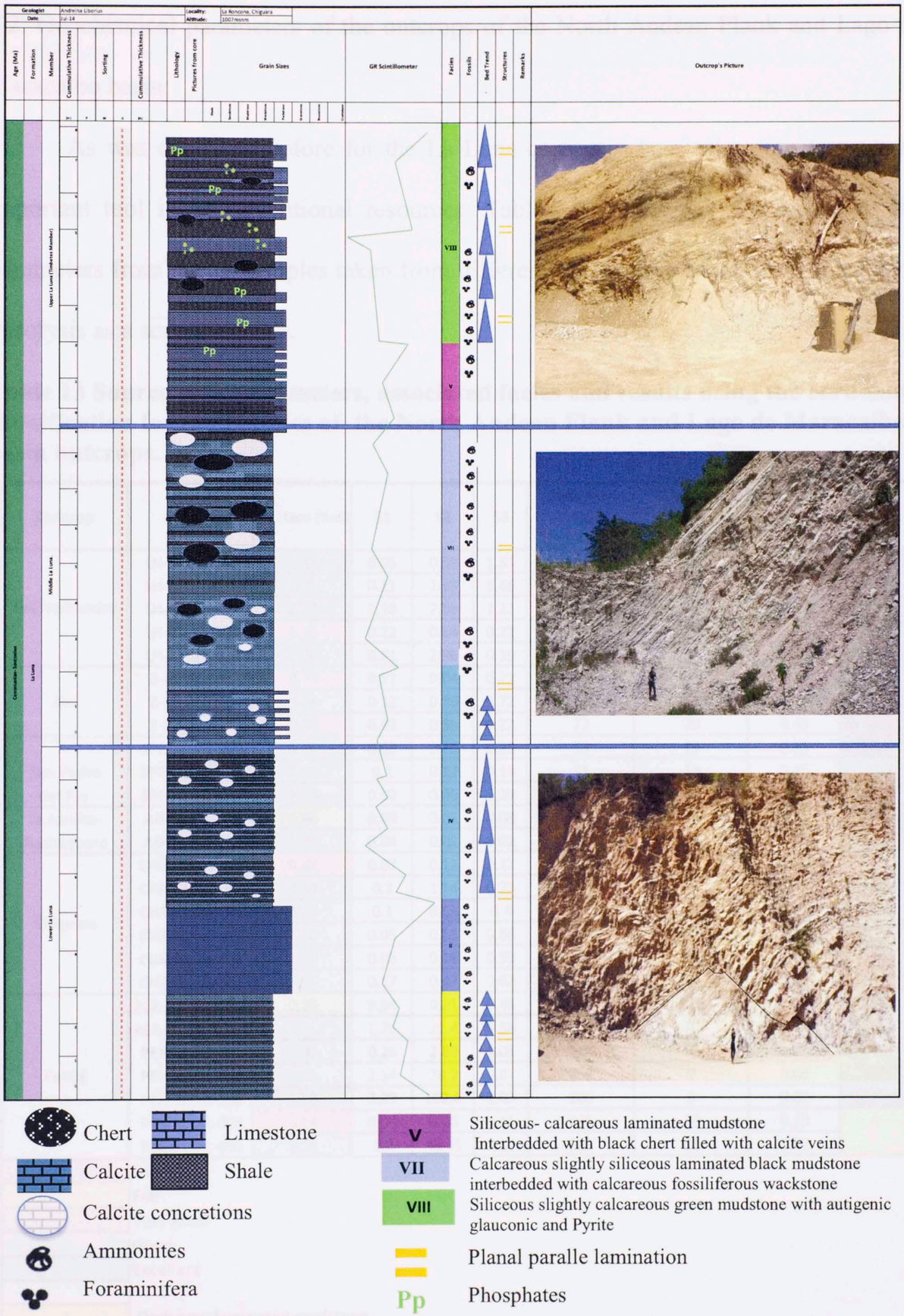

Figure 84 Geological profile using Ozzies logbook representing the geologic units (Vertical scale; lithological pattern; GR scintillometer and facies) in Flanco Perijanero outcrop.

5.2. Geochemical parameters of the outcrops of the North Andean Flank and Lago de Maracaibo basin:

As was described before for the La Luna core, geochemical parameters are an important tool in unconventional resources. Tables 13-18 display the results of the parameters from the 25 samples taken from different outcrops obtained from Rock Eval Pyrolysis as a screening tool.

Table 13 Source rock parameters, associated facies and results using the carbonate classification for the samples of the North Andean Flank and Lago de Maracaibo basin outcrops.

Outcrop	Sample	TOC Leco (%wt)	S1	S2	S3	Hydrogen Index S2x100/TOC	Oxygen Index (S3x100/TOC)	Production Index	Facies
Las Hernandez	LH-KL-AL-013	2.41	0.05	0.59	1.51	24	63	0.08	VI
	LH-KL-AL-012	3.1	0.11	1.49	1.46	48	47	0.07	
	LH-KL-AL-005	3.24	0.38	2.56	1.21	79	37	0.13	V
	LH-KL-AL-003	0.75	0.22	0.64	0.22	85	29	0.26	
	LH-KL-AL-001	2.29	0.81	2.96	0.19	129	8	0.21	
Zea	Z-KL-AL-003	0.74	0.51	0.64	0.21	86	28	0.44	VI
	Z-KL-AL-002	1.64	0.12	0.36	0.72	22	44	0.25	V
	Z-KL-AL-001	0.76	0.42	0.55	0.22	72	29	0.43	
San Pedro del Rio	SPR-KL-AL-004	1.18	0.08	0.15	0.22	13	19	0.35	V
	SPR-KL-AL-003	1.08	0.1	0.12	0.14	11	13	0.45	IV
	SPR-KL-AL-002	2.14	0.02	0.06	1.28	3	60	0.25	
La Azulita-Bachaquero	AB-KL-AL-003	0.46	0.09	0.01	0.08	2	18	0.9	V
	AB-KL-AL-001	1.86	0.04	0.01	1.02	1	55	0.8	
Chiguara	CHR-KL-AL-009	0.69	0.07	0.11	0.17	16	25	0.39	VII
	CHR-KL-AL-008	5.64	0.2	1.14	0.23	20	4	0.15	
	CHR-KL-AL-006	4.74	0.1	0.65	0.4	14	8	0.13	
	CHR-KL-AL-005	1.16	0.05	0.16	0.66	14	57	0.24	V
	CHR-KL-AL-004	1.57	0.05	0.16	0.59	10	38	0.24	
	CHR-KL-AL-001	1.15	0.17	0.47	0.62	41	54	0.27	
Perija	PER-KL-AL-008.2	0.22	0.04	0.21	0.46	98	214	0.16	VII
	PER-KL-AL-008.1	2.9	1.76	21.4	0.58	739	20	0.08	
	PER-KL-AL-007	1.92	0.26	2.69	1.01	140	53	0.09	IV
	PER-KL-AL-005	10.3	2.14	78.2	0.91	759	9	0.03	
	PER-KL-AL-004	12.8	3.29	102.4	1.03	800	8	0.03	
	PER-KL-AL-003	0.14	0.04	0.26	0.11	186	79	0.13	I
	PER-KL-AL-002	7.24	1.2	48.45	1.12	669	15	0.02	

	Poor
	Fair
	Very good
	Good
	Excellent
I	Dark gray laminated mudstone
IV	Laminated mudstone with limestone concretions and micropackstone
V	Siliceous- calcareous laminated mudstone interbedded with black chert filled with calcite veins
VI	VI. Siliceous- Calcareous mudstone interbedded with wackstone facies
VII	Slightly siliceous- calcareous laminated black mudstone interbedded with calcareous fossiliferous wackstone.

Table 14 Source rock parameters, associated facies and results using the shale classification in the the North Andean Flank and Lago de Maracaibo basin outcrops.

Outcrop	Sample	TOC Leco (%wt)	S1	S2	S3	Hydrogen Index (S2x100/TOC)	Oxygen Index (S3x100/TOC)	Production Index	Facies
Las Hernandez	LH-KL-AL-013	2.41	0.05	0.59	1.51	24	63	0.08	VI
	LH-KL-AL-012	3.1	0.11	1.49	1.46	48	47	0.07	
	LH-KL-AL-005	3.24	0.38	2.56	1.21	79	37	0.13	V
	LH-KL-AL-003	0.75	0.22	0.64	0.22	85	29	0.26	
	LH-KL-AL-001	2.29	0.81	2.96	0.19	129	8	0.21	
Zea	Z-KL-AL-003	0.74	0.51	0.64	0.21	86	28	0.44	VI
	Z-KL-AL-002	1.64	0.12	0.36	0.72	22	44	0.25	V
	Z-KL-AL-001	0.76	0.42	0.55	0.22	72	29	0.43	
San Pedro del Rio	SPR-KL-AL-004	1.18	0.08	0.15	0.22	13	19	0.35	V
	SPR-KL-AL-003	1.08	0.1	0.12	0.14	11	13	0.45	IV
	SPR-KL-AL-002	2.14	0.02	0.06	1.28	3	60	0.25	
La Azulita-Bachaquero	AB-KL-AL-003	0.46	0.09	0.01	0.08	2	18	0.9	V
	AB-KL-AL-001	1.86	0.04	0.01	1.02	1	55	0.8	
Chiguara	CHR-KL-AL-009	0.69	0.07	0.11	0.17	16	25	0.39	VII
	CHR-KL-AL-008	5.64	0.2	1.14	0.23	20	4	0.15	
	CHR-KL-AL-006	4.74	0.1	0.65	0.4	14	8	0.13	
	CHR-KL-AL-005	1.16	0.05	0.16	0.66	14	57	0.24	V
	CHR-KL-AL-004	1.57	0.05	0.16	0.59	10	38	0.24	
	CHR-KL-AL-001	1.15	0.17	0.47	0.62	41	54	0.27	
Perija	PER-KL-AL-008.2	0.22	0.04	0.21	0.46	98	214	0.16	VII
	PER-KL-AL-008.1	2.9	1.76	21.4	0.58	739	20	0.08	
	PER-KL-AL-007	1.92	0.26	2.69	1.01	140	53	0.09	IV
	PER-KL-AL-005	10.3	2.14	78.2	0.91	759	9	0.03	
	PER-KL-AL-004	12.8	3.29	102.4	1.03	800	8	0.03	
	PER-KL-AL-003	0.14	0.04	0.26	0.11	186	79	0.13	I
	PER-KL-AL-002	7.24	1.2	48.45	1.12	669	15	0.02	

	Poor
	Fair
	Very good
	Good
	Excellent
I	Dark gray laminated mudstone
IV	Laminated mudstone with limestone concretions and micropackstone
V	Siliceous- calcareous laminated mudstone interbedded with black chert filled with calcite veins
VI	VI. Siliceous- Calcareous mudstone interbedded with wackstone facies
VII	Slightly siliceous- calcareous laminated black mudstone interbedded with calcareous fossiliferous wackstone.

Table 13 and 14 show the results of the geochemical parameters using the two classifications mentioned before.

Due to the increment of clastic deposits, weathering and the percent of organic matter present at the surface that appears to have affected the mudstones, it's better to take into account the shale classification in the North Andean Flank where the results differ slightly: The carbonate classification identifies an excellent source rock in almost all the intervals but the shale classification shows a very good- good-fair source rock.

In Lago de Maracaibo Basin (Flanco Perijanero) the results differ in both classifications, the Carbonate classification displays an excellent source rock, while the shale classification differs in most intervals. As the Flanco Perijanero outcrop is located in Lago de Maracaibo Basin (the percent of carbonates increases in this area and this outcrop is the La Luna Formation stratotype in Venezuela, which is 90% carbonates), the carbonate source rock classification should be taken into account for this outcrop. Table 19 and 20 also display the facies associated with the La Luna core description.

5.2.1. Source Potential Logs of the North Andean and Lago de Maracaibo Basin

The following diagrams allow differentiating the outcrops based on their TOC and prospectively results. The first outcrop in this section is Las Hernandez outcrop. It represents the most prospective outcrop in the North Andean flank. This outcrop has already generated hydrocarbons. TOC ranges around 2.29- 3.24 wt % and the S2 (figure 86A) displays a fair value for oil potential in some samples (Figure 86B). Although the percentage of carbonate is high, some variations in TOC content are due to the deposition of chert and shales in the outcrop. The hydrogen index in figure 86C, show a response of mixed oil and gas towards the top of the outcrop. Pyrograms (Figure 85) also show that even when the S2 presents some potential, the S3 and S4 shows a large amount of organic matter when compared with the already generated (S1) and the potential (S2).

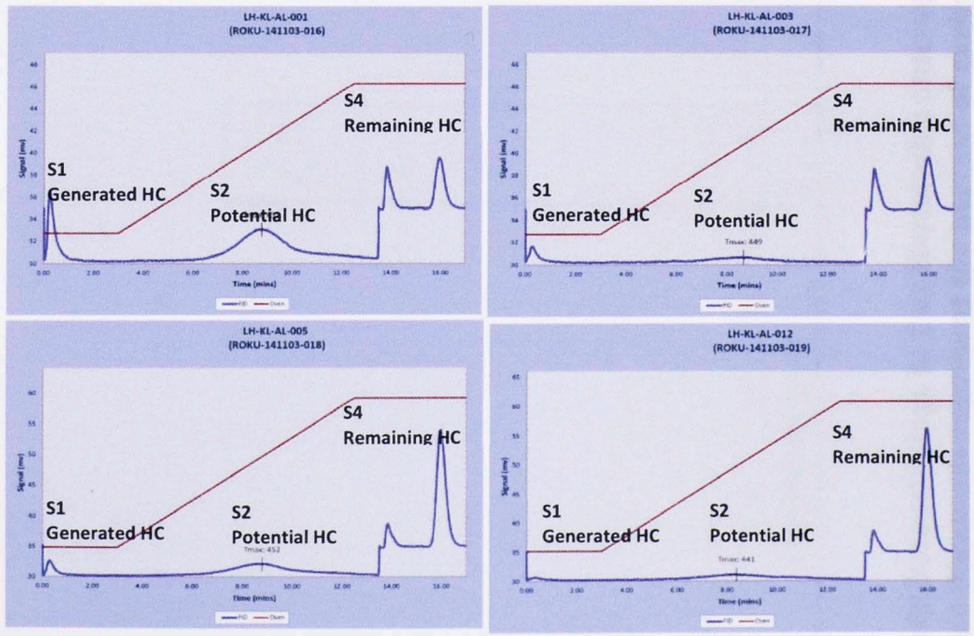

Figure 85 Pyrogram plots from Las Hernandez outcrop showing the Potential Hydrocarbon context in Facies V and VII (La Luna Upper interval).

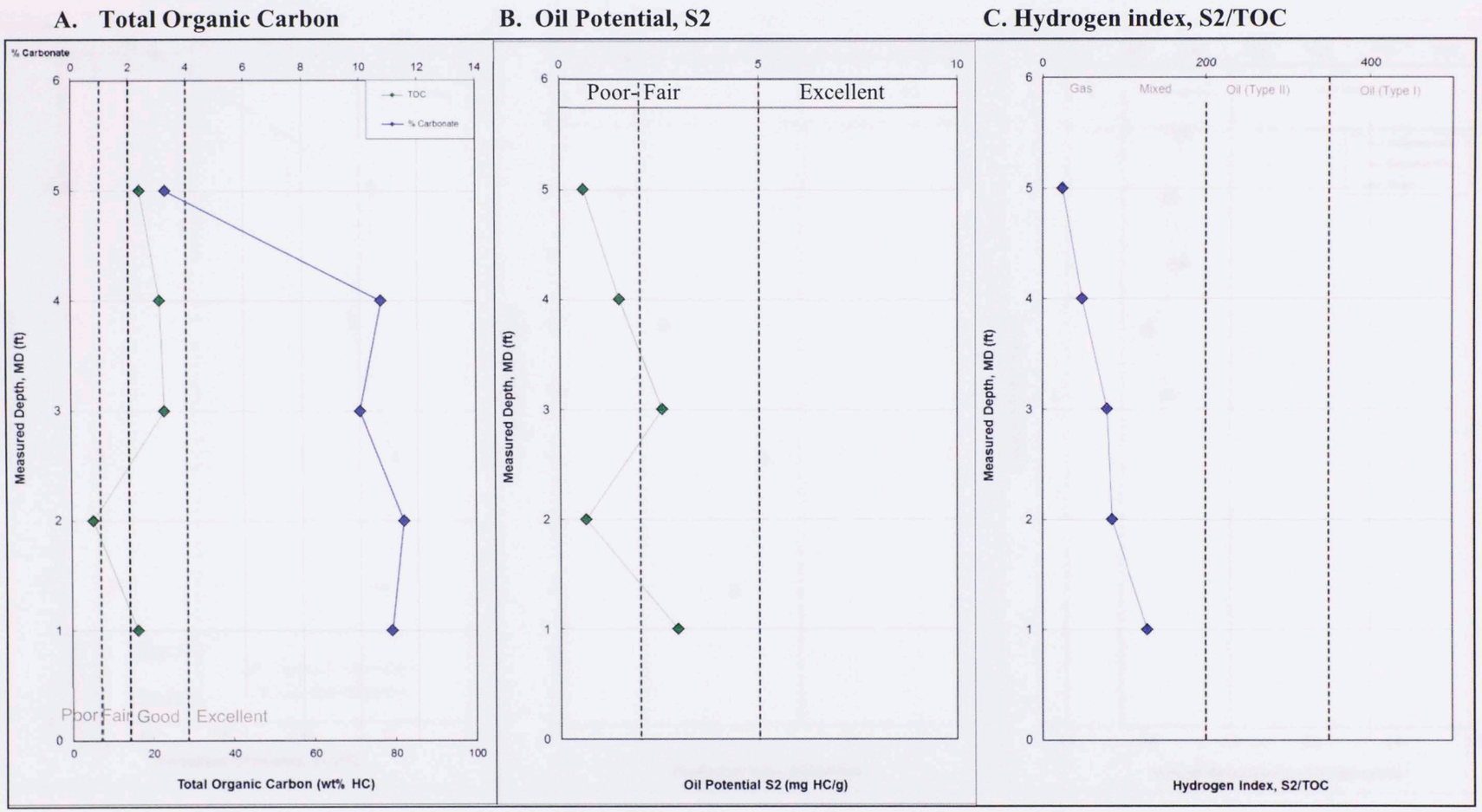

Figure 86 Source Potential logs in Las Hernandez outcrop. A) Total organic carbon (Green diamonds represent the TOC content and blue diamonds represent the percent of carbonates). B) Relationship between the S2 peak and the oil potential quality with depth. C) Relationship of the S2 peak between the TOC and the oil potential quality.

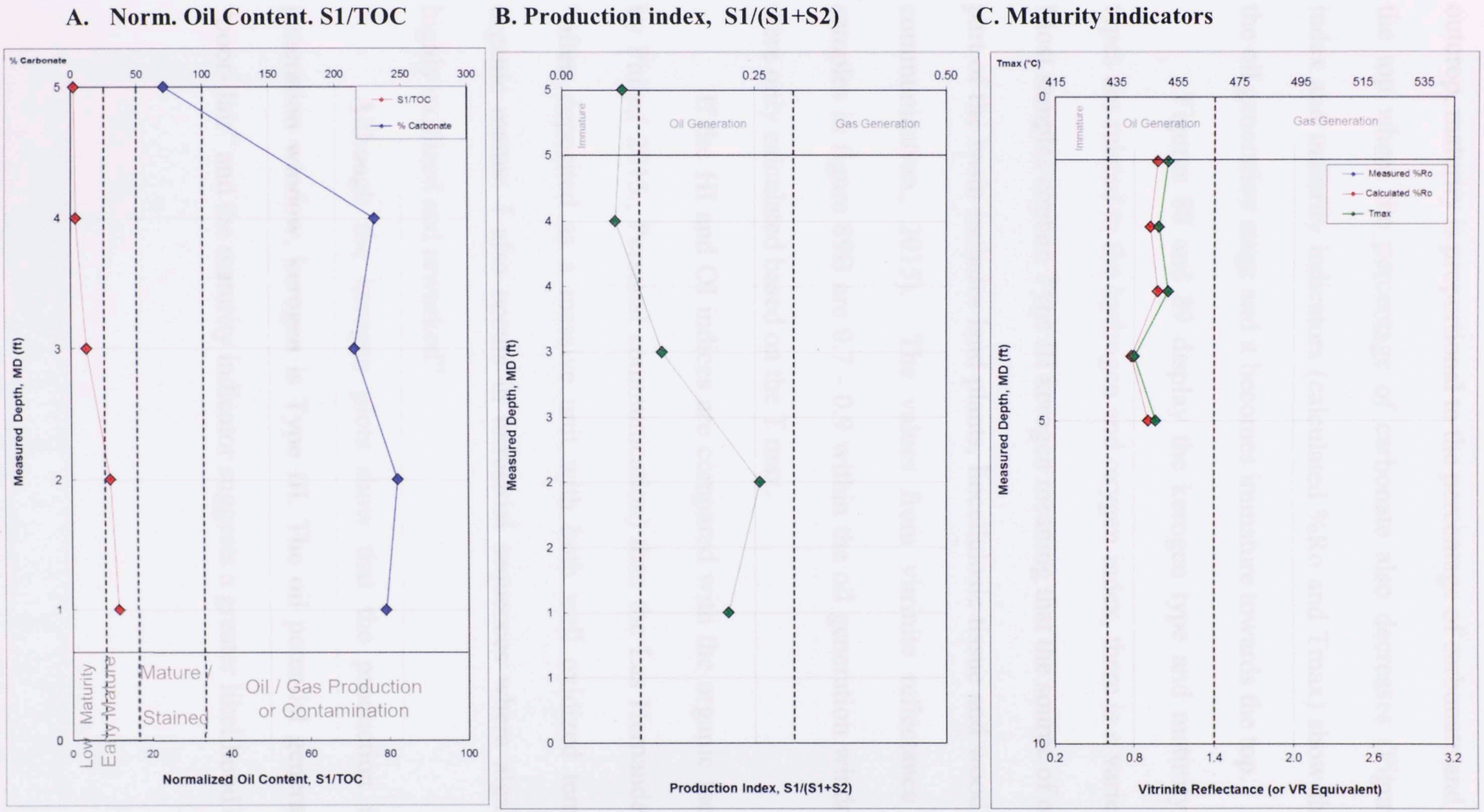

Figure 87 Maturity logs in Las Hernandez outcrop. A) Relationship of the S1 peak between the TOC and the percent of carbonates in Las Hernandez outcrop. B) Production index S1/ (S1+S2) with depth C. Maturity indicators (calculated vitrinite reflectance).

In figure 87, maturity logs in the Las Hernandez outcrop shows that in the basal outcrop, maturity is proportional to the percentage of carbonate and it decreases towards the top where the percentage of carbonate also decreases (Figure 87A). Production index and maturity indicators (calculated %Ro and Tmax) show that this outcrop is in the oil generation stage and it becomes immature towards the top.

Figures 88 and 89 display the kerogen type and maturity. Although kerogen types are related to the hydrogen and oxygen index, there is a variety of kerogen types. Most samples contain Type III kerogen meaning that the source of organic matter in this part of the basin includes land plants, liocellulosic tissue and wood (Philp, R.; personal communication., 2015). The values from vitrinite reflectance of Las Hernandez samples in figure 89B are 0.7 - 0.9 within the oil generation window, but these values were only calculated based on the T max.

If the HI and OI indices are compared with the organic facies model proposed by Philp,(2015., Personal communication) than the Las Hernandez outcrop relates as "often deposited as a massive unit with both well oxidized terrestrial and residual organic matter. I also occurs in terrestrial sequences where algal material has been highly oxidized and reworked"

Although the kerogen plots show that the production index is in the oil generation window, kerogen is Type III. The oil potential generation is classified as "poor- fair" and the maturity indicator suggests a greater likelihood of gas generation.

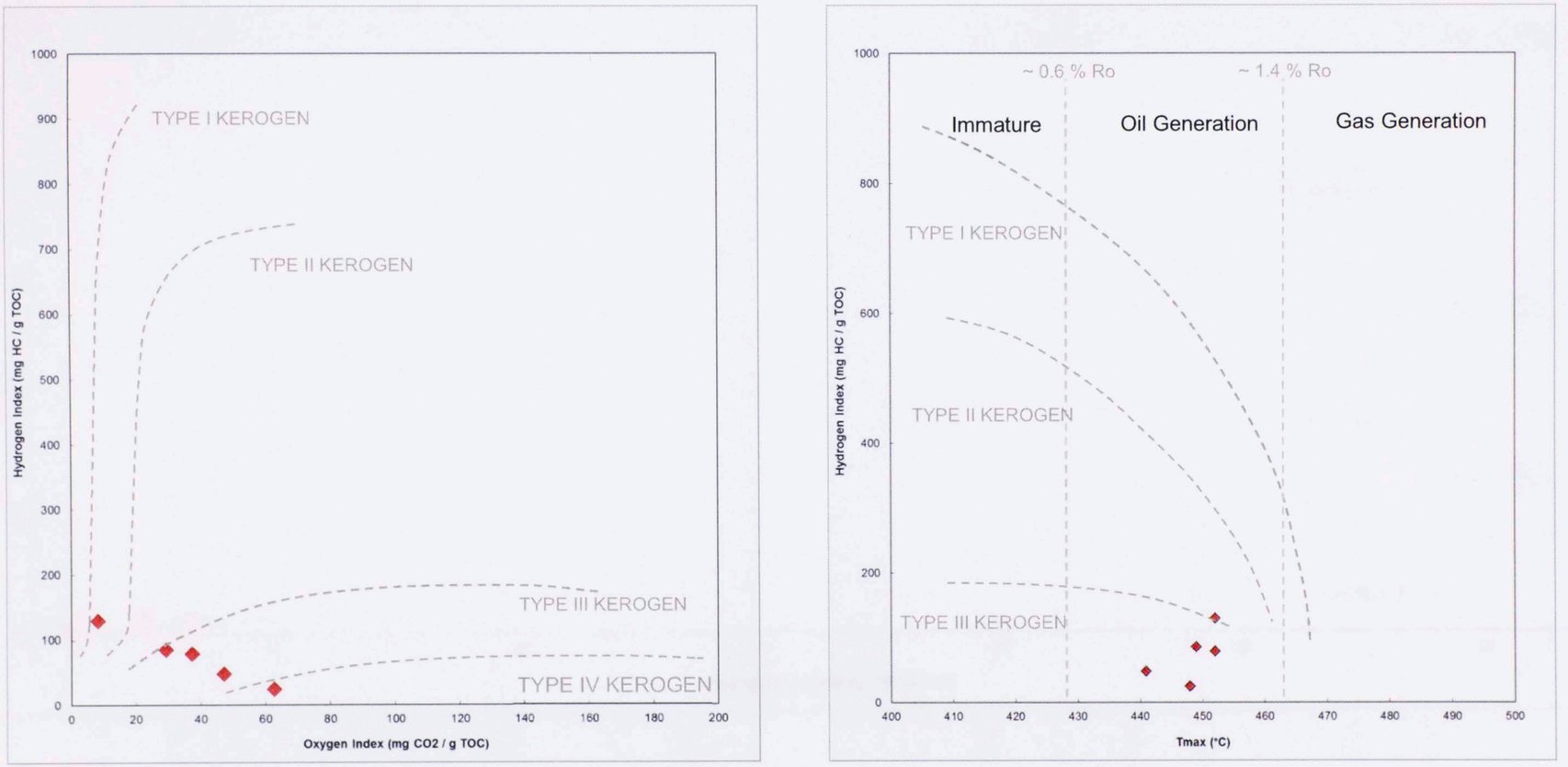

Figure 88 A) Pseudo Van Krevelen diagram showing four different types of kerogen at different maturity levels. B) Kerogen type and maturity plot that displays the relationship between the Tmax and the Hydrogen index. Red diamonds represent Las Hernandez samples.

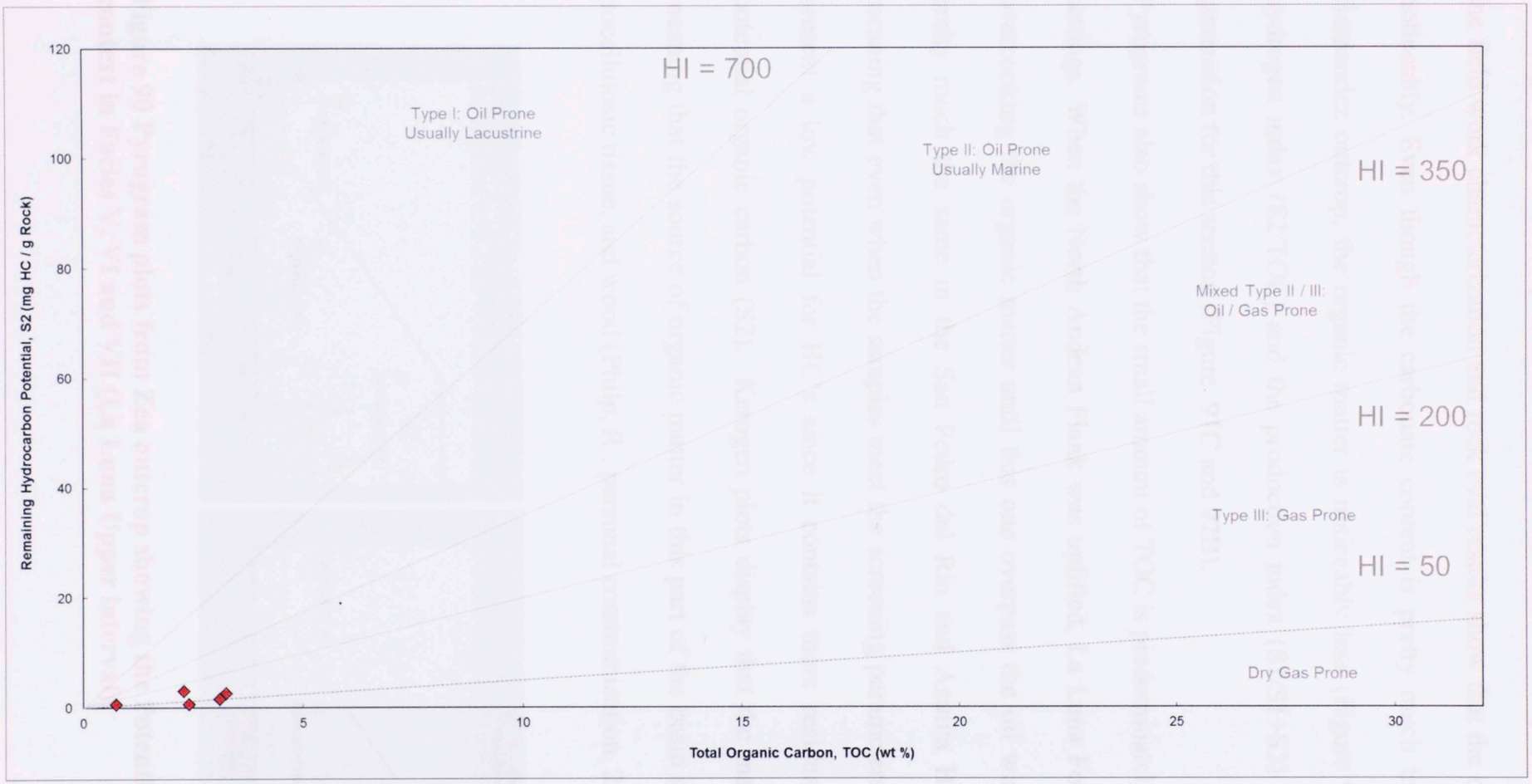

Figure 89 Kerogen Quality Plot that correlates TOC and S2. Red diamonds represent Las Hernandez samples.

Although the Zea outcrop is near the Las Hernandez outcrop (around 5.25km apart), the field work characterization and rock eval results show that the oil potential changes noticeably. Even though the carbonate content is pretty much the same as the Las Hernandez outcrop, the organic matter is noticeably less (Figure 91A and 91B). The hydrogen index (S2/TOC) and the production index (S1/S1+S2) establishes just gas generation for this section (Figure 91C and 92B).

Pyrograms also show that the small amount of TOC is predominately due to the tectonic settings. When the North Andean Flank was uplifted, La Luna Formation was heated overcooking the organic matter until this one overpass the oil window. This trend is pretty much the same in the San Pedro del Rio and Azulita Bachaquero outcrops meaning that even when the samples meet the screening parameters, the three outcrops present a low potential for HC's since it contains more residual carbon (S4) than potential organic carbon (S2). Kerogen plots display that the majority are Type III, meaning that the source of organic matter in this part of the basin includes land plants, liocellulosic tissue, and wood (Philp, R.; personal communication. 2015).

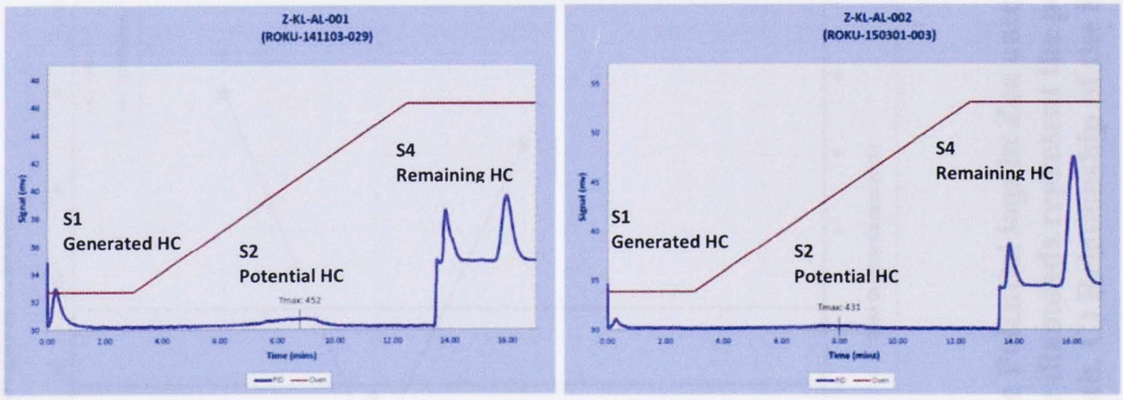

Figure 90 Pyrogram plots from Zea outcrop showing the Potential Hydrocarbon context in Facies V, VI and VII (La Luna Upper interval).

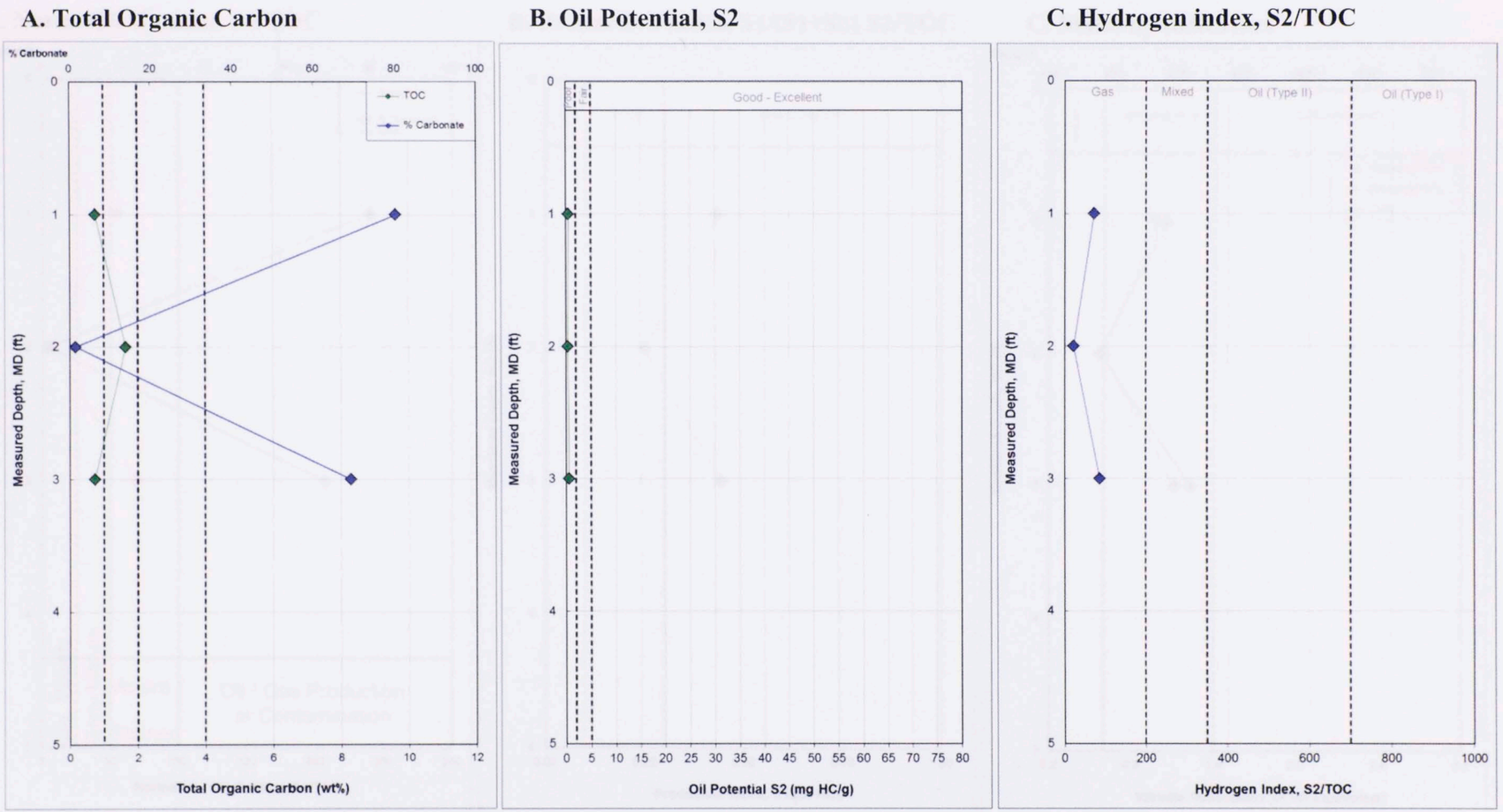

Figure 91 Source Potential logs in Zea outcrop. A) Percentage of TOC and Carbonates (Green diamonds represent the TOC content and blue diamonds represent the percent of carbonates). B) Relationship between the S2 peak and the Oil potential quality with depth. C) Relationship of the S2 peak between the TOC and the Oil potential quality.

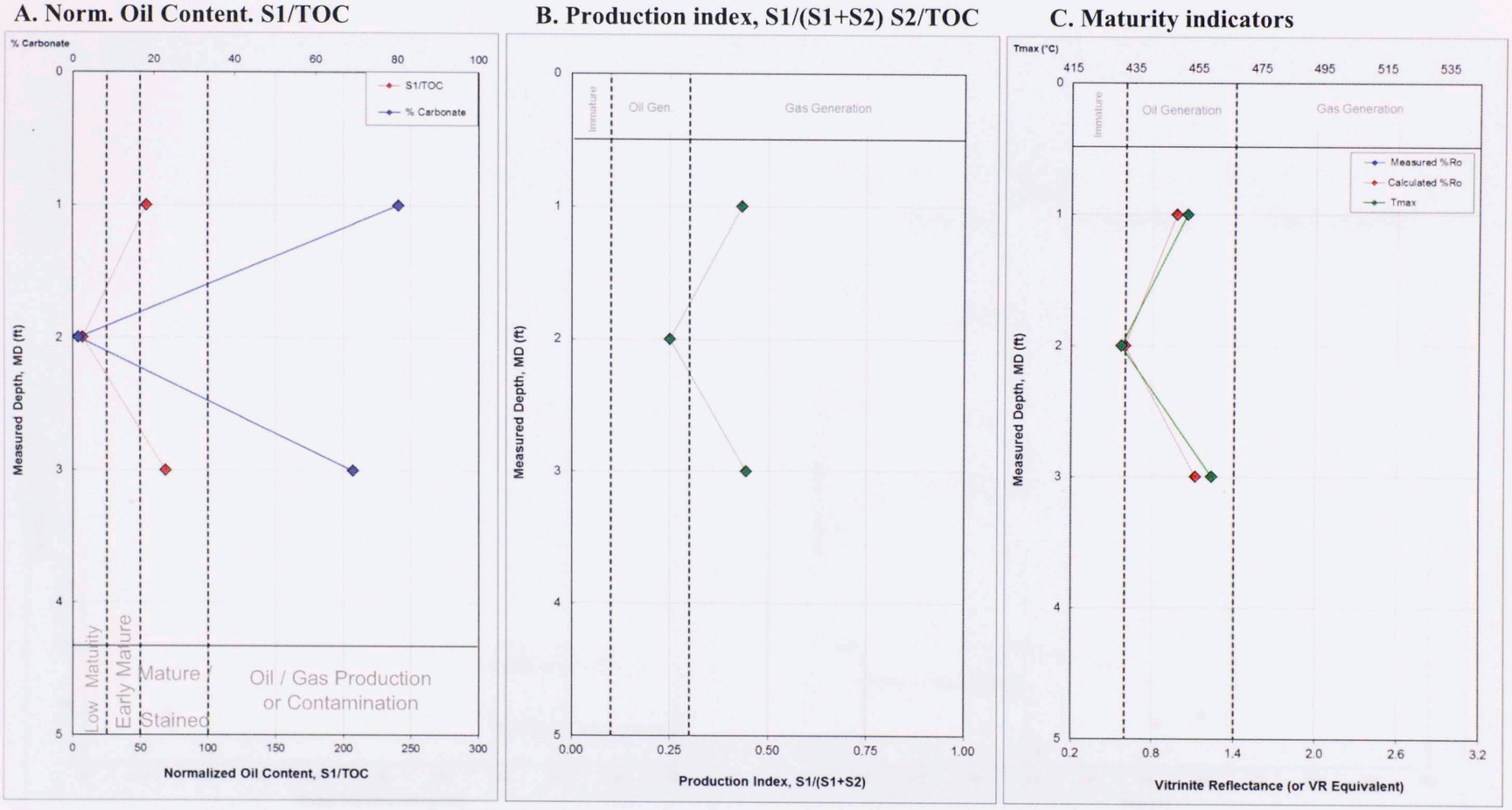

Figure 92 Maturity logs in Zea outcrop. A. Relationship of the S1 peak between the TOC and the percent of carbonates in Las Hernandez outcrop. B) Production index changes S1/ (S1+S2)) C) Maturity indicators (calculated vitrinite reflectance).

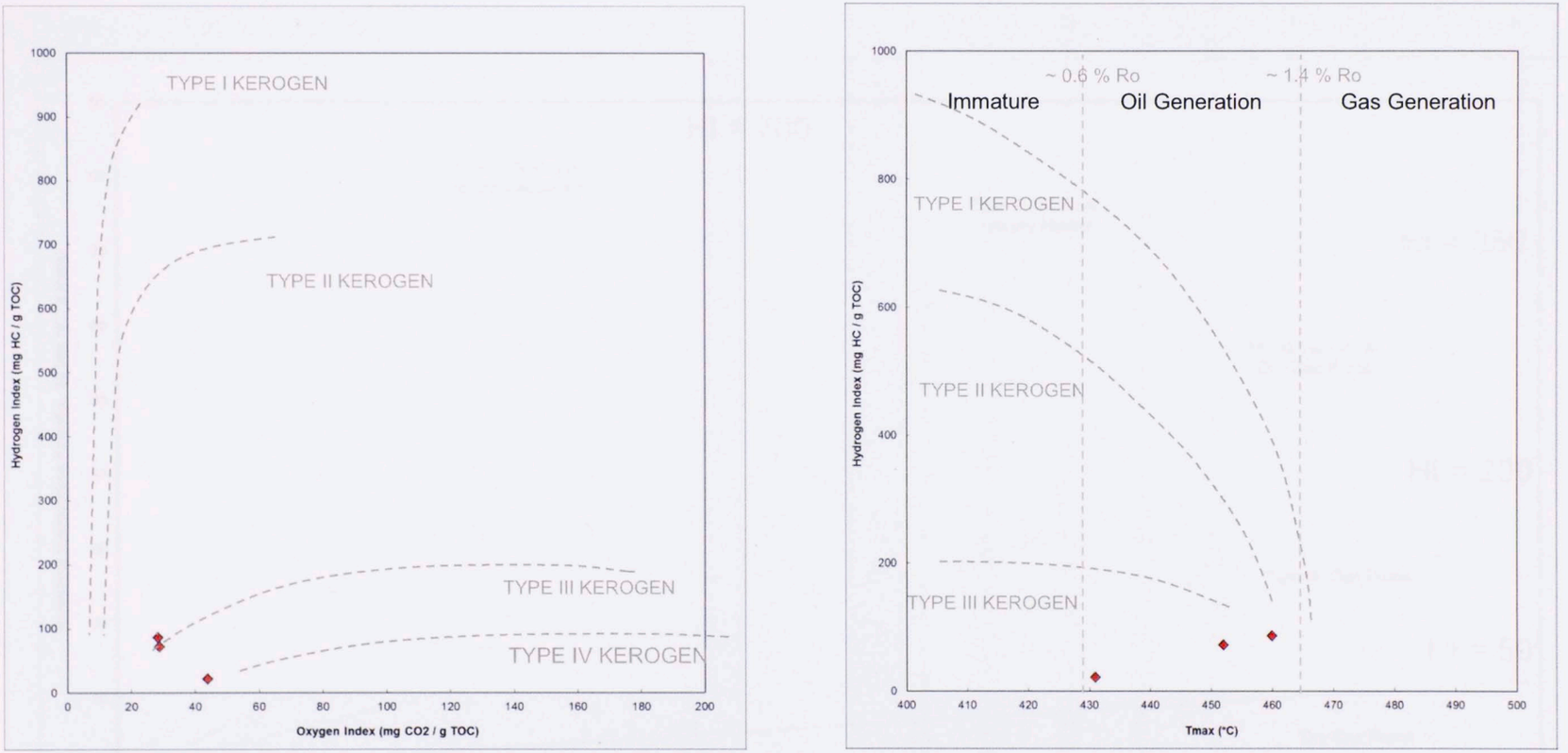

Figure 93 A. Pseudo Van Krevelen diagram showing four different types of kerogen at different maturity levels. B) Kerogen type and maturity plot that displays the relationship between the Tmax and the Hydrogen index. Red diamonds represent Zea samples.

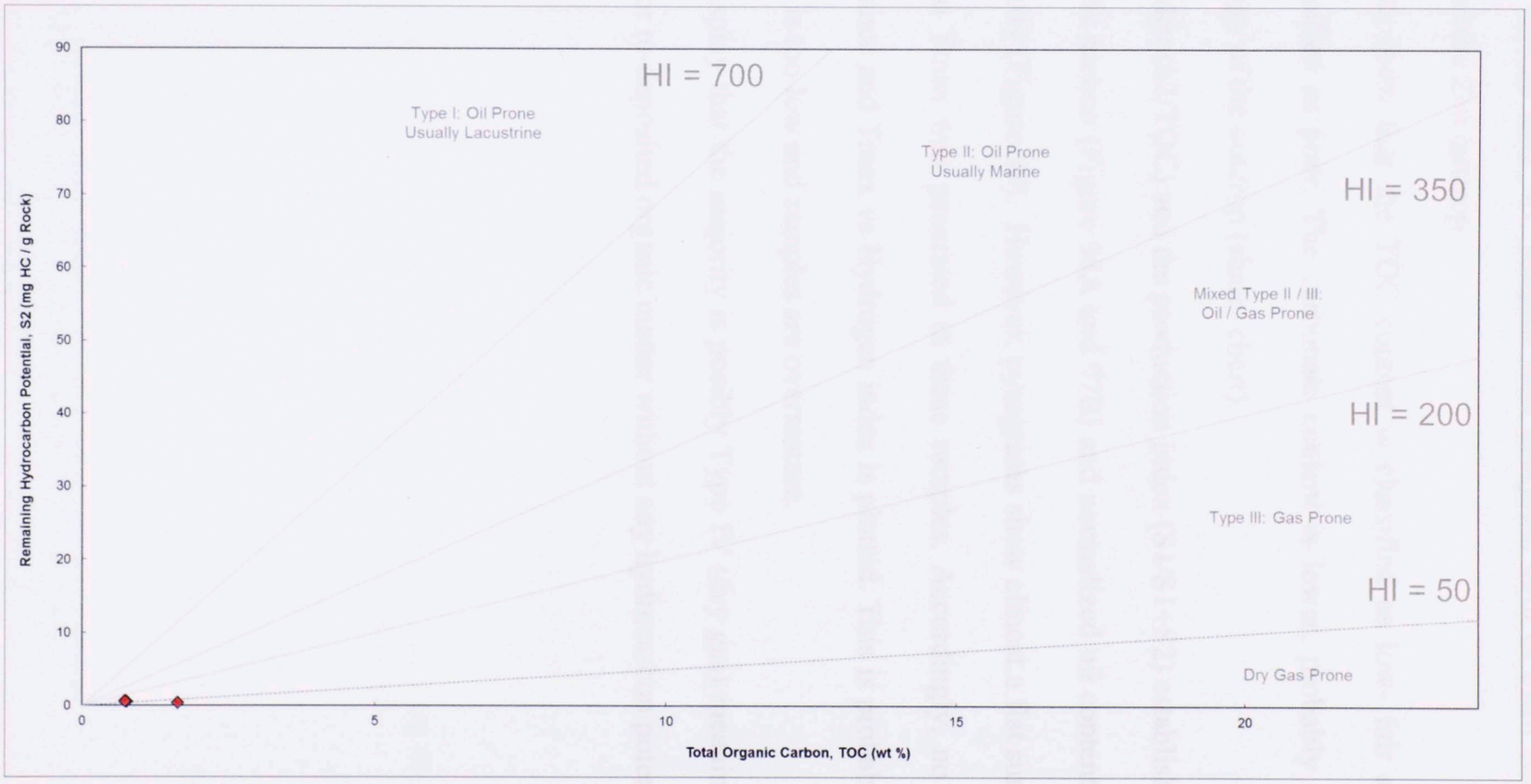

Figure 94 Kerogen Quality Plot that correlates TOC and S2. Red diamonds represent Zea samples.

La Azulita – Bachaquero is an outcrop with a noticeable content of organic matter and carbonate. Even though only two samples were analyzed, both of them shows almost the same trends as the Zea outcrop.

Rock eval results show that the TOC content is classified as low- fair and the oil potential is classified as poor. The carbonate content is lower, probably due to the change of lithology of the outcrop (shale- chert).

The hydrogen index (S2/TOC) and the production index (S1/S1+S2) establishes just gas generation for this section (Figure 96A and 97B) and normalized oil content (S1/TOC) shows low maturity (Figure 98). However, pyrograms show almost a flat surface in the S2 peak, thus no Tmax was generated in these samples. Accordingly, no calculated Vitrinite Reflectance and Tmax vs Hydrogen index is plotted. This is probably because the TOC content is too low and samples are overmature.

Kerogen plots display that the majority is posibly Type IV (dry gas) meaning that it is highly oxidized or re-deposited organic matter without any hydrocarbon potential.

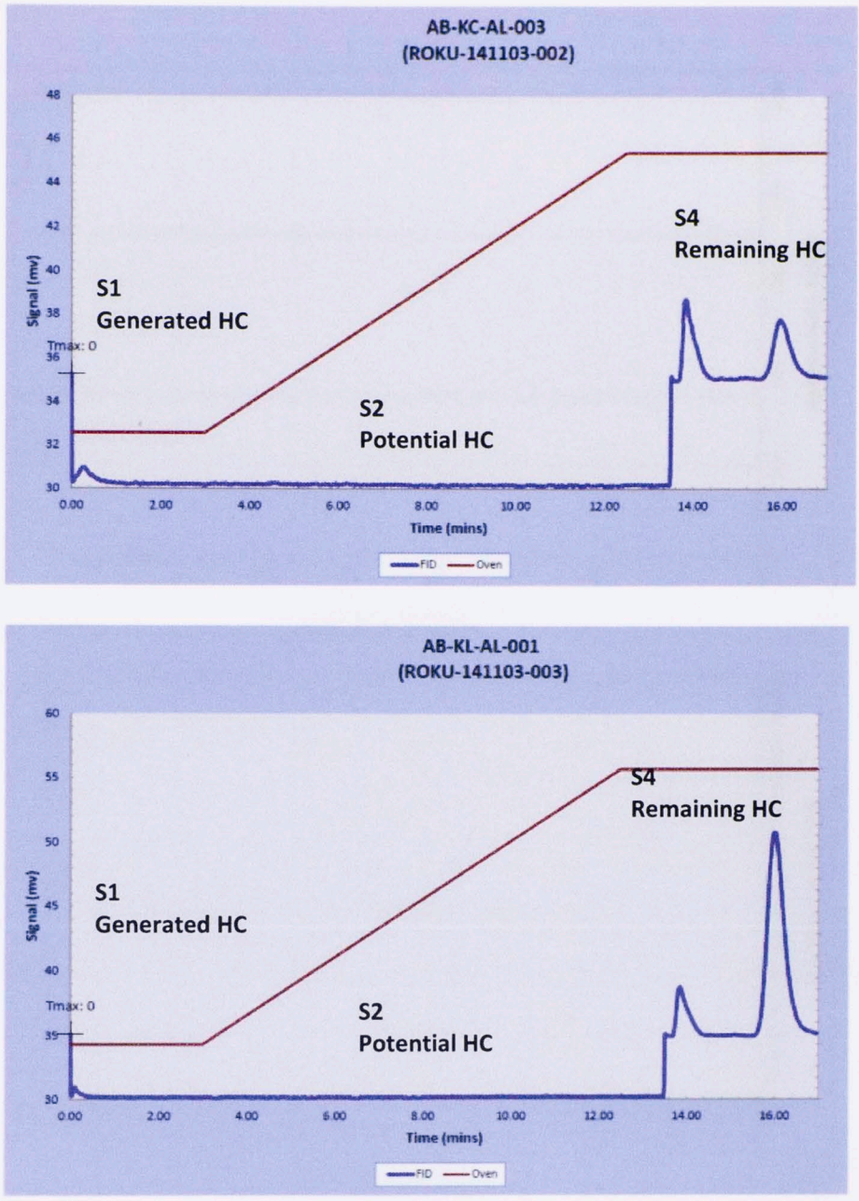

Figure 95 Pyrogram plots from Azulita-Bachaquero outcrop showing the Potential Hydrocarbon context in Facies I V and V (La Luna Upper interval).

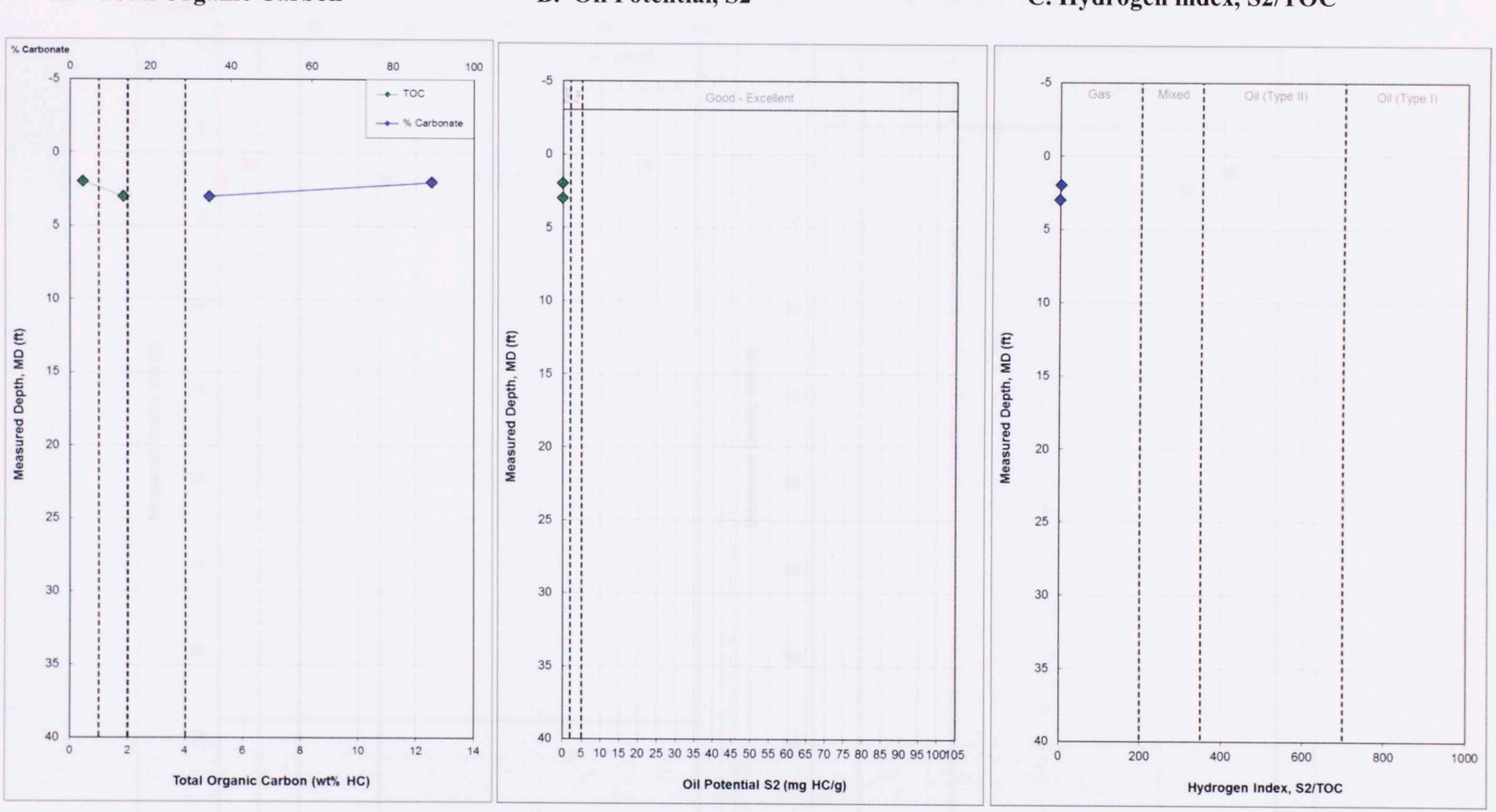

Figure 96 Source Potential logs in La Azulita – Bachaquero outcrop. A) Percentage of TOC and Carbonates (Green diamonds represent the TOC content and blue diamonds represent the percent of carbonates). B) Relationship between the S2 peak and the Oil potential quality with depth. C) Relationship of the S2 peak between the TOC and the Oil potential quality.

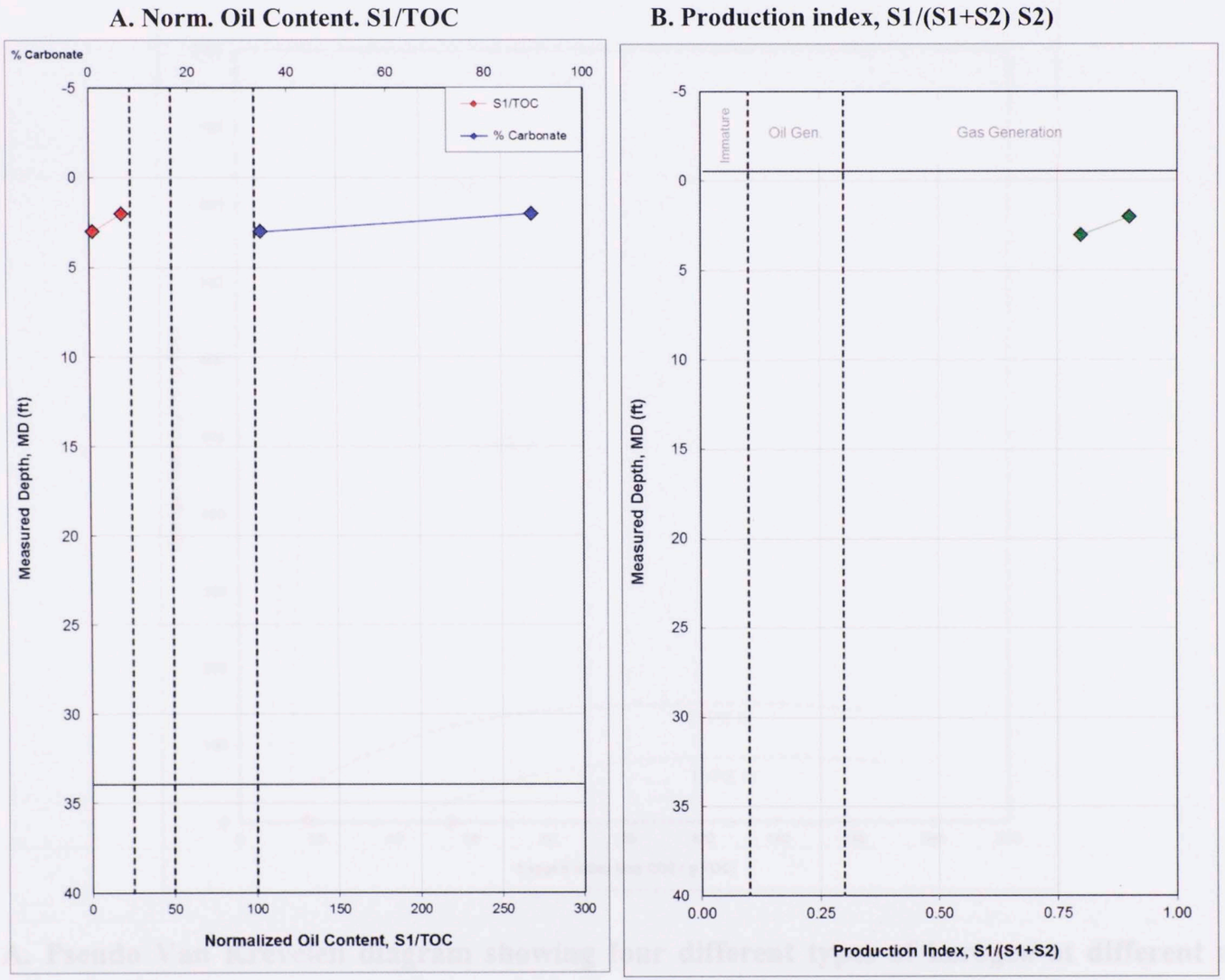

Figure 97 Maturity logs in Las Hernandez outcrop. A) Relationship of the S1 peak between the TOC and the percent of carbonates in Las Hernandez outcrop. B) Production index changes S1/ (S1+S2).

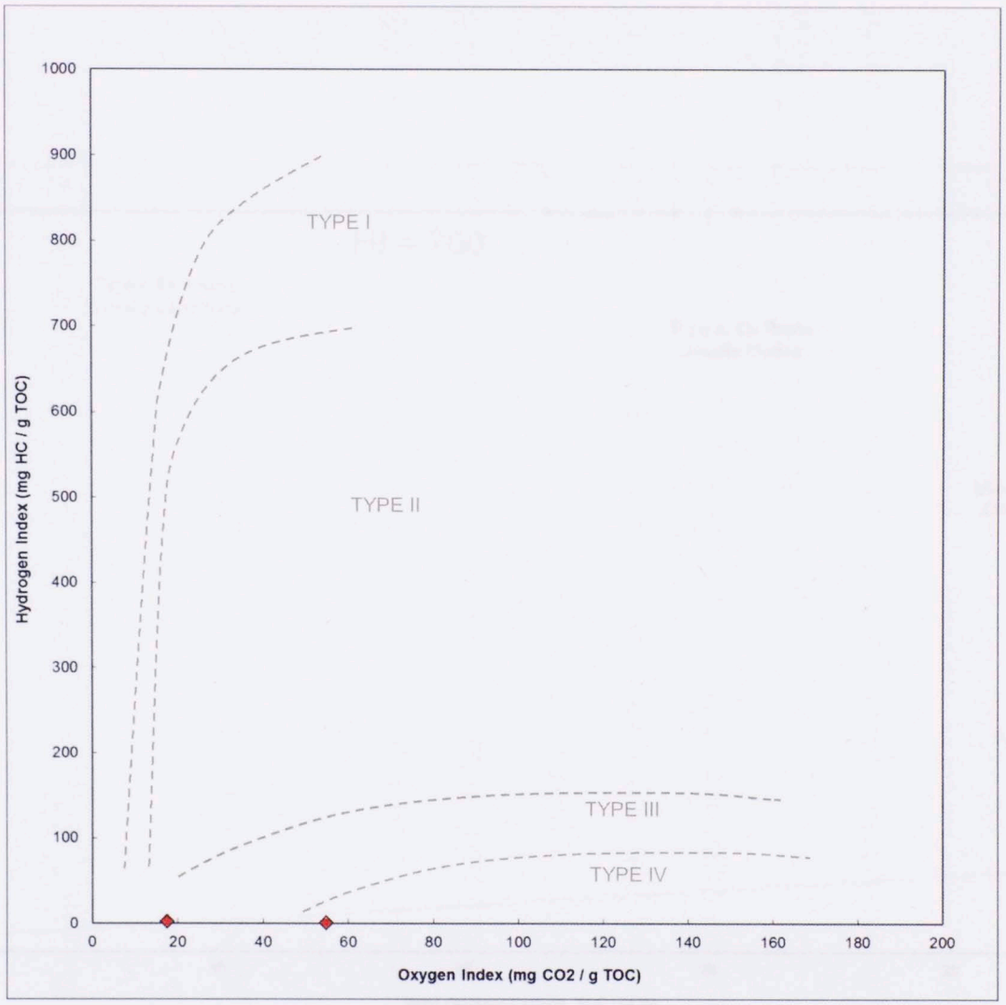

Figure 98 A. Pseudo Van Krevelen diagram showing four different types of kerogen at different maturity levels in Azulita- Bachaquero outcrop.

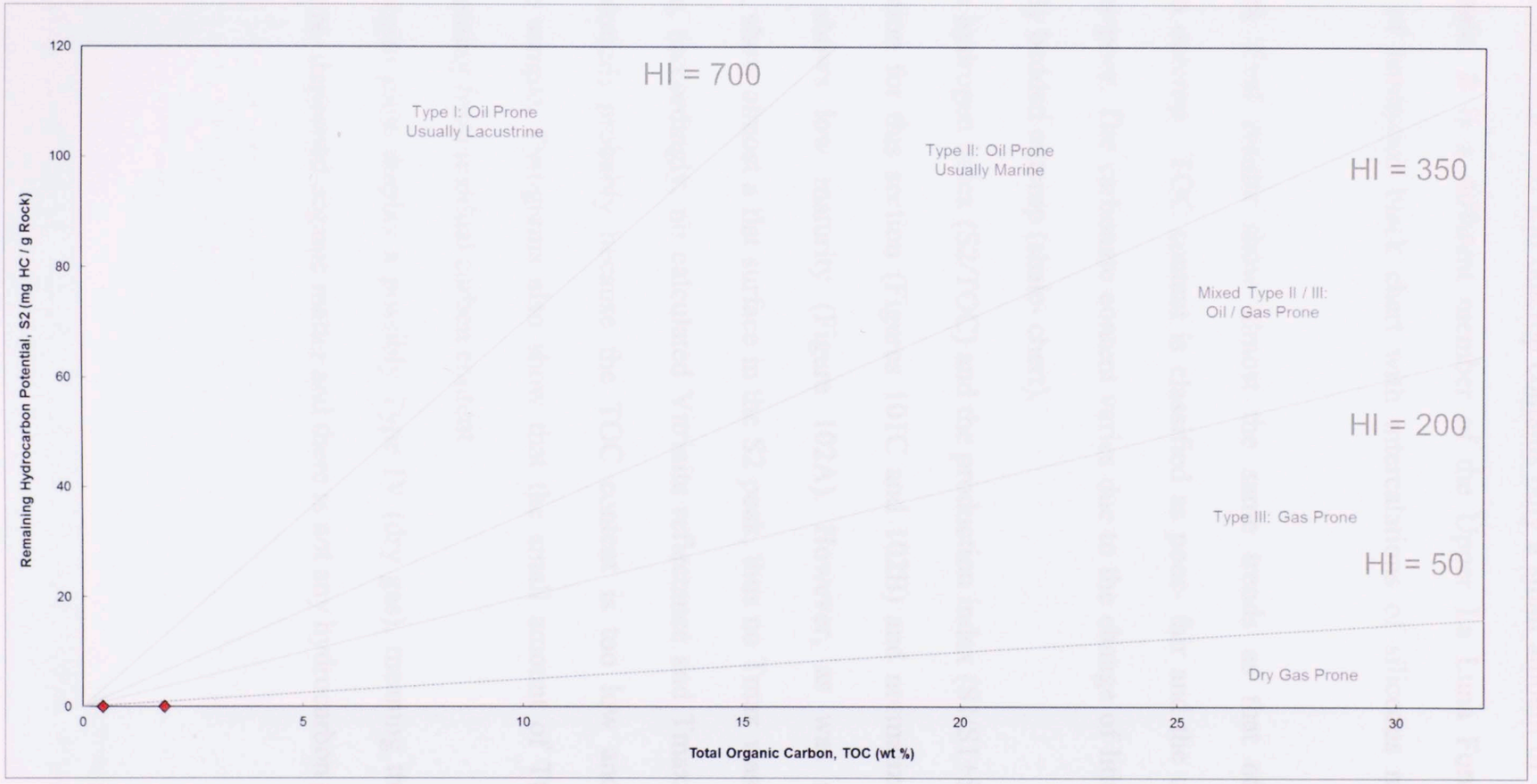

Figure 99 Kerogen Quality Plot that correlates TOC and S2. Red diamonds represent Azulita – Bachaquero samples samples.

The San Pedro del Rio outcrop contains only a small amount of organic matter and carbonate. It is a different member of the Upper La Luna Formation and is composed of laminated black chert with intercalations of siliceous mudstones and limestone.

Rock Eval results show almost the same trends as that of La Azulita-Bachaquero outcrop. TOC content is classified as poor- fair and the oil potential is classified as poor. The carbonate content varies due to the change of lithology and the rhythmically bedded outcrop (shale- chert).

The hydrogen index (S2/TOC) and the production index (S1/S1+S2) establishes gas generation for this section (Figures 101C and 102B) and normalized oil content (S1/TOC) shows low maturity (Figure 102A). However, as was stated before, pyrograms, show almost a flat surface in the S2 peak, thus no Tmax was generated for this sample, (accordingly, no calculated Vitrinite reflectance and Tmax vs Hydrogen index is plotted) probably because the TOC content is too low and it's also an overmature sample. Pyrograms also show that the small amount of TOC content is probably coming from residual carbon content.

Kerogen plots display a possibly Type IV (dry gas), meaning that it is highly oxidized or re- deposited organic matter and there is not any hydrocarbon potential.

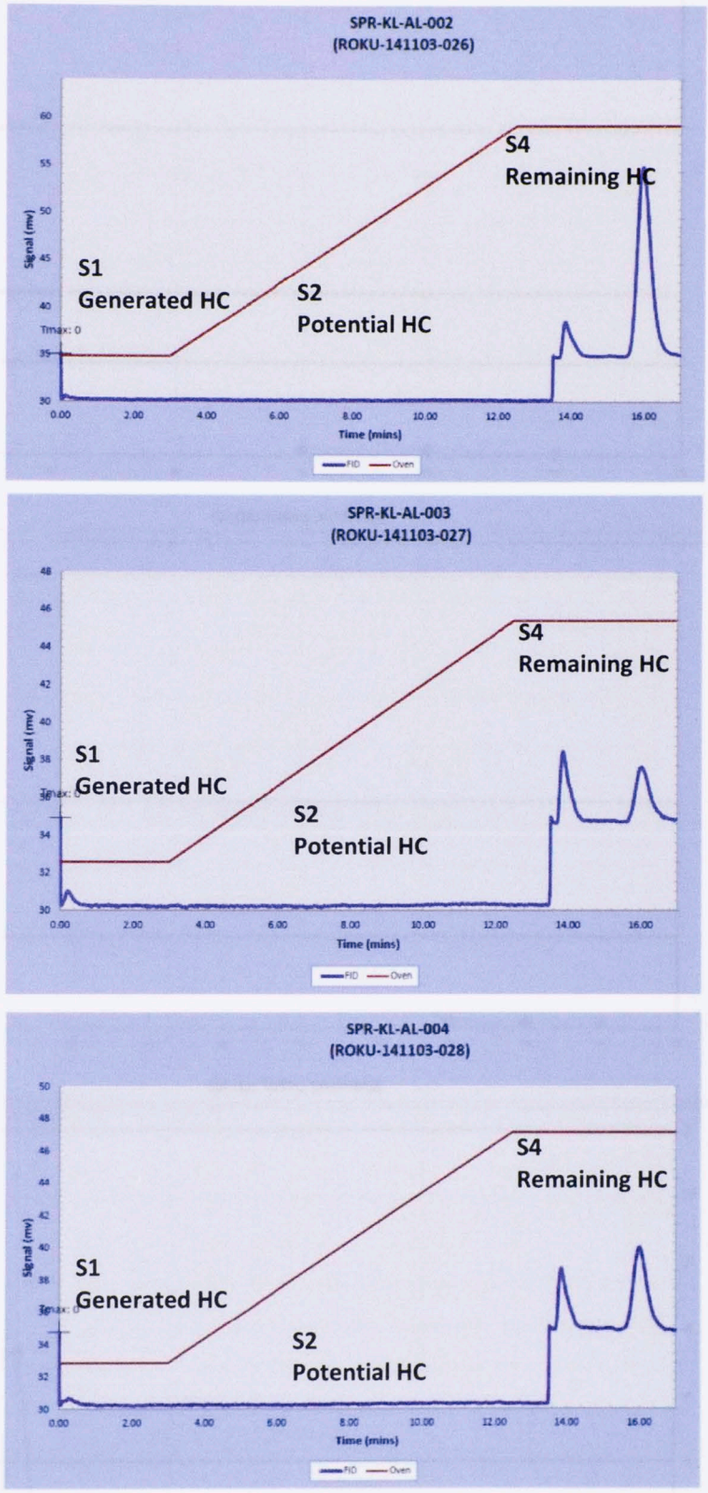

Figure 100 Pyrogram plots from San Pedro del Rio outcrop showing the Potential Hydrocarbon content in Facies I V and V (La Luna Upper interval).

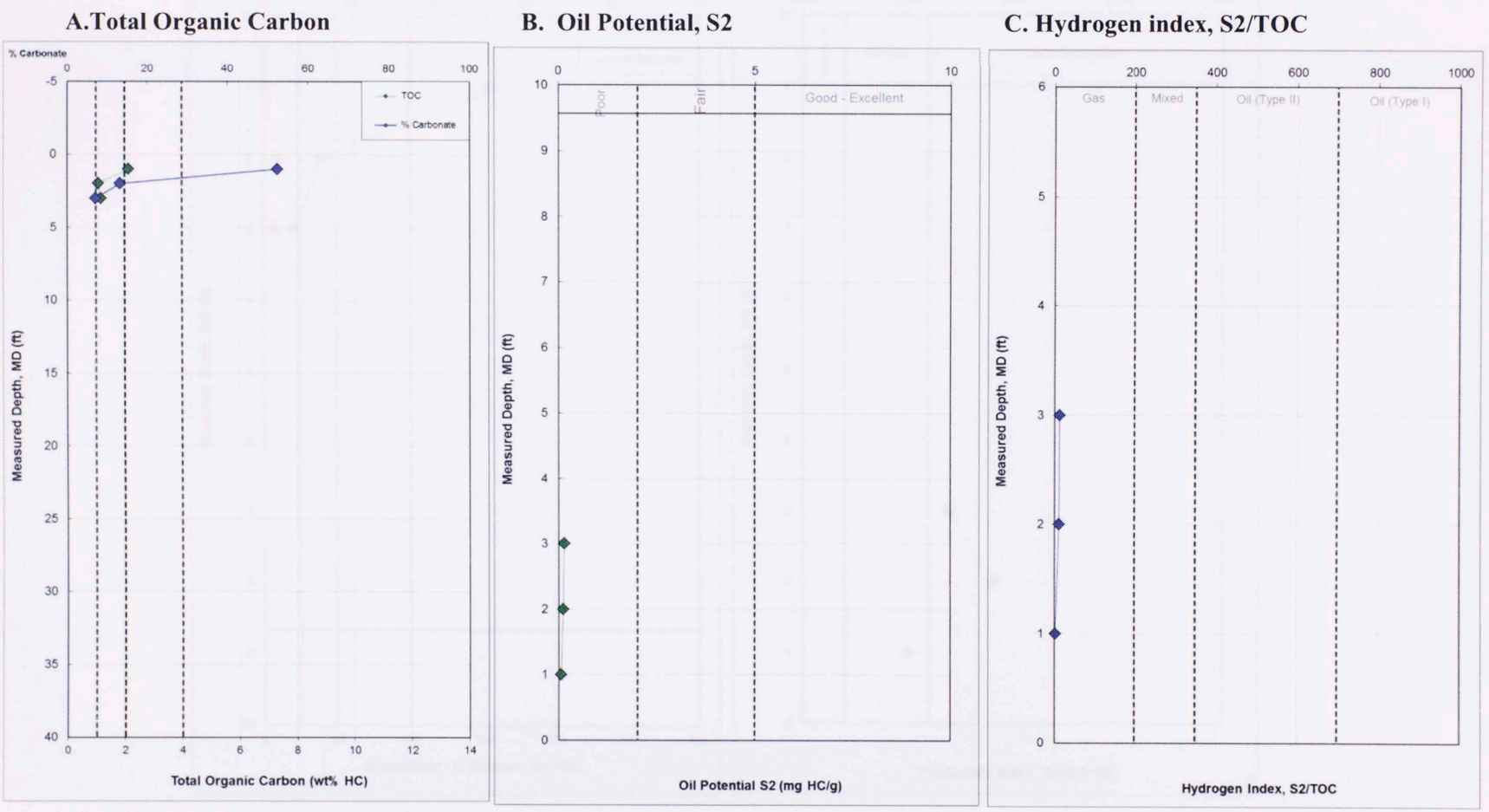

Figure 101 Source Potential logs in San Pedro del Rio outcrop. A) Percentage of TOC and Carbonates (Green diamonds represent the TOC content and blue diamonds represent the percent of carbonates). B) Relationship between the S2 peak and the Oil Potential quality with depth. C) Relationship of the S2 peak between the TOC and the Oil Potential quality.

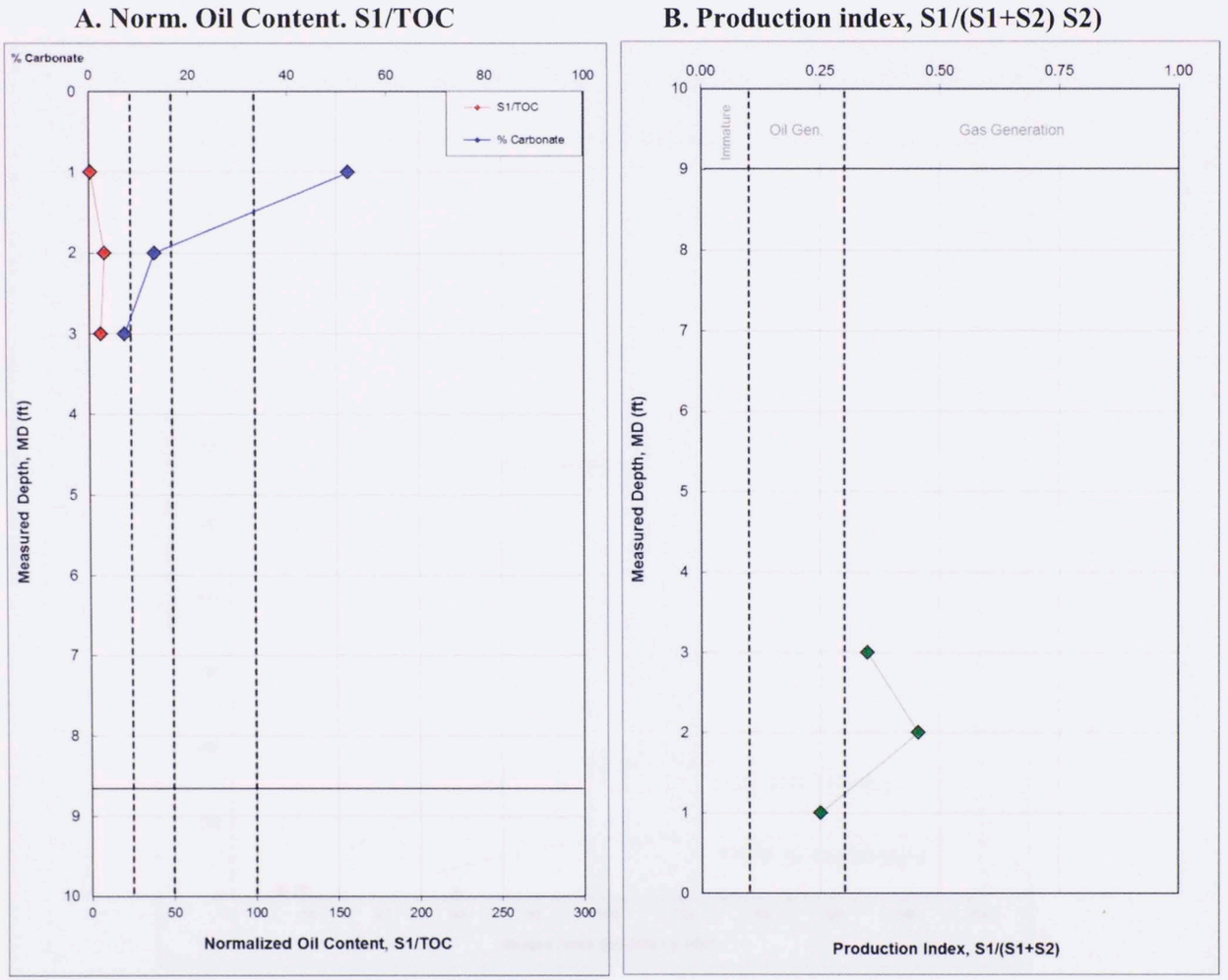

Figure 102 Maturity logs in Zea outcrop. A) Relationship of the S1 peak between the TOC and the percent of carbonates in the San Pedro del Rio outcrop. B) Production index with depth S1/ (S1+S2).

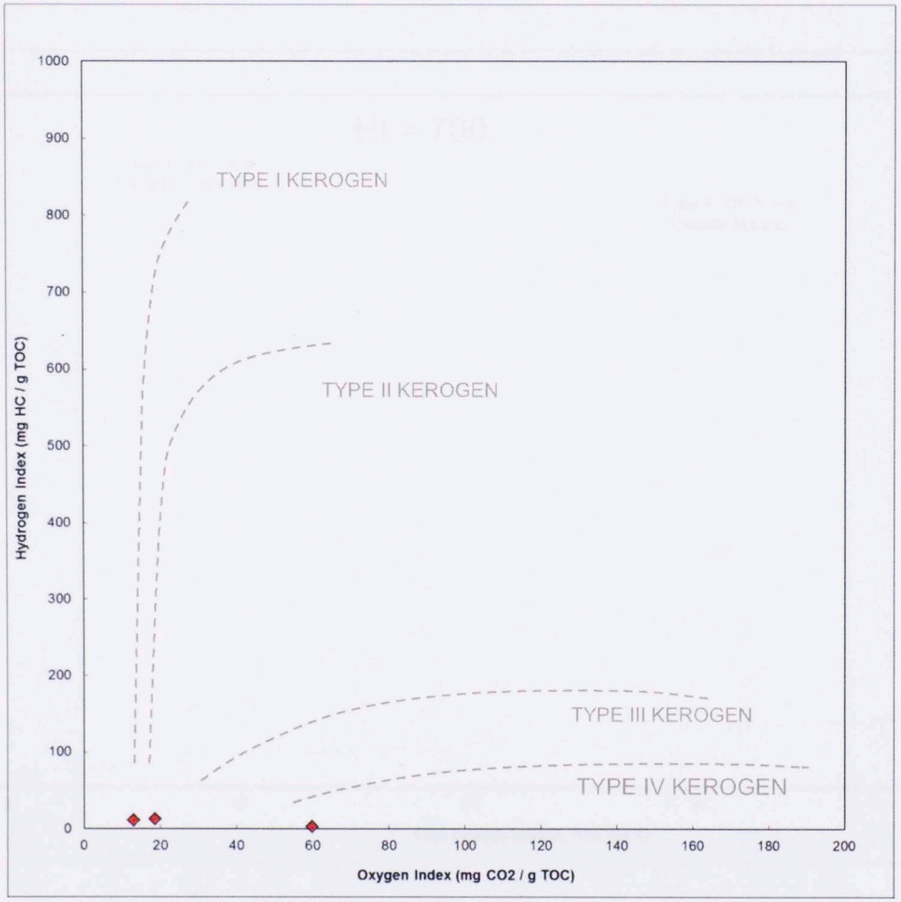

Figure 103 Pseudo Van Krevelen diagram showing four different types of kerogen at different maturity levels.

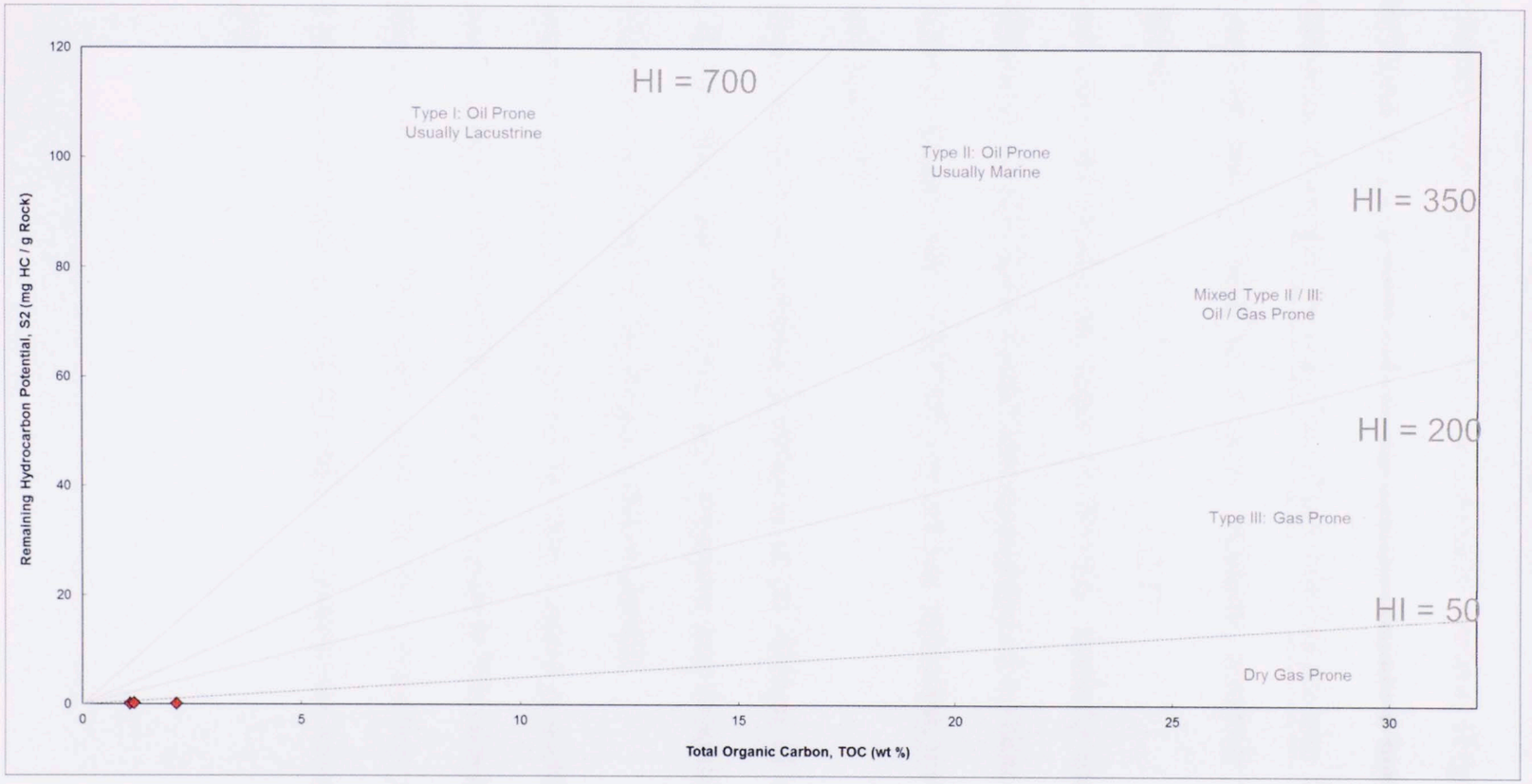

Figure 104 Kerogen Quality Plot that correlates TOC and S2. Red diamonds represent San Pedro del Rio samples.

Maturity logs in Chiguará show that TOC is inversely proportional to the carbonate content (the more TOC the less carbonate content) (Figure 107). The basal area of the Upper La Luna formation in this outcrop contains a high TOC content, and a lower percentage of carbonates which decreases towards the top. TOC content is 2.50 wt % on average and is classified as poor- excellent; however the oil potential is classified as poor.

Even when the production index (S1/S1+S2), maturity indicators (calculated vitrinite reflectance vs calculated Tmax) and normalized oil content (S1/TOC) show oil generation, the hydrogen index (S2/TOC) is too low indicating just gas generation for this section (Figure 107).

Pyrograms show no potential generation of oil. Almost all of them show a flat surface in the S2 peak, thus no Tmax was generated and accordingly, no calculated vitrinite reflectance and Tmax vs Hydrogen index is plotted.

Pyrograms also show that most of the TOC content is probably coming from a large amount of residual carbon in the outcrop (S1 peak to low compared to S4).

Although the Rock Eval plots show that the production index is in the oil generation window, kerogen is Type III and IV, meaning that kerogen is possibly gas and dry gas prone.

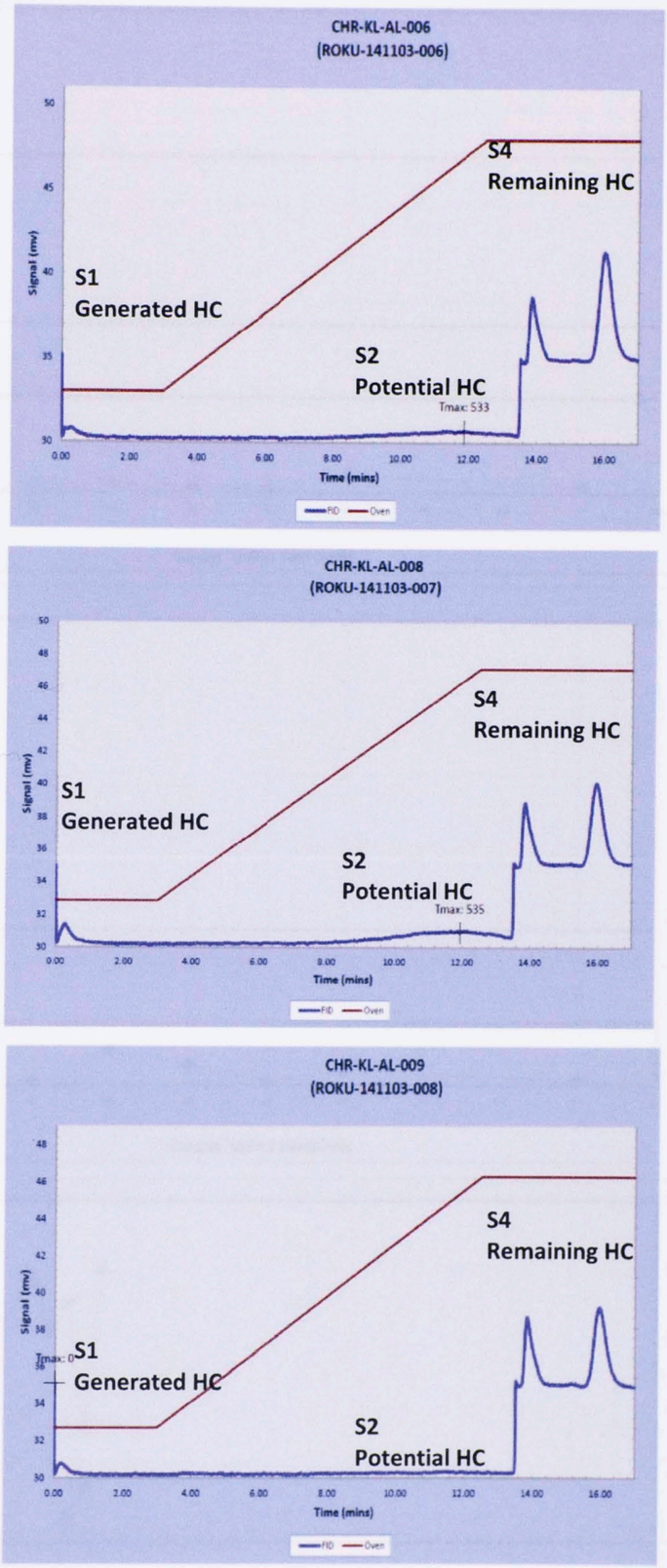

Figure 105 Pyrogram plots from Chiguará outcrop showing the Potential Hydrocarbon content in Facies V and VII (La Luna Middle and Upper interval).

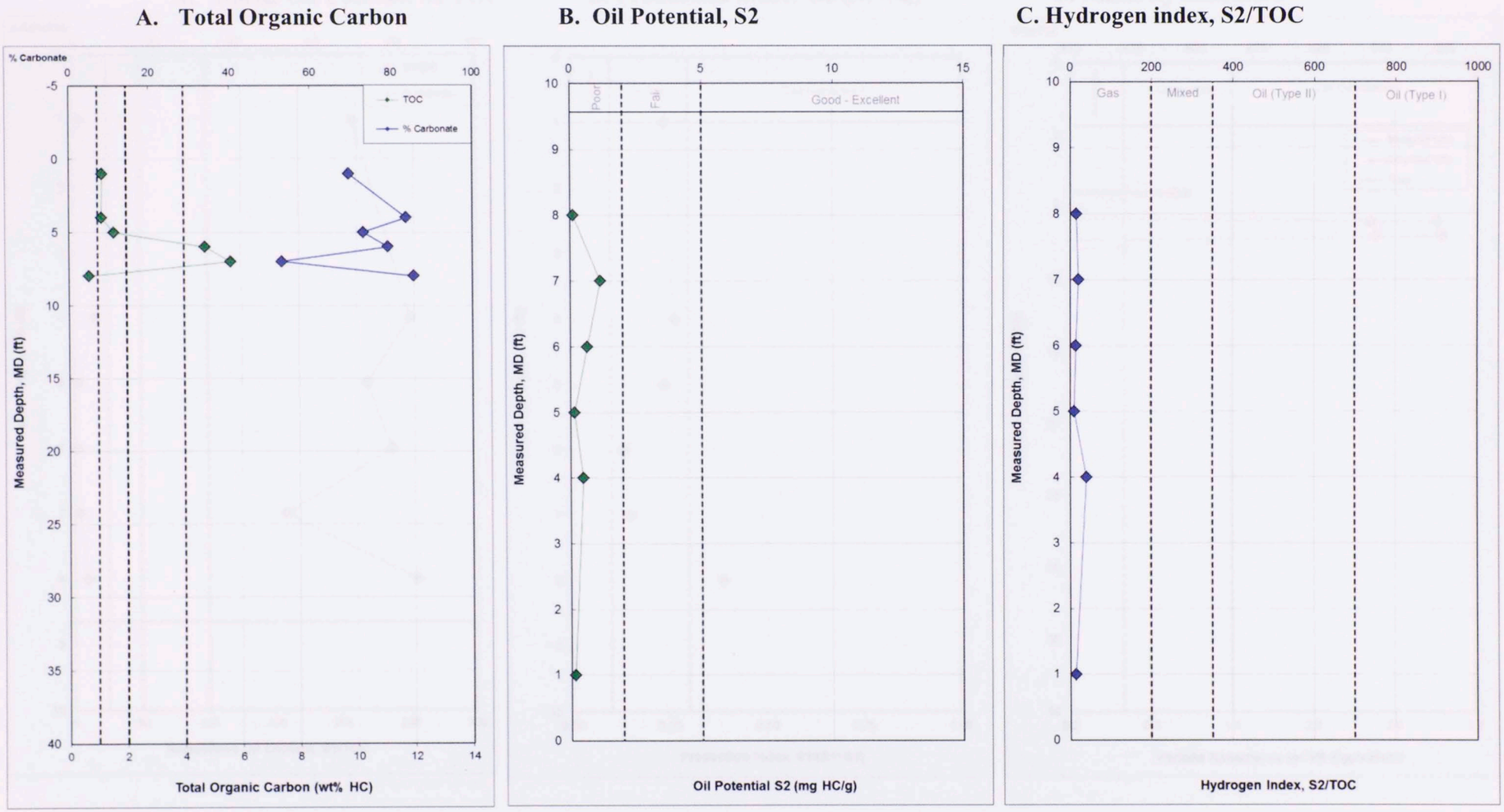

Figure 106 Source Potential logs in Chiguará outcrop. A) Percentage of TOC and Carbonates (Green diamonds represent the TOC content and blue diamonds represent the percent of carbonates). B. Relationship between the S2 peak and the Oil potential quality with depth. C) Relationship of the S2 peak between the TOC and the Oil potential quality.

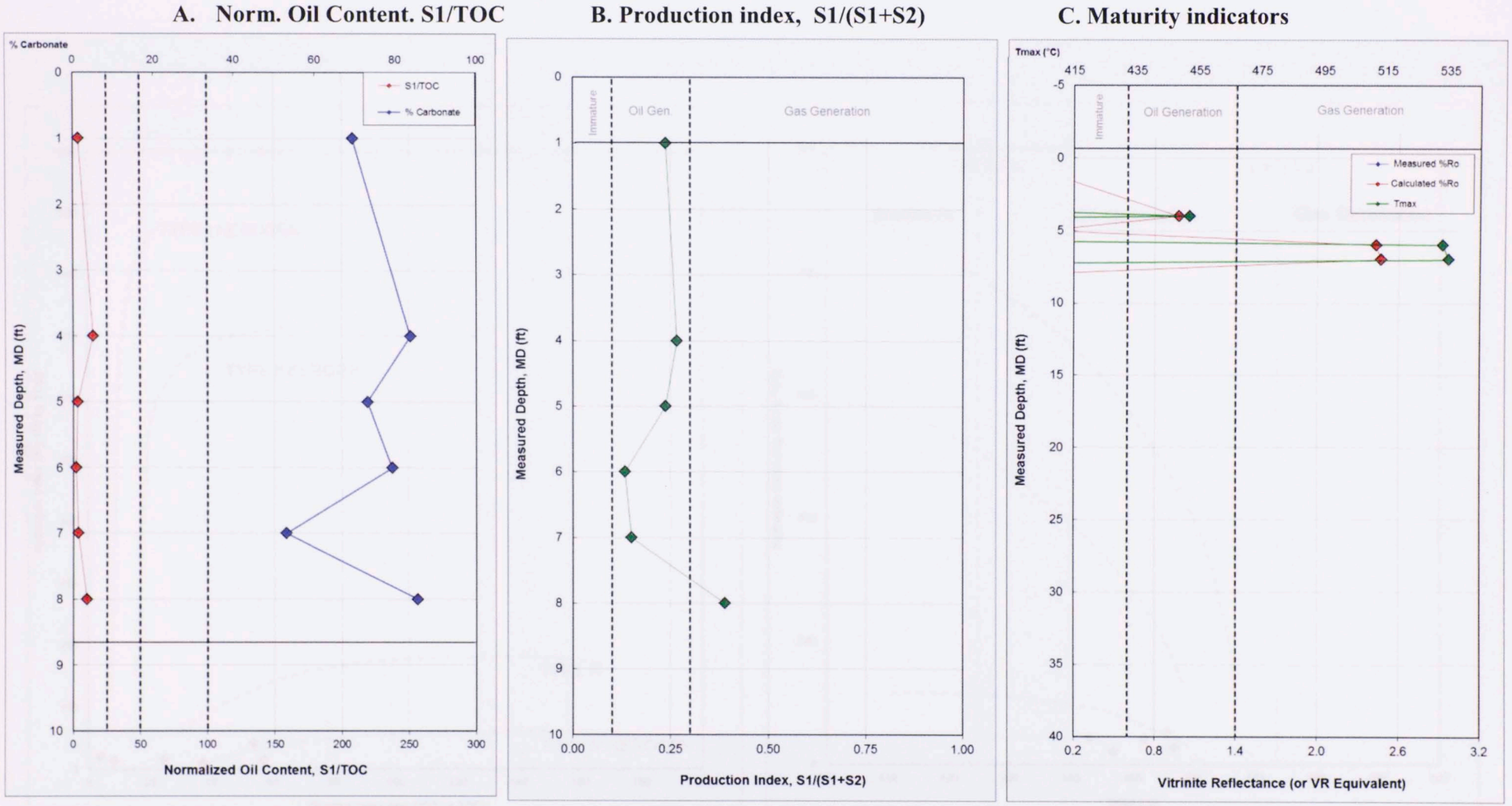

Figure 107 Maturity logs in Chiguará outcrop. A) Relationship of the S1 peak between the TOC and the percent of carbonates in Las Hernandez outcrop. B. Production index changes S1/ (S1+S2) C) Maturity indicators (calculated vitrinite reflectance).

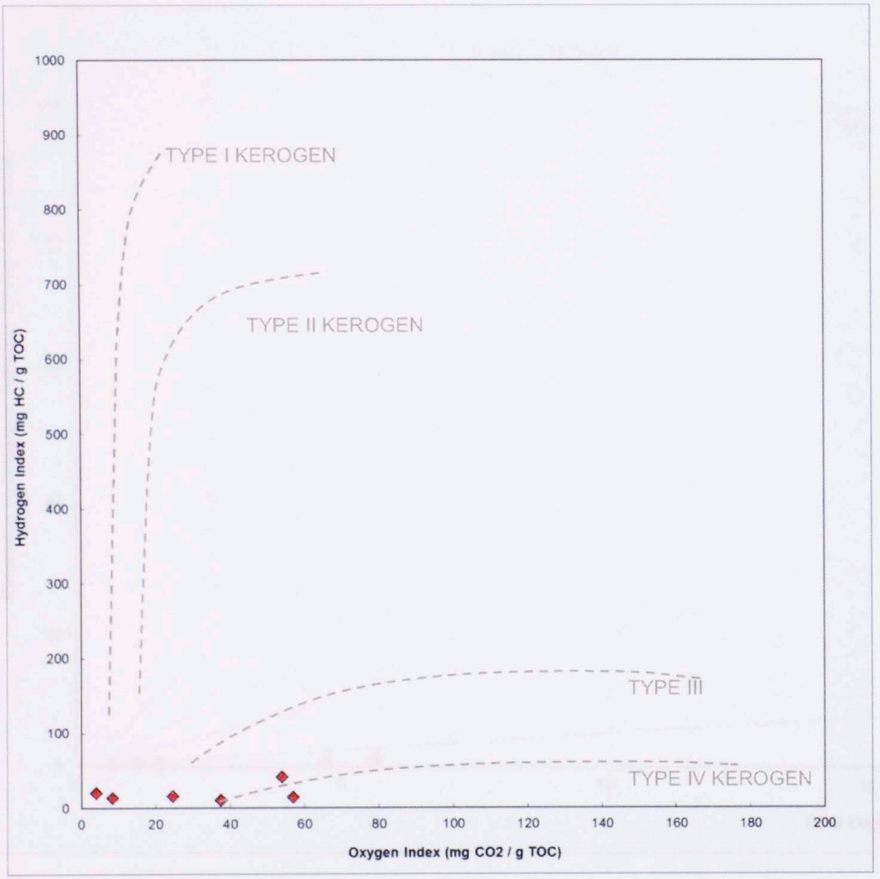

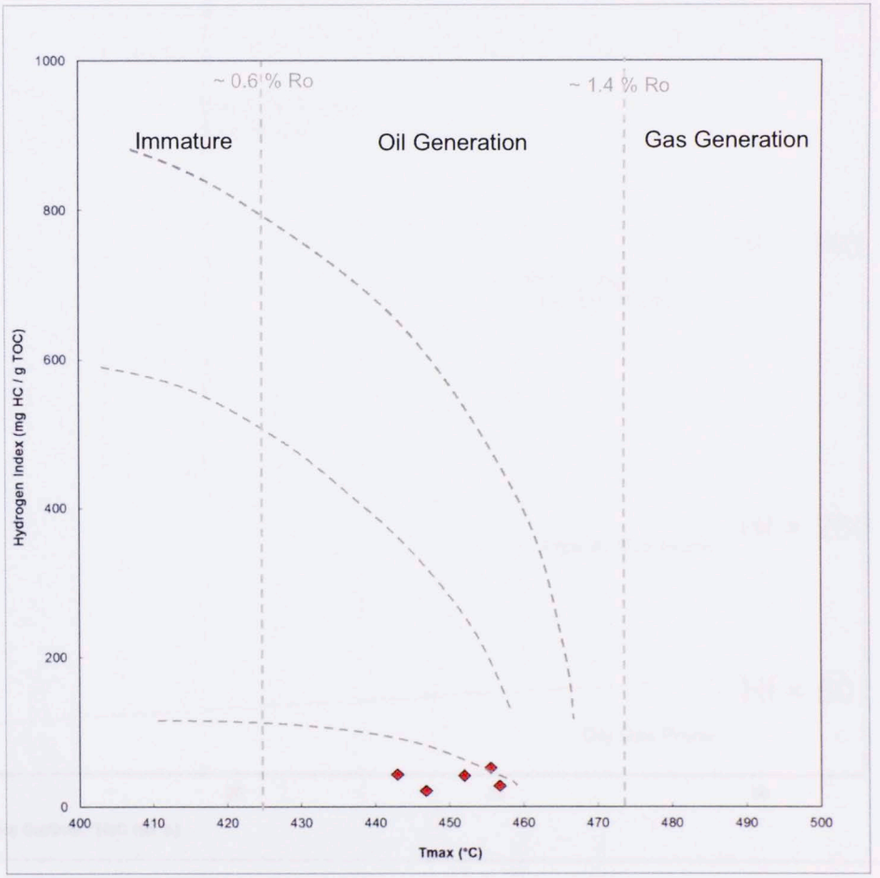

Figure 108 A) Pseudo Van Krevelen diagram showing four different types of kerogen at different maturity levels. B. Kerogen type and maturity plot that displays the relationship between the Tmax and the Hydrogen index. Red diamonds represent Chiguará samples.

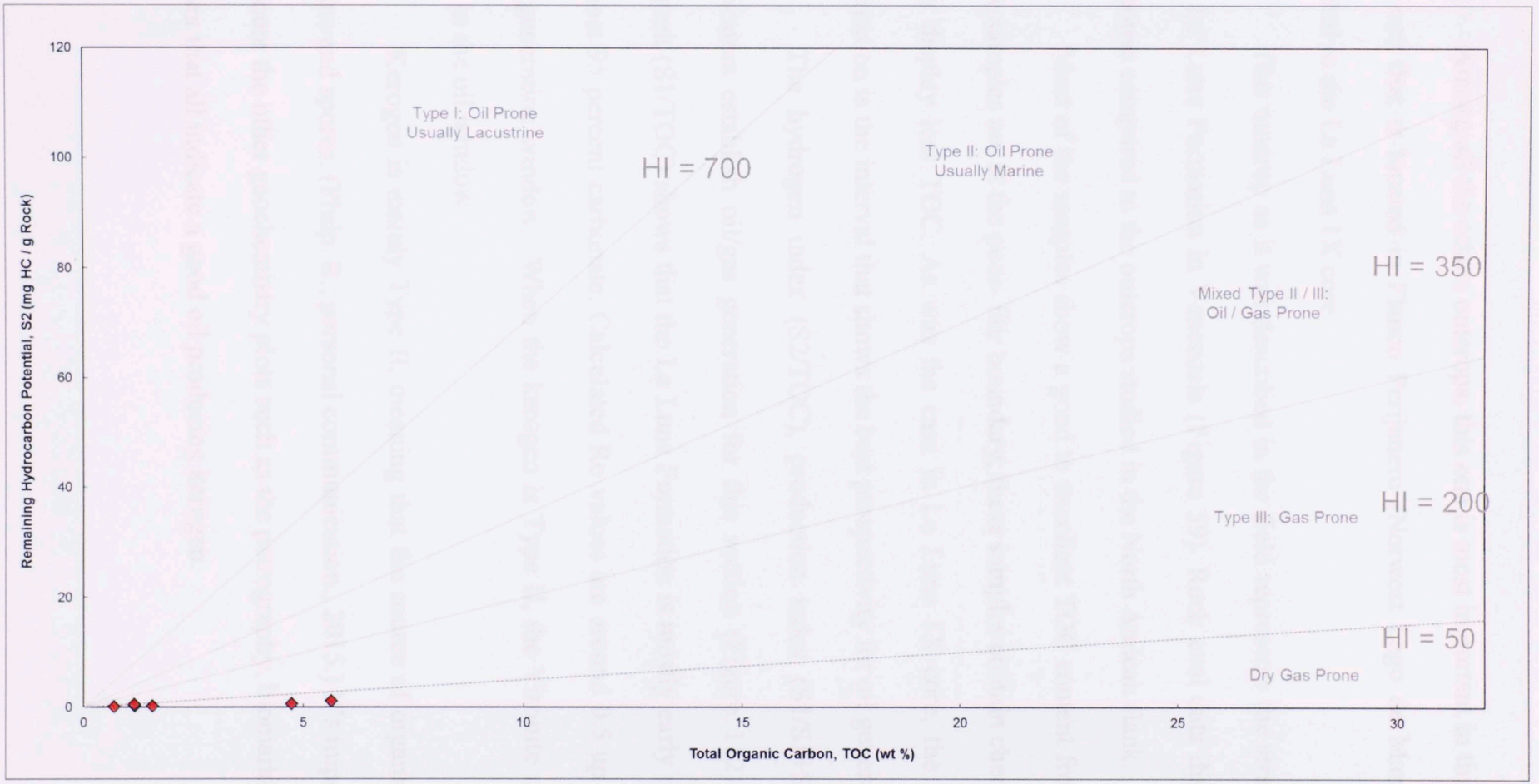

Figure 109 Kerogen Quality Plot that correlates TOC and S2. Red diamonds represent Chiguará samples.

Among all the others outcrops, this one is most important in this study since it is the one that is located in Flanco Perijanero (Norwest Lago de Maracaibo) and it is related to the La Luna 1X core.

This outcrop as it was described in the field represents the stratotype section of the La Luna Formation in Venezuela (Figure 59). Rock eval data displays a different response compared to the outcrops studied in the North Andean flank.

Most of the samples show a good to excellent TOC content from bottom to top. Few samples are at the poor- fair boundary; these samples contain chert concretions and thus display less TOC. As was the case in La Luna 1X core, the Middle La Luna Formation is the interval that shows the best prospectivity for oil generation.

The hydrogen index (S2/TOC), production index (S1/S1+S2) and maturity indicators establish oil/gas generation for this section (Figure 112). Normalized oil content (S1/TOC) shows that the La Luna Formation is mostly early mature with 60 to almost 95 percent carbonate. Calculated Ro values are around 0.5 up to 0.6 within the oil generation window. When the kerogen is Type II, the Vitrinite reflectance values are in the oil window.

Kerogen is mainly Type II, meaning that the source of organic matter includes resins and spores. (Philp, R.; personal communication., 2015.) It's important to take into account the other geochemistry plots such as the petrography, biomarkers and Hydrogen Index that all indicate a good oil producing kerogen.

Pyrograms shows a fair potential in the S2 peak compared with other outcrops (Figure 110) and although the S4 peak shows a high peak S2 still has a potential for hydrocarbon production.

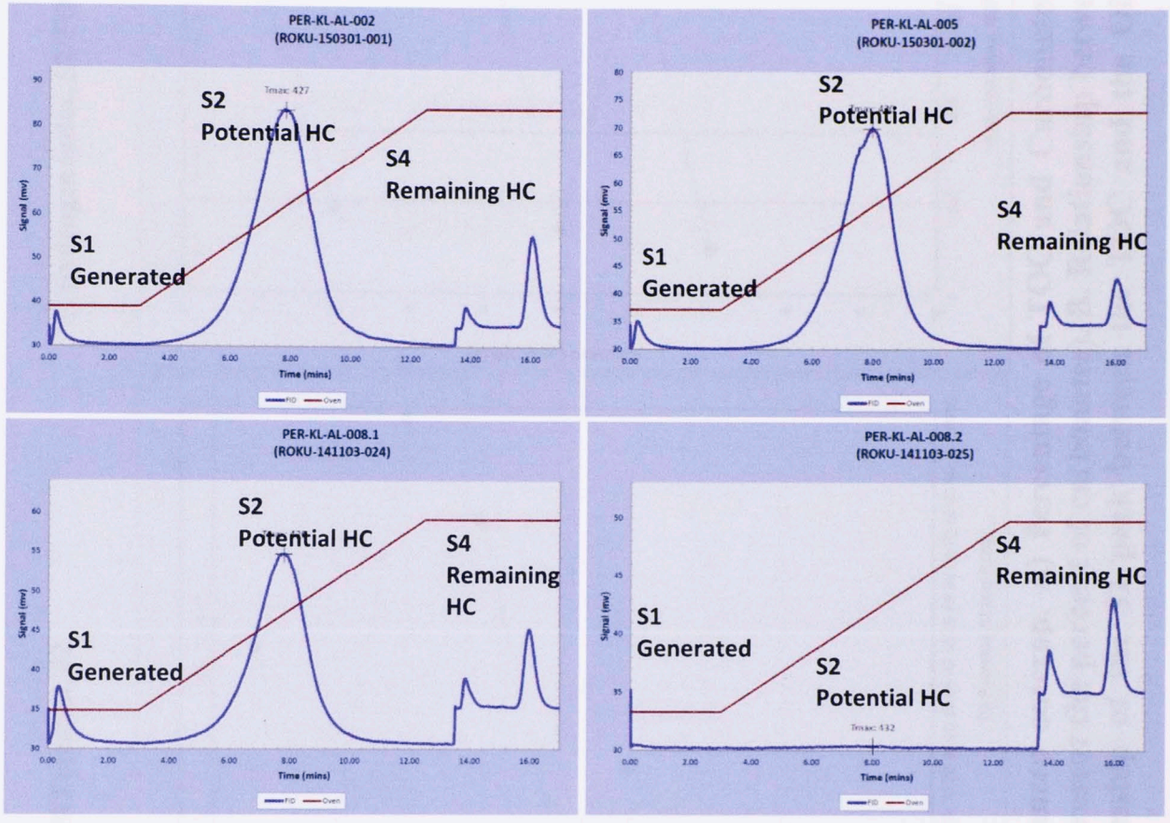

Figure 110 Pyrogram plots from Flanco Perijanero outcrop showing the Potential Hydrocarbon context in Lower, Middle and Upper La Luna interval.

A.Total Organic Carbon B. Oil Potential, S2 C. Hydrogen index, S2/TOC

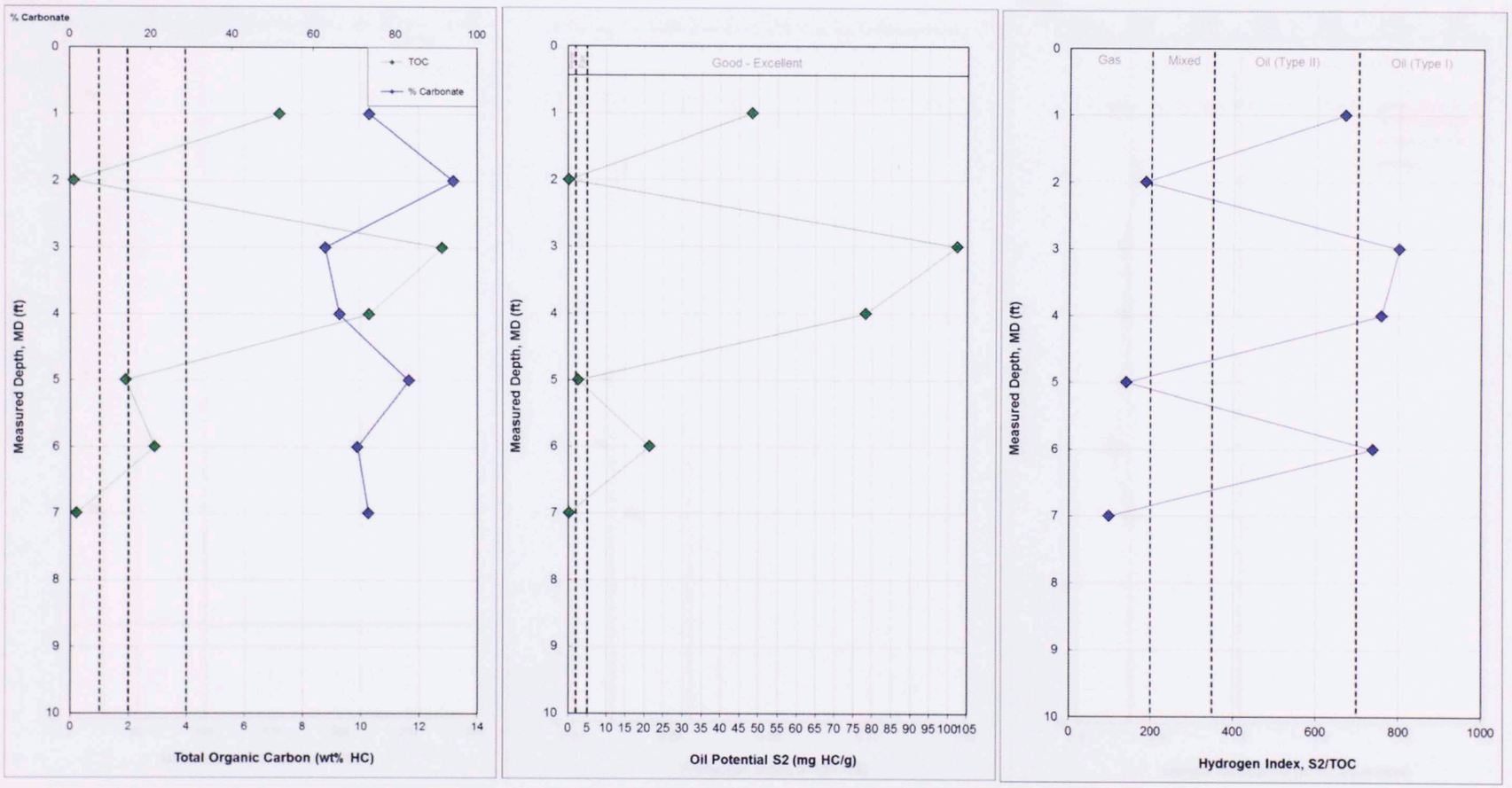

Figure 111 Source Potential logs in Flanco Perijanero outcrop. A) Percentage of TOC and Carbonates (Green diamonds represent the TOC content and blue diamonds represent the percent of carbonates). B. Relationship between the S2 peak and the Oil potential quality with depth. C) Relationship of the S2 peak between the TOC and the Oil potential quality.

A. Norm. Oil Content. S1/TOC B. Production index, S1/(S1+S2) C. Maturity indicators

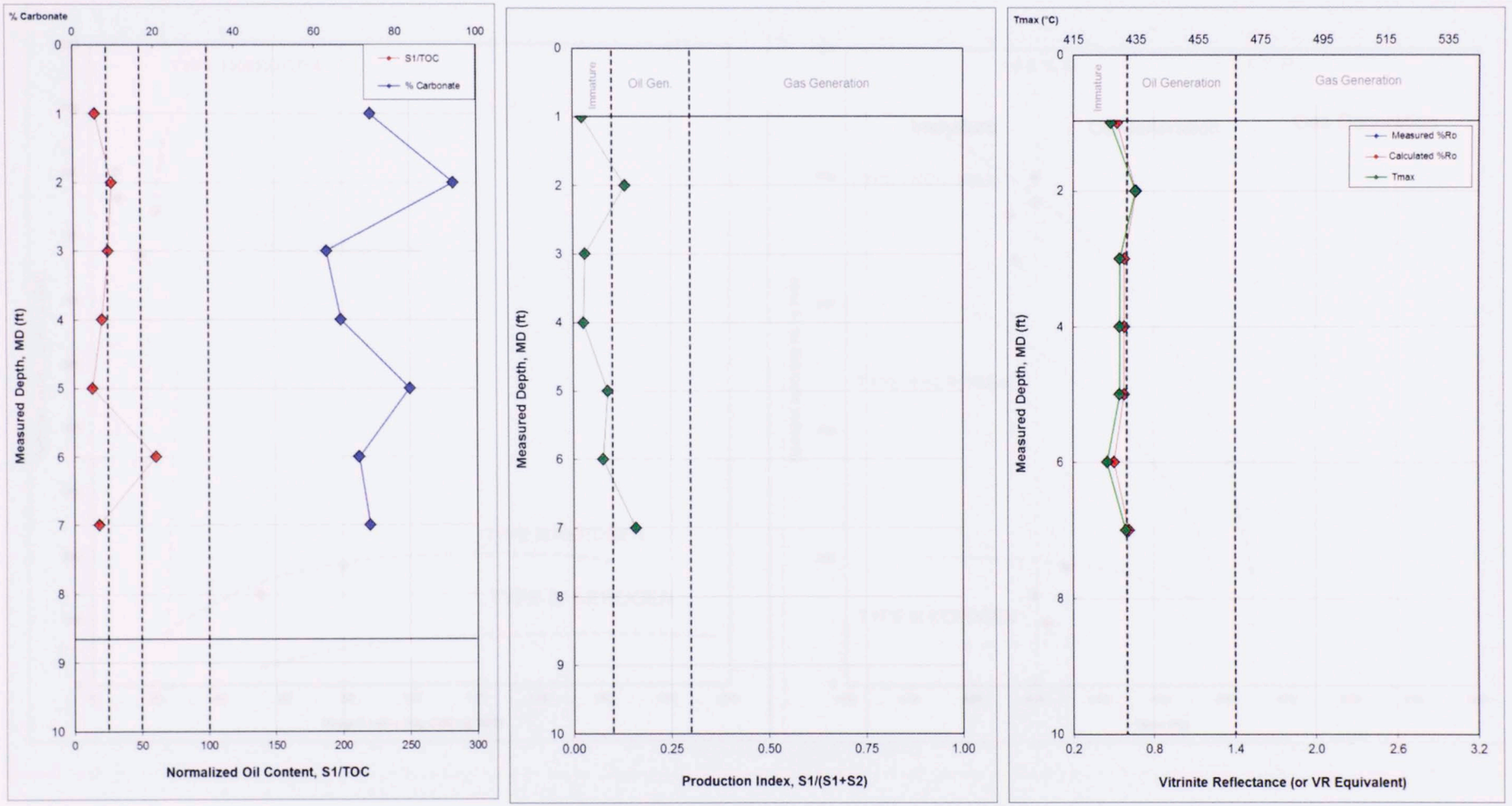

Figure 112 Maturity logs in Flanco Perijanero outcrop. A) Relationship of the S1 peak between the TOC and the percent of carbonates in Las Hernandez outcrop. B. Production index changes S1/ (S1+S2) C) Maturity indicators (calculated vitrinite reflectance).

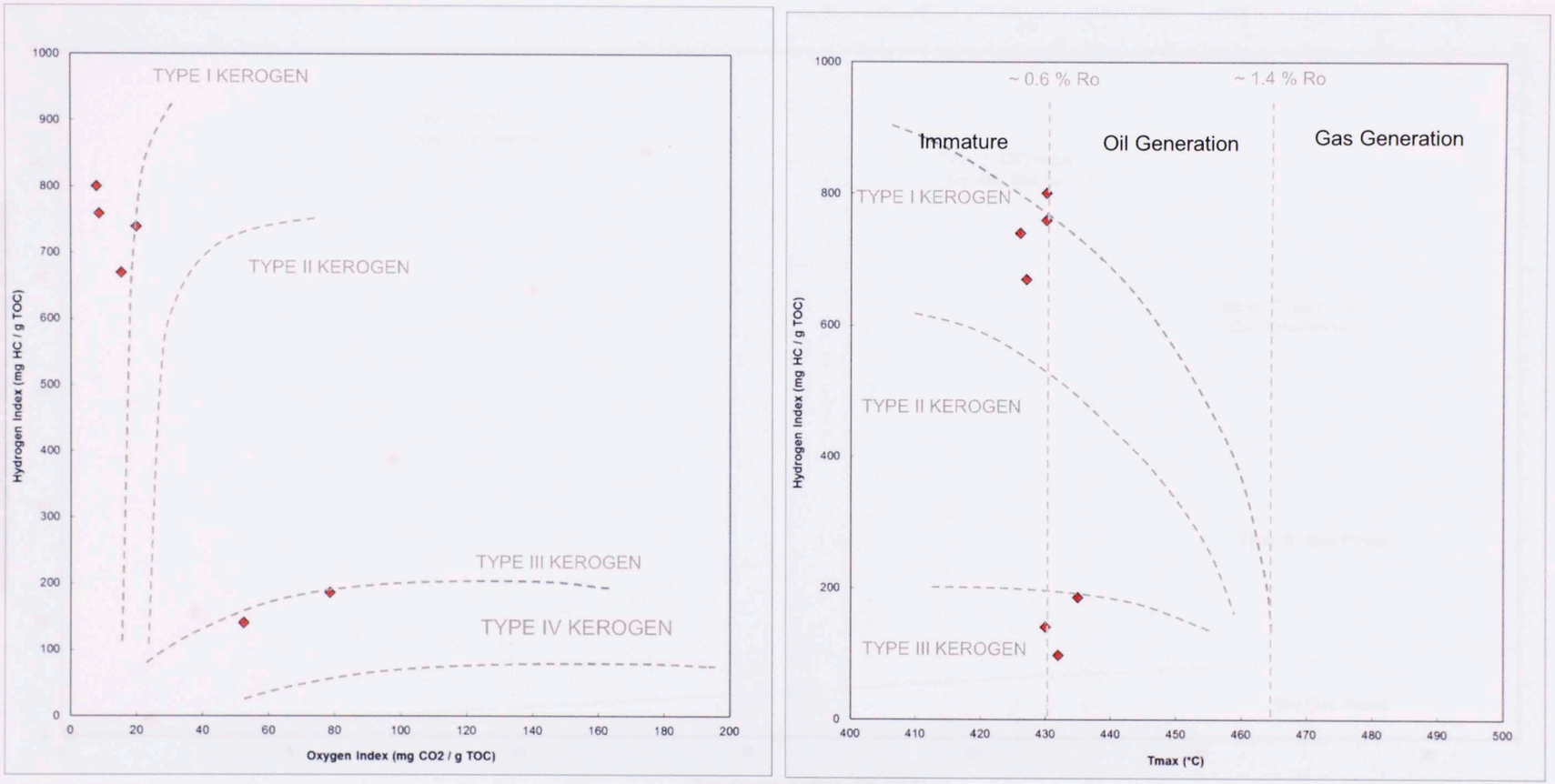

Figure 113 A) Pseudo Van Krevelen diagram showing four different types of kerogen at different maturity levels. B. Kerogen type and maturity plot that displays the relationship between the Tmax and the Hydrogen index. Red diamonds represent Flanco Perijanero samples.

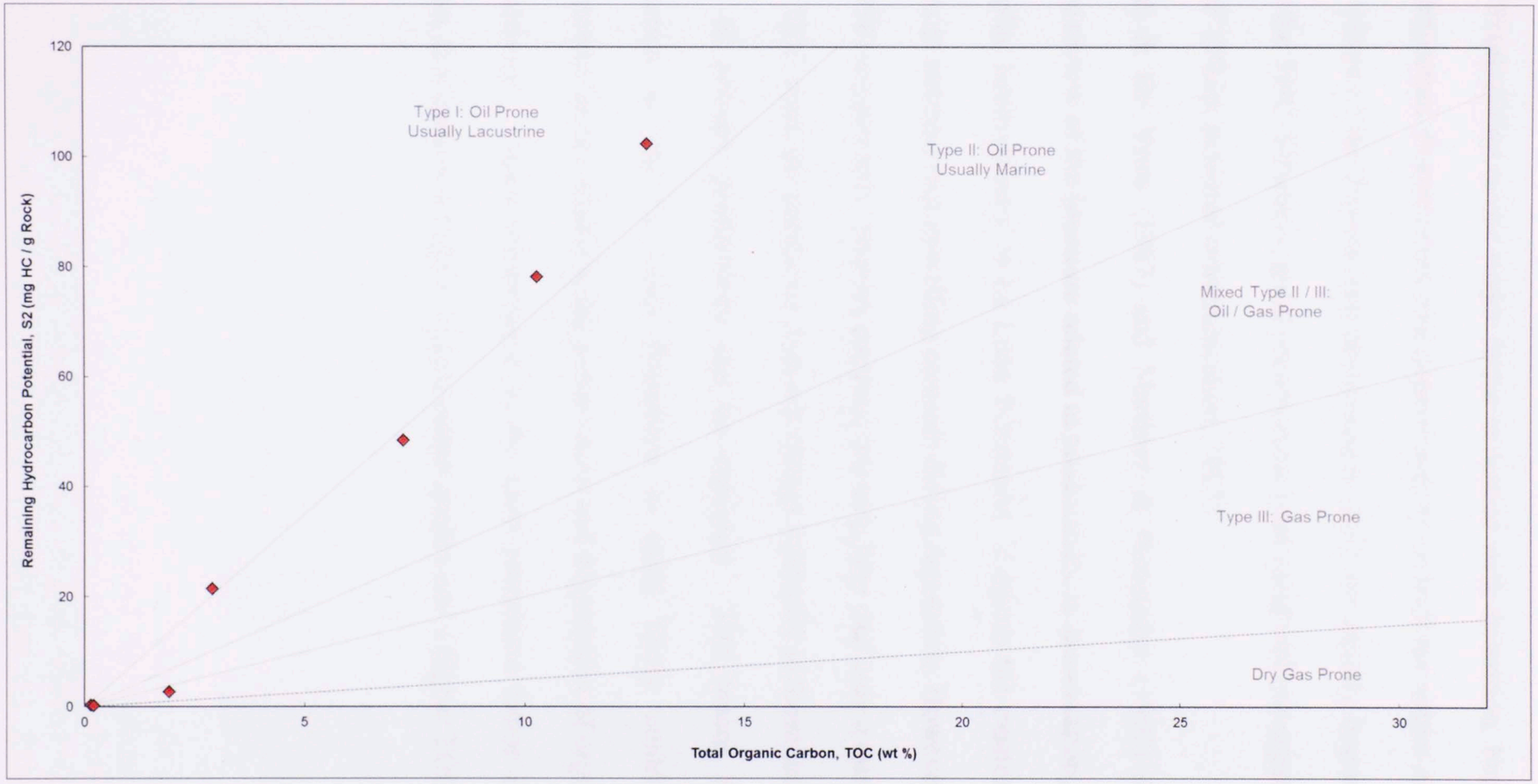

Figure 114 Kerogen Quality Plot that correlates TOC and S2. Red diamonds represent Flanco Perijanero samples.

5.3 Productivity/ Preservation

"Productivity is one major factor in source rock formation, but preservation is equally important. Preservation will depend mainly on both the nature of organic matter and the nature of the depositional environment. Both are equally important in order to preserve the TOC. Similarly, good preservation is no good without organic matter being produced" (Philp, personal communication, 2015).

Macellari & De Vries (1987) and Martinez & Hernandez (1992) state that in an extensive review of the literature related to productivity vs preservation, the lateral and stratigraphic heterogeneity of La Luna Formation suggests the existence of temporal variations in nutrient-rich upwelling currents during deposition. However, Perez-Infante et al. (1996) suggest that "primary productivity may have had only a minor influence on the final TOC since the parameter does not change markedly in those intervals where an increase in primary productivity can be expected. This means that their TOC interpretation in the La Luna Formation is more likely controlled by local environmental factors related to the preservation and degradation of organic matter than to productivity". Since preservation is the most prominent factor in the La Luna Formation, this leads to a higher organic matter quality and a higher TOC.

5.4 Petrography of outcrop samples

1. Las Hernández outcrop

This outcrop represents the most organic rich interval in the whole North Andean Flank. TOC values classify it as a very good- excellent source rock. Thin section 001 and 002 (Figure 115 and 116) show a packstone with a high percentage of organic matter matrix and high amount of recrystallized calcite. It has an abundance of fossils and dark-colored areas, thin brachiopods and gastropods are highly oriented and spicules of Echinoderms are in an organic-rich matrix. Algal structures and Foraminifera with uniserial morphology are characteristic in the sample. No porosity was found in this thin section. Bitumen content is low to moderate.

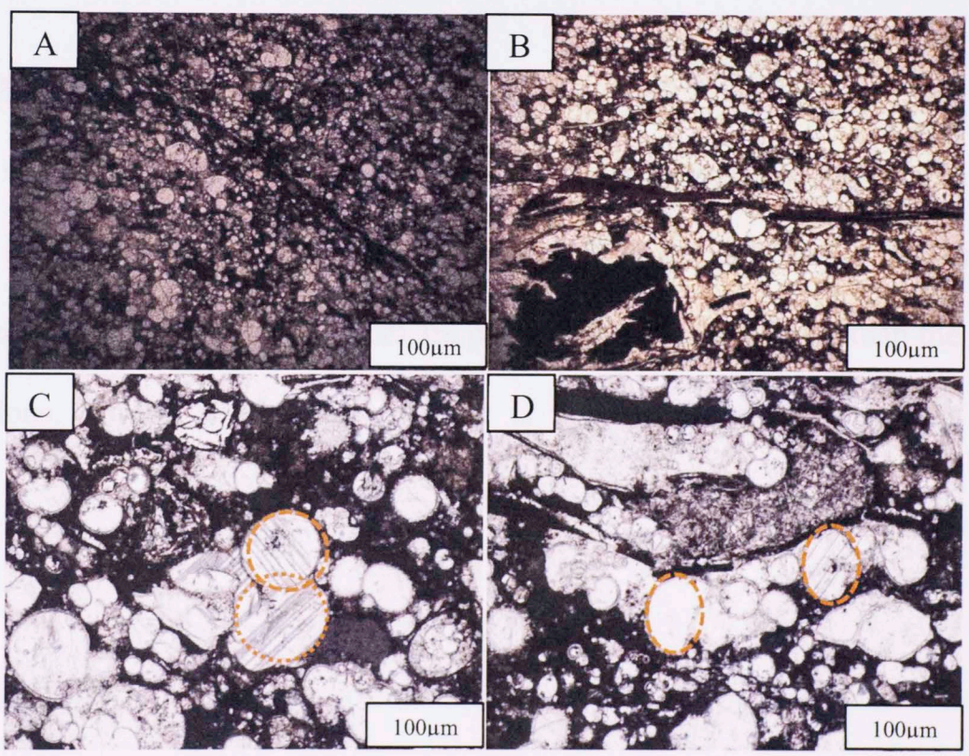

Figure 115 Photographs of thin section 001-Las Hernandez in plane polarized light. A) Big picture of the thin section represented by various types of fine-grained sediment and organic matter B) Big picture of the thin section represented by various types of fine- grained sediment and organic matter C) Foraminifera with uniserial morphology and calcite recrystallization D) Foraminifera with uniserial morphology partially recrystallized to calcite.

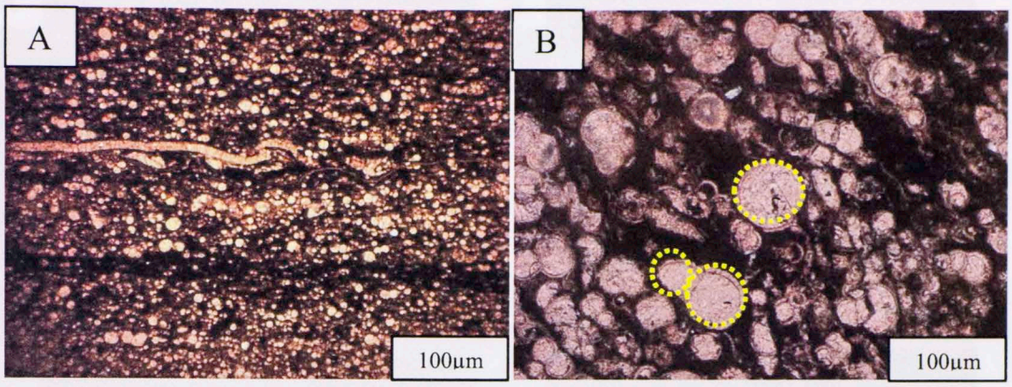

Figure 116 Photographs of thin section 002-Las Hernandez in cross polarized light. A) Big picture of the thin section represented by various types of fine- grained sediment and organic matter B) Foraminifera with uniserial morphology partially recrystallized to calcite in organic matter cement.

Thin section 003:

This wackstone represents the most organic-rich interval of the whole outcrop. Bitumen oil content is moderate. TOC is around 3.25 percent. Some shell fragments, brachiopods and uniserial foraminifera are present, but of smaller size than the prior two thin sections. Some interparticle porosity is present. Quartz overgrowths are also present.

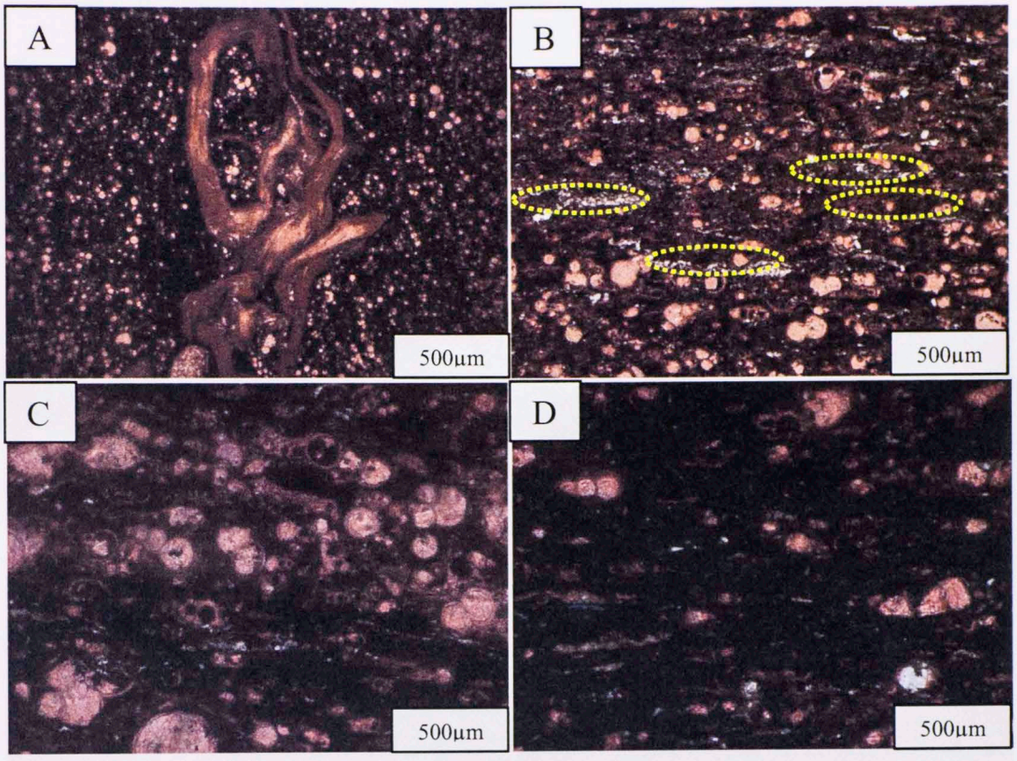

Figure 117 Photographs of thin section 003-Las Hernandez in cross polarized light. A) Big picture of the thin section represented by a brachiopod and uniserial foraminifera in an organic matter matrix (b and C) Foraminifera with uniserial morphology partially recrystallized to calcite in an organic matter cement with some interparticle porosity D) high amount of organic matter cement and some disperse foraminifera and interparticle porosity.

Thin section 004

This sample represents the contact between the Upper La Luna and The Tres Esquinas Member (Colon Formation). There is a remarkable difference between two types of cementation. Towards the right is organic rich "cement" with some brachiopods and unicellular foraminifera, and stylolites are present in a 45 degree angle, perpendicular to the bedding. Towards the left, the cement is composed of micrite and a

high increment of moldic and interparticle porosity. Some aragonite recrystallization is present around the foraminifera.

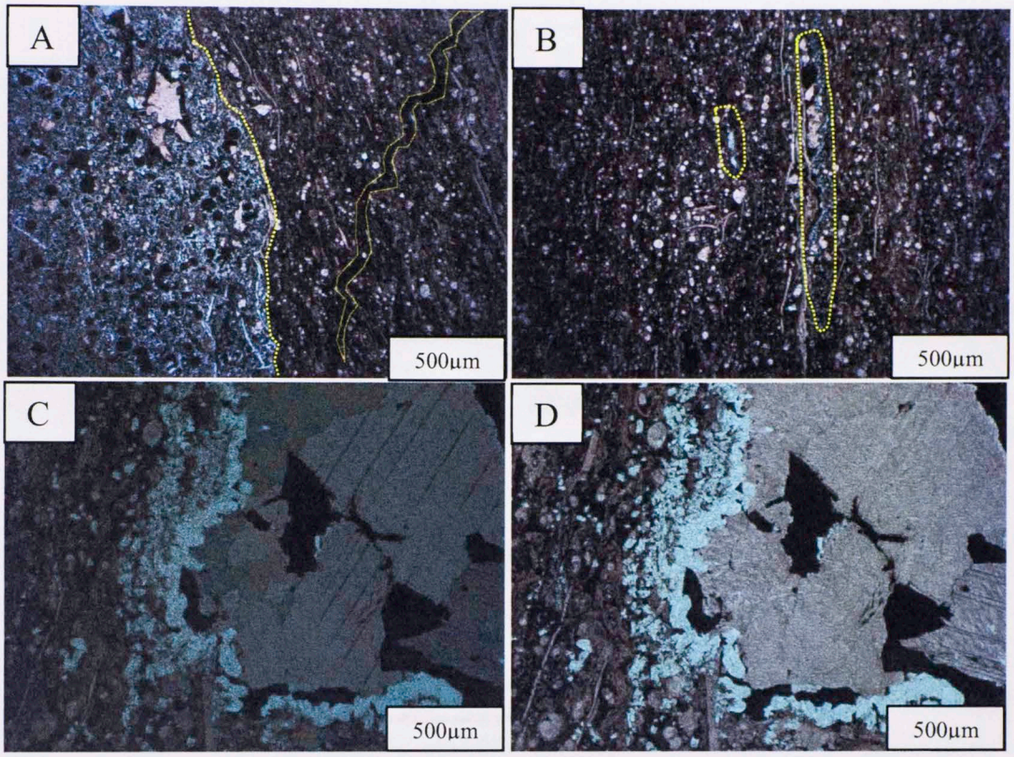

Figure 118 Photographs of thin section 004-Las Hernandez in cross polarized light. A) Big picture of the thin section represented the contact of Upper La Luna with Tres Esquinas Member. Organic matter content, stylolites and foraminifera are notorious in the right side. To the left an increment of moldic porosity is notorious in the sample B) Presence of some interparticle porosity in organic rich cement C) Interparticle porosity and aragonite recrystallization in an calcite clast (cross polarized light) D) Interparticle porosity and aragonite recrystallization in an calcite clast (plane polarized light).

2. Zea outcrop

Thin section 001 and 002 (Figure 119 and 120) show a wackstone with micrite cement and uniserial foraminifera completely recrystallized to calcite. Organic matter fragments, recrystallized micrite and equigranular calcite occur along with some bioclasts altered to micrite. Intraparticle and dissolution porosity are present. Pyrite

fragments are also characteristic in certain parts of the sample. Quartz overgrowths and the presence of pyrite fragments are also characteristic in certain parts of the sample.

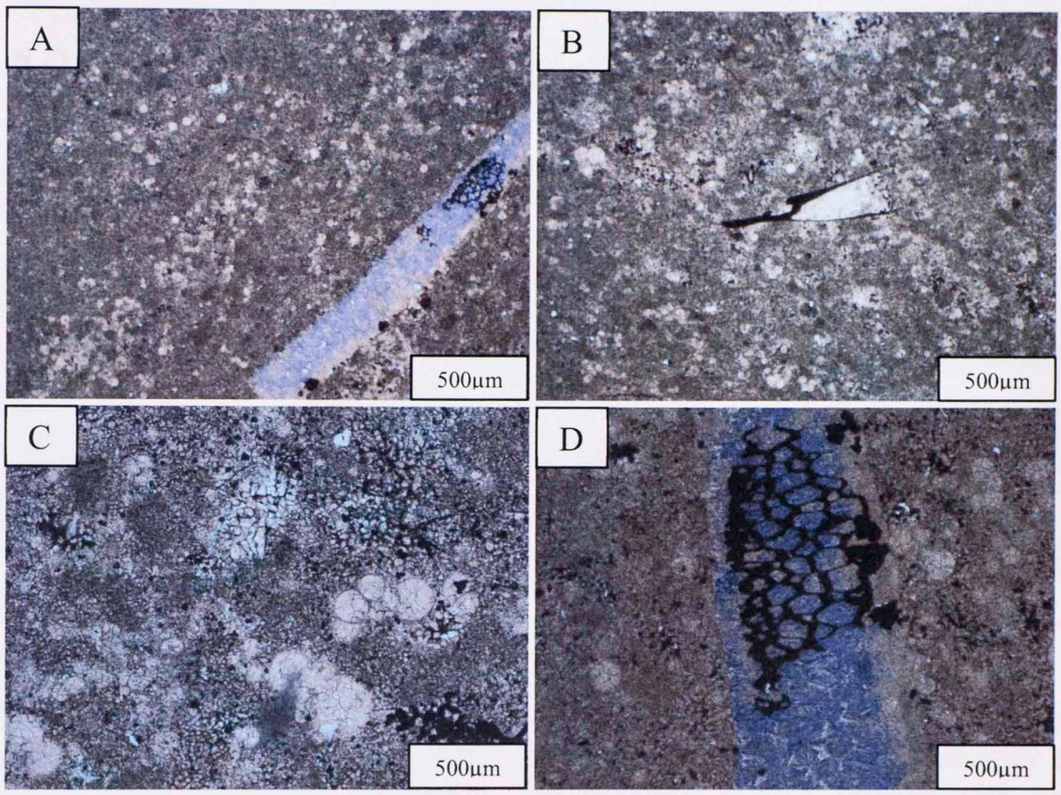

Figure 119 Photographs of thin section 001-Zea in cross polarized light. (a and B) Big picture of the thin section represented by micrite cement around the recrystallized foraminifera C) Recrystallized micrite, intraparticle porosity and pyrite fragments D) Micrite cement around the recrystallized foraminifera and pyrite replacement in echinoderm spicule.

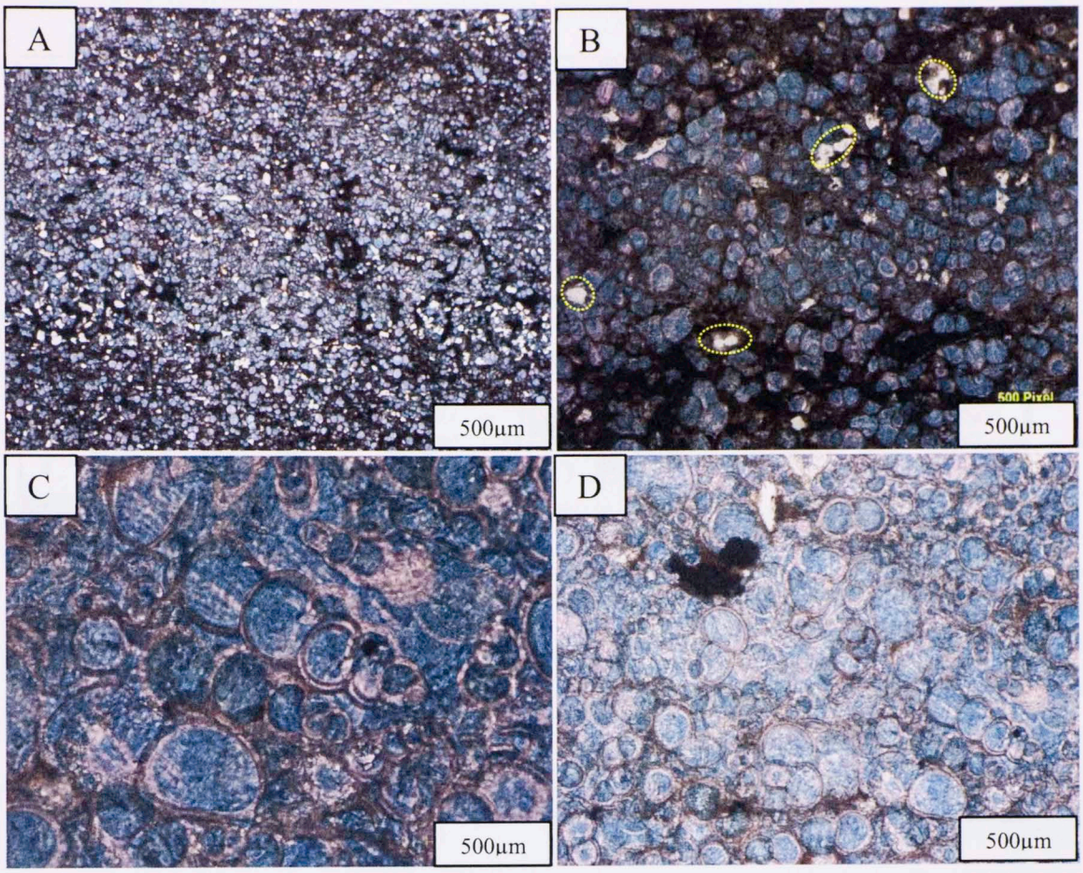

Figure 120 Photographs of thin section 002-Zea in cross polarized light. A) Big picture of the thin section represented by a packstone with organic matter cement around the recrystallized foraminifera B) Organic matter cement with uniserial foraminifera, Qtz fragments and pyrite (c and D) Interparticle and intraparticle porosity in uniserial foraminifera.

3. San Pedro del Rio outcrop

This packstone-wackstone (Figure 121) is predominately composed of abundant uniserial and multiserial foraminifera that have recrystallized to calcite in an organic-rich matrix. Stylolites and sparite veins are perpendicular to the bedding. Porosity is also found (intraparticle, interparticle, vug and fracture porosity). Siderite cement is also present and pyrite and dolomite are found as trace minerals.

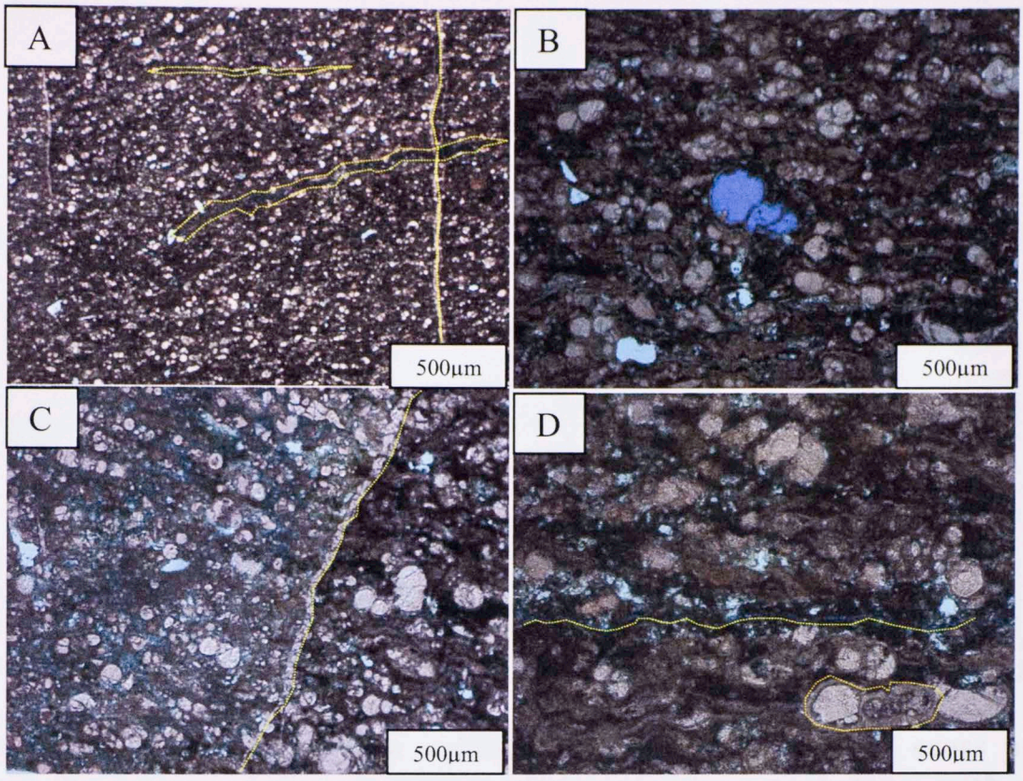

Figure 121 Photographs of thin section 001-Chiguara in cross polarized light. A) Big picture of the thin section represented by a packstone with multiserial foraminifera in organic rich cement B) Intraparticle and interparticle porosity around the foraminifera with some siderite cement C) Sparite veins perpendicular to the deposition and interparticle porosity D) Porosity by fracture and calcite recrystallization around the foraminifera.

4. Azulita- Bachaquero outcrop

This sample is a packstone with various types of smaller and finer- grained grains. Dolomite, pyrite and siderite fragments are dispersed in the matrix as are some intraparticle; interparticle moldic and dissolution porosity. Most of the foraminifera are recrystallized to calcite.

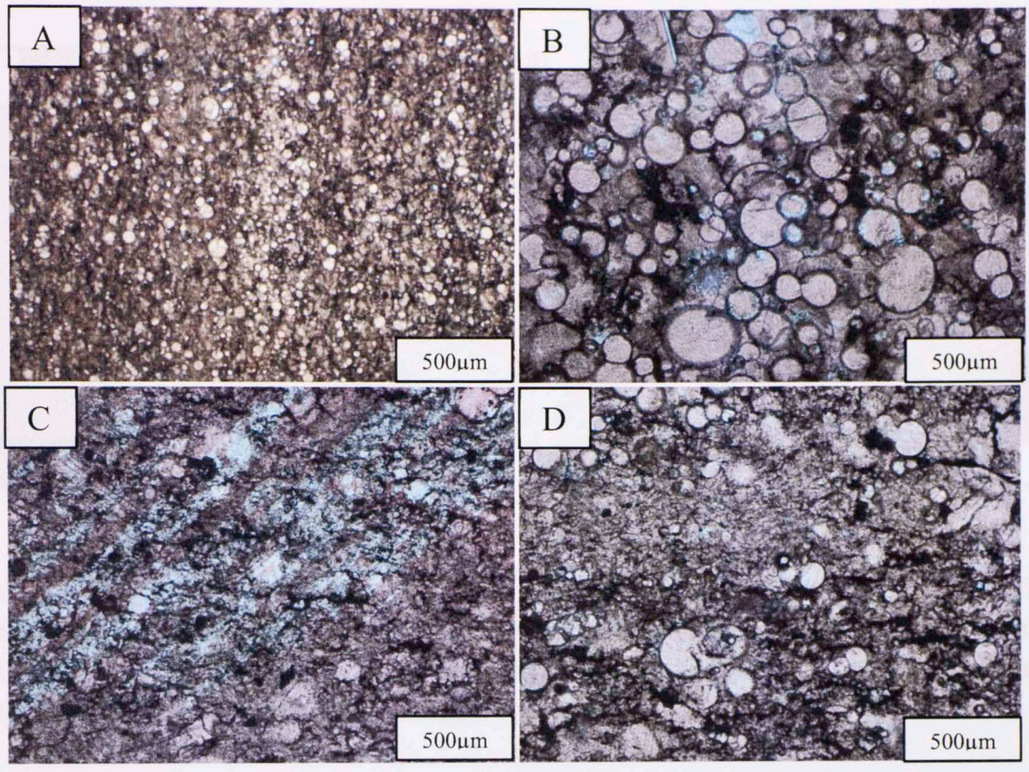

Figure 122 Photographs of thin section Azulita- Bachaquero in cross polarized light. A) Big picture of the thin section represented by a packstone- with uniserial foraminifera in micrite cement B) Moldic, intraparticle and interparticle porosity around the foraminifera C) Porosity by dissolution in a micrite matrix D) Calcite recrystallization of uniserial foraminifera.

5. Chiguará outcrop

Thin section 001

This sample represents a packstone with a high abundance of recrystallized and multiserial foraminifera in a micrite and organic-rich matrix. Some sparite- filled fractures and some interparticle porosity are present, as are dolomite and rhomboidal pyrite fragments.

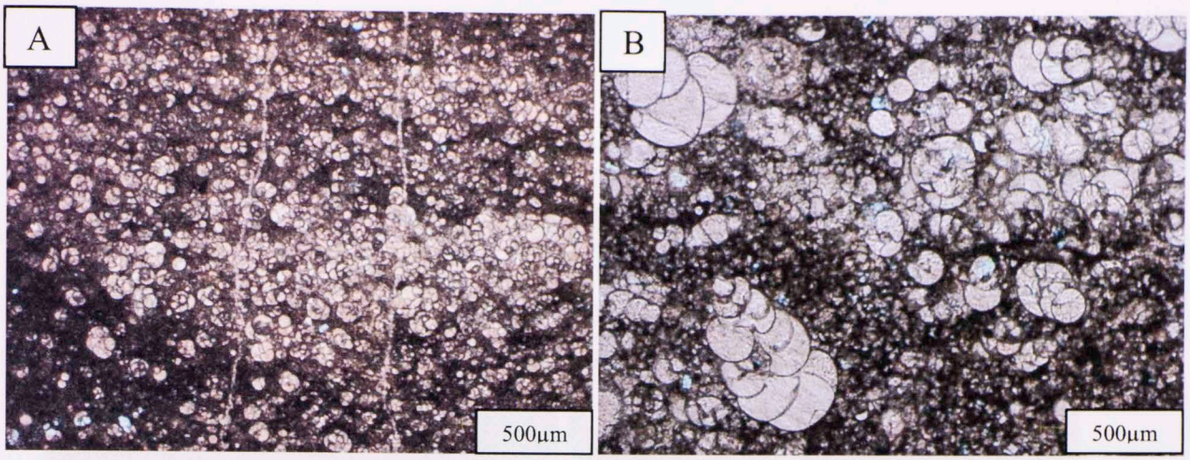

Figure 123 Photographs of thin section 001-Chiguara in cross polarized light. A) Big picture of the thin section represented by a packstone with multiserial foraminifera in micrite and organic rich matrix B) Calcite recrystallization of multiserial foraminifera with some intraparticle porosity.

Thin section 002

This packstone represents the Chejende Member of La Luna Formation in the North Andean flank. This sample shows recrystallized foraminifera, gastropods and shell fragments in an organic-rich matrix.

There is a higher abundance of fossils in some laminations. Bitumen is moderate and is observed in the matrix. A TOC value of 4.74 wt% shows this sample as an excellent source rock. Dolomite and pyrite fragments and some fracture porosity is present.

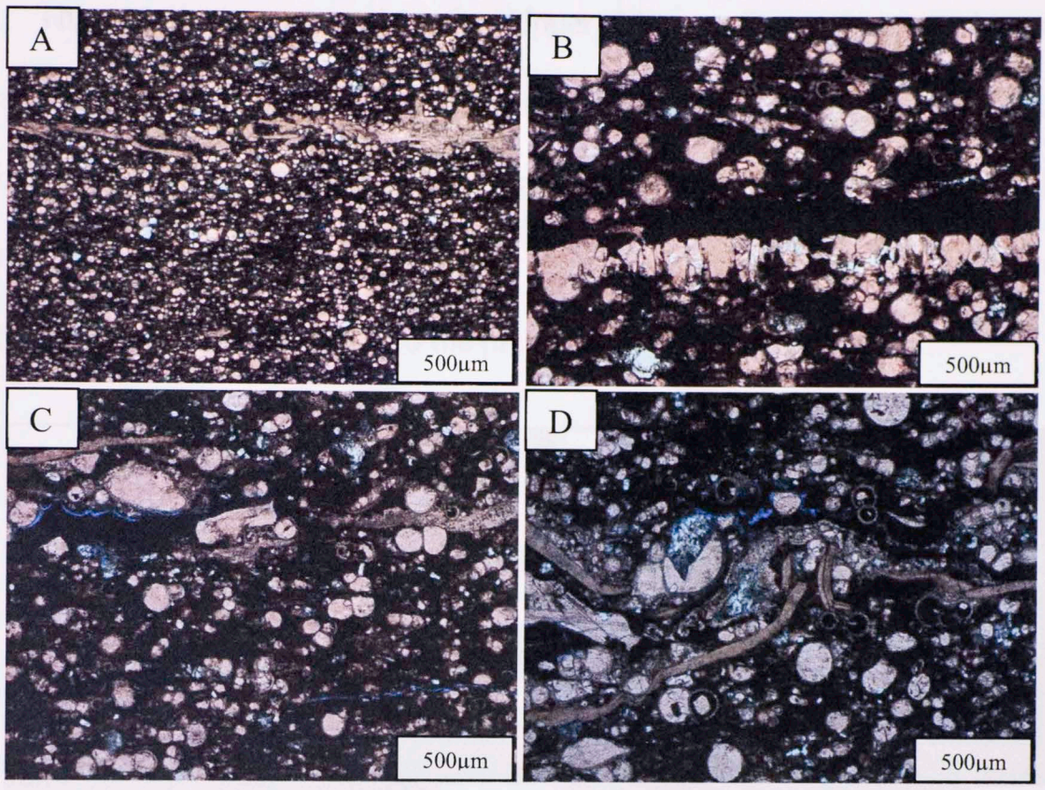

Figure 124 Photographs of thin section 002-Chiguara in cross polarized light. A) Big picture of the thin section represented by a packstone and a recrystallized foraminifera, gastropods and shell fragments in an organic rich matrix B) Dolomitization process in recrystallized fossils around an organic rich matrix C) Porosity by fracture D) Dolomitization process in recrystallized fossils around an organic rich matrix.

6. Flanco Perijanero outcrop

From the bottom to the top, samples represent the Lower, Middle and Upper La Luna formation stratotype. These thin sections are the ones that best represent the Lago de Maracaibo Basin since they are the closest ones to the La Luna IX core.

Thin section 001

This packstone represents the Upper Maraca Formation; it shows calcite recrystallized foraminifera, gastropods, fish remains and shell fragments in a micrite matrix. There is little diagenesis and small replacement of the original allochems to sparite. Uniserial and multiserial foraminifera are abundant and are well preserved. There is some fracture porosity and the presence of very small stylolites.

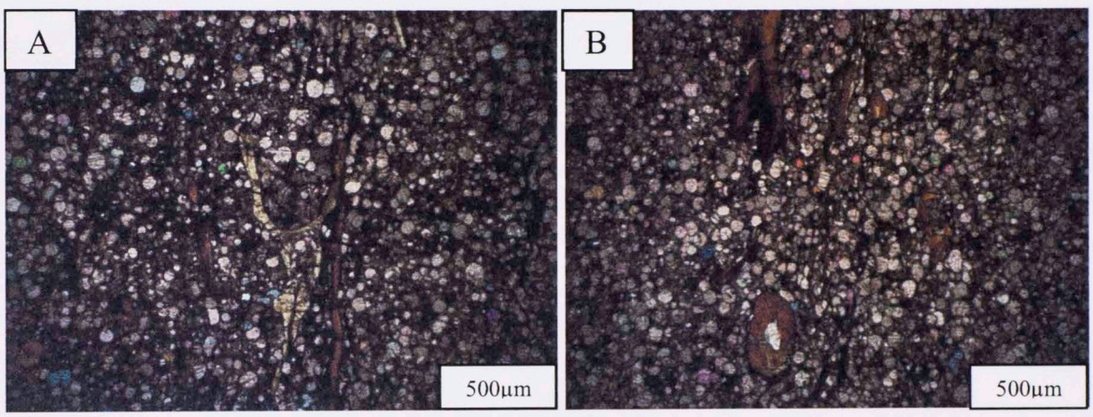

Figure 125 Photographs of thin section 001-Perija in cross polarized light. (A and B) Big picture of the thin section that represents a packstone with a good preservation of the foraminifera and shell fragments in a micrite cement.

Thin section 002

This mudstone with preserved foraminifera represents the Lower La Luna Formation in Lago de Maracaibo Basin. TOC for this section is around 7.24 wt. % and the S2 peak (Figure 111) is high, indicating an excellent interval of potential oil generation.

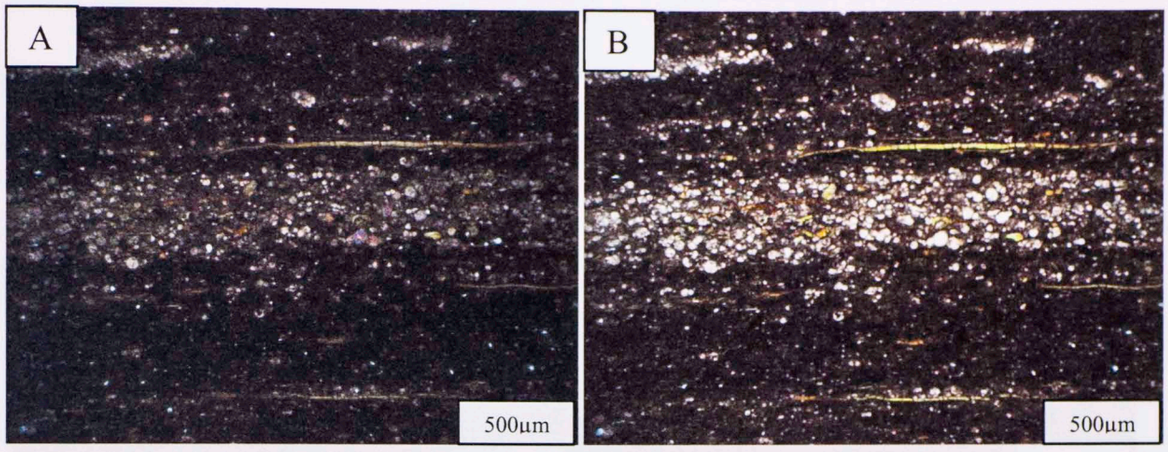

Figure 126 Photographs of thin section 002-Perija. A) Big picture of the thin section that represents a mudstone with a good preservation of the foraminifera and shell fragments in an organic rich matrix (cross polarized light) B) Big picture of the thin section that represents a wackstone with a good preservation of the foraminifera and shell fragments in an organic rich matrix (planar polarized light).

Thin section 003

This sample represents the boundary between the Lower and Middle La Luna interval in the La Luna stratotype (Lago de Maracaibo Basin). It is a mudstone in an organic matter-rich matrix with an abundance of calcite recrystallization of uniserial and multiserial foraminifera that shows similar features as in the La Luna 1X core. Bitumen content is moderate and the TOC shows high values (12.8 wt. %) and the S2 peak shows excellent potential for oil generation.

This rock also has the highest TOC value of the entire outcrop. Coarse Prism shells occur in this section (Figure 128) indicating they have undergone diagenetic modification (Scholle & Ulmer- Sholle, 2003). Some quartz and phosphates are also present in small amounts.

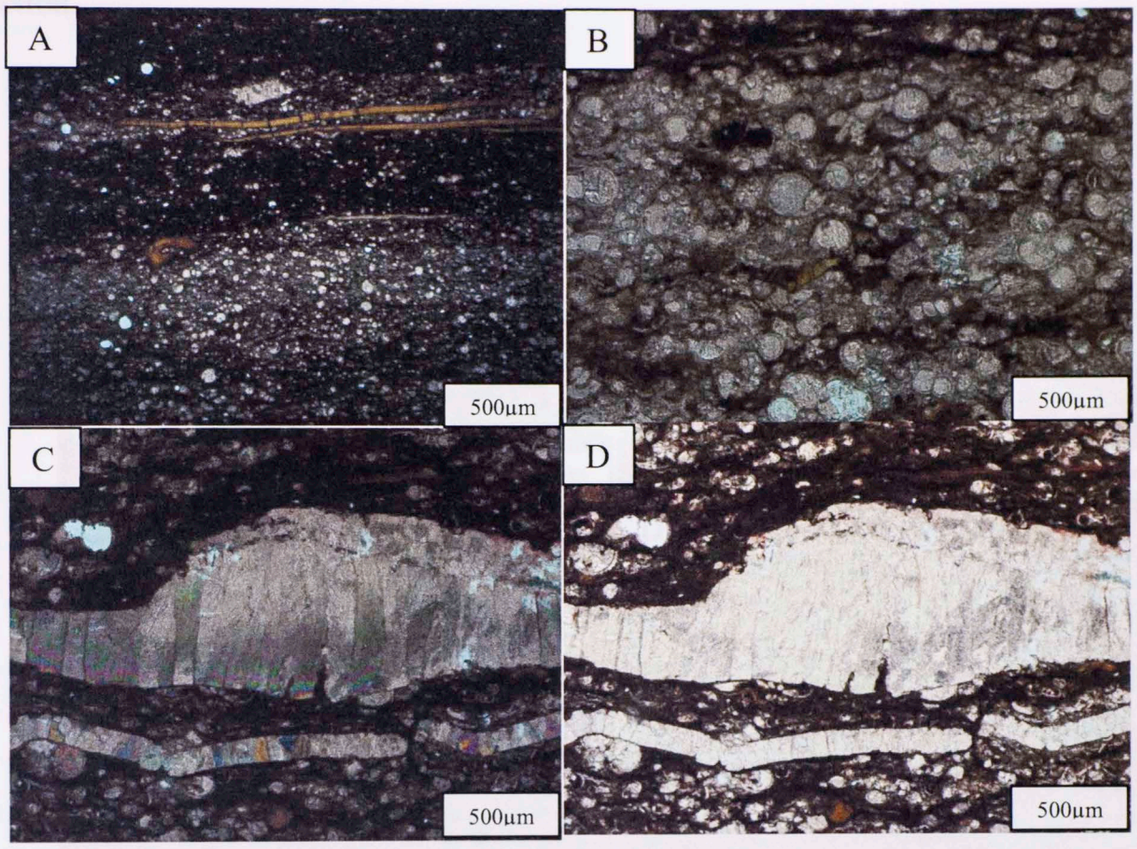

Figure 127 Photographs of thin section 003-Perija. A) Big picture of the thin section that represents a mudstone with a good preservation of the foraminifera and shell fragments in an organic rich matrix (cross polarized light) B) Big picture of the thin section that represents a wackstone with a good preservation of the foraminifera and shell fragments in an organic rich matrix (planar polarized light).

Thin section 004

This section represents the Upper La Luna interval. As previously stated, the Upper La Luna contains an abundance of glauconite. This sample is a packstone- grainstone with high amounts of foraminifera and shell fragments in a siderite cement.

Dolomitization is evident in some parts of the thin section. Porosity is interparticle and grain-to-grain. A large amount of transported phosphate is also visible in the thin section.

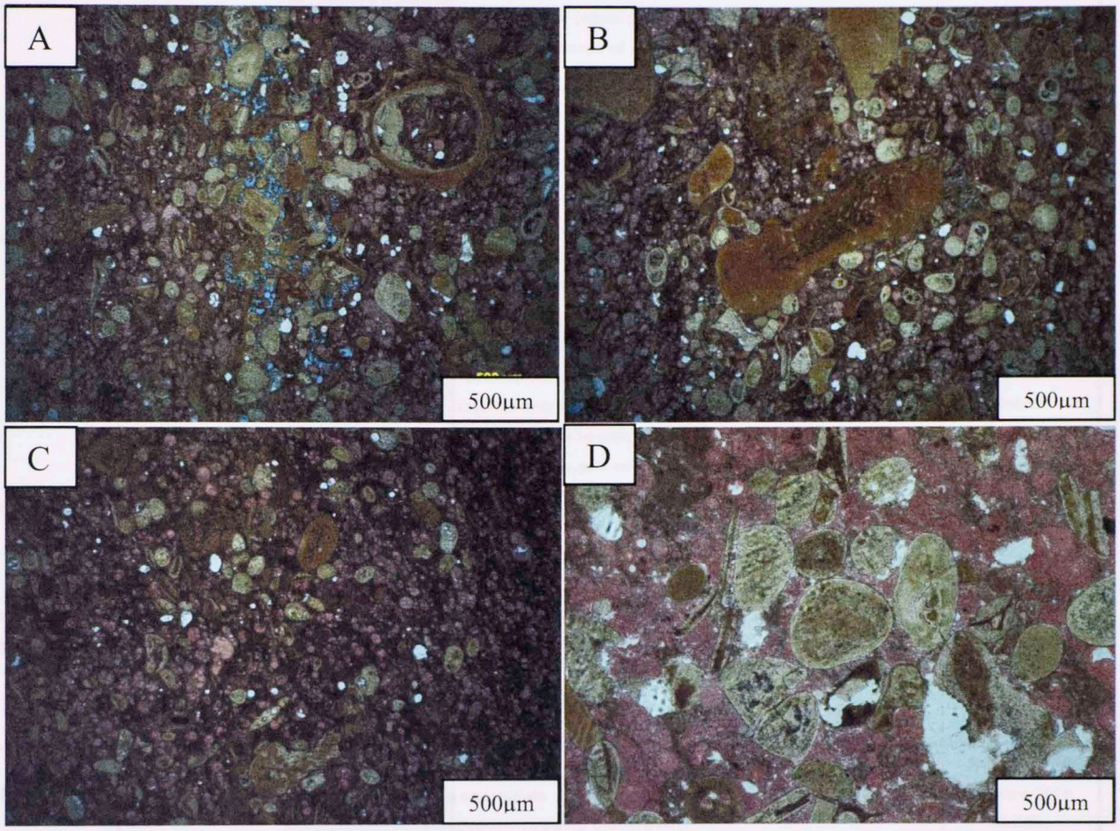

Figure 128 Photographs of thin section 004-Perija. (a, b and C) Big picture of the thin section that represents packstone- micrograinstone with high amounts of foraminifera and shell fragments in siderite cement (cross polarized light) with high abundance of glauconite and phosphates D) Presence of big glauconite grains.

Table 15 Chart summary of facies and major features of thin sections of La Luna outcrops.

Outcrop	Thin sections	Facies related	Mayor Features	Porosity
Las Hernandez	Thin section 001 and 002	V	Packstone with a high percentage of organic matter matrix and high amounts of recrystallized calcite.	No Porosity
	Thin section-003		Wackstone with the most organic-rich interval of the whole outcrop. Bitumen oil content content is moderate. TOC is around 3.25 Some shell fragments, brachiopods and uniserial foraminifera are present but of smaller size than the prior two thin sections.	Interparticle
	Thin section 4	VI	Wackstone with two types of cementation: Organic rich "cement" with some brachiopods and unicellular foraminifera, and stylolites and micrite and a high increment of porosity	Moldic Interparticle
Zea	Thin section 001 and 002	VI	Wackstone with micrite cement and uniserial foraminifera completely recrystallized to calcite	Interparticle Dissolution
San Pedro del Rio	Thin section 001 and 002	IV	Packstone-wackstone composed of abundant uniserial and multiserial foraminifera, stylolites and sparite veins	Intraparticle Interparticle Vug Fracture
Azulita-Bachaquero		VII	Packstone with finer-grained and smaller sediments Dolomite, pyrite and siderite fragments are disperse	Intraparticle Interparticle Moldic
Chiguara		V	Packstone with abundance of recrystallized and multiserial foraminifera in a micrite organic rich matrix. Sparite filled fractures	Interparticle
Flanco Perijanero	Thin section 001	I	Packstone and mudstone with recrystallized foraminifera gastropods, fish remains and shell fragments in a micrite matrix. Good Preservation and high TOC content	By fracture
	Thin section 003	IV	Boundary between the lower and middle La Luna interval mudstone in an organic matter-rich matrix with an abundance of calcite recrystallization High TOC values	Interparticle
	Thin section 004	VII	Packstone-grainstone Upper La Luna Interval with an abudance of glauconitic intervals Transport phosphates	Interparticle Grain to grain
I	Dark gray laminated mudstone			
IV	Laminated mudstone with limestone concretions and Packstone			
V	Siliceous- calcareous laminated mudstone interbedded with black chert filled with calcite veins			
VI	Calcareous slightly siliceous wackstone			
VII	Slightly siliceous- calcareous laminated black mudstone interbedded with calcareous fossiliferous wackstone.			

6. Sequence stratigraphic framework

"Sequence stratigraphy is the study of sedimentary rock relationships within a chronostratigraphic or geologic-time framework" (Slatt et al., 2011). According to Slatt, (2015) shales like the Barnett Shale, Woodford Shale, Marcellus Shale, Haynesville Shale, Eagle Ford Shale and the La Luna Shale exhibit stratigraphic zonation that indicates at least two scales of predictable relative sea level cyclicity. Thus, "a sequence stratigraphy model is established (Figure 129), consisting of a basal erosion surface of underlying strata (sequence boundary, SB) which can be combined with a younger transgresive surface of erosion (TSE), generally overlain by an organic rich transgresive system tract (TST) capped by a condensed section/maximum flooding surface (CS/mfs), which is overlain by downlapping highstand systems tract (HST) deposits" (Slatt, 2015). He also states, that a principal application of a sequence stratigraphic framework on shales is the correlation and mapping of sequence stratigraphic intervals in a systematic manner to develop relationships to geomechanical or geochemical characteristics for sweet spot identification.

6.1 Sequence stratigraphy of the La Luna formation:

The Mid- Late Cretaceous age represents one of the periods of more extensive distribution of organic-rich sediments in both deep and shallow-marine environments, throughout the world (Perez Infante et al, 1996). Organic carbon-rich sediments are related to Oceanic Anoxic Events with a lot of organic matter generated and preserved.

Perez- Infante et al. (1996) based their study on bulk- geochemical, micropaleontological and carbon- isotopic data to address local and global stratigraphic variability of lithofacies, biomarker composition and micropaleontological assemblages

that define the Cenomanian/ Turonian event in La Luna Formation. His study suggested that the anoxic event is related to a major global sea level rise. However, the highest sea level peak in the Late Cretaceous appears to occur sometime later in the Middle Turonian (91.5 and 90.3 MA; Haq et al., 1987). Davis & Pratt (1999) found for the same La Luna IX core that "High concentrations of organic carbon and trace metals in La Luna strata resulted from the combined influence of reduced terrigenous dilution of marine sediment associated with global sea level changes, elevated concentrations of dissolved trace metals associated with widespread oxygen depletion in the Atlantic basin, moderate accumulation rates of labile organic matter associated with episodically high primary productivity on the northern margin of South America and an unusually thick layer of sulfidic bottom water that periodically blanketed La Luna sediments".

6.2 Subregional sequence stratigraphic framework

According to Slatt et al. (2011), Relative Hydrocarbon Potential (RHP), (equation 1) is a geochemical parameter that is used as a paleoenvironmental indicator assuming that most of the samples are at similar levels of maturity. It also reflects the fluctuations in the oxygen level of the depositional environment and is used instead of the Hydrogen Index because it reduces the influence of organic matter maturation on the hydrogen index (Gomez, 2014).

$$\text{RHP}=\frac{S1+S2}{TOC} \qquad (1)$$

"Any change in S1 and S2 is not caused by maturity changes, but reflects changes in the amount of preserved organic matter (kerogen). Therefore, it can be

expected that under anoxic conditions in the depositional environment, larger amounts of organic matter (TOC) will be preserved in the sediment and the S2 peak will be greater than under oxic conditions, where less TOC is preserved and the S2 peak will be smaller. Thus, the calculated RHP value (S1 + S2/TOC) will be larger for sediment deposited under anoxic conditions than for sediment deposited under oxic conditions." (Slatt et al., 2011).

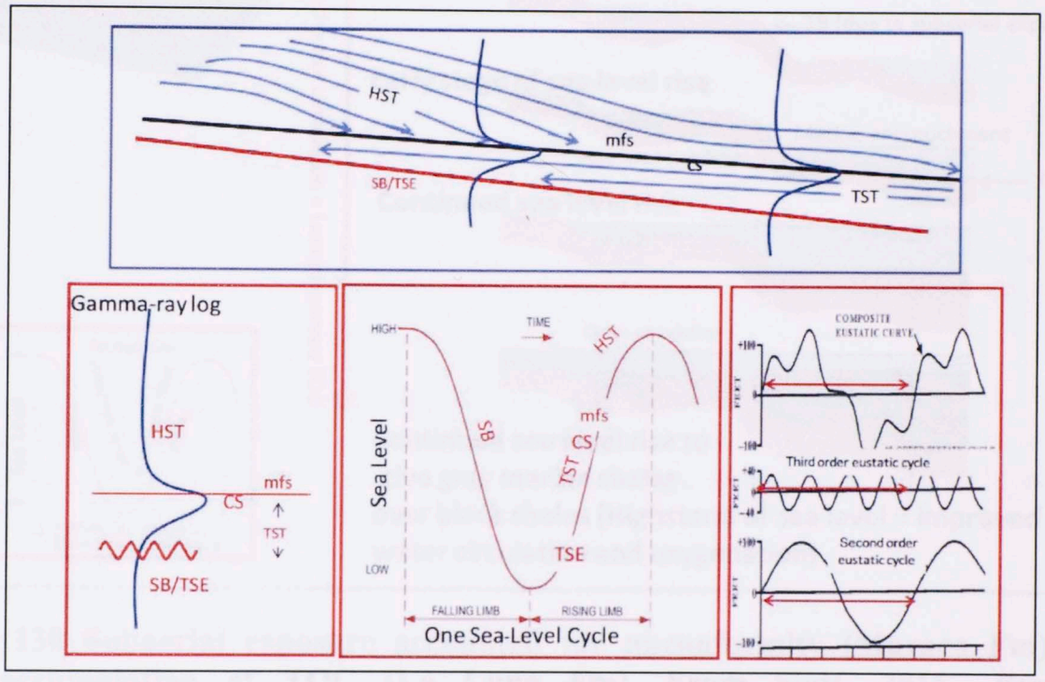

Figure 129 Generalized sequence – stratigraphic model of unconventional resource shales. SB, sequence boundary; TSE, transgresive surface of erosion; TST, transgresive systems tract; CS, condensed section; mfs, maximum flooding surface; HST, highstand system track. Two conceptual gamma ray logs are shown on the upper figure and on the lower left, to demonstrate the log responses of the different components. The lower-middle diagram is a relative sea level curve illustrating the positions or times within a sea level cycle when each component is formed. The lower diagram shows second and third order cycles and a composite relative sea level curve of these two orders of cyclicity. Lower right diagram is after *Van Wagoner et al.* (1990), *in Slatt et al.* (2011).

In order to have a better RHP resolution, a high amount of Rock Eval samples are needed, the RHP in this case cannot be determined since only 20 samples of Rock

Eval Analysis are available for this study and the changes of the sea level are not going to be reflected as would be expected.

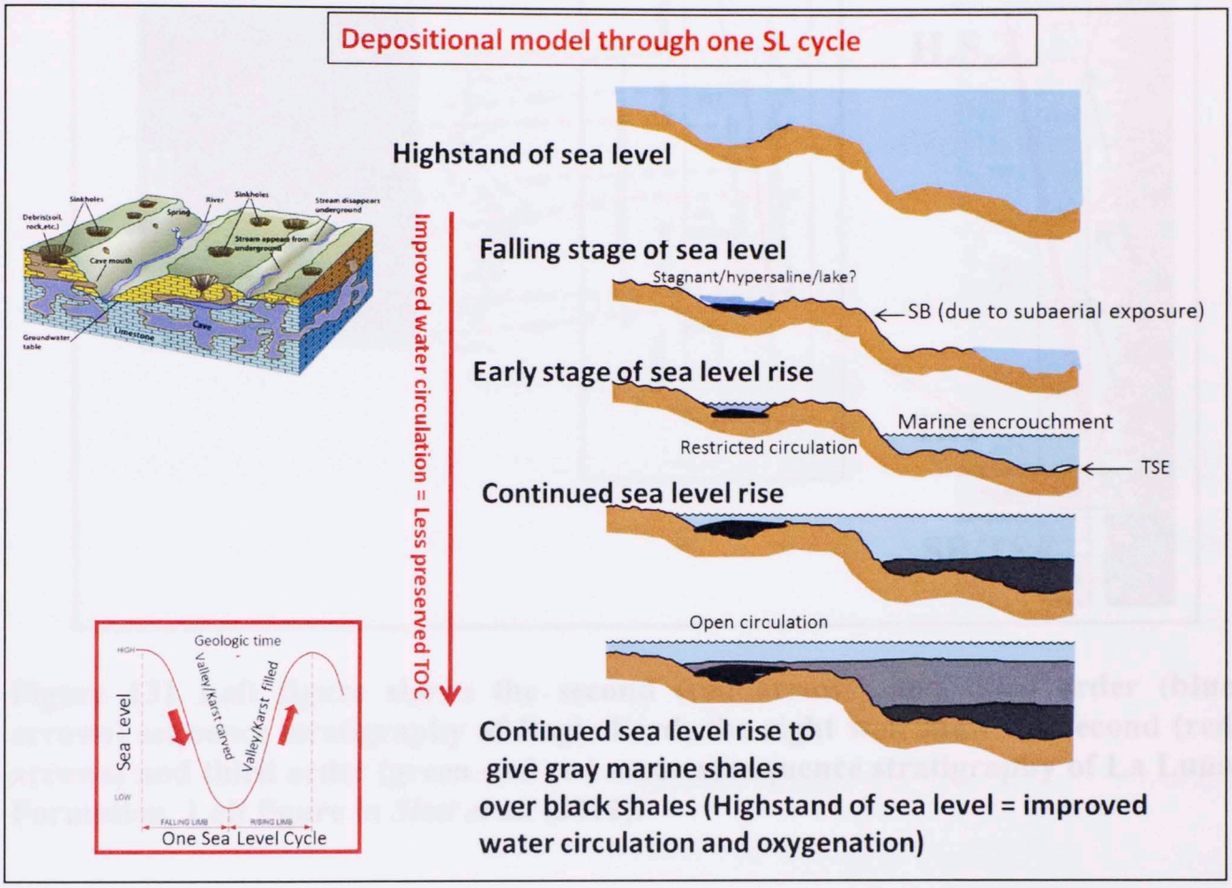

Figure 130 Subaerial exposure accounted for unconformity (Maraca Fm) and early accumulation of TOC (La Luna Fm). From Slatt, 2015., Personal communication).

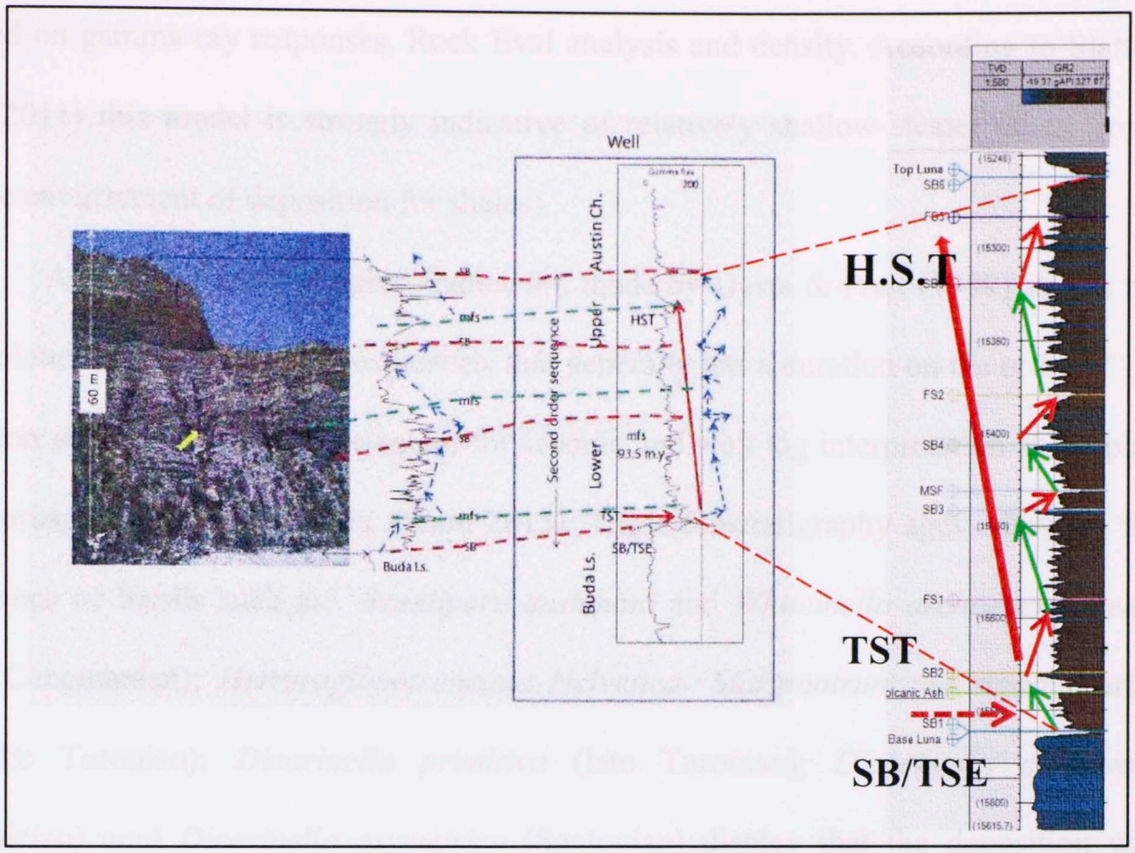

Figure 131 Left figure shows the second (red arrows) and third order (blue arrows) sequence stratigraphy of Eagle Ford; the right well show the second (red arrows) and third order (green and red arrows) sequence stratigraphy of La Luna Formation. Left figure in *Slatt et al.* (2011).

As is the case in the Eagle Ford (Figure 131), La Luna shows a gamma ray log response that diminishes progressively upward, indicating the sequence that begins with SB/TSE and ends with the HST in the La Luna IX well. It is also represented by a series of third order sequences of Highstand and Transgressive System Tracts overlying the erosional top of the underlying Maraca Formation (a shallow water platform with a subaerial exposure representing the unconformity before the deposition of La Luna Fm.) which constitutes the base of La Luna Formation (Figure 130).

Figure 131 shows the similitude of the Eagle ford shale with La Luna IX well and figure 132 shows a generalized sequence stratigraphic model for organic shales

based on gamma ray responses, Rock Eval analysis and density. According to Slatt et al. (2011) this model is strongly indicative of relatively shallow- water (shelf upper slope environment of deposition for shales).

A refined biostratigraphic framework made by Davis & Pratt (1999) allows the calculation of the third order sequences, that generally has a duration on the order of 1-5 million years and that also are useful for seismic and well log interpretation at the play and prospect generation levels. (Slatt, 2013). Those biostratigraphy ages show by the presence of fossils such as: *Rotalipora cushmani* and *Whiteinella archaeocretacea* (late Cenomanian); *Helveroglobotruncana Helvetica- Marginotruncana sigali* (Early-middle Turonian); *Dicarinella primitiva* (late Turonian); *Dicarinella concavata* (Conician) amd *Dicarinella asymetrica* (Santonian) display that the deposition was generated during the early Cenomanian through Santonian (Figure 133).

Figure 134 shows the sequence stratigraphic framework of La Luna formation based on results obtained from core, thin sections, GR response, Density log, Uranium; Thorium; Potassium, XRD, XRF and TOC from core (Passey, 1990).

Based on these responses, a cyclicity of third order surfaces (SB/TSE and MSF) were interpreted and correlated with three more wells in La Luna IX taking into account the distance between them (9985m between well 1 and La Luna 1X; 5593m between well 3 La Luna 1X and 6681 between well 4 and La Luna 1X). Flooding surfaces record a rapid increase of sea level rise and a Sequence Boundary is developed by erosion when sea level falls. Figure 135 and 136 show the sequence stratigraphic interpretation in a structural and a stratigraphic cross section.

From bottom to top, the Gamma ray response shows the erosional surface that was deposited after a relative sea level drop on the Maracaibo platform which produced a sequence boundary on the underlying Maraca Formation surface. Sea level rise in a short period of time allowed deposition of a marine transgressive deposit and a small flooding surface. This was followed by a low gamma ray and a high density response, forming the first highstand system tract (HST).

Associated volcanic ash deposits also were found in Lower La Luna as it was found in the Salada Member in Colombia by Gomez (2014). This origin of volcanic ash might be related to a volcanic arc located on the western margin of northern South America (Parnaud et al., 1995). After the other sequence boundary/ transgresive surface of erosion another third order sequence of sea level cycles formed. It is very noteworthy how a succession of Transgressive and Highstand System tracts are very characteristic of the La Luna Formation, especially in Lago de Maracaibo Basin. Transgressive system tracts (first MSF from bottom to top, Figure 134) that corresponds to the highest sea level rise during the Turonian (91.5 and 90.3 million years ago; Haq et al., 1987). It has a characteristic high gamma ray response, low and low uranium content. Another marine regression formed an HST, followed by two more cycles of sea level fall-rise, followed by another possible volcanic ash pulse seems to be reflected towards the top of La Luna Fm, however, this hypothesis has not been confirmed and other studies should be done. Another sea level rise is forming a second MFS, but this one is particularly characterized by glauconite and phosphate deposits. This was part of the final deposition of the La Luna Formation. According to Erlich et al. (2000) "Bottom water oxygen levels increased from the Late Santonian through the end of the

Cretaceous and ventilation of anoxic bottom waters may have been enhanced by more frequent or intense seasonal upwelling (caused by higher wind stress) and catastrophic overturn, as well as the removal of a key paleo-bathymetric barrier. Fish and marine reptile bone beds within the Tres Esquinas Member (La Luna Formation) are attributed to massive mortality during these events, and are correlative with similar Campanian units in eastern Colombia. During the Maastrichtian, increasing ventilation, combined with siliciclastic dilution, ultimately produced sediments with lower total organic carbon (TOC) content. The ending of this period is followed by a regressive trend (Colon Formation) with closure of the Tethys basin. In order to visualize a better sequence stratigraphy trend, figure 135 and 136 show a Stratigraphic and Structural cross section of third order sequences (TST and HST) in La Luna 1X.

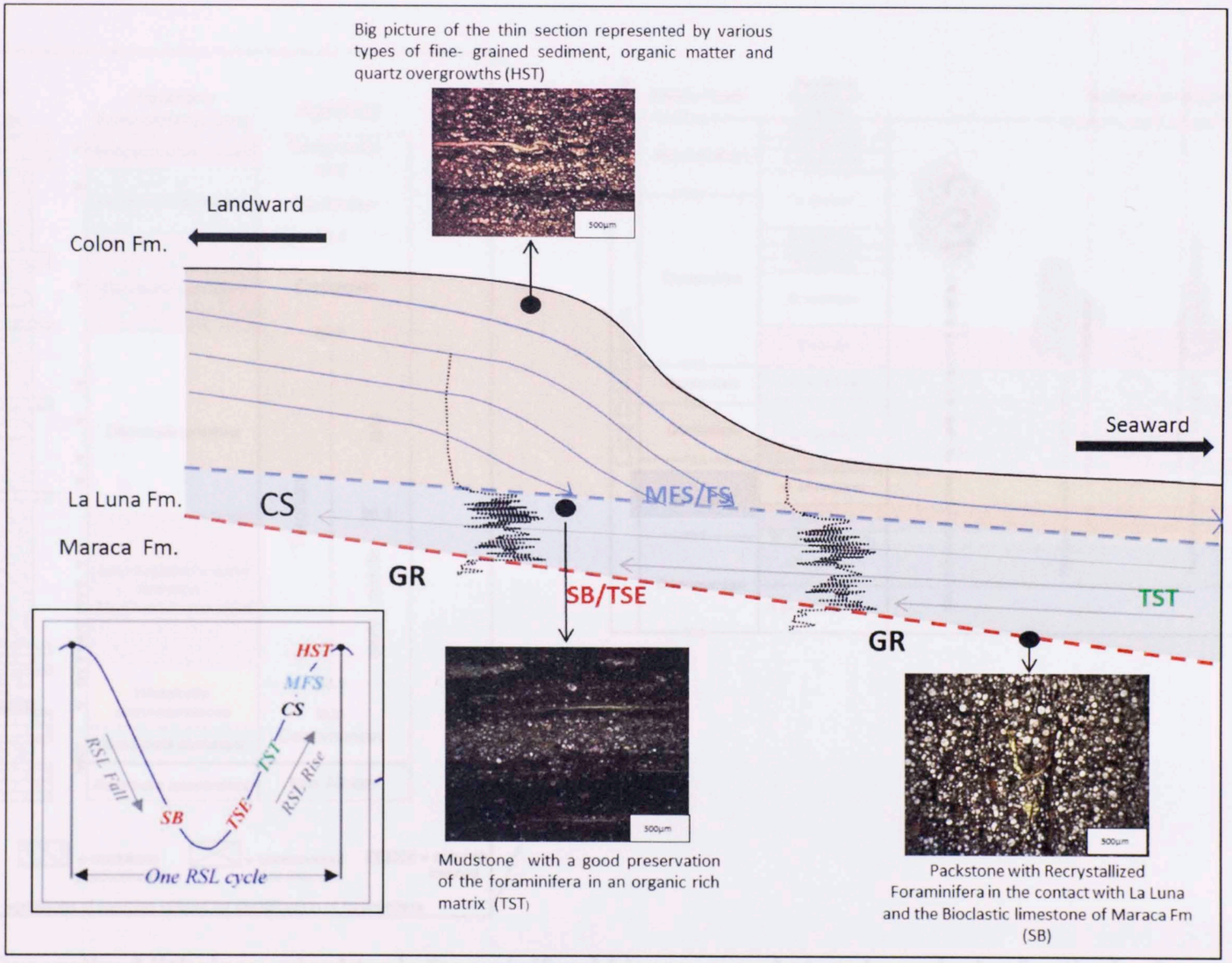

Figure 132 Generalized sequence stratigraphic model and the corresponding gamma ray log responses, with examples from La Luna Fm. (Modified from Slatt et al., 2012).

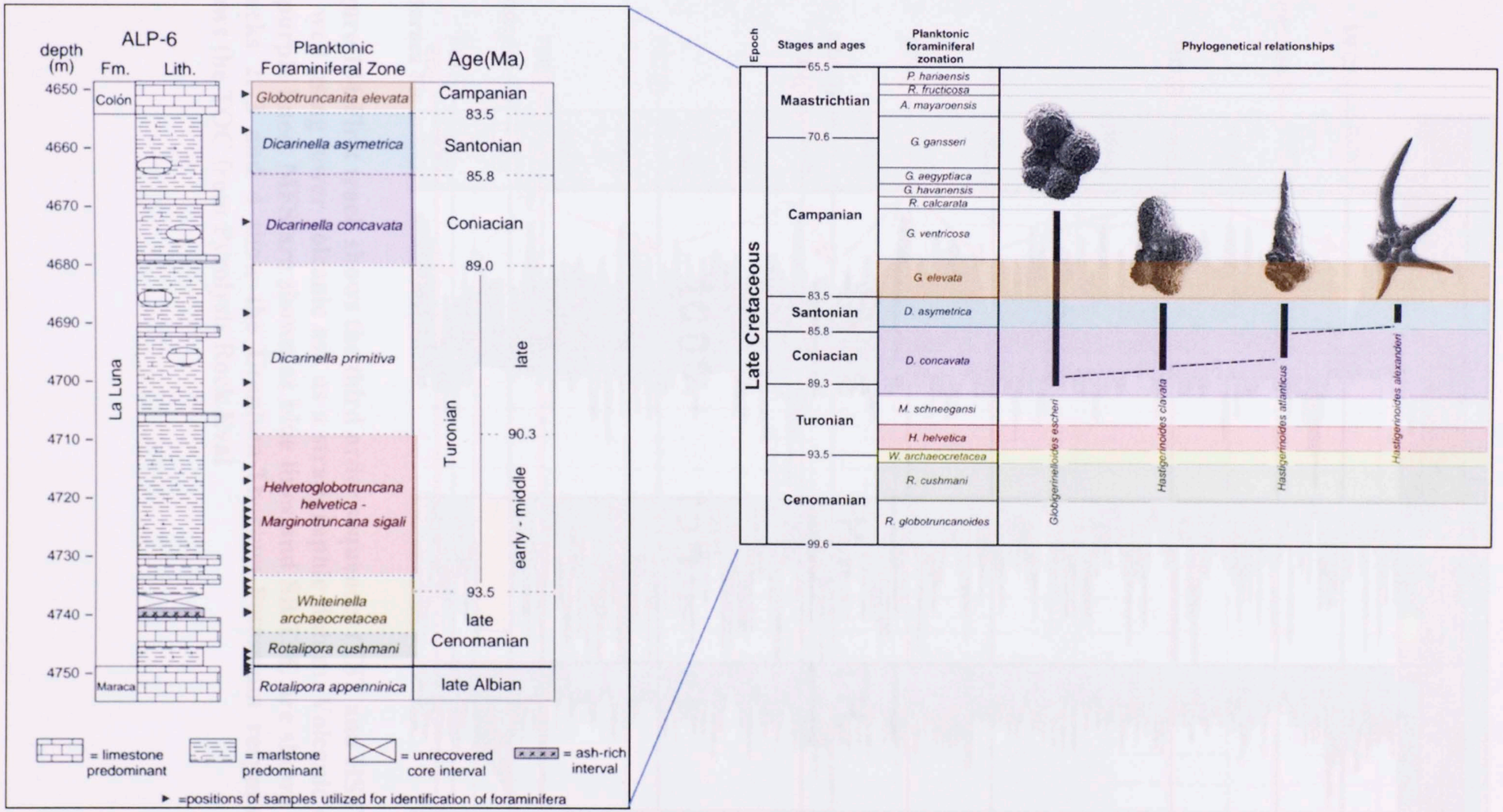

Figure 133 A) Generalized lithology, planktonic foraminiferal biozones, and stage boundaries for the La Luna Formation and surrounding units in La Luna IX. Biostratigraphy is determined after Sliter (1989). B) Age dates for stage boundaries taken from Gradstein et al. (1994), and middle-late Turonian boundary date from Kauffman et al. (1993).

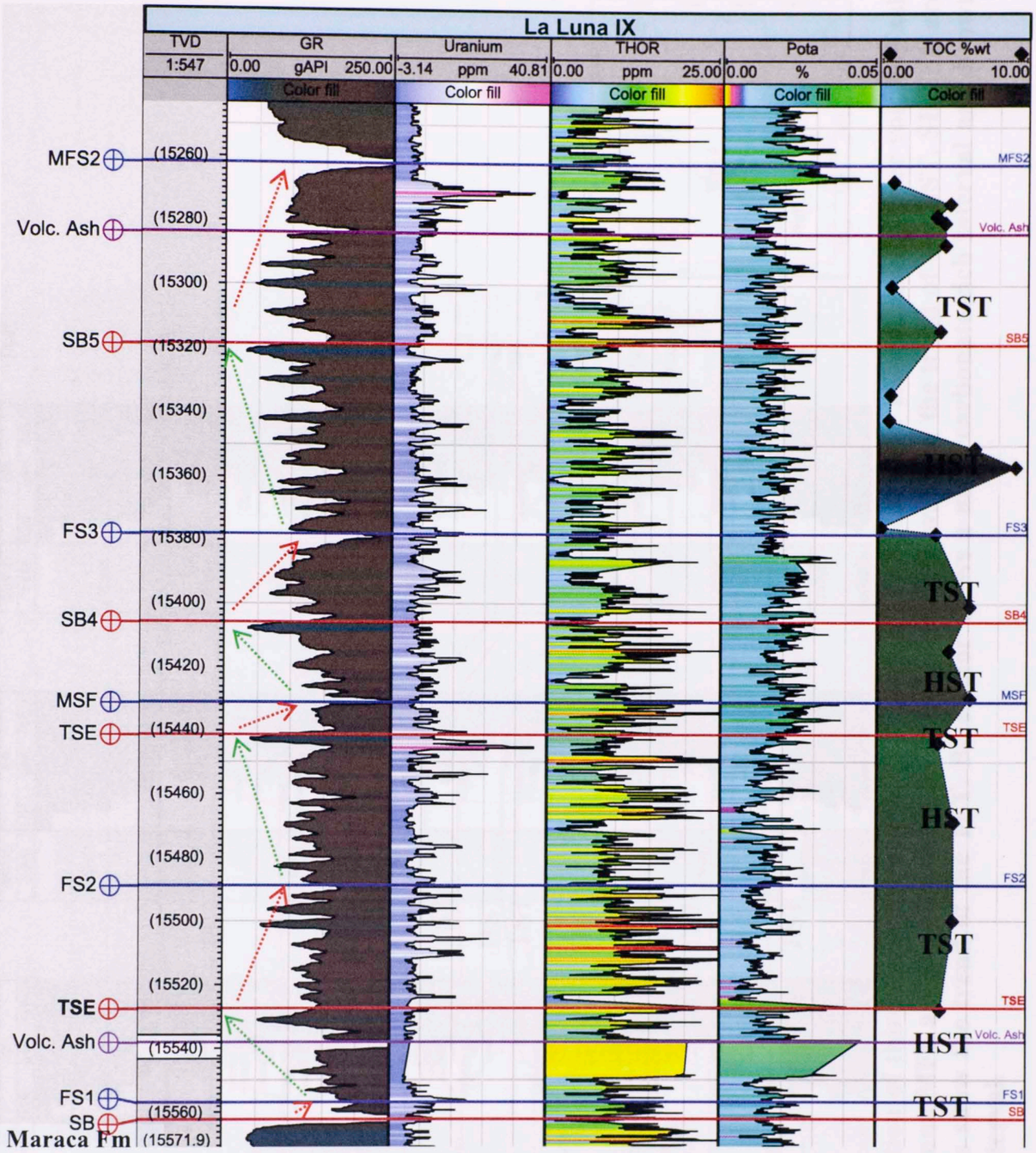

Figure 134 First track shows the third order sequences (TST and HST) in La Luna 1X well using lower volcanic ash as a stratigraphic datum. Volcanic ash is shown as purple lines; MFS are shown as blue lines and SB/TSE are shown as red lines. Tracks 2, 3 and 4 show the Uranium-Thorium-Potassium responses. Track 5 shows the TOC from Pyrolysis Rock Eval

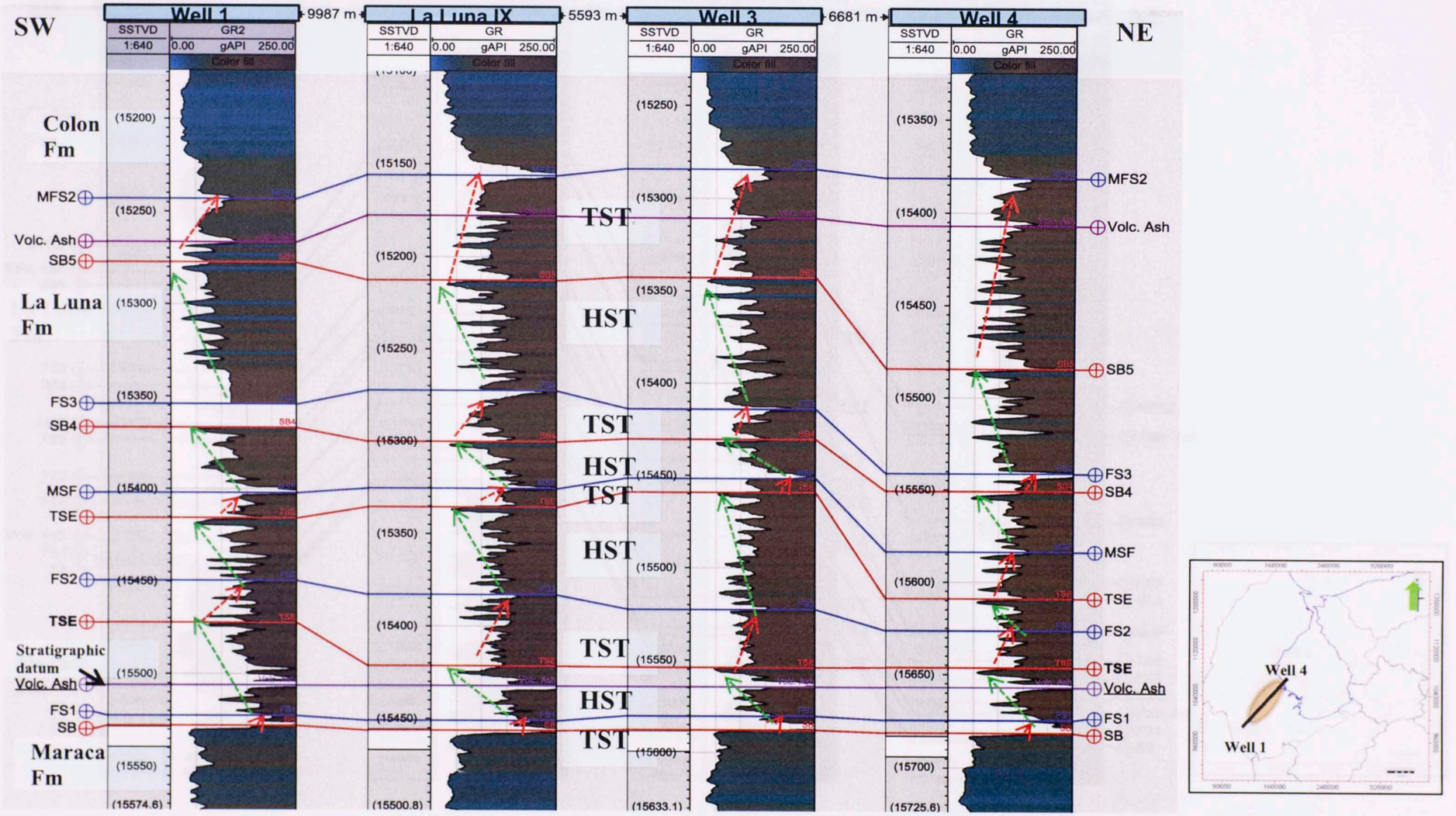

Figure 135 Stratigraphic cross section of third order sequences (TST and HST) in La Luna 1X well using lower volcanic ash (purple line) as a stratigraphic datum. MFS are shown as blue lines and green arrows show the trend of the HST. SB/TSE are shown as red lines and red arrows show the trend of the TST. Blue color shows a more carbonate-rich interval and brown color shows a more organic-rich interval.

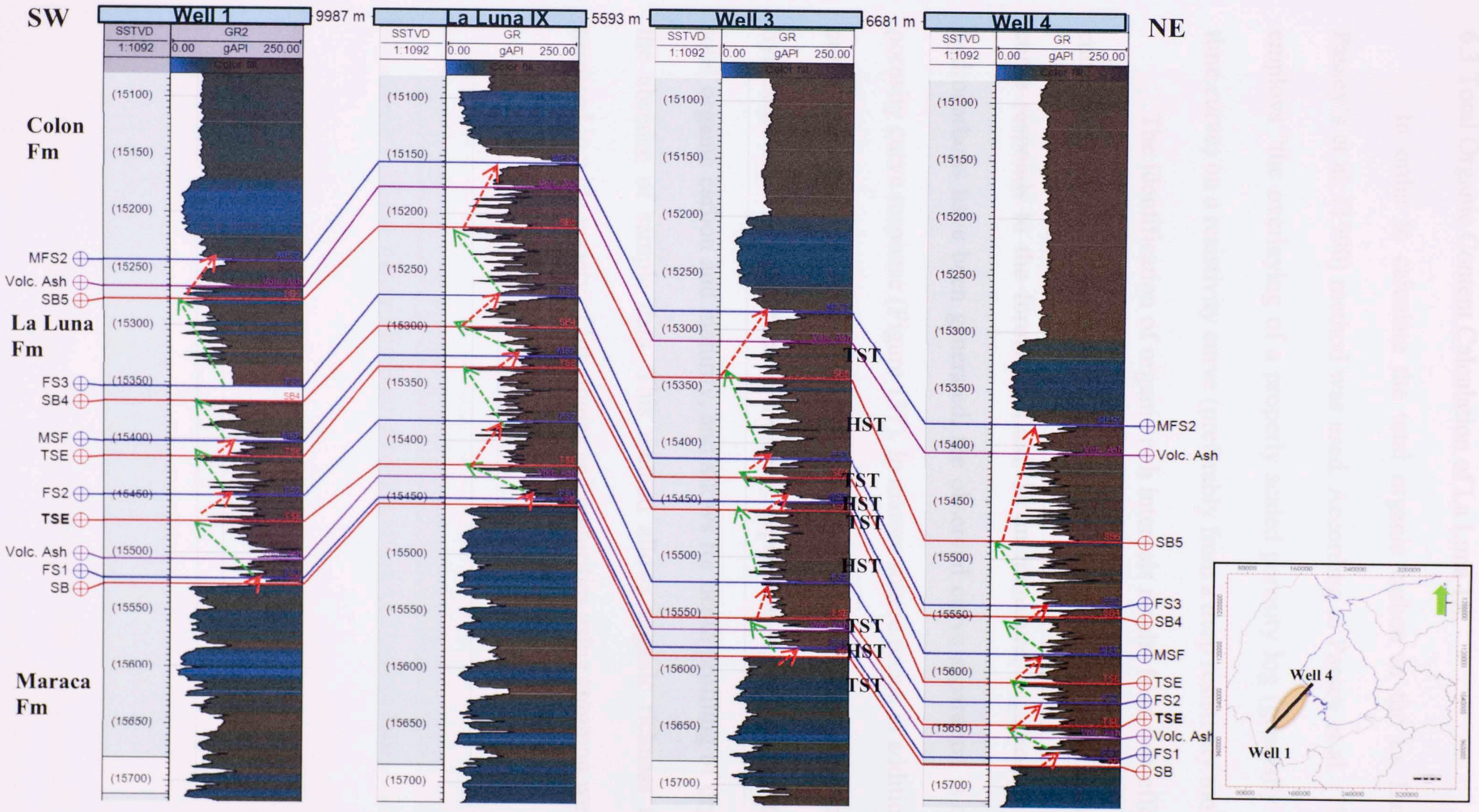

Figure 136 Structural cross section of third order sequences (TST and HST) in La Luna 1X well using volcanic ash are shown as purple lines. MFS are shown as blue lines and green arrows show the trend of the HST. SB/TSE are shown as red lines and red arrows show the trend of the TST. Blue color shows a carbonate-rich interval and brown color shows a organic-rich interval.

6.3 Total Organic Content Calculation of La Luna 1X

In order to calculate the total organic carbon in the La Luna 1X well, the Passey's et al. (1990) method was used. According to Passey et al. (1990), the method employs "the overlaying of a properly scaled porosity log (generally the sonic transit time curve) on a resistivity curve (preferably from a deep resistivity tool).

The identification of organic rich intervals results from two effects: the porosity curve responds to the presence of low density, low velocity kerogen, and the resistivity curve responds to the formation fluid. In an immature, organic-rich rock, where no hydrocarbons have been generated, the observed curve separation is due solely to the porosity curve response (Figure 137). In mature source rocks, in addition to the porosity curve response, the resistivity increases because of the presence of generated hydrocarbons. The magnitude of the curve separation in non- reservoirs is calibrated to total organic carbon and maturity, and allows for depth profiling of organic richness in the absence of sample data. This method allows organic richness to be accurately assessed in wide variety of lithologies and maturities using common well logs."

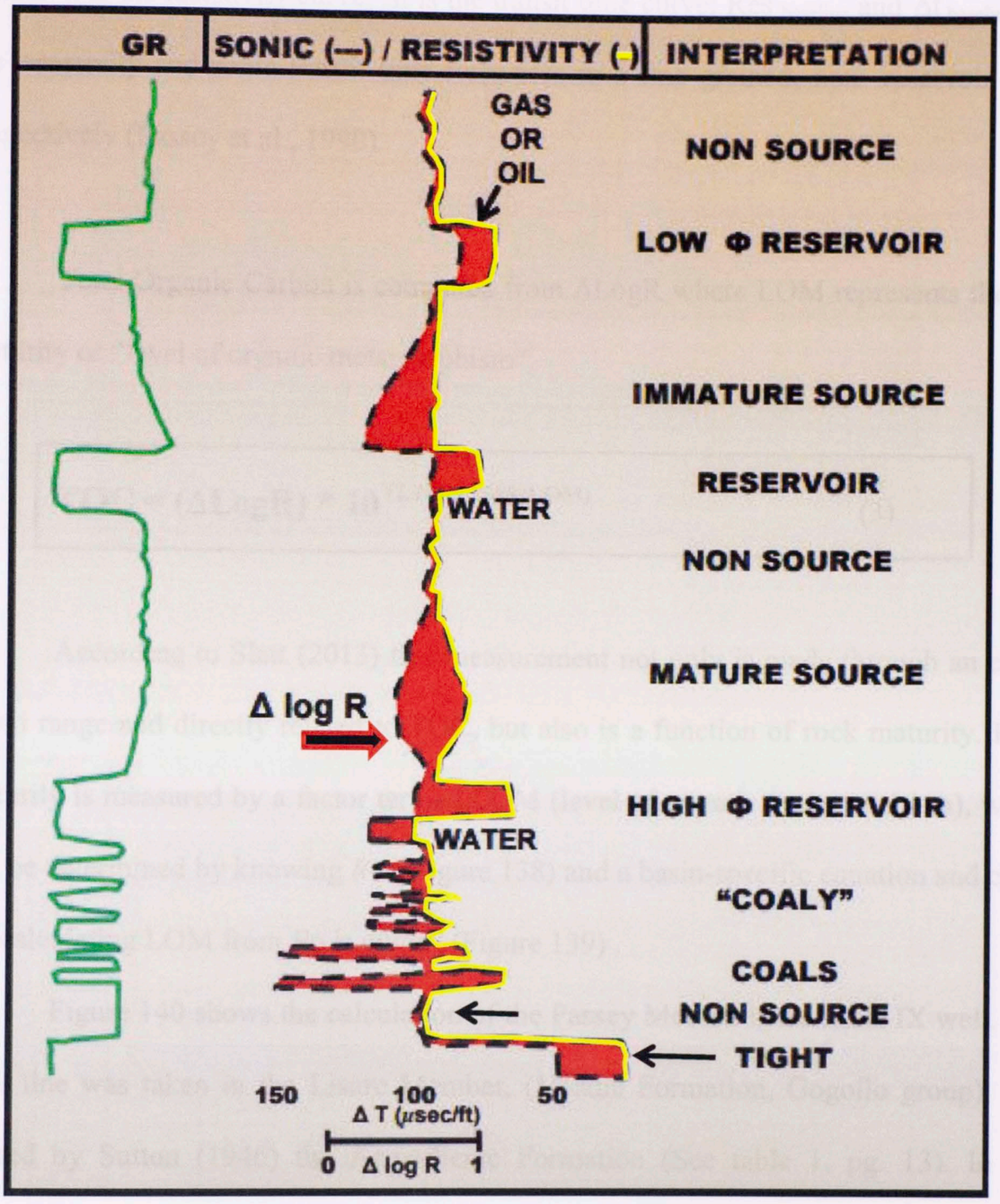

Figure 137 Sonic/ resistivity logs showing the Δlog R separation. After Passey et al. (1990).

$\Delta LogR$ is the separation between the porosity curve and deep resistivity curve and it's given by the following expression:

$$\Delta \text{LogR} = \log_{10}\left[\left(\frac{Res}{Res\ base\ line}\right) + 0.02 * (\Delta t - \Delta t_{\text{base line}})\right] \quad (2)$$

Where R is the resistivity curve, Δt is the transit time curve; $Res_{baseline}$ and $\Delta t_{baseline}$ are the resistivity and sonic transit time responses in a fine grained, non- reservoir rock, respectively (Passey et al., 1990).

Total Organic Carbon is computed from ΔLogR where LOM represents thermal maturity or "level of organic metamorphism":

$$TOC = (\Delta LogR) * 10^{(2.297-0.1688*LOM)} \quad (3)$$

According to Slatt (2013) this measurement not only is made through an entire depth range and directly related to TOC, but also is a function of rock maturity. Rock maturity is measured by a factor termed LOM (level of organic metamorphism), which can be determined by knowing *R*o (Figure 138) and a basin-specific equation and curve for calculating LOM from *R*o is given" (Figure 139) .

Figure 140 shows the calculation of the Passey Method in La Luna IX well. The base line was taken in the Lisure Member, (Middle Formation, Gogollo group), also named by Sutton (1946) the Aguardiente Formation (See table 1, pg. 13). In this member, sonic and resistivity logs overlap each other forming a fill with Gas or oil.

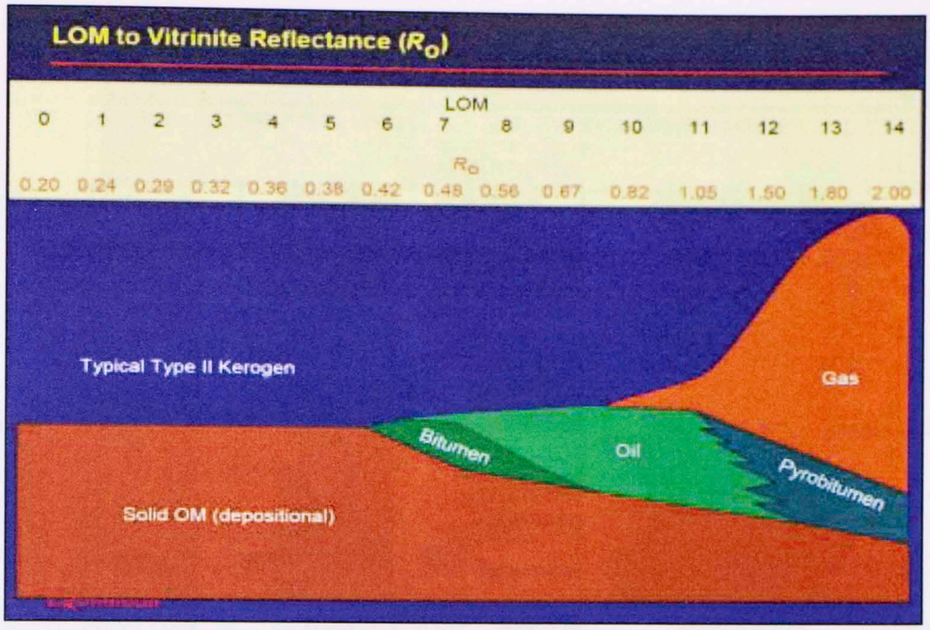

Figure 138 Relationship between LOM (level of organic metamorphism) and R_o. After Passey, from oral presentation (2012) in Slatt, 2013.



Figure 139 Relation between LOM and R_o for Woodford Shale basins in Oklahoma. Figure provided by J. Hooper in Slatt (2013).

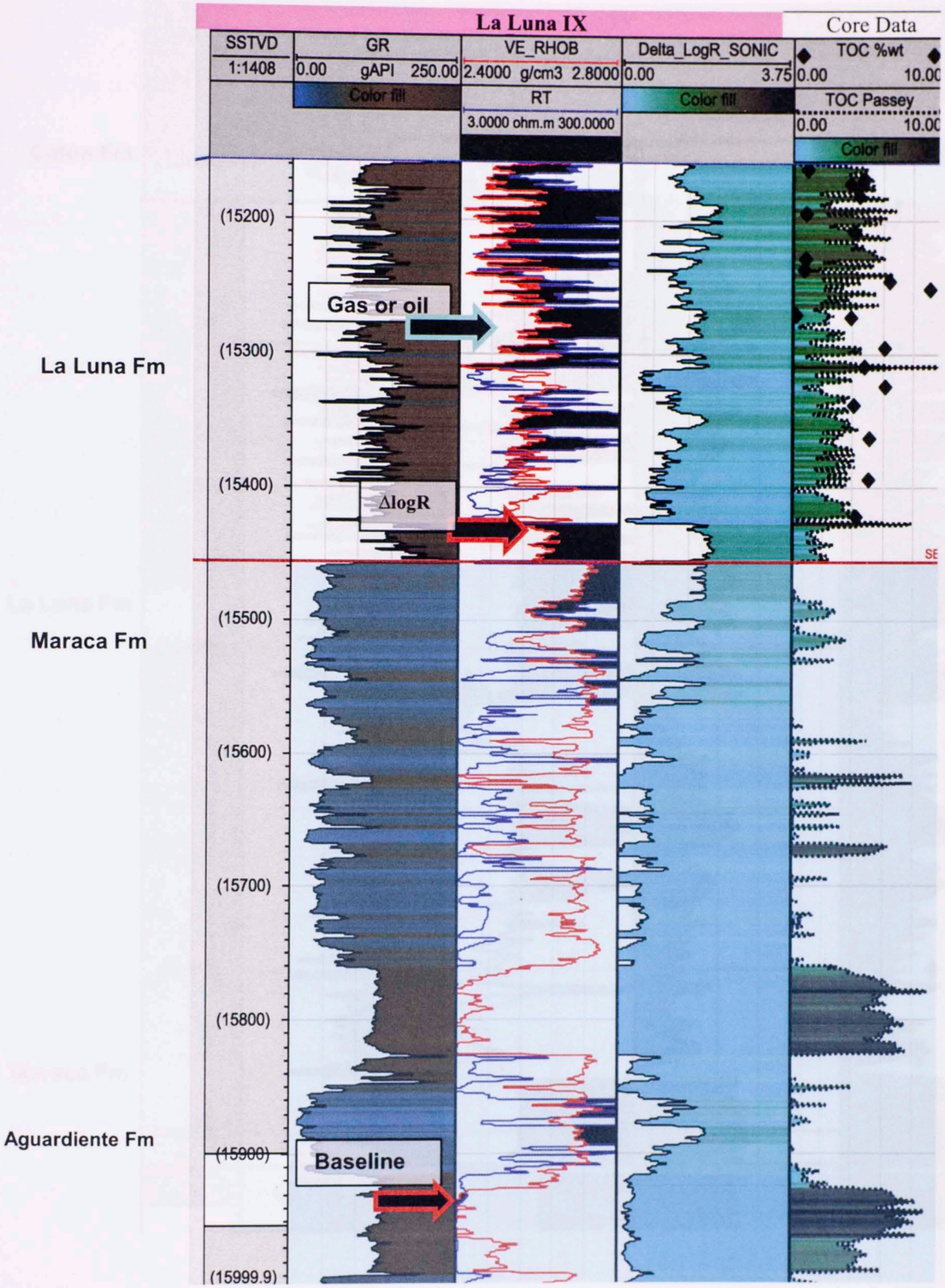

Figure 140 Track 1 corresponds to the GR profile related with the organic rich interval that shows in the Track 2. ΔlogR separations use the Sonic (VE_DT) and Resistivity (RT) overlay. Track 3 corresponds to the ΔlogR profile already generated by the two previous curves. Track 4 corresponds to the TOC data from core and TOC data predicted with the ΔlogR method and TOC Lithology predicted using (RT and VE_DT). Baseline was taken in Aguardiente Fm.

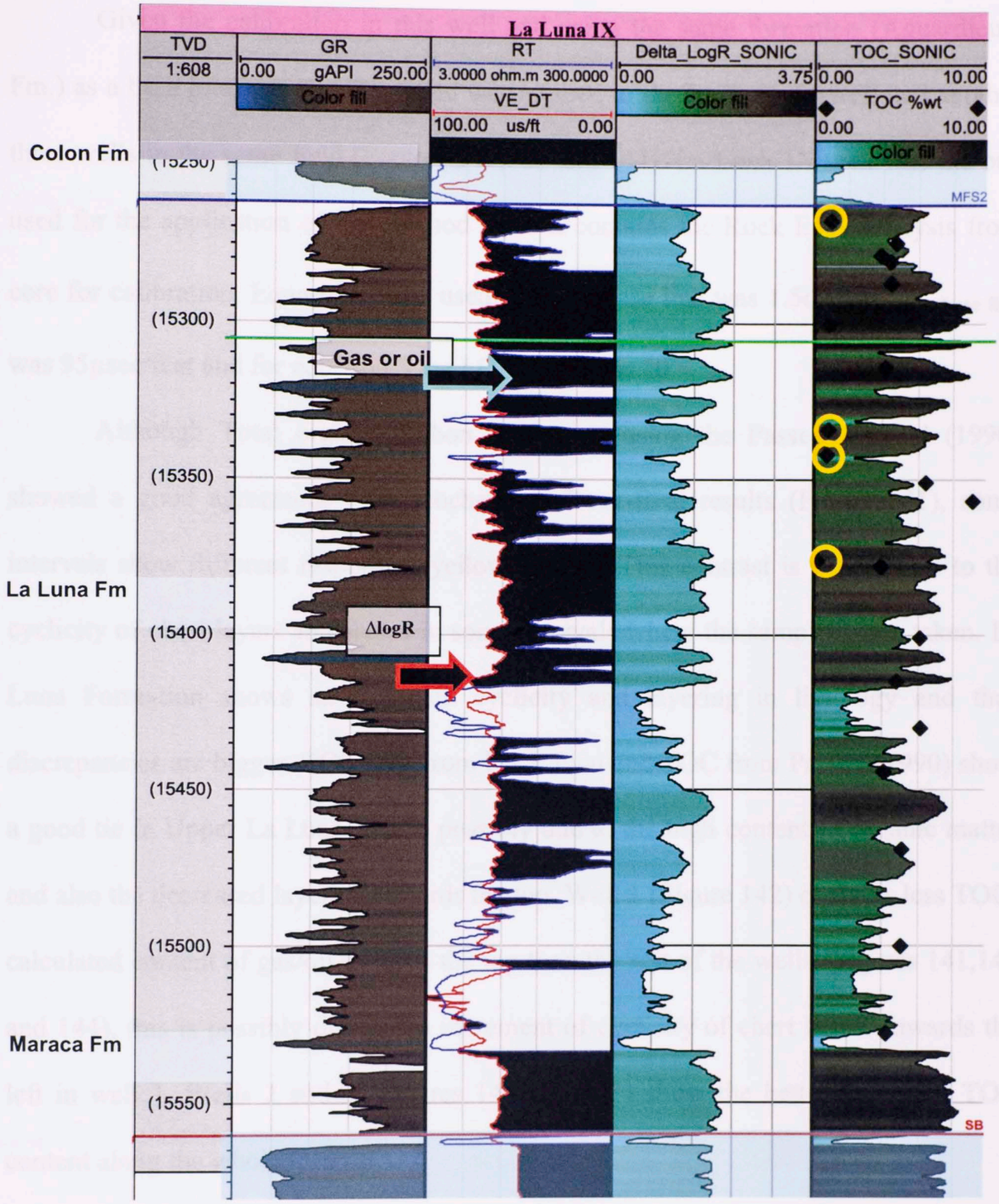

Figure 141 Track 1 corresponds to the GR profile related with the organic rich interval that shows in the track 2 ΔlogR separations using the Sonic (VE_DT) and Resistivity (RT) overlay. Track 3 corresponds to the ΔlogR profile already generated by the two previous curves. Track 4 corresponds to the TOC data from core and TOC data predicted with the ΔlogR method and TOC lithology predicted using (RT and VE_DT).Yellow circles show the low TOC content due to the presence of chert content.

Given the calibration in this well and using the same formation (Aguardiente Fm.) as a base line, the ΔlogR method was applied to the La Luna 1x well and another three wells in the same field (Figures 142,143 and 144). La Luna 1X well was the one used for the application of this method since it contains the Rock Eval Analysis from core for calibration. Equation 2 was used, the Res base line was 1.5ohm-m, $\Delta t_{\text{base line}}$ was 95μsec/feet and for equation 3 the LOM used was 10.

Although Total organic carbon estimation using the Passey Method (1990) showed a good agreement with geochemical Rock-Eval results (Figure 141), some intervals show different responses (yellow circles). This contrast is mainly due to the cyclicity of chert layers and shales in some intervals where the samples were taken. La Luna Formation shows an abundant cyclicity and layering in lithology and thus discrepancies are bigger. TOC data from Rock Eval and TOC from Passey (1990) show a good tie in Upper La Luna, this is possibly due to the high content of organic matter and also the decreased layering towards the top. Well 1 (Figure 142) contains less TOC-calculated content of gas/oil towards the top than the rest of the wells (Figures 141,143 and 144), this is possibly due to the increment of cyclicity of chert layers towards the left in well 1. Wells 2 and 3 (Figures 141 and 143) show the better estimated TOC content along the whole interval.

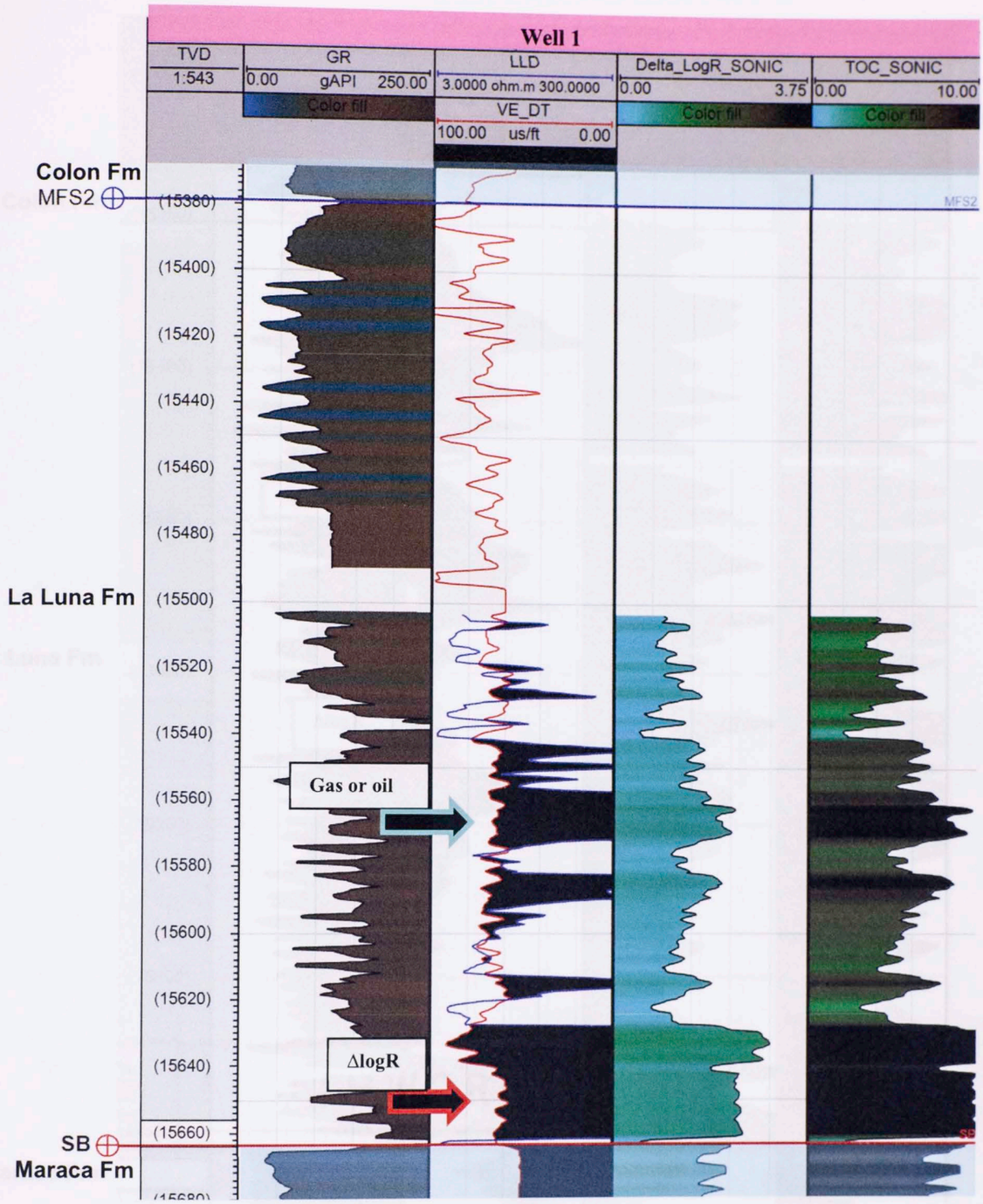

Figure 142 Track 1 corresponds to the GR profile related with the organic rich interval that shows in Track 2 ΔlogR separations using the Sonic (VE_DT) and Resistivity (RT) overlay. Track 3 corresponds to the ΔlogR profile already generated by the two previous curves. Track 4 corresponds to the TOC data predicted with the ΔlogR method. (Passey et al., 1990).

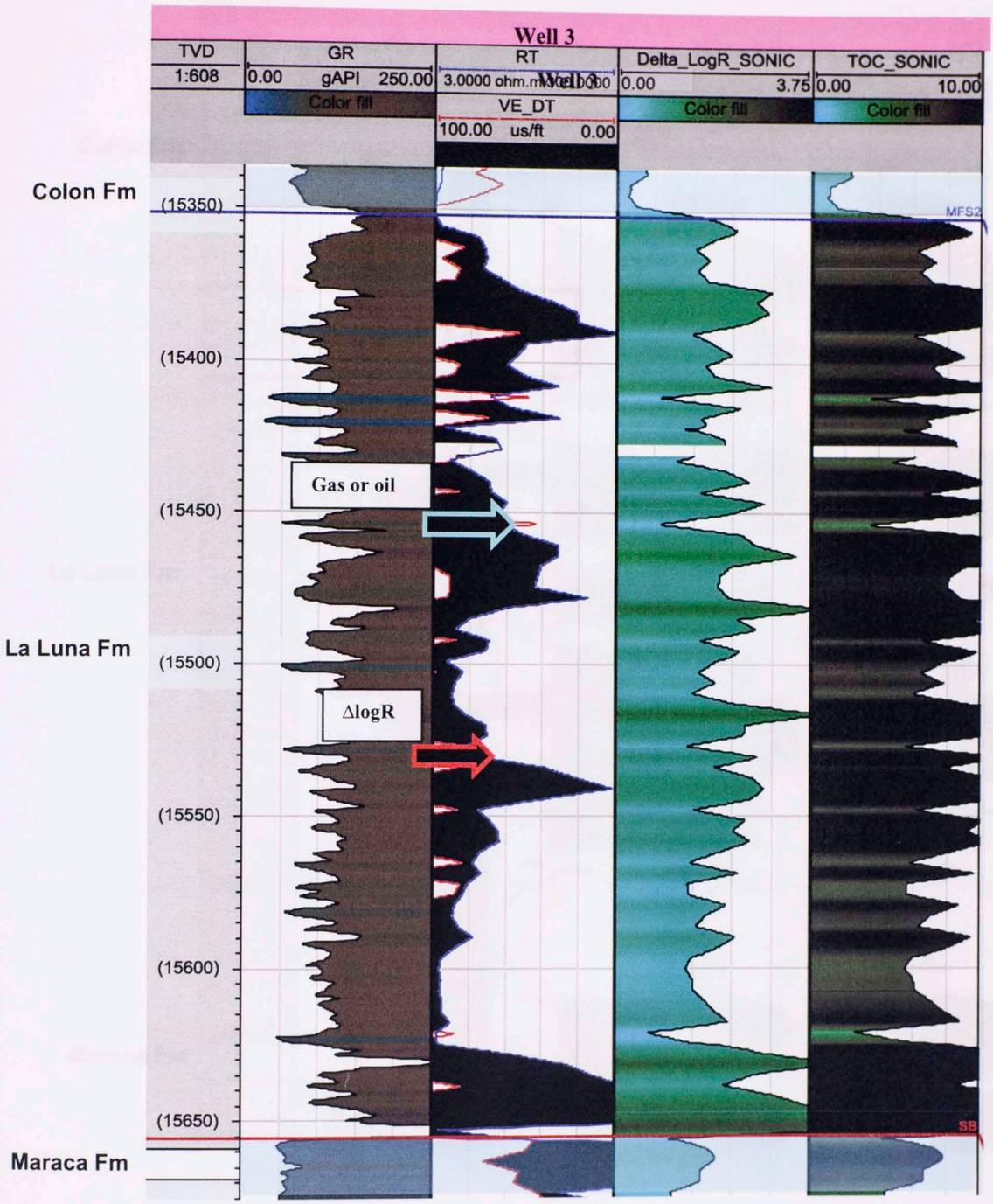

Figure 143 Track 1 corresponds to the GR profile related with the organic rich interval that shows in Track 2 ΔlogR separations using the Sonic (VE_DT) and Resistivity (RT) overlay. Track 3 corresponds to the ΔlogR profile already generated by the two previous curves. Track 4 corresponds to the TOC data predicted with the ΔlogR method. (Passey et al., 1990).

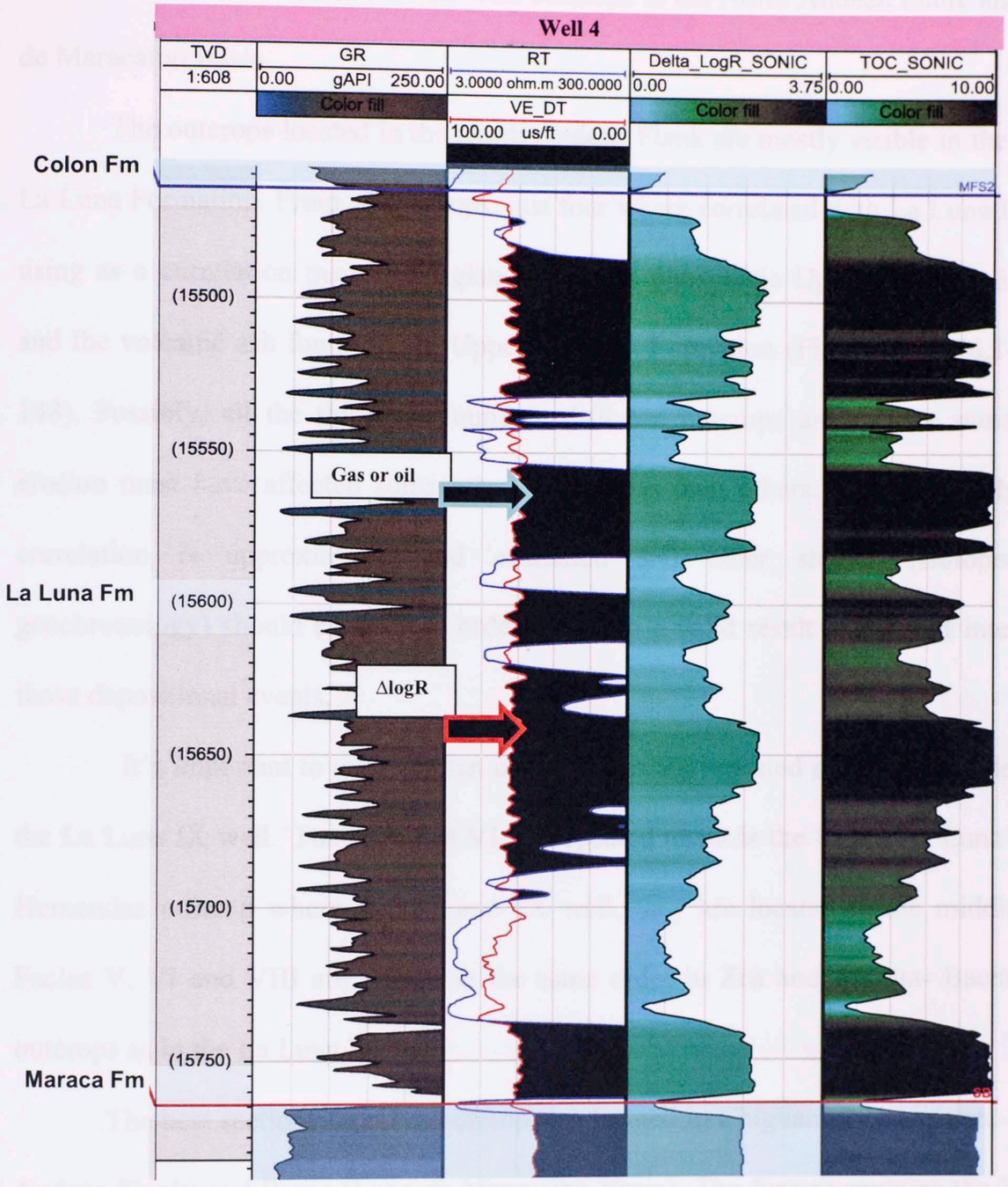

Figure 144 Track 1 corresponds to the GR profile related with the organic rich interval that shows in the Track 2 ΔlogR separations using the Sonic (VE_DT) and Resistivity (RT) overlay. Track 3 corresponds to the ΔlogR profile already generated by the two previous curves. Tract 4 corresponds to the TOC data predicted with the ΔlogR method. (Passey et al., 1990).

6.4 Correlation of La Luna 1X well with outcrops in the North Andean Flank and Lago de Maracaibo Basin

The outcrops located in the North Andean Flank are mostly visible in the Upper La Luna Formation. From all outcrops, just four where correlated with La Luna IX well using as a correlation marker the glauconitic and phosphatic Upper La Luna interval and the volcanic ash found in the Upper La Luna Formation (Figure 145,146,147 and 148). Possibly, all the thickness found in different outcrops are not the same since erosion must have affected some areas more areas than others. This means that this correlation is approximated and estimated and other studies (isotopes and geochronology) should be done in order to obtain a valid result that might intercalate those depositional events.

It's important to mention that not all facies are repeated in the same order as in the La Luna IX well. Facies V and VI are repeated towards the Upper La Luna in Las Hernandez outcrop where in La Luna 1X well, they are located in the middle part; Facies V, VI and VIII are almost in the same order in Zea and Azulita- Bachaquero outcrops as in the La Luna IX well. .

The best sections found in outcrop, are located in Chiguara (Merida state- North Andean Flank) and Perija (Lago de Maracaibo Basin). The former contains the Middle and Upper La Luna but the facies (as most of the outcrops located in the North Andean flank) are not deposited in the same order as in the La Luna IX. Facies III is repeated in the Upper La Luna. There is the possibility of another volcanic ash in the Upper La Luna Fm that has the same characteristics as Facies III in the La Luna IX core. This

interval of volcanic ash is not confirmed yet since any geochronology and isotopic studies have been done to establish a chronological marker.

The Perijá outcrop is the most important since it contains the entire section that is also related to the core and is located in the same area (Lago de Maracaibo Basin). In this section, some intervals do not exhibit the same facies order, but most are correlated with La Luna IX core. The same trend is shown starting at the Maraca/La Luna contact and ending in the phosphate sand glauconite-rich intervals which are characteristic of Upper La Luna/ Tres Esquinas Member.

Fossils are important for working out the relative ages of sedimentary rocks. By using biostratigraphy completed by students at the Universidad de los Andes-Venezuela in 2015 (Gerson & Paredes., 2015; Bastidas & Vielma., 2015) and the biostratigraphy completed by (Davis & Pratt, 1999) it was able to generate a correlation between the ages of the the outcrops of La Luna Formation in Zea and Las Hernandez with the La Luna IX core. Figure 149 and 150 show that most of the outcrops are corellated to the Upper la Luna Formation (Timbetes Member) showing a defined biohorizon with benthic and planktonic foraminifera. Planktonic foraminifera include *Heterohelix reussi*, *Heteroelix globulosa* y *Whiteinella sp.*, while the benthic species are comprised of *Orthokarstenia sp., Bolivina sp.* and *Lenticulina sp.,* therefore establishing the age as Conician- Campanian. (Gerson & Paredes., 2015; Bastidas & Vielma., 2015).

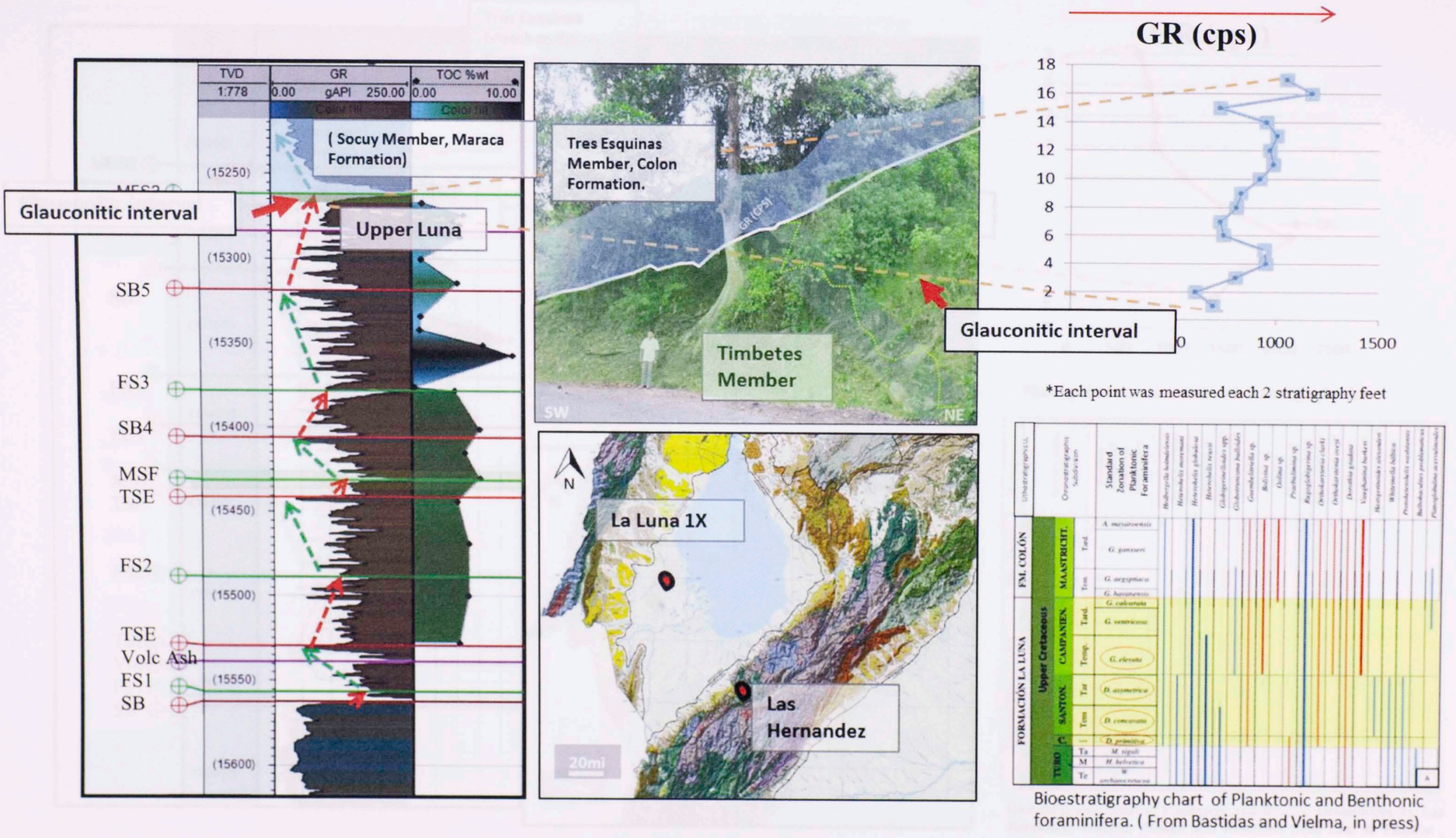

Bioestratigraphy chart of Planktonic and Benthonic foraminifera. (From Bastidas and Vielma, in press)

Figure 145 Estimated correlation between La Luna IX well and Las Hernandez outcrop. (Gamma ray measured in counts per second).

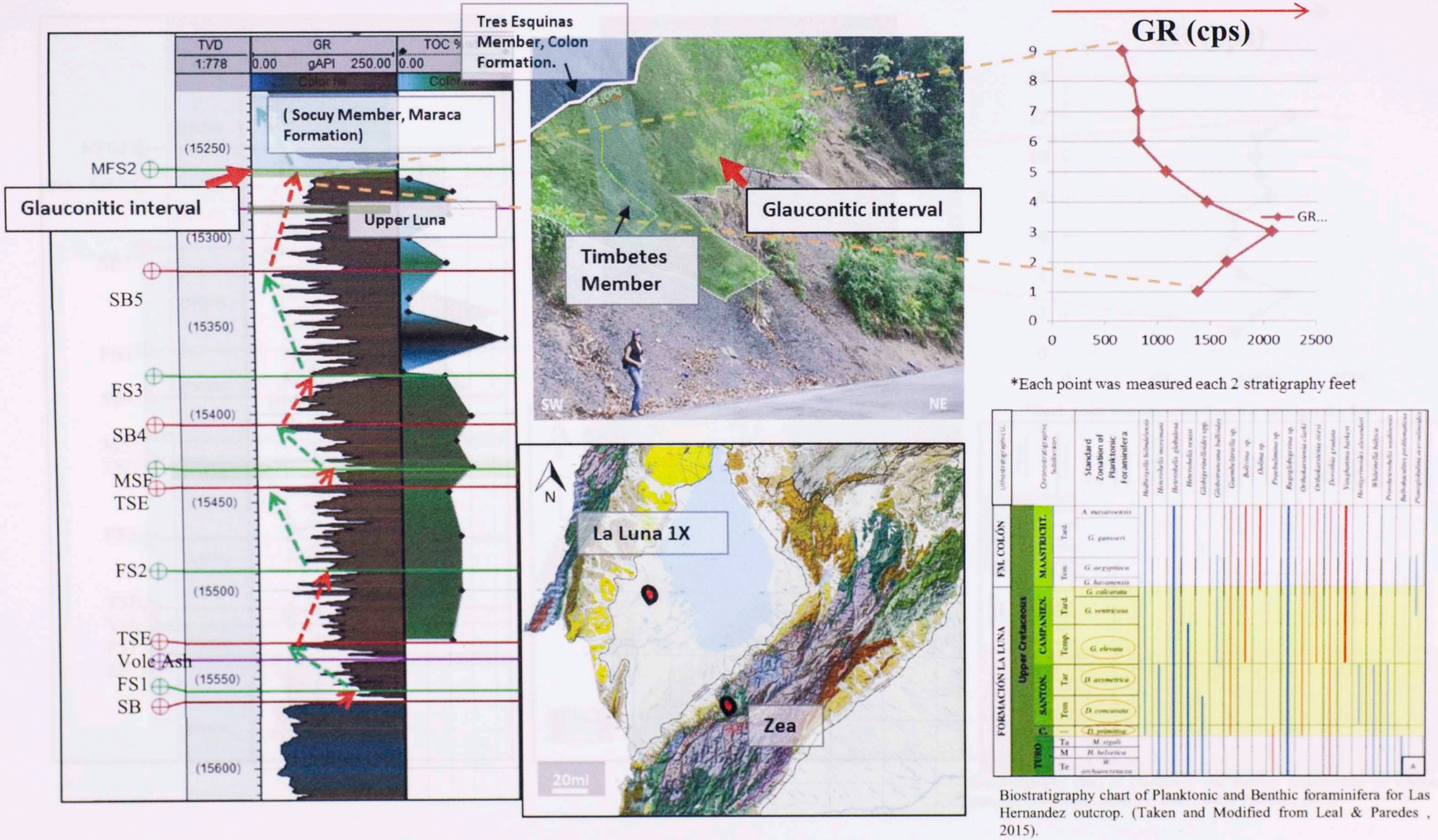

Biostratigraphy chart of Planktonic and Benthic foraminifera for Las Hernandez outcrop. (Taken and Modified from Leal & Paredes , 2015).

Figure 146 Estimated correlation between La Luna IX well and Zea outcrop. (Gamma ray measured in counts per second).

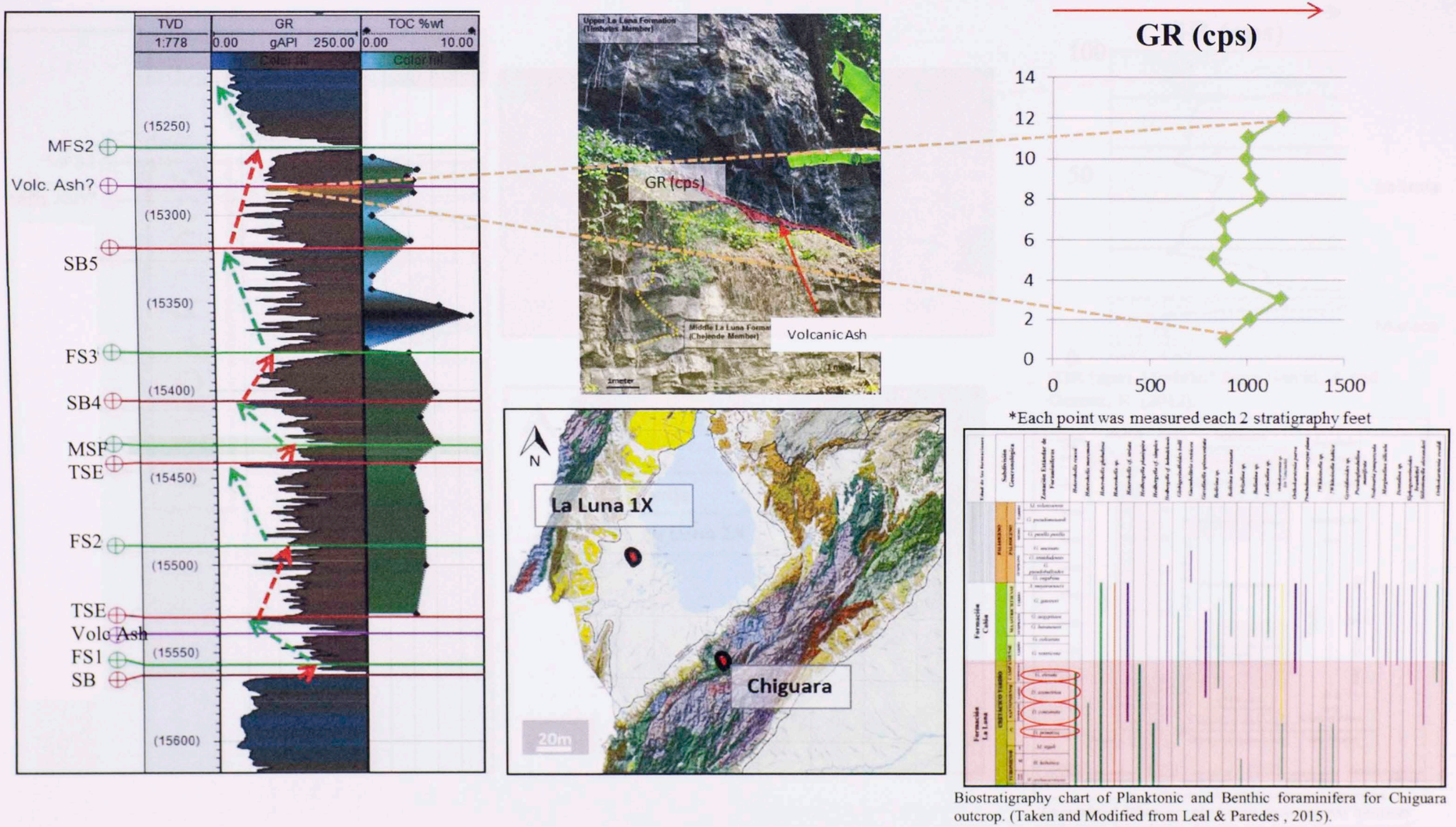

Biostratigraphy chart of Planktonic and Benthic foraminifera for Chiguara outcrop. (Taken and Modified from Leal & Paredes , 2015).

Figure 147 Estimated correlation between La Luna IX well and Chiguara outcrop. (Gamma ray measured in counts per second).

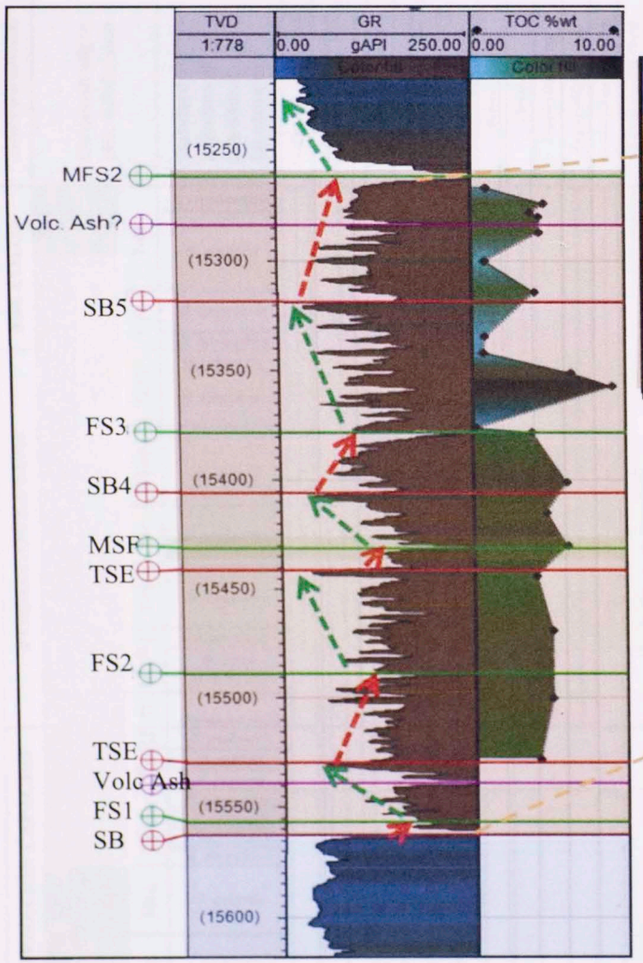

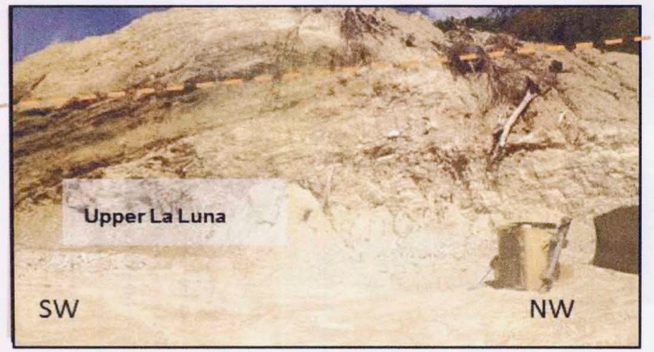

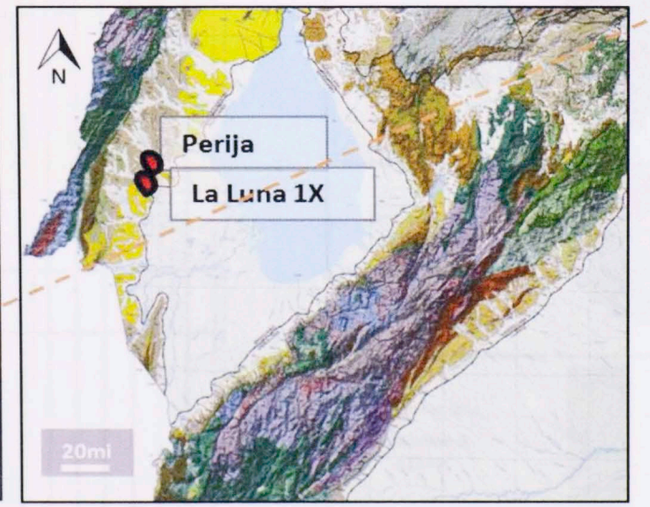

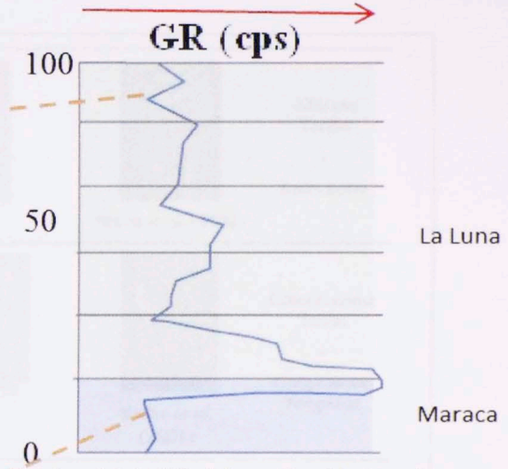

*GR (cps) Modified from Samid, A and Gomez, R. (2012).

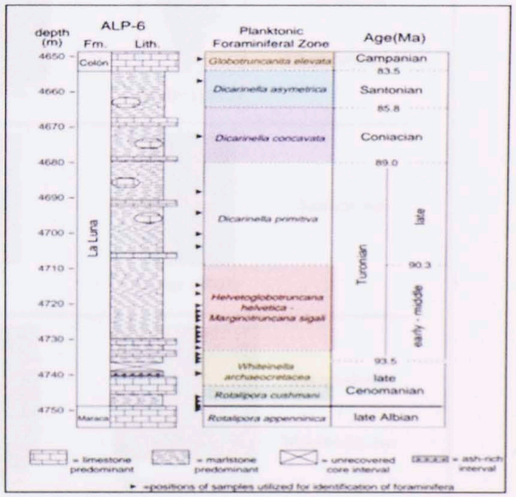

Generalized lithology, planktonic foraminiferal biozones and stage boundaries for the La Luna Formation and surrounding units in La Luna IX. From Davis & Pratt, 1999).

Figure 148 Estimated Correlation between La Luna IX well and Perijá outcrop. (Gamma ray measured in counts per second).

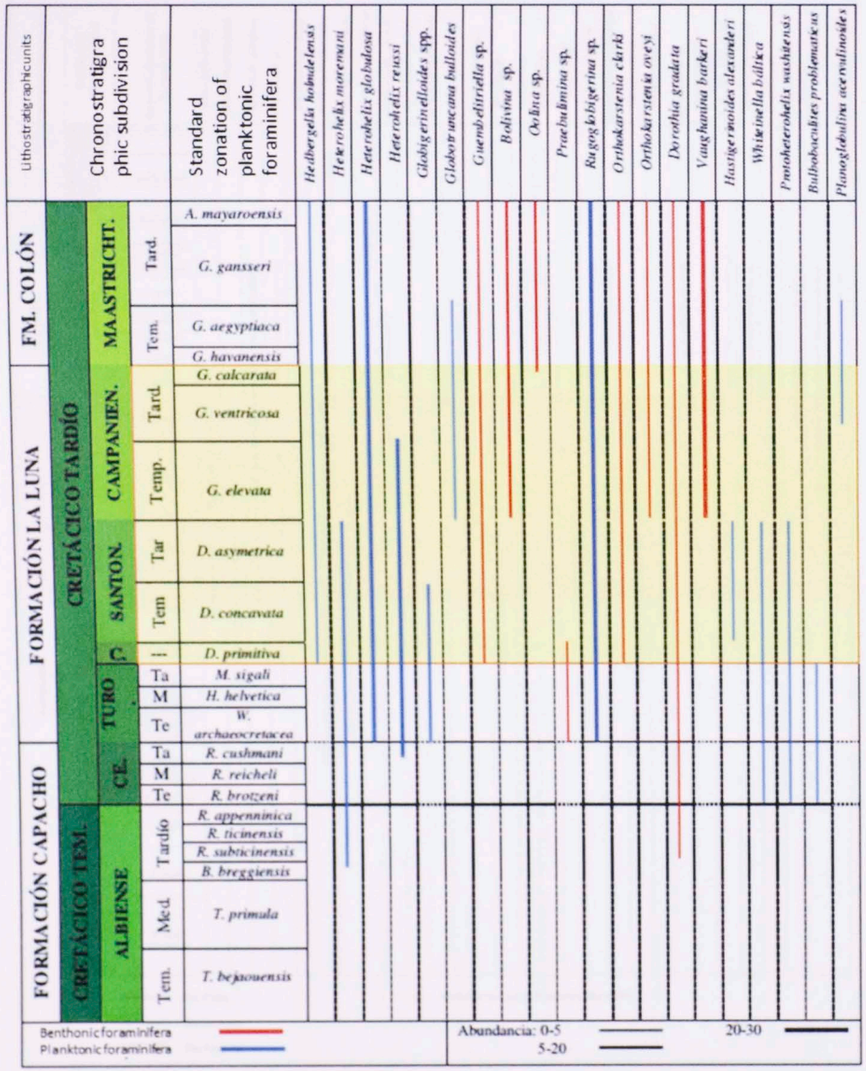

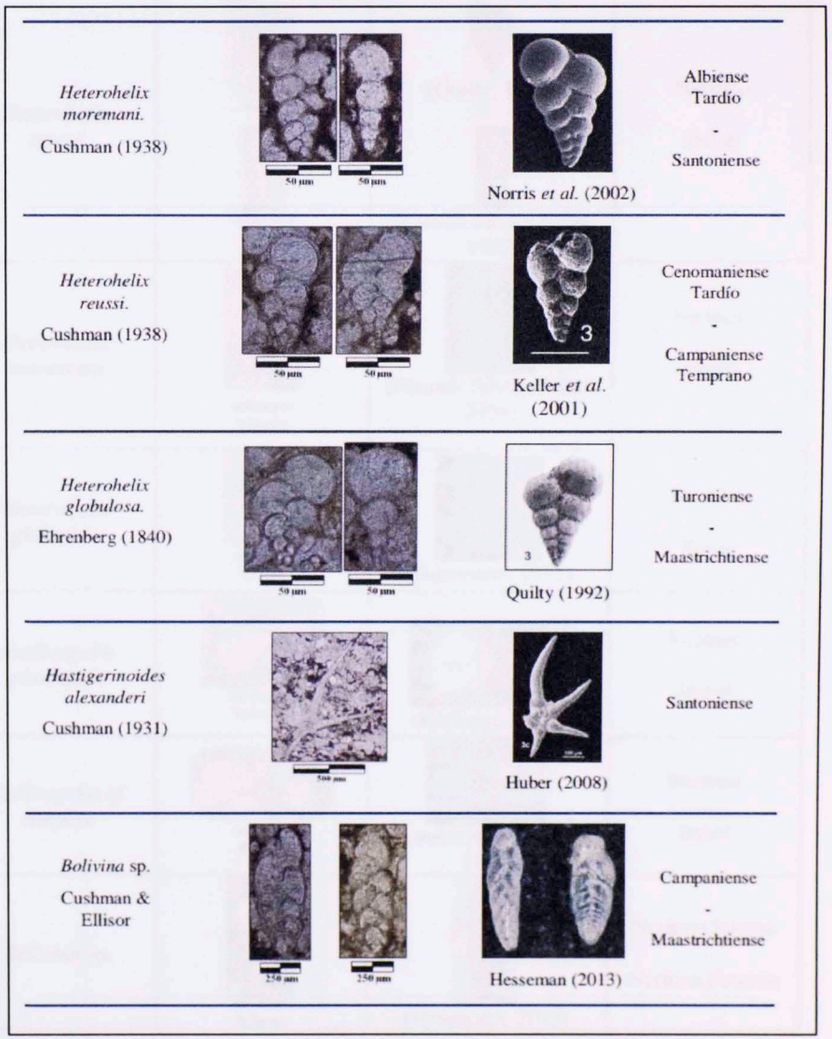

Figure 149 Identified foraminifera from Bastidas & Vielma (2015) and benthic-planktonic faunal distribution chart showing the standard zonation from Erlich (1999) in Bastidas & Vielma, 2015.

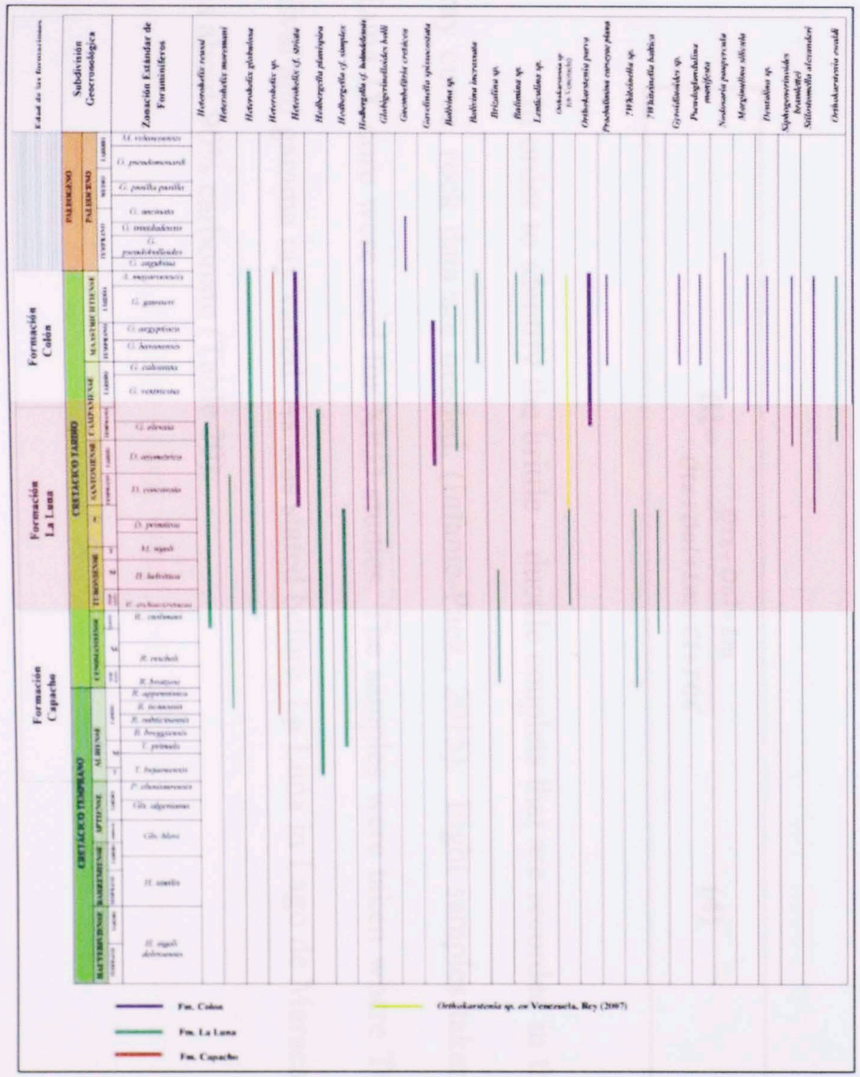

Heterohelix reussi	 0,25m  0,5mm	 (Quilty, 1992)  (Premoli Silva y Sliter, 1995)	Neritico - Batial
Heterohelix moremani	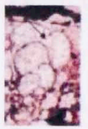 0,5mm	 (Premoli Silva y Sliter, 2004)	Neritico - Batial
Heterohelix globulosa	 0,25m	 (Hesemann, 2015)	Neritico - Batial
Hedbergella planispira	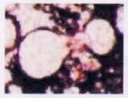 0,5mm	 (Kertznus, 2002)	Neritico - Batial
Hedbergella cf. simplex	 0,5mm	 (Premoli Silva y Sliter, 1995)	Neritico - Batial
***Bolivina* sp.**	 0,5mm	 (Hesemann, 2015)	Neritico Interno - Neritico Externo

Figure 150 Identified foraminifera from Gerson & Paredes (2015) and benthic-planktonic faunal distribution chart showing the standard zonation from Erlich (1999) in Gerson & Paredes, 2015.

7. Definition of the most prospective intervals

7.1 Brittleness index

"When a rock is subjected to increasing stress it passes through three successive stages of deformation: elastic, plastic, and fracture. Based on these behaviors it is possible to classify the rocks into two classes: ductile and brittle. If the rock has a smaller region of elastic behavior and a larger region of plastic behavior, absorbing much energy before failure, it is considered ductile. In contrast, if the material under stress has a larger region of elastic behavior but only a small region of plastic behavior, the rock is considered brittle" (Perez- Altamar, 2013).

Brittleness index is based on the mineral composition of the rock (Equation 4), dividing the most brittle minerals by the sum of the constituent minerals in the rock sample, (modified from Wang & Gale, 2009) as: Qtz: quartz, Lm: limestone and Dol: dolomite, Cl: Clay and TOC: Total organic carbon.

$$\mathbf{BI}=\frac{Qtz+Dol+Lm}{Qtz+Dol+Lm+Cl+TOC} \qquad (4)$$

In order to identify the brittle – ductile couplets that are recorded in the gamma ray curve, rock data are needed. (Infante-Paez., 2015). Eight samples taken from La Luna IX core were used for XRD studies. The samples were taken where TOC. Rock Eval and gamma ray varied. As was stated before, La Luna in Lago de Maracaibo Basin is about 90% carbonate (Table 20).

Table 16 Constituent minerals in the rock used for the Brittleness Index equation (modified from Wang & Gale, 2009)

DEPTH	Qtz	Dol	Lm	Cl	TOC	BI
15267	32.5	0.0	1.0	66.5	1.0	0.3
15300	4.1	0.0	95.9	0.0	0.9	1.0
15334	3.5	0.0	92.3	4.3	0.8	0.9
15357	36.1	36.1	59.2	0.0	9.1	0.9
15376	1.6	0.0	95.4	0.0	0.2	1.0
15401	3.8	0.0	96.2	0.0	6.1	0.9
15465	16.6	0.0	73.3	10.0	5.1	0.9
15528	24.7	0.0	28.8	46.9	4.2	0.5

Figure 151 shows the relationship of the brittle and ductile couplets BI, gamma ray, TOC wt% and RHP. Although the brittle- ductile couplets where based on the sequence stratigraphy (HST for Brittle areas and TST for ductile areas), few samples were used for the BI equation (modified from Wang & Gale, 2009) in the Middle La Luna Fm. It is recommended that more samples be taken to establish a better interpretation of the best intervals in La Luna IX well.

7.2 Target intervals

Although no porosity and oil saturation data were used to validate prospective intervals in this work, available data such as: geochemical parameters (TOC, S1, S2, Tmax and PI), TOC % (using Passey Method), OSI, BI, GR, Impedance, Density, carbonate, quartz and clay percent were used for the estimation of the three most prospective intervals in the cored well (Figure 151, 152 and 153).

The first interval from bottom to top has a thickness of 47 ft. and a BI of 0.85, H.S.T and related facies located in the sequence stratigraphic framework under facies V (Siliceous – calcareous laminated mudstone interbedded with black chert filled with calcite veins).

The second interval has a thickness of 25 feet and has a BI of 0.99. It is located below the H.S.T and related to facies V (Siliceous – calcareous laminated mudstone interbedded with black chert filled with calcite veins) as well.

The third interval contains a thickness of 59 feet and has an average BI of 0.93. It is facies VI and VII (Calcareous slightly siliceous wackstone and slightly siliceous calcareous laminated black mudstone interbedded with calcareous fossiliferous wackstone). This facies in particular, contains a bigger percent of carbonates and quartz compared with the rest of the La Luna interval.

It is important to explain that the variation in the geochemical patterns (Tmax, TOC, S1 and S2 peak) are due to the lithological variability of chert and shales present on La Luna Fm. Points that are surrounded by circles in the TOC track are chert samples (Figure 152), which affect the continuity of the geochemical parameters.

From the approximately 300 feet that La Luna formation contains in thickness, almost half of it is prospective. La Luna can be compared in thickness and organic matter content with the big Eagle Ford play. Therefore, if La Luna is exploited in Venezuela, it will show an excellent potential for unconventional development.

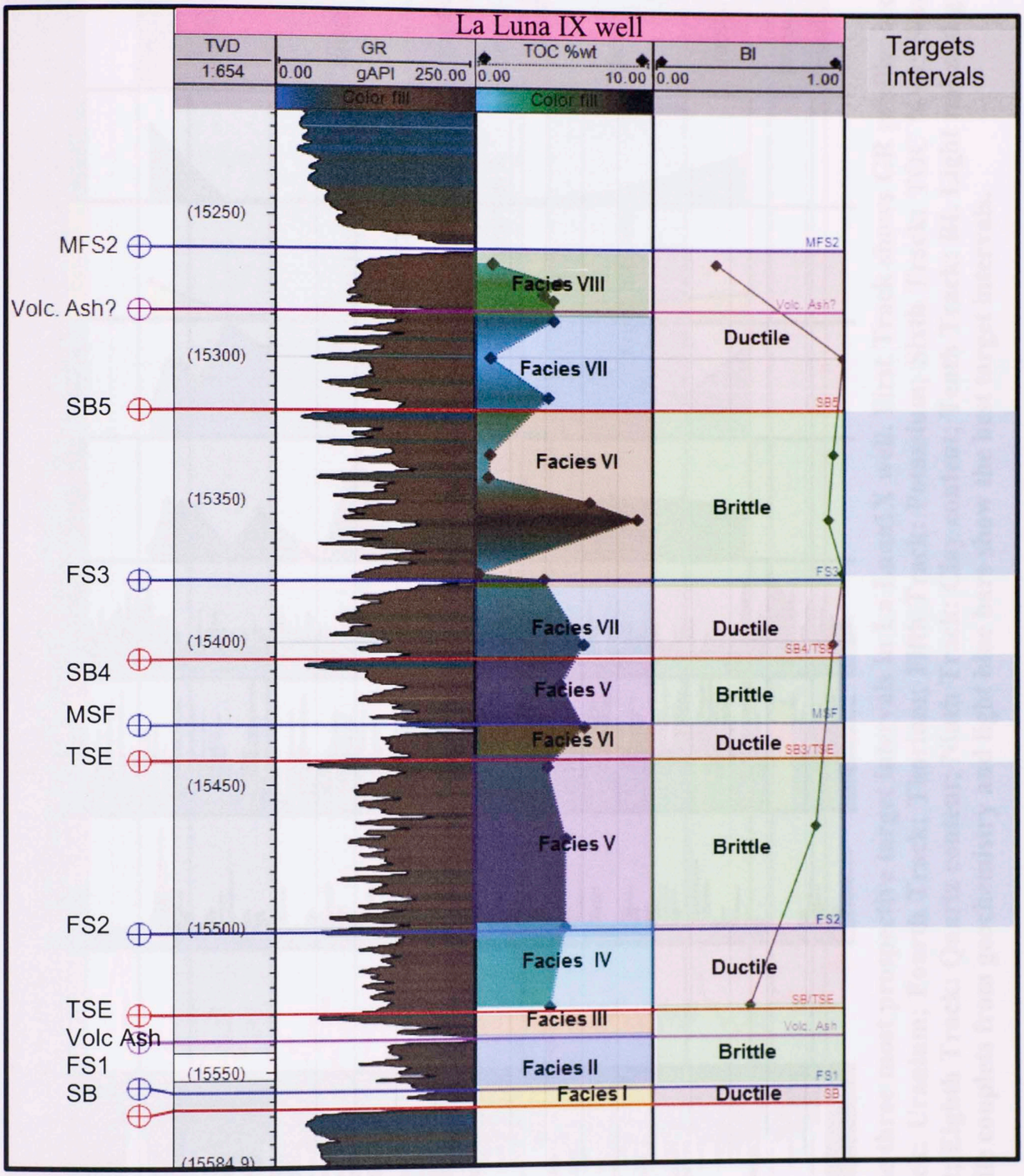

Figure 151 Relationship of the brittle and ductile couplets based on their stratigraphic correlation with the gamma ray, TOC % wt, BI and RHP. Blue squares show the best target intervals.

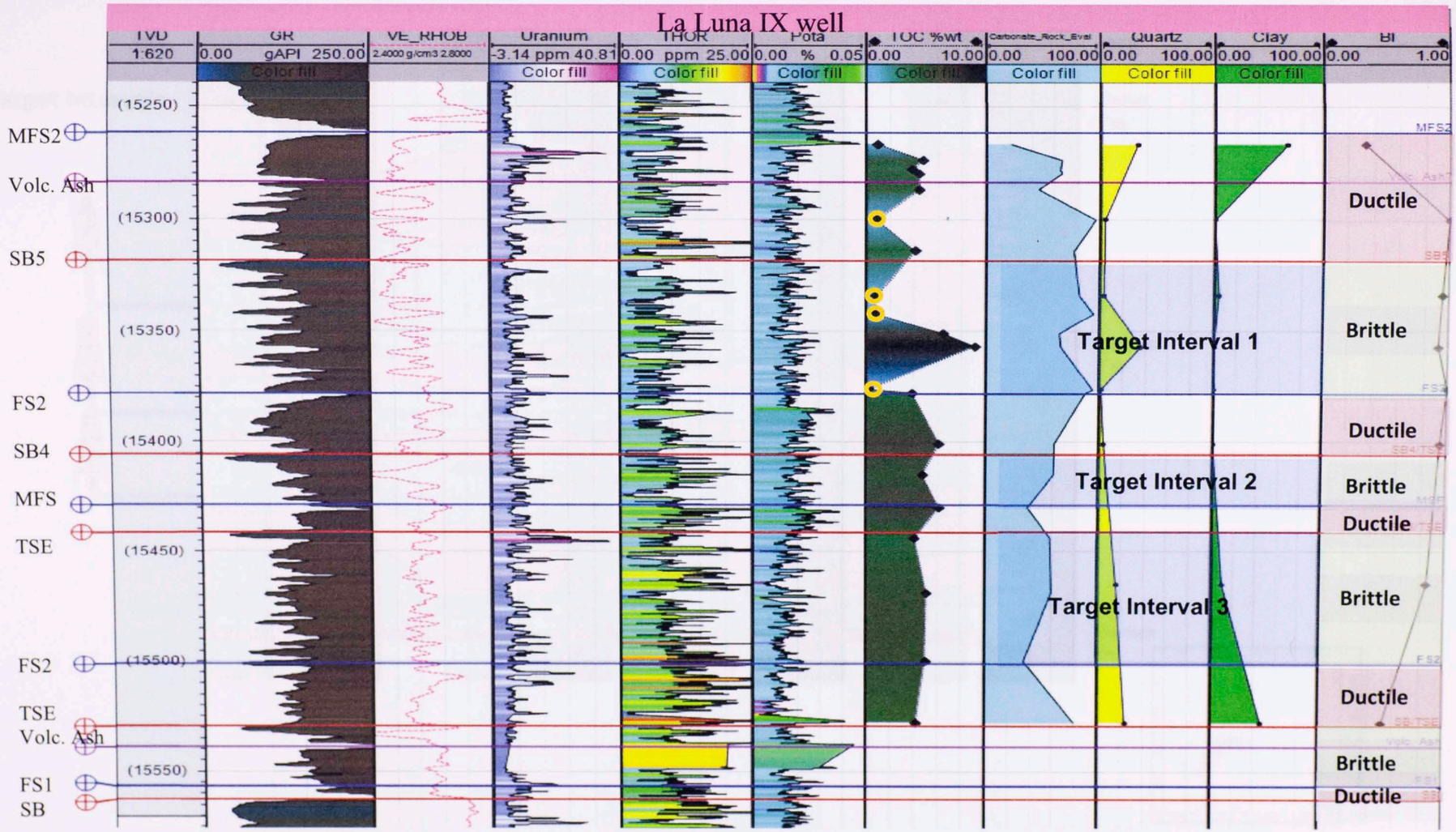

Figure 152 Definition of the three most prospective target intervals in La Luna1X well. First Track shows GR profile; second Track: Density; Third track: Uranium; Fourth Track: Thorium; Fifth Track: Potassium; Sixth Track: TOC %wt; Seventh Track: Carbonate content; Eighth Track: Quartz content; Ninth Track: Clay content; Tenth Track: BI. Light red and green bars show the brittle- ductile couplets from geochemistry and light blue bars show the best target intervals.

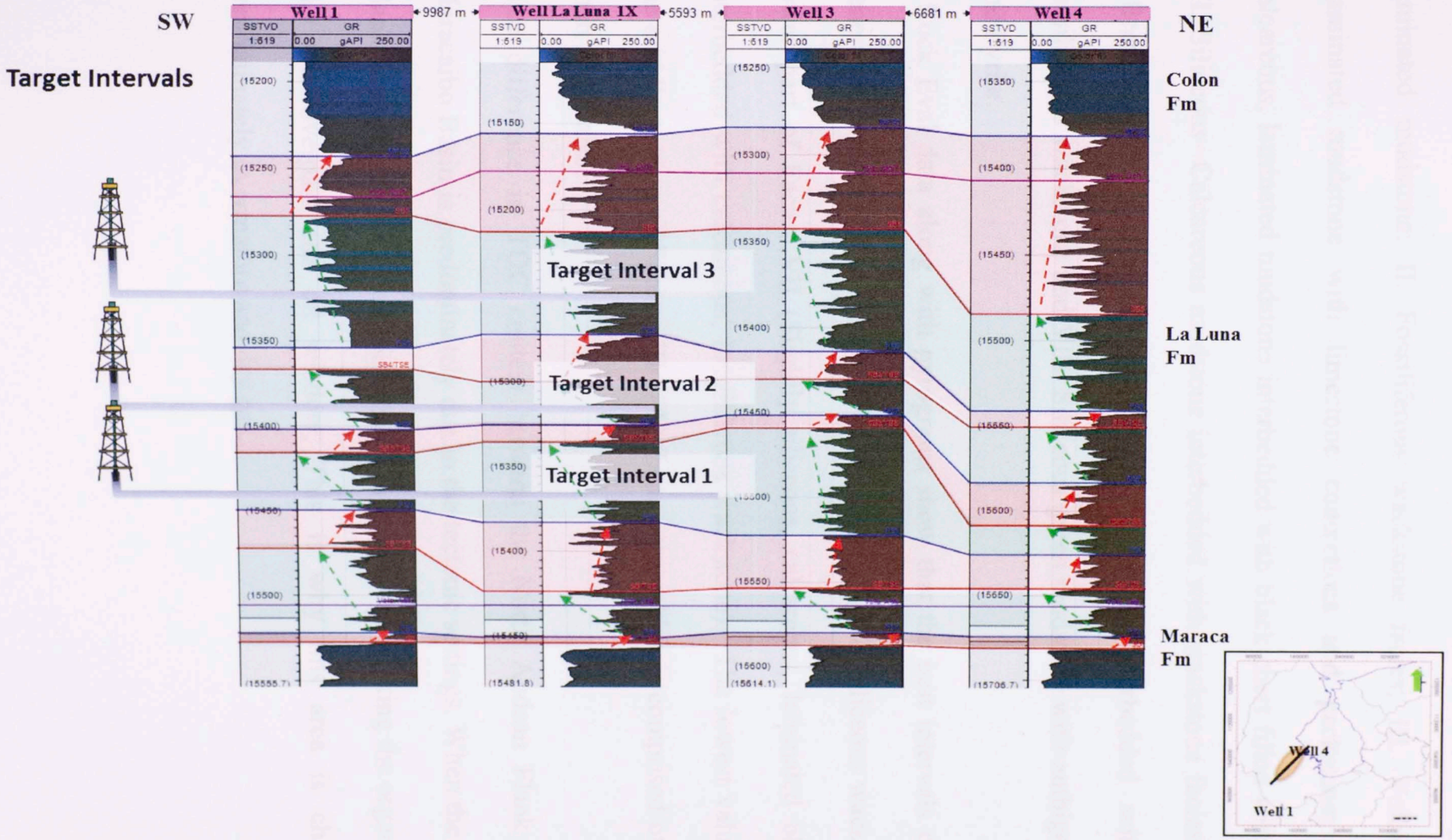

Figure 153 Stratigraphic cross section of third order sequences (TST and HST) in La Luna 1X well using lower volcanic ash (purple line) as a stratigraphic datum. MFS are shown as blue lines and green arrows show the trend of the HST. SB/TSE are shown as red lines and red arrows show the trend of the TST. Green color shows a more carbonate-rich interval and red color shows a more organic-rich interval.

Conclusions

-Eight facies were defined in the La Luna IX core from bottom to top: I. Dark gray laminated mudstone; II. Fossiliferous wackstone facies; III. Volcanic Ash; IV. Laminated mudstone with limestone concretions and packstone; V. Siliceous-calcareous, laminated mudstone interbedded with black chert filled with calcite veins; VI. Siliceous- Calcareous mudstone interbedded with wackstone facies; VII. Slightly siliceous- calcareous, laminated, black mudstone interbedded with calcareous, fossiliferous wackstone and VIII. Siliceous green mudstone with authigenic glauconite and Pyrite.

- Rock Eval data along with pyrograms show that the best intervals of potential oil generation are present in Facies VI (Calcareous, slightly siliceous wackstone) and the lower part of Facies VII (Slightly siliceous, calcareous, laminated black mudstone interbedded with calcareous, fossiliferous wackstone). The lowest values are seen in the middle section of Facies VII of La Luna core, which is comprised of alternation of chert and shales.

-The difference in TOC content between the North Andean Flank and Lago de Maracaibo Basin is predominately due to the tectonic settings. When the North Andean Flank was uplifted, La Luna Formation was heated overcooking the organic matter until this one overpass the oil window. This is why this area is characterized as predominately overmature and dry gas.

- As in the Eagle Ford, the La Luna shows a gamma ray log response that diminishes progressively upward, indicating the sequence begins with SB/TSE and ends with the HST in La Luna IX well. A series of third order sequences of Highstand and Transgressive System Tracts overlying the erosional top of the underlying Maraca Formation constitutes La Luna Formation.

-Three target intervals were identified in La Luna 1X well. The first interval from bottom to top has a thickness of 14.32 m. and a BI of 0.85. The second interval has a thickness of 7.60m and has a BI of 0.99. The third interval has a thickness of 18 m and has an average BI of 0.93.

References

Acuna, H., Gil, J., Riegstra J., Taha, M., Menier, M., et al. (1997). *Well Evaluation Conference Venezuela.*

Audemard, F., Romero, G., Rendon, H., & Cano, V. (2004). Quaternary fault kinematics and stress tensors along the southern Caribbean from fault slip data and focal mechanism solutions. *Science Direct*, 181-233.

Bastidas, J., & Vielma, C. (2015). *Evaluacion sedimentologica y Geoquimica de la Formacion La Luna para la prospeccion de Lulitas gasiferas en los poblados de Zea y Las Hernandez de Los estad.* Merida-Venezuela: Universidad de los Andes undergraduate Thesis.

Bellizia, A., & Pimentel, N. (1994). Terreno Mérida: un cinturón Alóctono Herciniano en la Cordillera de Los Andes de Venezuela. . *V Simposio Bolivariano Exploración Petrolera en las Cuencas Subandinas, Memoria , 271-299.*

Burkley, L.(1975). *Geochronology of the Central Venezuelan Andes.*. Ph. D. Thesis, Case Nester Reserve Univ. .

Canache, M., Pilloud, A., Cruz, J., & Gamarra., S. (1994). Stratigraphic revision of the Creataceous section of the Maraca river, Sierra de Perija, Venezuela. In *Proceedings of the 5th Simposio Bolivariano: Exploracion Petrolera en las cuencas Subandinas* (pp. pp.240-241). Puerto La Cruz, Venezuela.

Cobbold, P., Zanellaa, A., Rodriguesa, N., & Loseth, H. (2013). Bedding-parallel fibrous veins (beef and cone-in-cone): Worldwide occurrence and possible significance in terms of fluid overpressure, hydrocarbon generation and mineralization. *Marine and Petroleum Geology Volume 43*, 1-20.

Davis, C., & Pratt, L. (1999). Factors influencing organic carbon and trace metal accumulation in the Upper Cretaceous La Luna Formation of the western Maracaibo Basin, Venezuela. *Geological Society of America, Special Paper332*, 203-230.

Dos Santos, J., & Soto, G. (2002). *Caracterizacion diagenetica de los litotipos lodosos de la formacion La Luna en la seccion de La Quebrada Chiriria, estado Tachira.* Caracas: Universidad Central de Venezuela, Undergraduate Thesis.

Erlich, R. (1999). *Depositional Environments, Geochemistry, and Paleoceanography of upper cretaceous organic carbon- rich strata, Costa Rica and western Venezuela.* Austin, Texas: Vrije Universiteit.

Erlich, R., Macsotay, O., & Nederbragt, J (2000). Birth and Death of the Late Cretaceous "La Luna Sea", and Origin of the Tres EsquinasPhosphorites. *SEPM Research Conference*.

Gerson, A., & Paredes, E. (2015). *Caracterizacion sedimentologica y geoquimica de la sucesion Cenomanience- Campanience aflorante en la region de Chiguara. Estado Merida- Venezuela.* Merida-Venezuela: Universidad de los Andes undergraduate Thesis.

Gomez, A. (2014). *Integrated geological characterization and distribution of the salada Member, La Luna Formation, in the central area of the Middle Magdalena Basin, Colombia.* Norman, Oklahoma: M.S Thesis The University of Oklahoma.

Gomez, N. (2010). *Revista Mene*. Retrieved from //www.revistamene.com/nueva/docs/gas-natural-no-convencional.pdf

Gonzales-de-Juana, C., Iturral, J., & Picard Cadillat, Xavier. (1980). *Geologia de Venezuela y de sus Cuencas Petroliferas.* Caracas, Venezuela.

Hughes, J. (2013). A reality check on the shale revolution. *Nature 494*, 307-308.

Infante-Paez, L. (2015). *Seismically-Determined Distribution of Total Organic Carbon (TOC) in the woodford shale though integrated Reservoir Characterization, Payne County, Oklahoma.* Norman: Master Thesis The University of Oklahoma.

Jarvie, D., R.J, H., Ruble, T., & Pollastano, R. (2007). Unconventional shale gas systems: The Mississippian Barnett Shale of north central Texas as one model from thermogenic shale- gas assessment. In *AAPG Bulletin 91.* 475- 499.

Loubser, M., & Verryn, S. (2008). Combining XRF and XRD analyses and sample preparation. pp. 229, 238.

Newswire, P. (2012, July 20). *www.reporterlinker.com.* Retrieved July 20, 2014, from //www.reportlinker.com/p0829577/Montney-Shale-in-Canada-2012

Passey, Q., Creaney, S., Kulla, J., Moretti, F., & Stroud, J. (1990). A Practical Model for ORganic Richness from Richness from Porosity abnd Resistivity Logs. *AAPG Bulletin, V. 74 No. 12*, 1777- 1794.

Petroleos de Venezuela, Sociedad Anonima. (2012). *Proyecto de Investigacion en estudio de Formaciones Lutiticas como reservorio de gas natural en la Cuenca de Lago de Maracaibo.* Maracaibo, Venezuela.

Perez-Altamar, R. (2013). *Brittleness Estimation from Seismic Measurements in Unconventional Reservoirs:Application to the Barnett Shale.* Norman, Oklahoma: PhD Master Thesis.

Perez-Infante, J., Paul, F., & Max., F. (1996). Global and local controls influencing the deposition of the La Luna Formation (Cenomanian-Campanian), western Venezuela. *Elsevier, Volume 130, Issues 3-4*, 271-288.

Peter, C. (2013). Engineering energy: unconventional gas production: a study of shale gas in Australia. Australian Council of Learned Academies (ACOLA). Australia.

Philp, R. (2014). Formation and Geochemistry of Oil and Gas. In *Treatise on Geochemistry* (pp. 233-265). Second edition, vol 9. Oxford: Elsevier.

Renz, O. (1959). *Estratigrafía del Cretáceo en Venezuela occidental.* Caracas: Bol. Geol., 5(10): 3-48. Resumen (1960) Asoc. Venez. Geol., Min. y Petról., Bol. Inform., 3(7): 209.

Schlanger, S., & Jenkyns, H. (1976). Cretaceous anoxic events: causes and consequences. *Geol. Mijnbouw, 55*, 179-184.

Schlanger, S., Arthur, M., Jenkyns, H., & Scholle, P. (1987). The Cenomanian-Turonian oceanic anoxic event, Stratigraphy and distribution of organic rich beds and the marine 13C excursion. *J. Brooks and J. Fleet, Marine Petroleum Source Rocks, Geological Society London*, 371-399.

Scholle, P., & Ulmer-Scholle, D. (2003). *Petrography of Carbonate Rocks: Grains, textures, porosity, diagenesis.* Tulsa, Oklahoma: AAPG Memoir 77.

Schulz, H., Horsfield, B., & Sachsenhofer, R. (2010). Shale gas in Europe: a regional overview and current research activities. *Geological Society London, Petroleum Geology Conference series 2010 v.7*, (pp. 1079-1085). London.

Slatt, R. (2013). Sequence stratigraphy of the Woodford Shale and application to drilling and production. *AAPGDatapages/Search and Discovery*, Article No. 50792.

Slatt, R. (2012). Comparative Sequence Stratigraphy and Organic Geochemistry of Gas Shales: Commonality or coincidence? *Journal of Natural Gas Science and Engineering, v.8,*, p.68-84.

Slatt, R. (2012). Pore-to-regional-scale integrated characterization workflow for unconventional gas shales, in J. Breyer, ed., Shale reservoirs—Giant resources for the 21st century. *AAPG Memoir 97*, p. 1–24.

Slatt, R., & Rodriguez, N. (2012). Comparative sequence stratigraphy and organic geochemistry of gas shales: Commonality or coincidence? *Journal of Natural Gas Science and Engineering*, 68-84.

Slatt, R., McCullough, B., Molinares, C., Baruch, E., & Turner, B. (2015). Paleotopographic and Depositional Environment Controls on "Sweet Spot" Locations in. *Search and Discovery #80467 (2015)**.

Slatt, R., Philp, P., Abousleiman, Y., Singh, P., Perez, R., Portas, R., et al. (2011). Pore-to-regional-scale integrated characterization workflow for unconventional gas shales, in J. Breye. *Giant resources for the 21st century: AAPG Memoir 97*, 1-24.

Sutton, F. (1946). Geology of the Maracaibo Basin, Venezuela. *AAPG, Bulletin 30(10)*, 1621-1741.

Tissot, B. P., & Welte. (1984). Petroleum Formation and Occurrence. New York: 2 ed. Springer-Verlag.

Torres, E. (2013). *Unconventional Gas Shale Assessment of La Luna Formation, In the Central and South Areas of the Middle Magdalena Valley Basin, Colombia.* M.S Thesis University of Oklahoma.

Treanton, J., Turner, B., & Slatt, R. (2014). Outcrop derived inorganic geochemistry of the woodford shale; Murray county; Oklahoma. Houston, Texas.

Truskowski, I., & Galea-Alvarez, F. (1996). Late Cretaceous biostratigraphy of the La Luna Formation, Maracaibo Basin. *Second American Association of Petroleum Geologists/ Sociedad Venezolana de Geologos International Congress and Exhibition, Caracas.*, v.80,p.1341.

Truskowski, I., Galea-Alvarez, F., & Sliter, W. (1995). Cenomanian hiatus en Venezuela (abstract). In *Abstracts of the Geol. Soc. Am. Annual Meeting* (pp. PP A-303). New Orleans, Luisiana.

Turner, B., & Slatt, R. (2013). *Chemostratigraphy and its application to the Woodford Shale, Oklahoma.* Norman, Oklahoma: Institute of Reservoir Characterization, University of Oklahoma.

Villasmil, T. (2002). Retrieved from http://www.palacio.org/hablamos/0000009d.htm

Xu, X., Zhi, D., Liang, Y., & Zhang, H. (2011). Wu State Key; Status and development tendency of shale gas research. *Journal of Chengdu University of Technology.*

This volume is the property of the University of Oklahoma, but the literary rights of the author are a separate property and must be respected. Passages must not be copied or closely paraphrased without the previous written consent of the author. If the reader obtains any assistance from this volume, he or she must give proper credit in his own work.

I grant the University of Oklahoma Libraries permission to make a copy of my thesis/dissertation upon the request of individuals or libraries. This permission is granted with the understanding that a copy will be provided for research purposes only, and that requestors will be informed of these restrictions.

NAME [redacted]

DATE [redacted]

A library which borrows this thesis/dissertation for use by its patrons is expected to secure the signature of each user.

This thesis/dissertation by ANDREINA LIBORIUS PARADA has been used by the following persons, whose signatures attest their acceptance of the above restrictions.

NAME AND ADDRESS DATE

Revised 10/11/2012